

Experimental and Theoretical Investigation of a
Reductant-Activated Methodology for Covalent
Functionalization of 1T' Transition Metal
Dichalcogenides MoS₂ and WS₂

Thesis by
Ellen Yan

In Partial Fulfillment of the Requirements for
the Degree of
Doctor of Philosophy

The logo for the California Institute of Technology (Caltech), featuring the word "Caltech" in a bold, orange, sans-serif font.

CALIFORNIA INSTITUTE OF TECHNOLOGY
Pasadena, California

2021
(Defended May 18, 2021)

© 2021

Ellen Yan
ORCID: 0000-0003-3252-790X

Acknowledgements

Like all journeys, the path I took to arrive here was full of twists and turns, and people to thank who have influenced me to change, grow, and become the person that I am today. The fact that I am writing these words is evidence of the support that I have received over the years for which I am forever grateful. Since failure is an inevitable part of any journey, the progress that I have made depended in no small part upon the support that I have received, allowing me to extend further, dream bigger, and dare to do so in the first place.

First, I would like to thank my advisor, Nathan Lewis, for taking me on as a student, making this research possible, and providing the space for me to learn and grow. During times when I could not see the light at the end of the tunnel, you provided the trust and support that allowed me to stay on this path, for which I am forever grateful.

To Kim Papadantonakis and Bruce Brunschwig, thank you for being there throughout my journey. I am truly grateful for your insights, kindness, attention to detail, generosity, reliability, and attitude. Whatever the situation, it always felt more manageable after having a good chat with you, which is a treasure itself.

To Barbara Miralles, I cannot understate your professional contribution to the completion of my PhD. Without you, the entire process would fall apart. Thank you for being a constant in Noyes, always being a source of friendly conversation, and for holding the group together.

I would also like to thank my thesis committee members Professors Harry Gray, Paul Wennberg, and Kimberly See, for their time reviewing my candidacy proposals, my PhD proposals, and now this thesis. Thank you for your insights, comments, discussion, and contributions, without which I would not have made some of the insights herein.

To members of the Lewis Group, past and present: thank you all for your support, kindness, and willingness to lend a hand and your time. This project was inspired by the works of others in the group and could not exist without the help and input of Miguel, Renata, Mo, Azhar, Noah, and Paul K. Likewise, I also owe the fun times in Noyes to Michael, Jonathan,

Ethan, and Burt, with special thanks to Annelise, Kyra, and Pai for my sanity and well-being, whether it's the XPS requiring maintenance again, or life.

I also want to acknowledge Professor Bill Goddard, Soonho Kwon, Charles Musgrave, and Yufeng Huang for their time and advice getting me through the density functional theory calculations. Without them, an entire chapter would not exist. Thanks also goes to Sonjong Hwang for all his patience and help to obtain NMR data that was key to my research.

Besides my academic experience at Caltech, there are countless others who have been just as critical to my academic achievements and who made my non-academic experience just as memorable. I want to thank Barb Catlin for her selfless mentorship in the art of jazz, providing the structure and motivation that enabled me to grow my confidence by making the impossible possible. Thank you also to the staff and nurses who have supported my physical and mental health throughout these years such that I could continue doing research.

I want to acknowledge several teachers who made a tremendous impact in my life: my high school biology teacher, Monika Quinn, the most assertive critical thinker I had ever met, who used tough love to great effect and instilled a confident can-do attitude in her students; and two talented and highly effective undergraduate chemistry instructors whose teachings were the reason I chose chemistry as my major: Professors Andrew Dicks and Kristine Quinlan.

Finally, I would like to thank all my friends and family for their love, emotional support, guidance, and presence. Life and work happen at the same time, and when work is full of uncertainty as is often the case in science, one needs solid reserves of emotional support to be resilient and persevere. Thank you to my mom and dad for the childhood they provided me and giving me a sense of safety and stability. Thank you to my friends-at-a-distance: Kacy, Crystal, Michelle, for being there to support me and give me words of wisdom to work through the challenges in life. Thanks also to my friends-not-at-a-distance-except-in-a-pandemic: Porfirio, Manuel, Daniela, Jorge, Alejandro, Orika, Helen, David, Vin, Akshita, for the memories and experiences that have opened my mind and shifted my perspective, conversations that changed my philosophy and approach to life, and being amazing human beings whom I am so grateful to have had the pleasure of knowing.

Abstract

Chemically exfoliated MoS₂ (*ce*MoS₂) is a two-dimensional layered transition metal dichalcogenide in the 1T' phase that can be synthesized by intercalating and exfoliating MoS₂ of the thermodynamically stable and relatively inert 2H phase. Several functionalization techniques have emerged in the past decade to functionalize both the 2H and 1T' phases, with growing interest given the array of applications for MoS₂ in optoelectronics, catalysis, sensing, bioimaging, drug delivery, and photothermal treatment. To aid in this effort, we expanded upon a recently reported covalent functionalization method by developing a reduction-activated methodology to functionalize *ce*MoS₂ using one-electron metallocenes and showed that the coverage of a functional group increases as the reduction potential increases, allowing for greater control of the coverage. Using density functional theory (DFT), we found that the coverage of the smallest functional group, a methyl, is expected to be limited to ~64% per MoS₂ due to the steric hinderance associated with the methylation of sulfur sites that are adjacent to more than one methyl group. We also found that a similar coverage trend can be observed when applying reduction-activated functionalization to *ce*WS₂, albeit with a lower coverage at every potential that can be explained using DFT calculations as a difference in the thermodynamic favorability of the reaction. Reductant-activated functionalization provides a driving force that enables *ce*MoS₂ and 2H-MoS₂ to be functionalized when it is otherwise unreactive with electrophiles. Conceptualizing the work herein as part of a redox-activated functionalization method, there is an abundance of opportunity to explore oxidant- and reductant-activated functionalization on other chalcogenides, pnictides, and materials in the carbon and boron groups using both solution oxidants and reductants, as well as electrode-based electrochemical methods. Further exploration of redox-activated techniques expands the functionalization toolbox and enables researchers to develop application-specific functional materials.

Published Content and Contributions

Portions of this thesis have been drawn from the following publications and manuscripts in preparation.

E. X. Yan, M. B. Morla, S. Kwon, C. B. Musgrave, B. S. Brunschwig, P. A. Kempler, W. A. Goddard, N. S. Lewis, “Thermodynamic and kinetic limitations for covalent functionalization of 1T'-MoS₂: a model for methylation coverage on chemically exfoliated MoS₂” *in preparation*.

E.X.Y. performed the methyl functionalization calculations, analyzed the results, coded the coverage simulations, and made the figures; S.K. and C.M. provided input on the details of the calculations. The manuscript was prepared by E.X.Y. with input from co-authors.

E. X. Yan, R. Balgley, B. S. Brunschwig, N. S. Lewis, “Comparison of reactivity and methyl coverage obtainable using reductant-activated functionalization for chemically exfoliated MoS₂ vs WS₂” *in preparation*.

E.X.Y. and R.B. collected the data. E.X.Y. analyzed the data and made the figures. The manuscript was prepared by E.X.Y. with input from co-authors.

Reproduced in part with permission from

E. X. Yan, M. Cabán-Acevedo, K. M. Papadantonakis, B. S. Brunschwig, N. S. Lewis, “Reductant-Activated, High-Coverage, Covalent Functionalization of 1T'-MoS₂” *ACS Materials Lett.*, 2, 2, 2020.

doi: 10.1021/acsmaterialslett.9b00241

E.X.Y. collected and analyzed the data and made the figures. M.C. conceived of the project idea. The manuscript was prepared by E.X.Y. with input from co-authors.

Copyright 2020 American Chemical Society.

Table of Contents

Acknowledgements	iii
Abstract	v
Published Content and Contributions	vi
Table of Contents	vii
List of Figures	x
List of Tables	xvii
Chapter 1: Introduction to Molybdenum Disulfide	1
1.1 Properties and Phases of Molybdenum Disulfide	1
1.2 Areas of Research.....	2
1.3 MoS ₂ Functionalization Methods	3
1.4 Scope of This Thesis	5
Chapter 2: Reductant-Activated Functionalization of MoS₂	6
2.1 Introduction	6
2.2 Experimental Design.....	8
2.3 Results and Discussion.....	9
2.3.1 Characteristics of XPS, ATR-FTIR, NMR, and Raman spectra	9
2.3.2 Coverage as a function of reductant potential.....	13
2.3.3 Reactivity of <i>ce</i> MoS ₂ as a function of the halide leaving group	18
2.3.4 S _N 2 vs S _N 1 mechanism: reactivity of <i>ce</i> MoS ₂ with primary, secondary, and tertiary alkyl iodides.....	19
2.3.5 Electrochemical reduction-activated functionalization of <i>ce</i> MoS ₂	20
2.3.6 Reductant-activated functionalization of 2H-MoS ₂	21
2.4 Conclusion.....	23
Chapter 3: Density Functional Theory Modeling of 1T'-MoS₂ Methylation	24
3.1 Introduction	24
3.2 Computational Design.....	25
3.3 Results and Discussion.....	27
3.3.1 Potential dependence of 1T'-MoS ₂ on the number of electrons	27
3.3.2 Thermodynamic and kinetic differences during methylation of the two types of sulfur on 1T'-MoS ₂	29
3.3.3 Thermodynamics of progressive methyl functionalization of 1T'-MoS ₂ as a function of applied potential.....	34
3.3.4 Effects of neighboring methyl groups on the rotational barrier	41
3.3.5 Models of expected coverage under various constraints	45
3.4 Conclusion.....	51
Chapter 4: Comparison of Reductant-Activated Functionalization on WS₂ vs MoS₂ 53	
4.1 Introduction	53

4.2	Experimental Design	54
4.3	Results and Discussion.....	54
4.3.1	Methyl coverage of WS ₂ vs MoS ₂ using reductant-activated functionalization and influence of reaction time and temperature on coverage	54
4.3.2	Zeta potentials and particle sizes of <i>ce</i> WS ₂ , <i>ce</i> MoS ₂ , fct-WS ₂ , and fct-MoS ₂ ..	59
4.3.3	Comparison of the thermodynamics and kinetics of WS ₂ and MoS ₂ methyl functionalization using density functional theory modeling	62
4.4	Conclusion.....	65
Chapter 5: Conclusion and Outlook		67
Appendix A: Experimental and DFT Computational Methods		70
A.1	Materials	70
A.2	Synthesis of Chemically Exfoliated MoS ₂ (<i>ce</i> MoS ₂) and WS ₂ (<i>ce</i> WS ₂)	70
A.3	Reductant-Activated Functionalization of <i>ce</i> MoS ₂ and <i>ce</i> WS ₂	71
A.4	Preparation of <i>ce</i> MoS ₂ Electrodes and Open-Circuit Voltage Measurement	71
A.5	Sample Characterization	72
A.6	Density Functional Theory Methods	74
Appendix B: Details of X-ray Photoelectron Spectroscopy (XPS) Analysis		76
B.1	Analysis and Quantification of Coverage from XPS Data	76
B.1.1	Lineshapes.....	76
B.1.2	Constraints.....	76
Appendix C: Calculations and Conversions.....		79
C.1	Quantification of Coverage from ¹³ C MAS NMR Data	79
C.2	Work Functions of <i>ce</i> MoS ₂ and <i>ce</i> WS ₂	79
C.3	Effective Reduction Potential for One-Electron Reductants	79
C.4	Vibrational Frequencies of Methanethiol and Propanethiol	80
C.5	DFT Modeling of Grand Canonical Potential Free Energy	81
C.6	Calculations Using the Boltzmann Distribution and Eyring Equation.....	83
Appendix D: Modeling Coverage Code		85
D.1	Python Code for Modeling Coverage Distributions.....	85
D.1.1	Coverage distribution model for low-S with no neighbors (“0-neighbor max”).....	85
D.1.2	Coverage distribution model allowing a maximum of two functional groups in a row on low-S (“global 1-neighbor max”)	88
D.1.3	Coverage distribution model with at most one adjacent functional group to functionalization site at each step (“local 1-neighbor max”).....	90
D.1.4	Coverage distribution model allowing a maximum of three functional groups in a row on low-S (“global 3-in-a-row max”)	93
Appendix E: Geometries and Images of DFT Optimized Structures		96
E.1	1T'-MoS ₂ and Functionalized Structures.....	96
E.1.1	1T'-MoS ₂	96
E.1.2	(MoS ₂) ₁₆ CH ₃	97
E.1.3	(MoS ₂) ₁₆ (CH ₃) ₂	99
E.1.4	(MoS ₂) ₁₆ (CH ₃) ₃	100

E.1.5	(MoS ₂) ₁₆ (CH ₃) ₄	102
E.1.6	(MoS ₂) ₁₆ (CH ₃) ₅	105
E.1.7	(MoS ₂) ₁₆ (CH ₃) ₆	109
E.1.8	(MoS ₂) ₁₆ (CH ₃) ₇	112
E.2	1T'-MoS ₂ Initial, Transition and Final States of Reactions	114
E.2.1	(MoS ₂) ₁₆ + ClCH ₃ reactions on S7 and S10.....	114
E.2.2	(MoS ₂) ₁₆ (CH ₃) + ClCH ₃ reaction on S14.....	123
E.2.3	(MoS ₂) ₁₆ (CH ₃) ₂ + ClCH ₃ reaction on S5	127
E.2.4	(MoS ₂) ₁₆ (CH ₃) ₃ + ClCH ₃ reactions	130
E.2.5	(MoS ₂) ₁₆ (CH ₃) ₄ + ClCH ₃ reactions	137
E.2.6	(MoS ₂) ₁₆ (CH ₃) ₅ + ClCH ₃ reactions	149
E.3	1T'-WS ₂ Initial, Transition and Final States of Reactions	158
E.3.1	1T'-WS ₂	158
E.3.2	(WS ₂) ₁₆ + ClCH ₃ reaction on S7	159
Bibliography		164

List of Figures

- Figure 1.1. Top-down and side views along the *c*-axis and *b*-axis of 1H-, 1T-, and 1T'-MoS₂. Unit cells are outlined; actual cell parameter in the *c*-direction is larger than shown. The 1H structure is a single layer of the 2H phase..... 2
- Figure 1.2. MoS₂ functionalization methods that have been developed within the last decade, separated according to the phase of the functionalized MoS₂. 2H-MoS₂ has been functionalized using weakly bound species such as thiol and metal coordination on the edges and basal plane respectively, and with covalently bound species via thiol reaction with defects, defect-induced radical reactions, and reacting basal plane sulfurs with maleimides in thiol-ene reactions. 1T'-MoS₂ has been functionalized with electrophiles that are unreactive when combined with 2H-MoS₂ by chemically exfoliating 2H-MoS₂ to increase the sulfur nucleophilicity..... 4
- Figure 2.1. Reaction scheme for the covalent functionalization of MoS₂ and WS₂ via intercalation and exfoliation to form chemically exfoliated MS₂ (M = Mo, W), to which an electrophile can be added to functionalize the surface. Reductant-activated functionalization could be employed by adding a one-electron metallocene along with the electrophile. 7
- Figure 2.2. Energy diagram showing the relative energy positions of the *ce*MoS₂ Fermi level (eV vs vacuum) of relative to the formal potentials of five one-electron metallocene redox couples (V vs $E(\text{Fc}^{+/0})$). The *ce*MoS₂ Fermi level is based on the UPS measurement of the work function as shown in Figure 2.7 and the formal potentials are based on reported values⁸⁹ converted to $E^{0'}$ vs $E(\text{Fc}^{+/0})$ using the relationship $E(\text{Fc}^{+/0}) = 0.15 \text{ V vs SCE from } E(\text{Fc}^{+/0}) = 0.4 \text{ V vs SHE and } E(\text{SCE}) = 0.25 \text{ V vs SHE}$. The right box shows the molecules that were used to functionalize *ce*MoS₂... 9
- Figure 2.3. High-resolution XPS S2*p* for MoS₂, from top to bottom: *ce*MoS₂, after reacting with methyl iodide, 1-iodopropane, and 1-bromopropane, and MoS₂ after attempted reaction with 1-chloropropane. A third set of sulfur peaks was present in the XPS data for functionalized MoS₂ (orange peaks). 10
- Figure 2.4. (a) High-resolution XPS of Mo3*d* region for *ce*MoS₂ and methyl-MoS₂. No substantial differences were observed between the two spectra. (b) High-resolution XPS of the C1*s* region for functionalized methyl-MoS₂ and functionalized acetamide MoS₂. Carbon from the carbonyl group is visible in the latter case but not in the former due to overlap with the adventitious carbon peak. The latter result is consistent with previously reported XPS spectra for acetamide-MoS₂.¹⁹ (c) High-resolution XPS data for the halide regions (I3*d*, Br3*d*, or Cl2*p*) of the MoS₂ after the corresponding reaction. 11
- Figure 2.5. (a) ATR-FTIR and (b) ¹³C NMR spectra for, from top to bottom: *ce*MoS₂ (blue, NMR only), methyl-MoS₂ from methyl iodide (red), propyl-MoS₂ from 1-iodopropane (green), propyl-MoS₂ from 1-bromopropane (orange), and MoS₂ after attempted reaction with 1-chloropropane (purple, bottom). Characteristic C–H vibrations and carbon peaks appeared in the ATR-FTIR and NMR spectra,

- respectively, for functionalized MoS₂. Figure 2.5 reprinted with permission from the copyright holder, American Chemical Society. 11
- Figure 2.6. (a) Methyl coverage and the fraction of MoS₂ in the 1T' phase based on the S2*p* XPS peaks for methyl-MoS₂ synthesized using methyl iodide, as a function of the reductant used. Coverage data are the same as in Figure 2.8. The fraction of sulfur in the 1T' phase is consistently ~90% in all cases, suggesting that the variation in methyl coverage is not primarily due to the fraction of 1T' phase. Each experiment is plotted as a single point to show spread. (b) Emission spectra showing photoluminescence region of powder 2H-MoS₂ starting material, chemically exfoliated MoS₂, and functionalized MoS₂ for methyl-MoS₂ synthesized without reductant, with nickelocene, and with cobaltocene. Excitation was from a 532 nm diode pumped solid-state laser. Weak to no photoluminescence was observed before and after functionalization in the region where photoluminescence from mono/few-layer MoS₂ has typically been observed, likely due to the defect-rich nature of the powdered 2H-MoS₂ starting material..... 12
- Figure 2.7. Ultraviolet photoelectron spectra (UPS) for chemically exfoliated MoS₂, methyl-MoS₂, and propyl-MoS₂ synthesized using methyl iodide and 1-iodopropane, respectively. (a) The high binding energy cut-off used to obtain the work function for these powders. Displayed work function and error range is the average of three samples and the standard deviation. (b) Valence-band regime for the same samples, showing a ≤ 0.3 eV band gap, consistent with theoretical calculations.^{14, 16} Samples were not heated to remove adventitious carbon before obtaining spectra..... 14
- Figure 2.8. (a) Coverage per MoS₂ for MoS₂ functionalized with methyl iodide, 1-iodopropane, 1-bromopropane, and 1-chloropropane as a function of the effective potential for the no-reductant case (open-circuit voltage -0.07 V vs $E^0(\text{Fc}^{+/0})$, see Appendix A.4) and for the reductants ferrocene, nickelocene, octamethylnickelocene, cobaltocene, and decamethylcobaltocene, corresponding to -0.1 , -0.5 , -1.1 , -1.3 , and -1.9 V vs $E^0(\text{Fc}^{+/0})$. Coverages were quantified using the peak areas from high-resolution XPS S2*p* spectra, as the fraction of the total S2*p* peaks that corresponds to covalently functionalized sulfur. (b) Standard deviations in percentage (%std) of the functionalized S2*p* peak areas fitted during Monte Carlo simulations ($n = 400$) for a portion of the data presented in (a). Error bars are the standard deviations for the %std. Note that the mean for the %std are below 2% except for conditions involving 1-chloropropane and minimal functionalization, where a larger % error is expected. (c) High-resolution XPS of S2*p* for *ce*MoS₂ with two types of peak fitting: (top) three sets of S2*p* double peaks: one for 1T'-MoS₂, one for 2H-MoS₂, and one for sulfur defects (S*). This peak fitting was used to determine the percentage of sulfur in the 2H phase in *ce*MoS₂. The percentage of 2H-MoS₂ for all functionalized samples was constrained based on this fitting; (bottom) four sets of S2*p* peaks, the fourth (simulating S-C) constrained to have the same binding energy relative to the 1T'-MoS₂ as the functionalized S-C peak observed in *fct*-MoS₂ samples. This peak fitting was used to determine the error associated with peak fitting when using peak areas for coverage quantification. (d) ¹³C MAS NMR of ¹³C-methyl-MoS₂ functionalized under three conditions: without reductant, with

- nickelocene, and with cobaltocene. This technique is semi-quantitative and shows the trend of increasing coverage. Error bars indicate $\pm 10\%$ based on 5% error of external standard and an estimate of 5% error from peak fitting. 15
- Figure 2.9. (a) High-resolution XPS of $S2p$ region, (b) ATR-FTIR, and (c) ^{13}C CPMAS NMR data for the functionalization of $ce\text{MoS}_2$ with chloropropane in the presence of either octamethylnickelocene ($\text{Me}_8\text{Cp}_2\text{Ni}$) or cobaltocene (Cp_2Co). 17
- Figure 2.10. High-resolution XPS $S2p$ region for (a) $ce\text{MoS}_2$ functionalized with methyl iodide following the standard functionalization procedure detailed in Appendix A, (b) $ce\text{MoS}_2$ functionalized with methyl iodide after stirring for 3 days under ambient condition, and (c) $ce\text{MoS}_2$ stirred for 3 days with ferrocenium tetrafluoroborate ($[\text{Fe}(\text{C}_5\text{H}_5)_2]\text{BF}_4$) then functionalized with methyl iodide. No substantial differences were observed between the first and second conditions. Spectra of samples functionalized after oxidation of $ce\text{MoS}_2$ with ferrocenium (c) exhibited $S2p$ regions with a decreased fraction of functionalization and increased fraction of 2H-MoS_2 relative to spectra (a) or (b). 18
- Figure 2.11. High-resolution XPS $S2p$ spectra and (b) ^{13}C CPMAS NMR spectra of the products from reactions between $ce\text{MoS}_2$ and 1-iodopropane (top), 2-iodopropane (middle), and 2-iodo-2-methylpropane (bottom). Functionalization was minimal using 2-iodopropane and was unsuccessful using 2-iodo-2-methylpropane. 19
- Figure 2.12. Fraction of functionalized sulfur based on high-resolution XPS $S2p$ spectra of electrochemically functionalized $ce\text{MoS}_2$ drop cast on graphite electrodes. Five electrodes were used to test the five potentials shown, with each spot representing a single XPS measurement and three spots measured per sample. 20
- Figure 2.13. High-resolution XPS $\text{F}1s$ and $S2p$ spectra for four reactions using reductant-activated functionalization with nickelocene (Cp_2Ni), octamethylnickelocene ($\text{Me}_8\text{Cp}_2\text{Ni}$), and cobaltocene (Cp_2Co): (a) $ce\text{MoS}_2$ reacted with 4-fluorobenzyl bromide, (b) 2H-MoS_2 reacted with 4-fluorobenzyl bromide, (c) 2H-MoS_2 reacted with 1-bromo-4-fluorobutane, and (d) 2H-MoS_2 reacted with 2-iodo-1,1,1-trifluoroethane. The coverage per MoS_2 is shown to the left of the peak used to determine those values, with 0% indicating that no peak was fitted. Area in (d) assumes a 3:1 fluorine to sulfur ratio. 22
- Figure 3.1. Reaction scheme for the $1\text{T}'\text{-MoS}_2$ methylation reaction that will be discussed in this chapter, viewed along the b -axis (top) and c -axis (bottom) of the rectangular cell. Shown here is the first methylation reaction with $\text{S}7$ (see Figure 3.4 for numbering), with subsequent methylations differing only in the number of methyls on the MoS_2 surface in the initial and final states. The left side shows the initial state, with ClCH_3 suspended over the sulfur to be functionalized, and the right side shows the final state after the $\text{S}_{\text{N}}2$ reaction is finished. Both structures are the optimized geometry results using the methods described in Appendix A. 26
- Figure 3.2. From left to right, the starting $1\text{T}'\text{-MoS}_2$ structure obtained from literature, the transformation of the starting structure to a rectangular cell with 10 \AA of additional vacuum space (middle), and the expansion of the unit cell into a 16 MoS_2 supercell to allow more space to study methyl functionalization on the periodic surface. 28

- Figure 3.3. The effects of adding electrons to 1T'-MoS₂ containing 16 MoS₂ units on the (a) potential, in V vs SHE, and (b) free energy corrected by the free energy of electrons. The free energy in (a) appears to have a linear relationship with respect to the number of electrons due to the free energy contribution of additional electrons. The quadratic shape of the free energy with respect to the number of electrons is easily apparent when corrected linearly by the free energy contribution electrons (see Appendix C.5). Potential and free energy values were obtained using jDFTx after geometry optimization using VASP (see Appendix A.6 for methods)..... 28
- Figure 3.4. Top-down and side view of the rectangular unit cell of the minimized 1T'-MoS₂ supercell, color-coded to show the two types of sulfur in the unit cell: low-S and high-S, with low-S having a longer average Mo-S distance and high-S having a shorter average Mo-S distance and protruding further out-of-plane compared to the low-S. 29
- Figure 3.5. Free energy of (MoS₂)₁₆(CH₃) with methyl on either S6, S7, S10, or S11, the former two being low-S and the latter two being high-S. Geometry optimizations and free energy calculations were performed on solvated structures that were negatively charged with 2 electrons, resulting in structures with potentials -0.15, -0.16, -0.11, and -0.11 V vs SHE, respectively. 30
- Figure 3.6. (a) Thermodynamic favorability, ΔG , and (b) kinetic barrier, ΔG^\ddagger , of methylation on S7 and S10 of 1T'-MoS₂ as a function of potential based on interpolations of the initial, transition, and final state free energies (see Appendix C.5). (c) Side-view of the initial state, transition state, and final states for S7 and S10 methylation with negative charge of 2. 31
- Figure 3.7. The correlation between the barrier height and the free energy of reaction for S7 and S10 methylation, plotted using the same points as shown in Figure 3.6. The reaction potential varies along each curve and can be determined using Figure 3.6. 32
- Figure 3.8. Transition state S-C bond distance as a function of potential in V vs SHE. Each point is based on a single nudged elastic band calculation. As the potential becomes more negative, the S-C bond length increases, indicating that the transition state resembles the initial state more than the final state, consistent with the data in Figure 3.6 indicating a more exothermic reaction as the potential decreases. 33
- Figure 3.9. Top row: 1T-MoS₂ before and after geometry optimization. Bottom row: methylated 1T-MoS₂ before and after geometry optimization. Methylated 1T-MoS₂ resulted in a distorted structure. 34
- Figure 3.10. (a) Free energies of 2-methyl functionalization patterns that include one methyl on S7, minimized with a negative charge of 2. (b) MoS₂ surface prior to the addition of the 2nd methyl. 35
- Figure 3.11. (a) Free energies of 3-methyl functionalization patterns that include methyls on S7 and S14, minimized with a negative charge of 2, (b) the MoS₂ surface prior to the addition of the 3rd methyl. (c) Free energies of 4-methyl functionalization patterns that include methyls on S5, S7, and S14, minimized with a negative charge of 2, (d) MoS₂ surface prior to the addition of the 4th methyl. 35

- Figure 3.12. (a) Free energies of 5-methyl functionalization patterns that include methyls on S5, S7, S14, and S16, minimized with a negative charge of 4.2, (b) the MoS₂ surface prior to the addition of the 5th methyl. (c) Free energies of 6-methyl functionalization patterns that include methyls on S5, S7, S13, S14, and S16, minimized with a negative charge of 4.2, (d) MoS₂ surface prior to the addition of the 6th methyl. 36
- Figure 3.13. The ΔG of the methylation reaction vs potential for the 5th and 6th methylations, indicated in the notation with numbers corresponding to methylated sulfurs, brackets around the most recent methyl position, a prefix indicating the number of neighbors for the bracketed position, and “h” to indicate high-S positions. 37
- Figure 3.14. The free energy of the methylation reaction, ΔG , vs potential for the 4th and 5th methylations, comparing the effect of neighboring groups on the ΔG value. For the 4th methylation reaction (blue solid and dashed lines), 0N-5-7-14-(16) and 1N-5-7-(13)-14 functionalizes a sulfur adjacent to 0 and 1 methyl group respectively. For the 5th methylation reaction (orange solid and dashed lines), 1N-5-7-13-14-(16) and 2N-5-7-(13)-14-16 functionalizes sulfurs adjacent to 1 and 2 methyl groups, respectively. The 5-methyl reactions result in the same pattern of methyls on the surface. 38
- Figure 3.15. (a) Free energies of 7-methyl functionalization patterns that include methyls on S5, S7, S13, S14, S15, and S16, minimized with a negative charge of 1, (b) MoS₂ surface prior to the addition of the 7th methyl. 38
- Figure 3.16. Potential in V vs SHE of the final state products (MoS₂)₁₆(CH₃)_x + Cl, with a fixed negative charge of 2 in the unit cell, depending on the number of methyls added to the surface ($x = 1, 2, 3, 4, 5$ or 6). The potential of the final products becomes more negative as the number of methyls increases due to additional electrons in the system. 39
- Figure 3.17. The free energy of the methylation reaction, ΔG , vs potential for all methylation reactions, where XN stands for X neighbors for the methyl being added, the numbers representing the sulfur positions that are methylated, and brackets surround the position undergoing the methylation reaction. Potentials corresponding to experimental conditions in Chapter 2 are marked with vertical lines..... 40
- Figure 3.18. Examples of methyl patterns and the corresponding notation to indicate the pattern and the rotating methyl. (a) Example where the rotating methyl has one neighbor, (b) an example where the rotation methyl has 0 neighbors, (c) and (d) are examples where the rotating methyl has 2 neighbors. Note that positions 13 and 16 are adjacent due to the periodic repeat of the unit cell..... 42
- Figure 3.19. The rotational barrier for clockwise methyl rotation by 120 ° of various methyl patterns as a function of (a) the number of neighbors adjacent to the rotating methyl, and (b) the number of methyl groups on the MoS₂ surface per unit cell. The unique pattern and methyl rotation is specified in the legend notation as XN-A*[-B] where X is the number of neighbors next to the rotating methyl, A, B, etc. are the positions with methyls, and the asterisk (*) indicates the rotating methyl..... 43
- Figure 3.20. Histograms of the coverage distributions from simulations of the random functionalization of a 100×100 grid ($N = 2000$, 30 bins) of four models and the resulting average and standard deviations. Half of the sites represent low-S and half represent high-S; high-S are not functionalized in any of these models: (a) the “0-

neighbor max” model that only allows functionalization on sites surrounded by empty sites, (b) the “global 1-neighbor max” model that allows functionalization if the result is no more than 1 neighbor adjacent to any group on the surface, (c) the “local 1-neighbor max” model that allows functionalization if the site being functionalized has at most 1 neighbor at the time of addition, and (d) the “global 3-in-a-row max” model that allows functionalization if the resulting layout has no more than 3 functional groups in a row. 47

Figure 3.21. Top-down views of the final product for 3 reactions: 1N-5-7-(13)-14 (left), 1N-5-7-13-14-(16) (middle), and 2N-5-7-(13)-14-16 (right). The latter two reactions result in the same pattern of methylation on S5, S7, S13, S14, and S16. For 1N-5-7-13-14-(16) (middle), the most recent methyl added is on S16, whereas for 2N-5-7-(13)-14-16 (right), the most recent methyl added is on S13. 49

Figure 4.1. X-ray photoelectron spectra (XPS) of W4*f* and S2*p* regions for *ceWS*₂ and methyl-*WS*₂ synthesized with iodomethane and no reductant. Black dots are the raw data points and lines fit the peaks according to different species. For pure W-containing compounds, W5*p*_{3/2} separates well from W4*f*. However, for samples in which W has several chemical states, the W5*p*_{3/2} signal from lower chemical states overlaps with W4*f*_{5/2} peak from higher chemical states,¹⁰⁰ which we also observe here. 55

Figure 4.2. Ultraviolet photoelectron spectra (UPS) of chemically exfoliated MoS₂ and WS₂ samples prepared and transferred under inert atmosphere. (a) The high binding energy cutoff and linear fits used to obtain the work function of drop cast nanosheets. (b) Valence-band regime for the same samples, showing a band gap near zero, consistent with reported calculations.^{14, 16} 56

Figure 4.3. (a) Methyl coverage on *ceMoS*₂ and *ceWS*₂ after reacting with methyl iodide in the presence of various one-electron metallocene reductants as a function of the effective solution potential. The effective solution potentials were determined by correcting the formal potential with a 50:1 reductant-to-oxidant ratio for ferrocene, nickelocene, octamethylnickelocene, cobaltocene, and decamethylcobaltocene in order of reductant strength. Coverage increases as reductant strength increases for both materials, and decreases beyond cobaltocene, while *ceWS*₂ consistently achieves lower coverage compared to *ceMoS*₂. Lines are linear fits using least squares linear regression of points excluding those for decamethylcobaltocene. (b) Methyl coverage per MS₂ (M = Mo, W) after reacting with iodomethane either with no reductant added or in the presence of ferrocene, as determined by fitting XPS spectra. Individual points represent a single experiment and hollow symbols indicate the average with standard deviation as error bars. No substantial differences can be observed between these two conditions for either *ceMoS*₂ or *ceWS*₂. 57

Figure 4.4. (a) Methyl coverage on *ceWS*₂ after reacting with methyl iodide in the presence of no reductant or with octamethylnickelocene as a function of reaction time. In both graphs, results from each reaction are shown as individual points to convey the distribution of values. Opacity is set of 60% to allow visualization of overlapping points. (b) Methyl coverage on *ceWS*₂ after reacting with methyl iodide in the presence of various reductants (none, octamethylnickelocene, cobaltocene, and

- decamethylcobaltocene) as a function of reaction temperature. No substantial differences were observed between room temperature and 50 °C, while coverage stayed the same or decreased for reaction temperatures above 50 °C. 58
- Figure 4.5. Charge density plot of 1T'-MoS₂ and 1T'-WS₂ using density functional theory (DFT) calculations after optimizing the structures. Charge density was calculated for neutral 1T'-MoS₂ and 1T'-WS₂, and with a -1 charge for both cases, to simulate a net charge of 0.25 per MS₂ (M = Mo, W). The neutral charge density plot was subtracted from the -1 charge density plot for both cases to obtain the charge density difference whose isosurface is shown above. Both structures show similar distribution of the excess negative charge. 59
- Figure 4.6. (a) Particle sizes of *ce*MoS₂, *ce*WS₂, *ce*MoS₂ + ICH₃, and *ce*WS₂ + ICH₃, as a function of time after sample preparation plotted on a log₁₀ *y*-axis. Linear fits are made using least squares linear regression. The accuracy of particle size measurements decreases for values above 1 μm. The increase in particle size after methyl functionalization indicate increased aggregation. (b) Mobility measurements using dynamic light scattering of suspensions of *ce*MoS₂, *ce*WS₂, *ce*MoS₂ + ICH₃, and *ce*WS₂ + ICH₃, as a function of time since sample preparation. For both plots, each point is an individual measurement, with each cluster containing 10 data points, and each point is set to 60% opacity to visualize the distribution of overlapping points. Values plotted here were used to obtain the zeta potentials plotted in Figure 4.7 using the Smoluchowski model. 60
- Figure 4.7. Zeta potential measurements for solutions of *ce*MoS₂, *ce*WS₂, *ce*MoS₂ + ICH₃, and *ce*WS₂ + ICH₃. Each point represents an individual measurement, with 60% opacity to show overlapping points. Left graph zooms in on the time frame from 5–25 minutes after sample preparation to show changes in zeta potential immediately after methyl iodide is added to *ce*MoS₂ and *ce*WS₂. Linear fits were made using least squares linear regression. 61
- Figure 4.8. Interpolation in 0.1 V intervals of (a) the free energy and (b) the barrier height, of adding ClCH₃ to S7 (Figure 3.1) on 1T'-MoS₂ and WS₂. The free energies and barrier heights are calculated by subtracting the initial state grand canonical potential from the final state grand canonical potential (for the free energy) or the transition state grand canonical potential (for the barrier height) at fixed potential for each reaction. 63

List of Tables

Table 2.1. The standard reduction potential for each redox couple, the effective reduction potential assuming 50:1 ratio of reductant to oxidant, and the potential on an absolute energy scale using $E(\text{Fc}^{+/0}) = 0.4 \text{ V vs } E_{\text{SHE}}$ (standard hydrogen electrode) and $E_{\text{SHE}} = 4.44 \text{ V vs } E_{\text{Vac}}$	16
Table 3.1. Coverage per MoS_2 obtained experimentally using reductant-activated functionalization and theoretically using simulations, expressed as an average and standard deviation. The theoretical results were obtained using simulations based on different assumptions on the allowed number of neighbors on a local vs global scale. Experimental results are based on data shown in Figure 2.8.....	48
Table 4.1. Zeta potentials for solutions of $ce\text{MoS}_2$, $ce\text{WS}_2$, with and without methyl iodide, as a function of time after preparation. Averages and standard deviations are based on 10 measurements, each of which is plotted in Figure 4.7.....	62
Table C.5.1. List of all vibrational frequencies calculated using density functional theory (B3LYP with basis set 6-311G**) for methanethiol and propanethiol, assigned to experimental peaks from methyl- MoS_2 and propyl- MoS_2 (synthesized using methyl iodide and 1-iodopropane, respectively). A description is provided for characteristic (experimental) or high-intensity (theoretical) peaks. Calculated frequencies that contained substantial contribution from the S–H bond were not used to assign peaks due the absence of this bond in experimental samples.	80

Chapter 1: Introduction to Molybdenum Disulfide

1.1 Properties and Phases of Molybdenum Disulfide

Crystalline molybdenum disulfide (MoS_2) belongs to the class of group VI transition metal dichalcogenides (TMD) of the form MX_2 ($\text{M} = \text{Mo}, \text{W}; \text{X} = \text{S}, \text{Se}$).¹⁻³ MoS_2 consists of layers of two-dimensional (2D) sheets held together by van der Waals forces and can be found naturally in its thermodynamically stable phase as the mineral molybdenite.⁴ Given its 2D composition and weak interlayer van der Waals forces, MoS_2 , along with other anisotropic 2D materials, can be exfoliated chemically or mechanically to produce few- and mono-layer sheets of varying size depending on the synthesis technique.⁵⁻⁷ Reducing the thickness of the crystal to atomically thin (less than 10 nm) layers results in confinement effects that can drastically change the properties of 2D materials.⁸⁻¹⁰ In semiconducting MoS_2 , reducing the thickness from greater than 4 layers (bulk MoS_2) to a single layer results in an indirect to direct bandgap transition, as well as a widening of the bandgap from 1.2 to 1.9 eV.¹⁰⁻¹¹

MoS_2 has several common polymorphs: the 2H, 3R, and 1T phases, the last of which may refer to the perfectly octahedral phase but is also sometimes used to refer to several distorted octahedral phases, the most common being the 1T' and 1T'' phases.^{2, 9, 12-14} In the phase nomenclature, the integer represents the number of layers in the unit cell, and the letter represents the type of symmetry (H = hexagonal, R = rhombohedral, T = tetragonal). The 2H phase is the thermodynamically stable phase, the 3R can be produced under specific low-temperature synthetic conditions,¹⁵ and the 1T is a metastable phase that spontaneously distorts to the 1T'' and 1T' phases, with 1T' being the most stable of the three and possessing a >0.7 eV barrier to its transformation to the 1H phase.^{14, 16} Even so, the 1T' does eventually convert back to the 2H phase at room temperature in the absence of stabilizing factors such as surface functionalization.¹⁷⁻¹⁹ The 2H and 3R phases are semiconducting, the 1T phase is metallic, and the distorted 1T' phase is quasi-metallic with a small bandgap of 0.1 eV.^{16, 20-21} Figure 1.1 illustrates the 1H (a single layer of the 2H phase), 1T, and 1T' phases, with the latter being the primary phase of concern in this work.

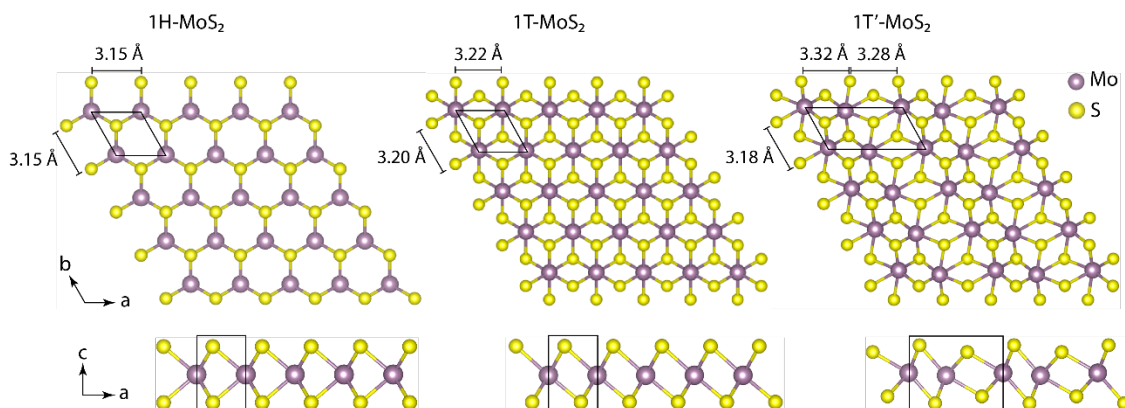


Figure 1.1. Top-down and side views along the c -axis and b -axis of 1H-, 1T-, and 1T'-MoS₂. Unit cells are outlined; actual cell parameter in the c -direction is larger than shown. The 1H structure is a single layer of the 2H phase.

1.2 Areas of Research

The majority of MoS₂ research applications studied have been of either 2H-, 1T-, or 1T'-MoS₂. The 2H phase is used for applications that require a bandgap, and the 1T/1T' for applications that benefit from greater conductivity and that do not require a bandgap. These two phases can be combined synergistically to make multiphase materials, such as by using phase conversion or cross-linking to make MoS₂ transistors from the 2H phase and metallic contacts from the 1T/1T' phase.²²⁻²³

2H-MoS₂ has been investigated for applications in optoelectronics,²⁴⁻²⁵ sensing,²⁶⁻³⁴ and for biological uses in photothermal imaging and drug delivery.³⁵⁻³⁸ For example, substrate-bound 2H-MoS₂ has been studied as a light absorber in flexible electronics and photovoltaics^{3,24} and as a sensing material for gas and piezoelectric sensors,²⁶⁻³⁴ while free-floating 2H-MoS₂ has been studied for targeted drug delivery that exploits the high surface area to volume ratio of MoS₂ nanosheets,^{36,38} for photothermal imaging as a near-infrared absorber,^{36,39-40} and for catalysis in hydrodesulfurization.⁴¹⁻⁴² In contrast, due to the metallic nature of 1T'-MoS₂, researchers have studied this phase for use in electrocatalysis as a hydrogen evolution catalyst,⁴³⁻⁴⁸ antibacterial coatings via generation of reactive oxygen species,⁴⁹⁻⁵⁰ in gas and electrochemical sensors,^{26,51} and for bioimaging.³⁹

Investigations into MoS₂ applications are still in their infancy, with renewed interest in 2D materials growing after 2011 since the unambiguous identification of single-layer graphene in 2004.⁵²⁻⁵³ Although MoS₂ found its application as a low friction solid lubricant since at least the 1940s, interest in studying the properties and applications of atomically thin MoS₂ recently increased 10-fold since 2011, along with interest in 2D materials in general as we look beyond graphene.⁵⁴ Thus, new methodologies for manipulating and modifying MoS₂ are continuing to emerge, and the current list of applications represents only a snapshot in time that will no doubt grow as researchers continue to explore the potentials of this material.

1.3 MoS₂ Functionalization Methods

Surface functionalization with small molecules is a common method of manipulating the material surface properties at a molecular level in order to imbue the material with desirable nano and macroscopic properties for a particular application.⁵⁵⁻⁶⁷ On MoS₂, the different phases are intimately linked to the design of the functionalization methodology, since the reactivity of surface atoms are determined in large part by the electronic structure which is in turn determined by the crystal structure.⁶⁸

The 2H phase, being the thermodynamically stable phase, is relatively air-stable and unreactive at the surface.⁶⁹ This is beneficial for transistor applications as it allows the construction of devices that can be exposed to varying atmospheres, including air, without inducing a drastic change in the device behavior, whereas air-sensitive transistor materials such as perovskites require an additional layer to protect against atmospheric oxygen and water.⁷⁰⁻⁷¹ However, the other side of the double-edged sword of a relatively unreactive surface is that changing the surface properties of the 2H phase via surface functionalization is nontrivial and requires exploiting regions or mechanisms with higher reactivity.⁷² For example, sulfur vacancies, which form during synthesis and are responsible for *n*-type behavior, are common throughout the surface of natural and synthetic 2H-MoS₂.⁷³⁻⁷⁴ The absence of an acceptor (the sulfur) increases the reactivity of neighboring sulfur atoms and enables these sulfurs near the vacancy to participate in radical reactions with diazonium radicals.⁷² Notably, functionalization of these initial sulfurs near vacancies also induces

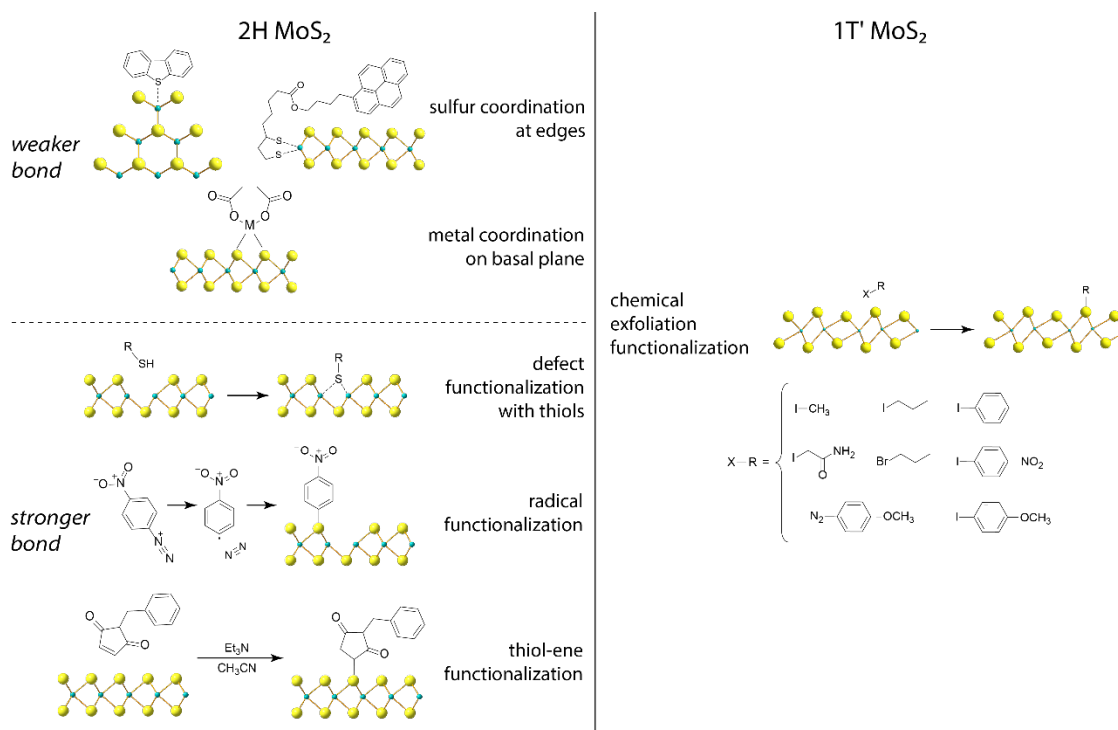


Figure 1.2. MoS₂ functionalization methods that have been developed within the last decade, separated according to the phase of the functionalized MoS₂. 2H-MoS₂ has been functionalized using weakly bound species such as thiol and metal coordination on the edges and basal plane respectively, and with covalently bound species via thiol reaction with defects, defect-induced radical reactions, and reacting basal plane sulfurs with maleimides in thiol-ene reactions. 1T'-MoS₂ has been functionalized with electrophiles that are unreactive when combined with 2H-MoS₂ by chemically exfoliating 2H-MoS₂ to increase the sulfur nucleophilicity.

higher reactivity in *its* neighboring sulfurs, and the propagation of reactivity continues until the surface is covered, limited only by steric hinderance. Other reactions that rely on the nucleophilic attack of sulfur such as with radical polymerization,⁷⁵ and thiol-ene reactions with maleimides,⁷⁶⁻⁷⁸ may propagate by a similar mechanism although their mechanism has not yet been modeled. In addition to the reactivity induced in neighboring sulfurs, sulfur vacancies can themselves act as electron acceptors and the exposed metal atom can be functionalized with a nucleophile such as a thiol.^{57, 79-81} By contrast, the 1T' phase is metastable and can be synthesized via chemical or electrochemical intercalation and exfoliation, whereby excess negative charge is stored in the MoS₂ during intercalation, and the addition of a protonated solvent like water exfoliates the material into nanosheet suspensions of chemically exfoliated MoS₂ (*ce*MoS₂).^{5, 7, 82} A consequence of the intercalation and excess negative charge is that the sulfur nucleophilicity increases and

*ce*MoS₂ readily reacts with good electrophiles that the 2H phase is unreactive towards.^{19, 83-85} The 1T' phase is stabilized by surface functionalization; in its absence, this phase converts to the 2H phase over a period of days to weeks.¹⁹ Figure 1.2 details the various methods that have been developed to functionalize 2H- and 1T'-MoS₂, including the above examples as well as examples of coordination functionalization either by sulfur coordination to exposed edge-site metals,⁸⁶⁻⁸⁷ or by metal coordination to the basal plane sulfurs.⁵⁵

1.4 Scope of This Thesis

This thesis works towards understanding and developing the intercalation and chemical exfoliation functionalization methodology for 1T'-MoS₂ as illustrated in the right side of Figure 2.1. In Chapter 2, we describe reductant-activated functionalization, a systematic method of controlling the functional group coverage on chemically exfoliated MoS₂ (*ce*MoS₂). We also explore the types of electrophiles that are compatible and react with *ce*MoS₂ by changing the leaving group and steric hinderance of the electrophile and share our preliminary results for electrochemical functionalization and for functionalizing 2H-MoS₂. In Chapter 3, we use density functional theory (DFT) modeling to explain the experimental coverage limits observed in the previous chapter and extend our insights from a DFT case study to explain the experimental upper and lower limits of functionalization by simulating random functionalization under various constraints. Chapter 4 extends the reductant-activated methodology to chemically exfoliated tungsten disulfide (*ce*WS₂), and we explore the differences between *ce*WS₂ and *ce*MoS₂ in their behavior and properties before and after functionalization, coupled with DFT calculations to support the observed experimental differences in coverage. Finally, we conclude in Chapter 5 by summarizing our findings and providing an outlook for future work and ways in which our reductant-activated functionalization method can be expanded and improved upon to develop a holistic understanding of redox-activated functionalization on TMDs and on analogous materials.

Chapter 2: Reductant-Activated Functionalization of MoS₂

2.1 Introduction

Chemically exfoliated MoS₂ (*ce*MoS₂) has been synthesized by intercalation and exfoliation in water as early as the 1980s,⁸⁸ with further characterization of the resulting 1T' phase and restacked structures performed in the 1990s.¹⁷ Several decades passed before *ce*MoS₂ was functionalized by small molecule electrophiles in 2015 in two separate instances, via mechanisms that occurred only on *ce*MoS₂ and not on the 2H-MoS₂ starting material.^{19, 84} These studies demonstrated how the phase of the material could be used to induce reactivity for a specific type of reaction, and how materials within the group VI TMDs (MoS₂, WS₂, MoSe₂, WSe₂) underwent similar reactions. Specifically, chemical intercalation and exfoliation that results in the 1T' phase imparts surface chalcogens with greater nucleophilicity compared to the starting 2H phase, such that the once unreactive 2H TMDs could react with diazonium salts and alkyl and aryl iodides in the 1T' phase.^{19, 83-84} The reported coverage reached a high of 29% per MoS₂, similar to the amount of excess charge determined previously for *ce*MoS₂ (25%), prompting the conclusion that the coverage appeared to be limited by amount of excess charge stored in the sheets.^{17, 19} Verifying this hypothesis and the potential for further functionalization by determining the limits of this method remained unexplored at that time.

Based on this hypothesis that the reaction is limited by the amount of negative charge in *ce*MoS₂ following intercalation and exfoliation, we hypothesized that the reaction should proceed further if the *ce*MoS₂ is given additional negative charge after the stored charge is depleted (i.e. after the stored charge has been transferred into S–C bonds), by using a form of “reductant-activated” functionalization. This approach is supported by evidence of the effectiveness of oxidant-activated functionalization that has been used to functionalize silicon surfaces and nanoparticles.⁸⁹⁻⁹⁰ For both silicon surfaces and nanoparticles, increasing the solution oxidation potential by increasing the oxidant strength increases the coverage of surface Si–O bonds when the oxidant strength is higher than some threshold. This threshold

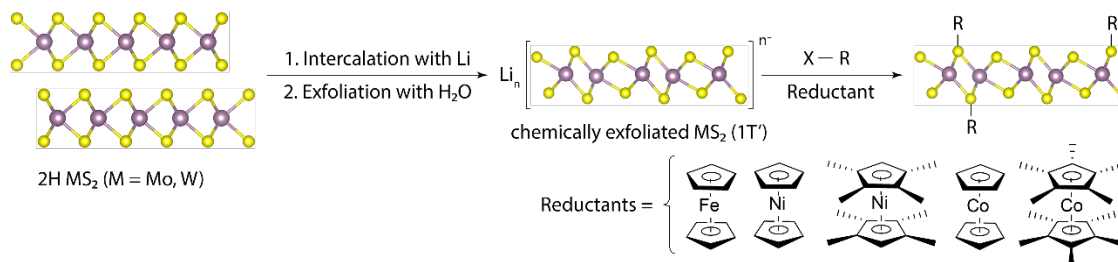


Figure 2.1. Reaction scheme for the covalent functionalization of MoS_2 and WS_2 via intercalation and exfoliation to form chemically exfoliated MS_2 ($\text{M} = \text{Mo, W}$), to which an electrophile can be added to functionalize the surface. Reductant-activated functionalization could be employed by adding a one-electron metallocene along with the electrophile.

varies between bulk and nanoparticle and even between nanoparticles of different sizes below 10 nm, because the reaction kinetics depends on participation of electrons from the valence band and its position varies with the size of the nanoparticle.⁹⁰ The key idea is that, to favor the formation of Si–O bonds, the valence band of silicon must be capable of being oxidized in order to generate a hole that can then be localized by the nucleophilic attack of a nucleophile such as an alcohol, carboxylic acid, amine, thiol, or phosphine. It follows that the oxidant strength must be enough to generate a solution potential that is positive of the valence band to allow electron flow from the valence band to the oxidant. In a similar but reverse fashion, this work uses reductants to activate *ceMoS₂* functionalization by transferring electrons from the reductant to *ceMoS₂* via the scheme shown in Figure 2.1, which occurs when the reductant potential is more negative than that of the *ceMoS₂* Fermi level (E_F) (Figure 2.2).

In addition to evaluating the utility of reductant-activated functionalization on *ceMoS₂*, we also sought to determine whether the nucleophilic addition mechanism is concerted ($\text{S}_{\text{N}}2$) or 2-step ($\text{S}_{\text{N}}1$), where the loss of the leaving group precedes nucleophilic attack in the latter case. For an $\text{S}_{\text{N}}2$ mechanism, the reaction kinetics should decrease with greater steric hinderance (primary > secondary > tertiary electrophiles), whereas for an $\text{S}_{\text{N}}1$ mechanism, the reaction proceeds when the cation intermediate can be stabilized (tertiary > secondary > primary). For either mechanism, the reaction kinetics should decrease with decreasing effectiveness of the leaving group; for halides this means $\text{I} > \text{Br} > \text{Cl}$ in reactivity. Given the existing evidence of functionalization with primary alkyl halides before we began this work,

we hypothesized that the S_N2 mechanism is highly likely, and the S_N1 mechanism may be a possibility for tertiary alkyl halides.

We explored the effects of reductant potential on the coverage of $ceMoS_2$ and the coverage limits that can be achieved under the optimized scenario, which we will discuss in the following sections. In addition, we verified that the S_N2 mechanism is indeed the predominant mechanism by functionalizing $ceMoS_2$ with primary, secondary, and tertiary alkyl iodides, the results of which suggest that the S_N1 mechanism does not occur for any of these molecules. Finally, we tested electrochemical functionalization of $ceMoS_2$ /graphite electrodes and applied this reductant-activated functionalization on 2H- MoS_2 .

2.2 Experimental Design

To evaluate the effects of reductant-activated functionalization at different reductant strengths while keeping the form of the reductant and the steric hinderance of the functional group consistent, we used one-electron metallocene reductants as the source of negative charge and the following small molecules to functionalize $ceMoS_2$: methyl iodide to test the maximum coverage limit, 1-iodopropane, 1-bromopropane, and 1-chloropropane to compare the leaving group effect, and 1-iodopropane, 2-iodopropane, and 2-iodo-2-methylpropane as the primary, secondary, and tertiary alkyl halides to verify the S_N2 over the S_N1 mechanism. The reductants were selected based on their solution potential relative to the Fermi level of $ceMoS_2$ as measured by ultraviolet photoelectron spectroscopy (UPS), with one reductant below the Fermi level (ferrocene), and four above (nickelocene, octamethylnickelocene, cobaltocene, decamethylcobaltocene). Figure 2.2 shows the relative reductant potentials vs the $ceMoS_2$ E_F , and the molecules used in this study. Detailed descriptions of the materials and synthetic methods can be found in Appendix A.

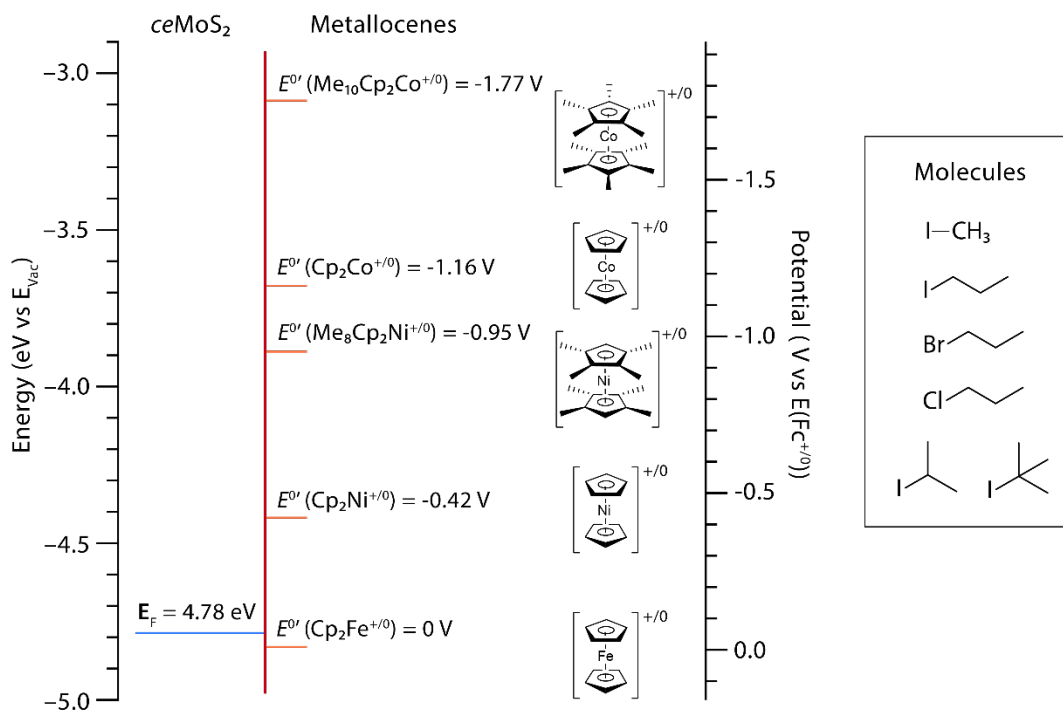


Figure 2.2. Energy diagram showing the relative energy positions of the $ceMoS_2$ Fermi level (eV vs vacuum) of relative to the formal potentials of five one-electron metallocene redox couples (V vs $E(Fc^{+/0})$). The $ceMoS_2$ Fermi level is based on the UPS measurement of the work function as shown in Figure 2.7 and the formal potentials are based on reported values⁸⁹ converted to $E^{0'}$ vs $E(Fc^{+/0})$ using the relationship $E(Fc^{+/0}) = 0.15$ V vs SCE from $E(Fc^{+/0}) = 0.4$ V vs SHE and $E(SCE) = 0.25$ V vs SHE. The right box shows the molecules that were used to functionalize $ceMoS_2$.

2.3 Results and Discussion

2.3.1 Characteristics of XPS, ATR-FTIR, NMR, and Raman spectra

The organic moieties of functionalized $ceMoS_2$ were characterized using attenuated total reflection Fourier-transform infrared spectroscopy (ATR-FTIR) and solid state ^{13}C cross-polarization magic-angle spinning nuclear magnetic resonance spectroscopy (^{13}C CPMAS NMR). The coverages were quantified by fitting the multiple peaks in the $S2p$ high-resolution spectra obtained from X-ray photoelectron spectroscopy (XPS), with the peaks at ~ 162.4 eV binding energy assigned to sulfur atoms bonded to carbon (S-C). No additional peaks were observed at higher binding energies relative to the 2H-MoS₂ sulfur peak at 163.2 eV, suggesting a lack of functionalization for the 2H phase consistent with previous studies showing that 2H-MoS₂ could not be functionalized with alkyl halides such as iodoacetamide.

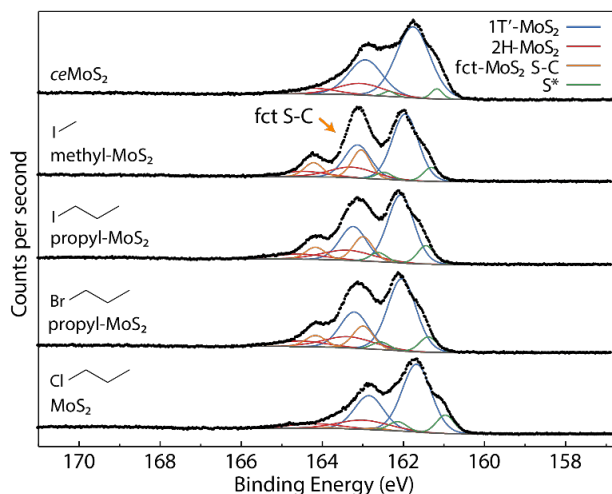


Figure 2.3. High-resolution XPS $S2p$ for MoS_2 , from top to bottom: $ce\text{MoS}_2$, after reacting with methyl iodide, 1-iodopropane, and 1-bromopropane, and MoS_2 after attempted reaction with 1-chloropropane. A third set of sulfur peaks was present in the XPS data for functionalized MoS_2 (orange peaks).

Figure 2.3 shows the $S2p$ XPS peak fitting for functionalized MoS_2 (fct- MoS_2) compared to that of unfunctionalized $ce\text{MoS}_2$. Detailed peak-fitting parameters are provided in Appendix B.

In addition to XPS peaks attributed to the functionalized sulfur, $1T'$, and $2H$ MoS_2 phases, a shoulder was observed at ~ 160.8 eV binding energy in $ce\text{MoS}_2$, in accord with the binding energy of Li_2S , which can form during lithiation.⁹¹ This

peak may also be due to the formation of inner-edge defects (S^*) from desulfurization during lithiation, as the generation of vacancies tends to shift the sulfur peak to lower binding energy.⁴⁷ This shoulder accounts for $\sim 3\%$ of the total sulfur in $ce\text{MoS}_2$. High-resolution spectra in the molybdenum and halide regions showed no evidence of changes to the molybdenum oxidation states and showed minimal residual halide, indicating removal of the reactant alkyl halide (Figure 2.4). Quantification of the surface coverage were calculated from the high-resolution $S2p$ region since the $\text{C}1s$ peaks were convoluted with peaks from adventitious carbon for methyl groups. As an aside, if functional groups containing carbons adjacent to electronegative atoms were used, such as carbonyl groups, these carbons would be far enough away from adventitious carbon to be observable in the $\text{C}1s$ spectrum. Such is the case for acetamide- MoS_2 as shown in Figure 2.4b.

Characteristic methyl and methylene peaks associated with methyl and propyl moieties were observed in the IR and NMR spectra (Figure 2.5). The characteristic IR vibrations for the C–S bond stretch, C–H bend, and C–H stretches were at 694 , $946/1289$, and 2906 cm^{-1} for methyl- MoS_2 , and were 727 , 1257 , and $2862/2924/2955$ cm^{-1} for propyl- MoS_2 . These peak

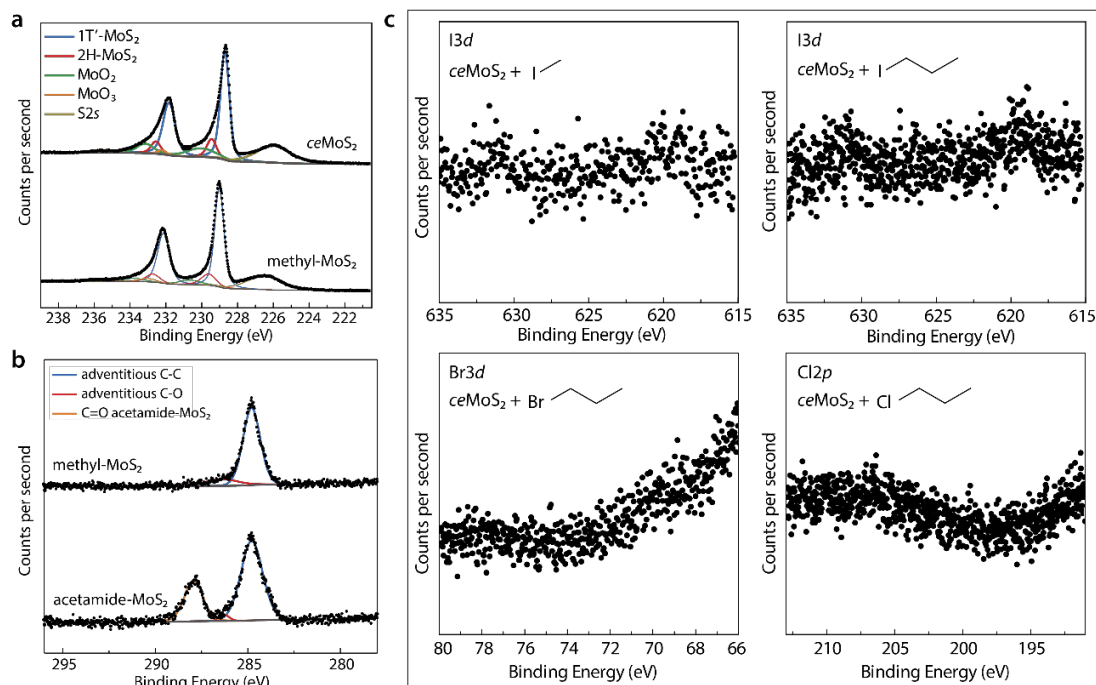


Figure 2.4. (a) High-resolution XPS of Mo3d region for *ce*MoS₂ and methyl-MoS₂. No substantial differences were observed between the two spectra. (b) High-resolution XPS of the C1s region for functionalized methyl-MoS₂ and functionalized acetamide MoS₂. Carbon from the carbonyl group is visible in the latter case but not in the former due to overlap with the adventitious carbon peak. The latter result is consistent with previously reported XPS spectra for acetamide-MoS₂.¹⁹ (c) High-resolution XPS data for the halide regions (I3d, Br3d, or Cl2p) of the MoS₂ after the corresponding reaction.

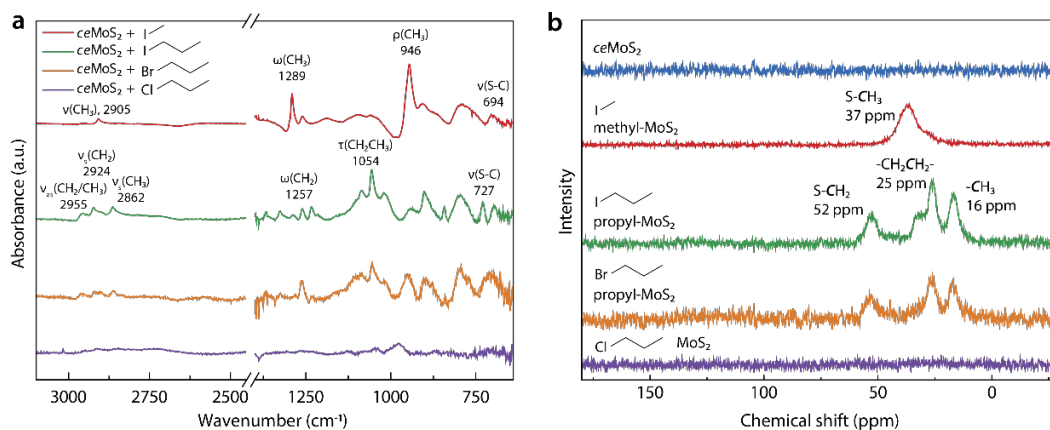


Figure 2.5. (a) ATR-FTIR and (b) ¹³C NMR spectra for, from top to bottom: *ce*MoS₂ (blue, NMR only), methyl-MoS₂ from methyl iodide (red), propyl-MoS₂ from 1-iodopropane (green), propyl-MoS₂ from 1-bromopropane (orange), and MoS₂ after attempted reaction with 1-chloropropane (purple, bottom). Characteristic C-H vibrations and carbon peaks appeared in the ATR-FTIR and NMR spectra, respectively, for functionalized MoS₂. Figure 2.5 reprinted with permission from the copyright holder, American Chemical Society.

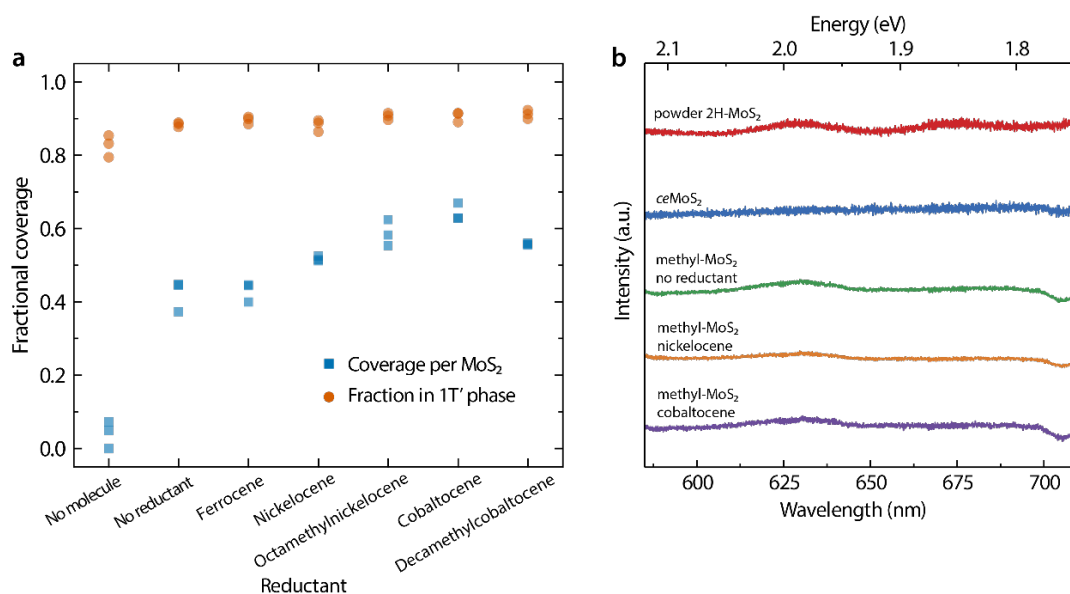


Figure 2.6. (a) Methyl coverage and the fraction of MoS₂ in the 1T' phase based on the S2p XPS peaks for methyl-MoS₂ synthesized using methyl iodide, as a function of the reductant used. Coverage data are the same as in Figure 2.8. The fraction of sulfur in the 1T' phase is consistently ~90% in all cases, suggesting that the variation in methyl coverage is not primarily due to the fraction of 1T' phase. Each experiment is plotted as a single point to show spread. (b) Emission spectra showing photoluminescence region of powder 2H-MoS₂ starting material, chemically exfoliated MoS₂, and functionalized MoS₂ for methyl-MoS₂ synthesized without reductant, with nickelocene, and with cobaltocene. Excitation was from a 532 nm diode pumped solid-state laser. Weak to no photoluminescence was observed before and after functionalization in the region where photoluminescence from mono/few-layer MoS₂ has typically been observed, likely due to the defect-rich nature of the powdered 2H-MoS₂ starting material.

assignments were made based on DFT calculations for optimized methanethiol and propanethiol (Appendix C, Table C.5.1) to simulate the S–C bond. Furthermore, the carbon peaks at 37 and 52 ppm in the NMR spectra of ¹³C-methyl-MoS₂ (synthesized from ¹³C-methyl iodide) and propyl-MoS₂, respectively, are expected for carbons covalently bound to a sulfur atom, as thiols and sulfinic acids deshield the α -carbon and cause a downfield shift in the carbon peak.⁹² The two other types of carbon for propyl-MoS₂ synthesized from 1-iodopropane or 1-bromopropane were also observed, at 16 and 25 ppm, respectively. Consistent with previous reports of *ce*MoS₂ covalent functionalization, the proportion of 1T' to 2H in the functionalized product remained the same after functionalization, and the Raman spectra for functionalized *ce*MoS₂ were similar to that of pure *ce*MoS₂ (Figure 2.6a). No notable photoluminescence (PL) was observed before or after functionalization in the 2H or 1T' phase at the typical PL energy range for MoS₂ mono- and few-layers (~600–650 nm or

1.9–2.1 eV)⁹³ because of the defect-rich nature of the powder 2H-MoS₂ starting material (Figure 2.6b).

2.3.2 Coverage as a function of reductant potential

The coverage for methyl-MoS₂ was 41% ± 4% (average ± standard deviation, $N=3$), slightly higher with previously published 30% coverage for the maximum coverage using methyl iodide and *ce*MoS₂.¹⁹ If the coverage obtained in the absence of reductant is limited by the charge density stored in the *ce*MoS₂, we would expect that the coverage would increase with negative charge injection. In addition, removing charge from *ce*MoS₂ prior to the reaction would reduce the surface methyl coverage. On the other hand, if this coverage reflected a sterically limited packing density, then negative charge injection should have minimal effect.

We sought to evaluate whether an appropriately chosen reducing agent could transfer negative charge to *ce*MoS₂ or functionalized *ce*MoS₂, thereby enabling further functionalization after consumption of the initially stored negative charge. The coverage produced by functionalization was thus determined as a function of the reducing strength of the metallocenes present during the functionalization reaction. Five metallocenes, ferrocene (Cp₂Fe), nickelocene (Cp₂Ni), octamethylnickelocene (Me₈Cp₂Ni), cobaltocene (Cp₂Co), and decamethylcobaltocene (Me₁₀Cp₂Co), provided reduction potentials that spanned a range from above to below the Fermi levels (E_F) of *ce*-, methyl-, and propyl-MoS₂, estimated using ultraviolet photoelectron spectroscopy (UPS) to determine the work function of 3 samples of each material drop cast onto p^+ -Si (Figure 2.7). The average work function of 4.78 eV obtained from these measurements is close to literature reports of the 1T MoS₂ work function of 4.7 eV that were determined using UPS as well.²³ This shift towards lower work function in methyl- and propyl-MoS₂ may be due to the contribution of the dipole, which has been a well-documented effect on silicon band edges,^{67, 94-95} but may also be due to the trapping of negative charges contributed by the reductants in the S–C bonds themselves, increasing the number of electrons in the bands as the coverage increases.

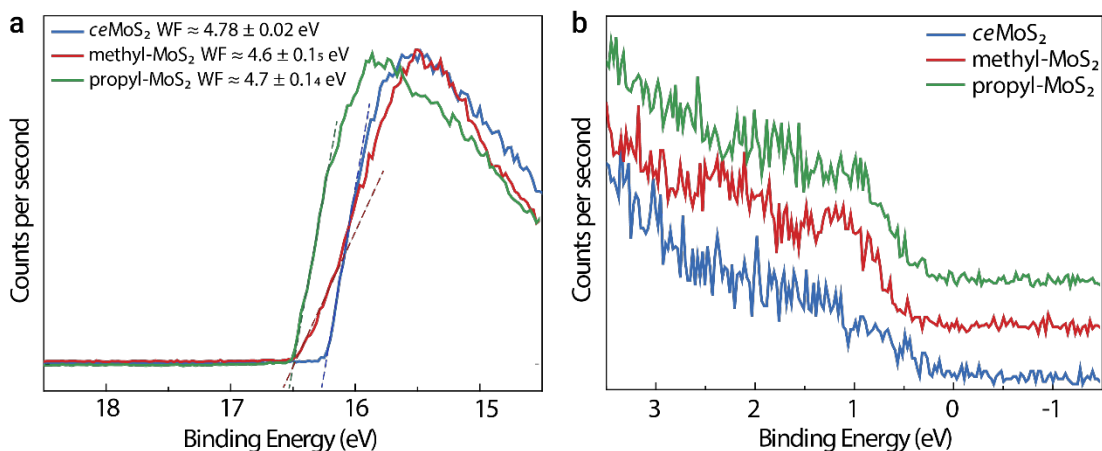


Figure 2.7. Ultraviolet photoelectron spectra (UPS) for chemically exfoliated MoS₂, methyl-MoS₂, and propyl-MoS₂ synthesized using methyl iodide and 1-iodopropane, respectively. (a) The high binding energy cut-off used to obtain the work function for these powders. Displayed work function and error range is the average of three samples and the standard deviation. (b) Valence-band regime for the same samples, showing a ≤ 0.3 eV band gap, consistent with theoretical calculations.^{14, 16} Samples were not heated to remove adventitious carbon before obtaining spectra.

Figure 2.8a describes the change in functional group coverage as a function of the effective solution potential as determined by the reductant, or in the no-reductant case, by the open-circuit voltage of a *ce*MoS₂ electrode (see Appendix A for measurement details). The effective reduction potentials, E_{eff} , of the metallocene solutions ranged from -0.1 to -1.9 V vs ferrocenium/ferrocene ($\text{Fc}^{+/0}$) and were estimated by assuming a reductant to oxidant concentration ratio of 50:1, as detailed in Table 2.1.⁹⁶ All reactions were performed in triplicate with error bars indicating the standard deviation. To assess the significance of the area under the fitted S–C curve in XPS spectra, unfunctionalized *ce*MoS₂ spectra, in which the S–C bond is absent, were fit with the additional sulfur peaks at the S–C binding energy (Figure 2.8c), resulting in a “coverage” of $4\% \pm 3\%$ ($N=3$). Thus, we interpret that S–C bond formation occurred only for XPS S2*p* peaks with coverage values above $\sim 10\%$ in the absence of additional data such as NMR. Figure 2.8b shows the standard deviations of the peak areas ($\sim 1\text{--}3\%$) obtained from Monte Carlo simulations for each sample, indicating that the trends in Figure 2.8a are well outside the range of error that can be attributed to errors in XPS peak fitting. In addition to quantification by XPS, ¹³C MAS NMR on *ce*MoS₂ functionalized with ¹³C-methyl iodide with and without nickelocene and cobaltocene, verified the trend of increasing coverage with reductant strength (Figure 2.8d).

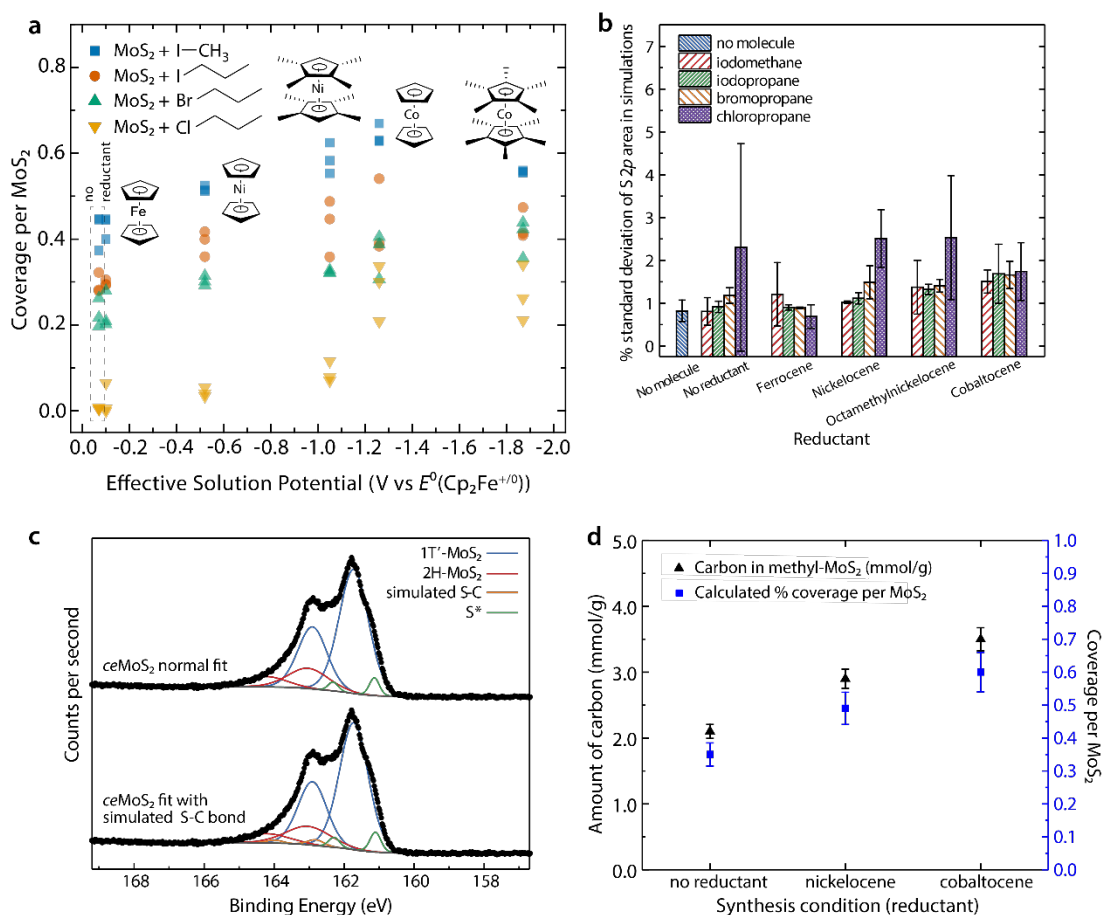


Figure 2.8. (a) Coverage per MoS₂ for MoS₂ functionalized with methyl iodide, 1-iodopropane, 1-bromopropane, and 1-chloropropane as a function of the effective potential for the no-reductant case (open-circuit voltage -0.07 V vs $E^0(\text{Fc}^{+/0})$, see Appendix A.4) and for the reductants ferrocene, nickelocene, octamethylnickelocene, cobaltocene, and dexamethylcobaltocene, corresponding to -0.1 , -0.5 , -1.1 , -1.3 , and -1.9 V vs $E^0(\text{Fc}^{+/0})$. Coverages were quantified using the peak areas from high-resolution XPS S_{2p} spectra, as the fraction of the total S_{2p} peaks that corresponds to covalently functionalized sulfur. (b) Standard deviations in percentage (%std) of the functionalized S_{2p} peak areas fitted during Monte Carlo simulations ($n = 400$) for a portion of the data presented in (a). Error bars are the standard deviations for the %std. Note that the mean for the %std are below 2% except for conditions involving 1-chloropropane and minimal functionalization, where a larger % error is expected. (c) High-resolution XPS of S_{2p} for *ce*MoS₂ with two types of peak fitting: (top) three sets of S_{2p} double peaks: one for 1T'-MoS₂, one for 2H-MoS₂, and one for sulfur defects (S*). This peak fitting was used to determine the percentage of sulfur in the 2H phase in *ce*MoS₂. The percentage of 2H-MoS₂ for all functionalized samples was constrained based on this fitting; (bottom) four sets of S_{2p} peaks, the fourth (simulating S-C) constrained to have the same binding energy relative to the 1T'-MoS₂ as the functionalized S-C peak observed in *fc*-MoS₂ samples. This peak fitting was used to determine the error associated with peak fitting when using peak areas for coverage quantification. (d) ¹³C MAS NMR of ¹³C-methyl-MoS₂ functionalized under three conditions: without reductant, with nickelocene, and with cobaltocene. This technique is semi-quantitative and shows the trend of increasing coverage. Error bars indicate $\pm 10\%$ based on 5% error of external standard and an estimate of 5% error from peak fitting.

Table 2.1. The standard reduction potential for each redox couple, the effective reduction potential assuming 50:1 ratio of reductant to oxidant, and the potential on an absolute energy scale using $E(\text{Fc}^{+/0}) = 0.4 \text{ V vs } E_{\text{SHE}}$ (standard hydrogen electrode) and $E_{\text{SHE}} = 4.44 \text{ V vs } E_{\text{vac}}$.

Reductant (A^-)	Standard Reduction Potential for (A/A^-) vs $E(\text{Fc}^{+/0})$ (V)	Effective Reduction Potential, 50:1 reductant to oxidant vs $E(\text{Fc}^{+/0})$ (V)	Potential vs E_{vac}
Ferrocene (Cp_2Fe)	0	-0.10	4.74
Nickelocene (Cp_2Ni)	-0.42	-0.52	4.32
Octamethylnickelocene ($\text{Me}_8\text{Cp}_2\text{Ni}$)	-0.95	-1.05	3.79
Cobaltocene (Cp_2Co)	-1.16	-1.26	3.58
Decamethylcobaltocene ($\text{Me}_{10}\text{Cp}_2\text{Co}$)	-1.77	-1.87	2.97

As expected, exposure to the ferrocene solution did not result in a substantial change in coverage. Figure 2.8a shows an approximately linear increase in coverage for methyl iodide, 1-iodopropane, and 1-bromopropane as the strength of the reductant increases from ferrocene ($E_{\text{eff}} = -0.1 \text{ V vs Fc}^{+/0}$) to cobaltocene ($E_{\text{eff}} = -1.3 \text{ V vs Fc}^{+/0}$). At even higher reduction potentials using decamethylcobaltocene ($E_{\text{eff}} = -1.9 \text{ V vs Fc}^{+/0}$), the coverage did not increase and even appears to decrease, possibly due to competing side reactions and reduction of methyl iodide. Thus, the highest coverage achieved peaked using cobaltocene at ~64%, which amounts to ~32% of all sulfurs being functionalized. This coverage is lower than we hypothesized, considering that silicon surfaces can achieve ~100% methyl coverage with an Si-Si distance of 3.8 Å on Si(111),⁹⁷ compared to the S-S distance of ~3.3 Å on *ce*MoS₂. To assess the factors contributing to this coverage and understand the point at which the coverage is limited by sterics, we will use density functional theory (DFT) calculations, discussed in Chapter 3.

In reactions involving 1-chloropropane, S-C bonds were only visible in the XPS data for reactions performed in the presence of the two strongest reductants used: cobaltocene or decamethylcobaltocene. Because of the similarity of some XP spectra to spectra for unfunctionalized *ce*MoS₂, ¹³C NMR and ATR-FTIR were used to verify that

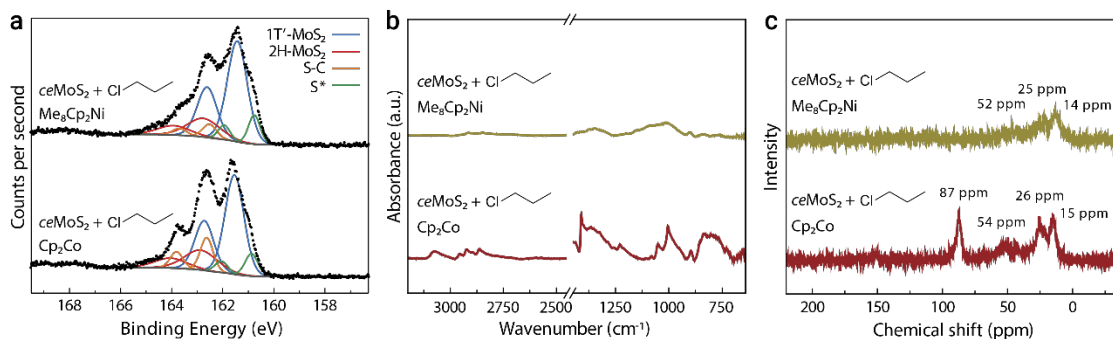


Figure 2.9. (a) High-resolution XPS of S_{2p} region, (b) ATR-FTIR, and (c) ¹³C CPMAS NMR data for the functionalization of *ce*MoS₂ with chloropropane in the presence of either octamethylnickelocene (Me₈Cp₂Ni) or cobaltocene (Cp₂Co).

functionalization was successful using cobaltocene, whereas minimal coverage resulted when octamethylcobaltocene was used (Figure 2.9). Notably, the NMR peak positions and peak splitting for propyl-MoS₂ synthesized using chloropropane and cobaltocene were in accord with those for propyl-MoS₂ (Figure 2.5). However, an additional peak was present at 87 ppm, and the intensity of the peak at 54 ppm was relatively small, consistent with a downfield shift for the anchoring carbon that can be observed in R-CH₂-O species. An additional 4% of both molybdenum and sulfur oxides were observed in the XPS data for the chloropropane/cobaltocene functionalization compared to functionalization using iodopropane, further suggesting a linkage through metal or sulfur oxides.

To evaluate the effects of removing charge density using a metallocene oxidant, *ce*MoS₂ was oxidized by stirring in DMF containing ferrocenium tetrafluoroborate for 3 days, prior to reaction of the *ce*MoS₂ with methyl iodide. The overall composition of the products showed a 15% increase in 2H-MoS₂ and a 15% decrease in S-C bonds relative to *ce*MoS₂ handled in a nominally identical way but not exposed to ferrocenium tetrafluoroborate, which showed a coverage of 35%, as expected (Figure 2.10). In another experiment, *ce*MoS₂ was oxidized with ferrocenium tetrafluoroborate for 4 hours instead of 3 days, followed by methyl iodide, which yielded 49% coverage, similar to the case with no oxidant. These results suggest that removal of negative charge affects the coverage by destabilizing the 1T' phase and favoring the reversion to the 2H phase. This reasoning is consistent with the hypothesis that the 2H to 1T' phase transformation occurs due to the stabilization of the 1T' phase by negative charge

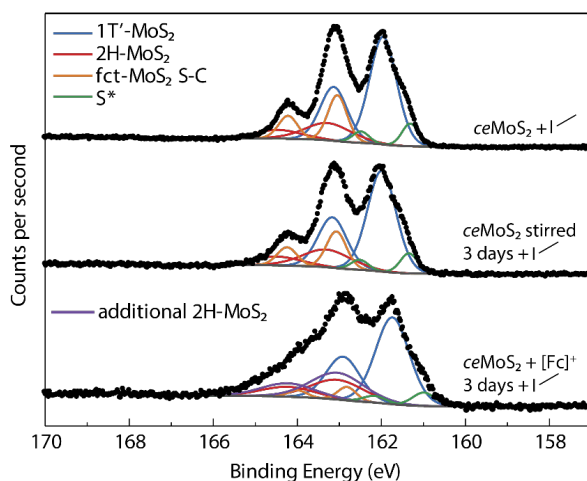


Figure 2.10. High-resolution XPS $S2p$ region for (a) $ceMoS_2$ functionalized with methyl iodide following the standard functionalization procedure detailed in Appendix A, (b) $ceMoS_2$ functionalized with methyl iodide after stirring for 3 days under ambient condition, and (c) $ceMoS_2$ stirred for 3 days with ferrocenium tetrafluoroborate ($[Fe(C_5H_5)_2]BF_4$) then functionalized with methyl iodide. No substantial differences were observed between the first and second conditions. Spectra of samples functionalized after oxidation of $ceMoS_2$ with ferrocenium (c) exhibited $S2p$ regions with a decreased fraction of functionalization and increased fraction of 2H- MoS_2 relative to spectra (a) or (b).

injection. We would like to deconvolute the effects of the charge density as opposed to the phase on $ceMoS_2$ reactivity, since these two processes can both occur in the presence of an oxidant prior to methyl iodide addition. From these results, it is clear that sections of $ceMoS_2$ that convert back to the 2H phase are excluded from functionalization, but it remains unclear whether oxidized $ceMoS_2$ in the 1T' phase react with methyl iodide. Future experiments in this area will need to elucidate the kinetics of 3 processes to determine a suitable experiment design: $ceMoS_2$ oxidation, phase transition, and the functionalization reaction.

2.3.3 Reactivity of $ceMoS_2$ as a function of the halide leaving group

1-iodopropane, 1-bromopropane, and 1-chloropropane were chosen as the set of molecules to explore the dependence of reactivity on the leaving group while keeping the steric effects as similar as possible between molecules. Figure 2.3 shows the XPS, and Figure 2.5 ATR-FTIR, and ^{13}C CPMAS NMR spectra for $ceMoS_2$ before and after functionalization by methyl iodide (methyl- MoS_2), 1-iodopropane (propyl- MoS_2), 1-bromopropane (propyl- MoS_2), and 1-chloropropane. The XPS, ATR-FTIR, and NMR spectra all suggest the presence of propyl groups on $ceMoS_2$ after reacting with 1-iodopropane and 1-bromopropane, whereas 1-chloropropane resulted in neither an S-C XPS peak, C-H IR stretches, nor carbon peaks in the ^{13}C NMR, suggesting that 1-chloropropane was unreactive with $ceMoS_2$. The three types of propyl carbons can be clearly seen for propyl- MoS_2

synthesized from either 1-iodopropane or 1-bromopropane, at 16, 25, and 52 ppm. These results show clearly difference in reactivity comparing alkyl halide electrophiles with iodine and bromine leaving groups as opposed to chlorine and demonstrate that chloride leaving groups are not sufficiently good leaving groups to react with *ce*MoS₂.

2.3.4 S_N2 vs S_N1 mechanism: reactivity of *ce*MoS₂ with primary, secondary, and tertiary alkyl iodides

The reactivity of *ce*MoS₂ with primary, secondary, and tertiary alkyl halides was compared using 1-iodopropane, 2-iodopropane, and 2-iodo-2-methylpropane, respectively. For an S_N2 mechanism, we would expect that the order of decreasing reactivity goes primary > secondary > tertiary, whereas for an S_N1 mechanism we would expect the reverse order of decreasing reactivity. If both mechanisms can be used, then both 1-iodopropane and 2-iodo-2-methylpropane should be able to functionalize *ce*MoS₂, the former via a planar transition state, and the latter via a planar carbocation. What we observe in the XP and NMR spectra for these reactions, as shown in Figure 2.11, indicated rather that 2-iodopropane reacted minimally with *ce*MoS₂, and 2-iodo-2-methylpropane was unreactive entirely. Therefore, the

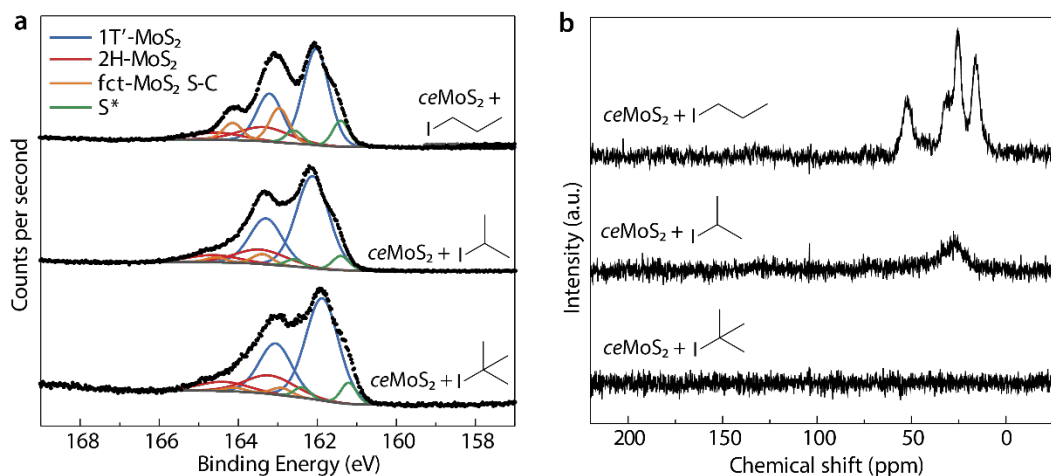


Figure 2.11. High-resolution XPS S_{2p} spectra and (b) ¹³C CPMAS NMR spectra of the products from reactions between *ce*MoS₂ and 1-iodopropane (top), 2-iodopropane (middle), and 2-iodo-2-methylpropane (bottom). Functionalization was minimal using 2-iodopropane and was unsuccessful using 2-iodo-2-methylpropane.

reaction proceeds via an S_N2 mechanism and primary alkyl halides with a favorable leaving group are the most promising reagents to functionalize 1T'-MoS₂.

2.3.5 Electrochemical reduction-activated functionalization of *ce*MoS₂

Since the proposed mechanism for increased coverage using reductant-activated functionalization relies upon electron transfer from the metallocenes to the *ce*MoS₂, any process capable of donating electrons to *ce*MoS₂ should enable control over the coverage. To test this hypothesis, we tested the electrochemical functionalization method by applying a negative bias for 2 hours to an electrode made from drop cast *ce*MoS₂ on graphite in a solution of 0.10 M tetrabutyl ammonium perchlorate and 0.10 M methyl iodide in acetonitrile. This concentration roughly matches the concentration of methyl iodide in the metallocene solution-based experiments. The experimental details of the electrochemical measurement are given in Appendix A.

Figure 2.12 plots the fraction of functionalized sulfur determined from fitting the XPS S2*p* peaks. One electrode was tested at each potential, and each spot represents a single XPS

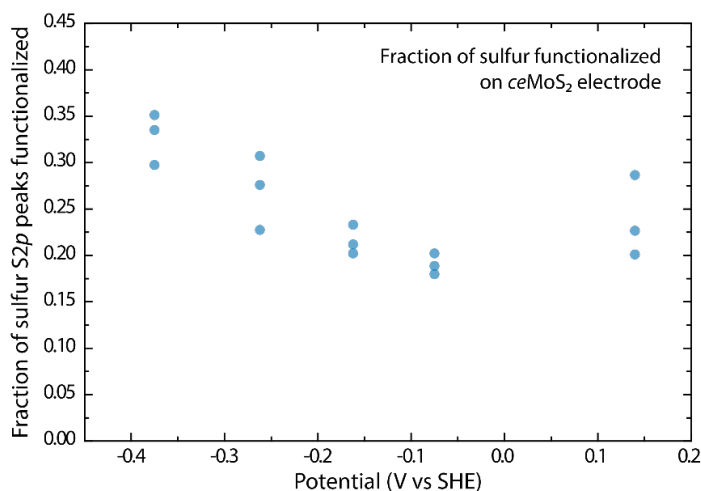


Figure 2.12. Fraction of functionalized sulfur based on high-resolution XPS S2*p* spectra of electrochemically functionalized *ce*MoS₂ drop cast on graphite electrodes. Five electrodes were used to test the five potentials shown, with each spot representing a single XPS measurement and three spots measured per sample.

measurement at a particular spot on the electrode. From this preliminary data, we can see that the coverage increases with reduction potential. Since the electrodes are drop cast with multiple layers of *ce*MoS₂ but only the uppermost layer is exposed, additional assumptions need to be made to obtain the surface coverage. The roughness of drop cast nanosheets presents additional

complications due to the porousness of the electrode. Also, since these results were obtained using one electrode per potential, additional experiments with multiple electrodes per potential should be tested in the future to gain greater confidence in the quantitative trend.

2.3.6 Reductant-activated functionalization of 2H-MoS₂

In a preliminary excursion to see whether the reductant-activated functionalization technique can be applied to functionalize 2H-MoS₂ that is otherwise unreactive with an electrophile, we tested three electrophiles containing fluorine end groups to provide a non-sulfur peak for semi-quantitative analysis: 4-fluorobenzyl bromide, 1-bromo-4-fluorobutane, and 2-iodo-1,1,1-trifluoroethane. These molecules are shown in Figure 2.13 with the corresponding F1s and S2p XPS spectra obtained after reductant-activated functionalization using either nickelocene, octamethylnickelocene, or cobaltocene. In all cases, cobaltocene resulted in the presence of organic fluorine on the surface of 2H-MoS₂ at ~688 eV binding energy, whereas no fluorine was observed for any of the nickelocene or octamethylnickelocene conditions on 2H-MoS₂. Ionic fluoride was also observed in the case of 2-iodo-1,1,1-trifluoroethane at ~684.5 eV (Figure 2.13d), likely from dissociation of fluoride from the organic molecule at some point during the reaction. We also tested 4-fluorobenzyl bromide with *ce*MoS₂ (Figure 2.13a) and found that fluorine reacted with *ce*MoS₂ under all three conditions, thus showing that the nucleophilic addition of MoS₂ to an electrophile is substantially less favored in the 2H phase as opposed to the 1T'. Since there was no clear delineation between the functionalized and unfunctionalized sulfur peaks on 2H-MoS₂, we used the peak areas for fluorine and sulfur to obtain the coverage values shown in Figure 2.13, each corrected by a relative sensitivity factor determined using the *ce*MoS₂ functionalization assuming that the fluorine to sulfur ratio is 1:1 for functionalization 4-fluorobenzylbromide, resulting in a sensitivity of 0.334 for sulfur if the fluorine sensitivity is taken to be 1. The relative sensitivity factors are known to deviate between instruments as well. From the semi-quantitative analysis of the fluorine and sulfur ratios, we found that the coverage for 4-fluorobenzyl bromide on *ce*MoS₂ were approximately 35%, 36%, and 37% using nickelocene, octamethylnickelocene, and cobaltocene, respectively. On 2H-MoS₂, no fluorine was observed using nickelocene and octamethylnickelocene, and using cobaltocene we observed

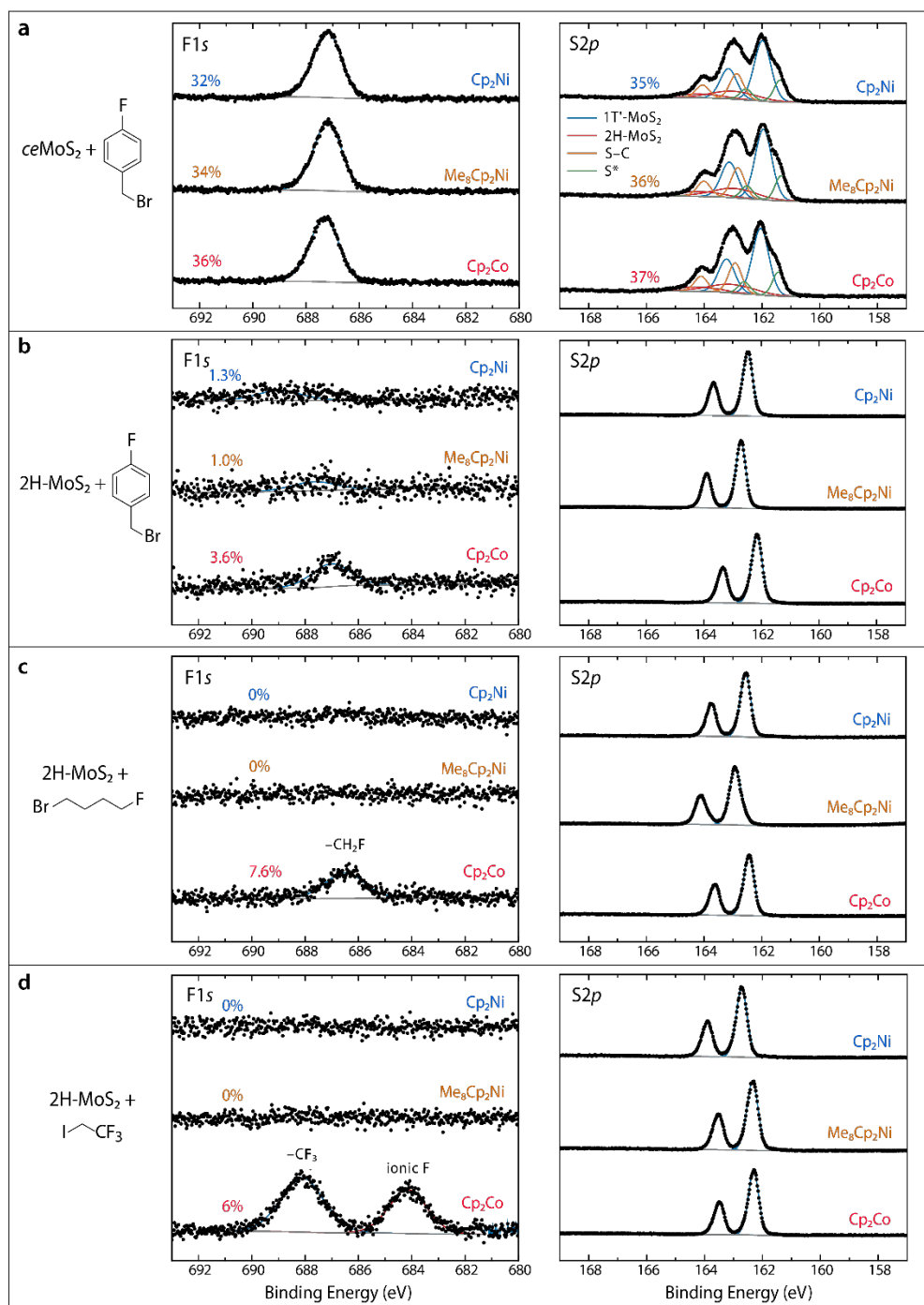


Figure 2.13. High-resolution XPS F1s and S2p spectra for four reactions using reductant-activated functionalization with nickelocene (Cp_2Ni), octamethylnickelocene (Me_8Cp_2Ni), and cobaltocene (Cp_2Co): (a) $ceMoS_2$ reacted with 4-fluorobenzyl bromide, (b) 2H-MoS₂ reacted with 4-fluorobenzyl bromide, (c) 2H-MoS₂ reacted with 1-bromo-4-fluorobutane, and (d) 2H-MoS₂ reacted with 2-iodo-1,1,1-trifluoroethane. The coverage per MoS₂ is shown to the left of the peak used to determine those values, with 0% indicating that no peak was fitted. Area in (d) assumes a 3:1 fluorine to sulfur ratio.

a coverage of ~4% for 4-fluorobenzyl bromide, ~8% for 1-bromo-4-fluorobutane, and ~6% for 2-iodo-1,1,1-trifluoroethane. Note that only one trial was performed for each experimental condition.

2.4 Conclusion

In this chapter, we have shown that primary alkyl halides with an iodide or bromide leaving group are the most promising reagents for reductant-activated functionalization of *ce*MoS₂ and that either addition or removal of negative charge can increase or decrease the amount of functionalization via S–C bond formation. Further, a reductant-activated functionalization method has been developed that allows for control over the degree of coverage of covalently attached surface functional groups on *ce*MoS₂ and enables functionalization by weak electrophiles that are otherwise non-reactive toward *ce*MoS₂. Similarly, electrochemical functionalization can be used to inject negative charge to control the fraction of functionalized sulfur on drop cast *ce*MoS₂. Reductant-activated functionalization with metallocenes can also be used to functionalize otherwise unreactive 2H-MoS₂ in preliminary work of a limited number of trials. Our observations that redox chemistry influences the coverage achievable during functionalization inform the understanding of the charge-transfer mechanisms governing surface functionalization. In addition to understanding the charge transfer and fundamental surface chemistry of *ce*MoS₂ by using one-electron reductants, the reductant-activated functionalization method described herein introduces additional control for mixed-functionalization surfaces. Future work should also investigate which electrophiles are particularly amenable to functionalizing 2H-MoS₂ with more statistical characterization.

In the following chapter, we use DFT modeling of the packing to elucidate the factors behind the coverage limit of ~64% that was observed experimentally, considering that this coverage per MoS₂ implies that less than half of all sulfurs are functionalized. In Chapter 4, we extend this method to WS₂ to compare the effects of the metal on functionalization S–C bond formation and to begin the exploration of the generality of this method for analogous materials.

Chapter 3: Density Functional Theory Modeling of 1T'- MoS₂ Methylation

3.1 Introduction

Theoretical research has been an insightful tool for researchers to obtain a deeper understanding of their experimental observations and to screen for materials on which to focus research efforts. On the topic of functionalization, density functional theory (DFT) modeling of diazonium radical functionalization on 2H-MoS₂ provided a model and explanation for the mechanism by which functionalization propagated along the surface, revealing that this propagation relied on vacancy- and functionalization-induced reactivity in neighboring sulfurs.⁷² Such an insight would not have been extremely difficult to attain using the currently available experimental techniques. In Chapter 2, we discussed the experimentally determined effects of one-electron metallocenes on the coverage of methyl and propyl functional groups on *ce*MoS₂, a process which we call reductant-activated functionalization. We noted that the highest coverage achieved was ~64% and involved the use of the cobaltocene reductant. In this chapter, we use density functional theory (DFT) calculations to assess whether this coverage can be predicted using theoretical calculations and discuss the major factors that contribute to the coverage limitations in this system.

It has been demonstrated experimentally that *ce*MoS₂ is in the 1T' phase based on scanning transmission electron microscopy and photoemission spectroscopy.^{14, 17, 20} Theoretical works have predicted that the 1T phase is unstable and distorts spontaneously to the metastable 1T' phase.^{13, 16} However, this distinction with regards to chemically exfoliated TMDs was not widely acknowledged in the literature until after 2017, after which time several studies highlighted that *ce*MoS₂ was in the 1T' rather than the 1T phase.^{12, 20} Indeed, the 2015 covalent functionalization studies upon which the work in Chapter 2 is based refers to the phase of *ce*MoS₂ as 1T throughout the discussion, with a single sentence devoted to suggesting that the phase may not be perfectly octahedral contrary to the illustrations provided.¹⁹ Although this distinction may appear benign to those who are concerned

primarily with the conduction properties, for which 1T and 1T' are both well-suited given their metallic and quasi-metallic natures, this distinction becomes important when theoretical work is performed with the intent of explaining experimental observations or being used to predict expected outcomes prior to investing in experimentation. Theoretical studies have suggested that not only is the 1T phase dynamically unstable and 0.8 eV and 0.3 eV higher than the 2H and 1T' phases respectively,¹³ hydrogen adsorption studies on 2H-, 1T-, and 1T'-MoS₂ showed that adsorption energies differed by a minimum of a factor of 2 between 1T and 1T', with the 1T' being more favorable for hydrogen adsorption.¹⁶ Thus, it is important for structural distortions present in experimental results to be reflected as accurately as possible in the modeled structures to obtain meaningful results. To this end, previous DFT studies on the effects of functional groups on the stabilization and bandgap tuning on 1T-MoS₂⁹⁸ cannot be applied to our work in Chapter 2. We hope that the work contained in this chapter serves as a springboard for others to build upon when it comes to modeling the effects of functionalization on chemically exfoliated TMDs in the 1T' phase.

The scope of this chapter will focus on the methylation reaction of 1T'-MoS₂ with an alkyl halide. We begin with an exploration of the thermodynamics and kinetics for the first methylation, then proceed with determining the positions and order of subsequent methylations on the surface. Through this process, we will discuss insights into the important parameters influencing whether methylation will occur and the effects of applied potential on the thermodynamics and kinetics of a reaction. From these insights we construct a model to simulate the random addition of functional groups given a set of constraints to show the expected upper bound of coverage for a methyl group on *ce*MoS₂ and how this value is related to the experimental coverages discussed in Chapter 2.

3.2 Computational Design

The reaction we will model throughout this chapter is the addition of methyl chloride (ClCH₃) to 1T'-MoS₂ using a unit cell that contains 16 MoS₂ units as shown in Figure 3.1, using the methods described in Appendix A.6. The reason for using methyl chloride as opposed to methyl iodide, the latter of which was used experimentally in Chapter 2, is that

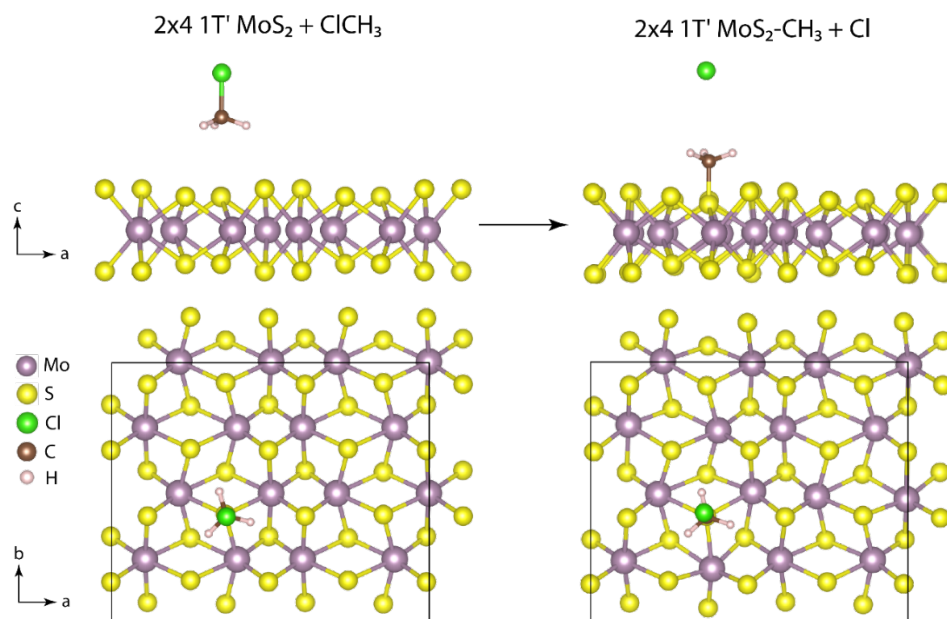


Figure 3.1. Reaction scheme for the 1T'-MoS₂ methylation reaction that will be discussed in this chapter, viewed along the *b*-axis (top) and *c*-axis (bottom) of the rectangular cell. Shown here is the first methylation reaction with S7 (see Figure 3.4 for numbering), with subsequent methylations differing only in the number of methyls on the MoS₂ surface in the initial and final states. The left side shows the initial state, with ClCH₃ suspended over the sulfur to be functionalized, and the right side shows the final state after the S_N2 reaction is finished. Both structures are the optimized geometry results using the methods described in Appendix A.

the pseudopotentials for iodine (and bromine) in the VASP software used to minimize the geometry were incompatible with solvation in the system, whereas the pseudopotentials for chlorine were compatible and we deemed the inclusion of implicit solvation in the calculation to be most relevant. Since chlorine is a weaker leaving group than iodine, the results from this model cannot be applied as readily to experimental data but can still serve as a useful measure of the relative trends that will allow us to observe changes in the kinetics and thermodynamics as methylation proceeds.

Our goal is to understand 1T'-MoS₂ methylation on both the thermodynamic and kinetic level, at various stages of coverage. To obtain the thermodynamics of a reaction (ΔG), the free energy of the final state of a reaction is subtracted by the initial state of a reaction, with the initial and final states resembling the examples shown in Figure 3.1. To obtain the kinetic barrier of a reaction (ΔG^\ddagger), we used climbing nudged elastic band (NEB) to obtain the transition state at saddle point of the reaction surface, and subtracted the initial state free

energy from the transition state free energy. To obtain the ΔG and ΔG^\ddagger values as a function of potential, we used the grand canonical potential kinetics method (detailed in Appendix C.5) to obtain the free energies of the initial, transition, and final states as a function of potential. Since kinetic barrier calculations are computationally expensive, these calculations were limited to studying the addition of the first methyl on the surface, whereas the thermodynamics was investigated for the addition of the 1st to the 6th methyl since only initial states and final states are required for each reaction.

3.3 Results and Discussion

3.3.1 Potential dependence of 1T'-MoS₂ on the number of electrons

A cornerstone of our analysis for the remainder of this chapter depends upon transforming the free energies of structures optimized under fixed charge to a free energy value as a function of potential, to facilitate the comparison with the experimental results of Chapter 2. To obtain this relationship, 1T'-MoS₂ was optimized with varying amounts of added negative charge (electrons), and the free energy and potential of the resulting structure was obtained using jDFTx as described in Appendix A. Before we show this relationship, first we discuss the steps taken to optimize the 1T'-MoS₂ slab.

A periodic slab of 1T'-MoS₂ that consists of 16 MoS₂ units in the unit cell was constructed based on a previously optimized 1T'-MoS₂ structure obtained from literature.¹⁴ The hexagonal cell was converted to a rectangular cell, the vacuum spacing was increased from 20 Å to 30 Å, and the unit cell was converted to a supercell containing 16 MoS₂ units to allow additional space for functionalization reactions both vertically and horizontally, since this is a periodic slab. This process is illustrated in Figure 3.2. Figure 3.3a shows the relationship of potential in V vs SHE as a function of the number of electrons added to the MoS₂ slab. Each point is an individual optimization and free energy calculation, whereby the structure was optimized using VASP and a single-point free energy calculation was performed using jDFTx. Thus, the potential is reflective of changes in optimized structure as a result of adding negative charge to the system. Using the grand canonical potential kinetics

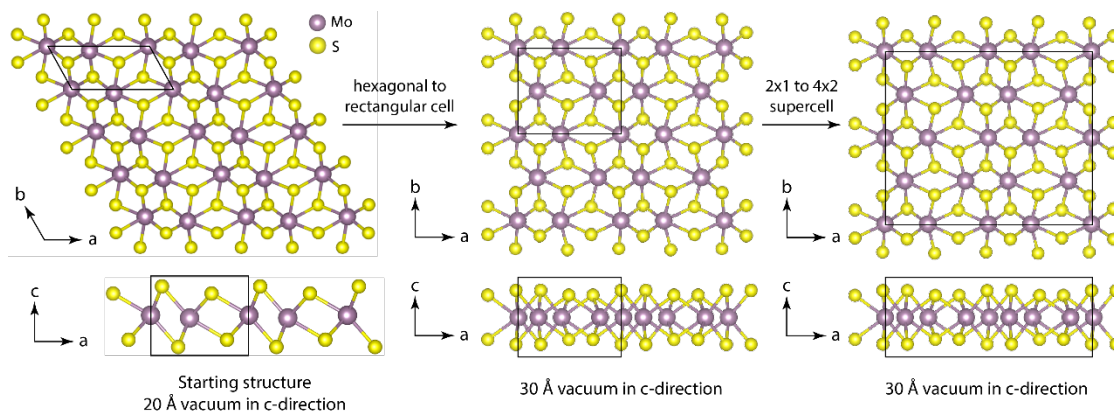


Figure 3.2. From left to right, the starting 1T'-MoS₂ structure obtained from literature, the transformation of the starting structure to a rectangular cell with 10 Å of additional vacuum space (middle), and the expansion of the unit cell into a 16 MoS₂ supercell to allow more space to study methyl functionalization on the periodic surface.

method (see Appendix C.5), we can visualize the change in free energy corrected by the free energy of electrons to obtain the thermodynamically stable amount of charge (Figure 3.3b), which occurs when there are ~ 1.8 additional electrons per 16 MoS₂. This method will be used for all optimized structures discussed in the following sections, including the initial, transition, and final states of reactions, to assess the thermodynamic and kinetic implications as a function of applied potential.

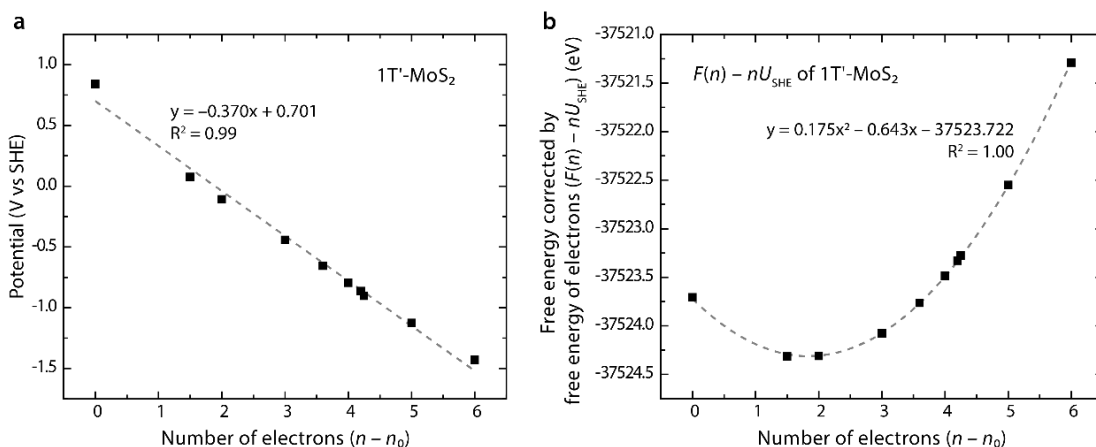


Figure 3.3. The effects of adding electrons to 1T'-MoS₂ containing 16 MoS₂ units on the (a) potential, in V vs SHE, and (b) free energy corrected by the free energy of electrons. The free energy in (a) appears to have a linear relationship with respect to the number of electrons due to the free energy contribution of additional electrons. The quadratic shape of the free energy with respect to the number of electrons is easily apparent when corrected linearly by the free energy contribution electrons (see Appendix C.5). Potential and free energy values were obtained using jDFTx after geometry optimization using VASP (see Appendix A.6 for methods).

3.3.2 Thermodynamic and kinetic differences during methylation of the two types of sulfur on 1T'-MoS₂

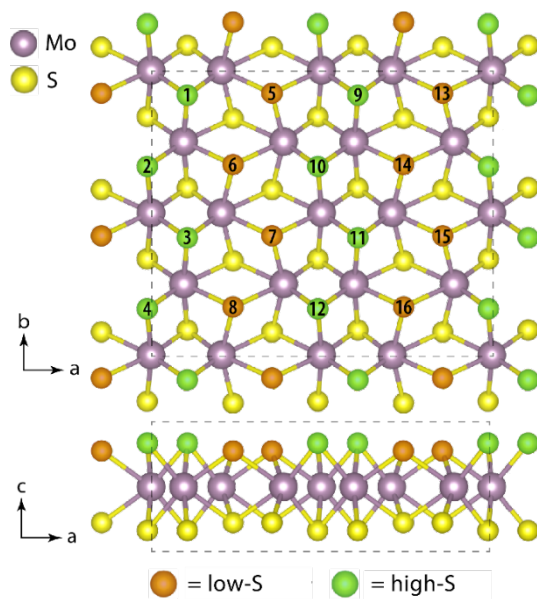


Figure 3.4. Top-down and side view of the rectangular unit cell of the minimized 1T'-MoS₂ supercell, color-coded to show the two types of sulfur in the unit cell: low-S and high-S, with low-S having a longer average Mo-S distance and high-S having a shorter average Mo-S distance and protruding further out-of-plane compared to the low-S.

The first aspect of methylation that we wanted to understand is how the two different types of sulfur, which emerge because of the distortion of the 1T phase to the 1T' phase, differ in their reactivity towards nucleophilic addition with methyl chloride. These two types of sulfur we will refer to as “low-S” and “high-S” sulfur, as shown in Figure 3.4, following the nomenclature used in previous computational studies of 1T'-MoS₂.¹⁶

Prior to investigating the thermodynamics and kinetics of the methylation reaction, we ascertained that methylated MoS₂ of a particular

type of sulfur results in a structure that has little intra-type free energy variation within either low-S or high-S, and a much larger inter-type free energy variation between low- and high-S using two sulfurs of each type: S6 and S7 for low-S, S10 and S11 for high-S. Figure 3.5 graphs the free energy of S6-, S7-, S10-, and S11-functionalized MoS₂, showing that the free energy of methylated MoS₂ depends largely on whether it is high-S or low-S, with little variation within the low-S and high-S groups. Thus, we selected S7 and S10 as the low-S and high-S sulfurs to study the first methyl group addition reaction to MoS₂.

Figure 3.6 shows the relationships between the thermodynamic favorability (ΔG) of methylation on S7 and S10 in terms of the final state free energy minus the initial state free energy, and the kinetic barrier of a reaction (ΔG^\ddagger) calculated from the transition state free

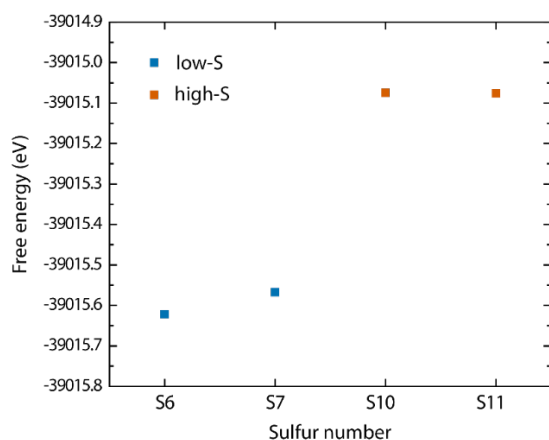


Figure 3.5. Free energy of $(\text{MoS}_2)_{16}(\text{CH}_3)$ with methyl on either S6, S7, S10, or S11, the former two being low-S and the latter two being high-S. Geometry optimizations and free energy calculations were performed on solvated structures that were negatively charged with 2 electrons, resulting in structures with potentials -0.15 , -0.16 , -0.11 , and -0.11 V vs SHE, respectively.

energy minus the initial state free energy. The computations for ΔG and ΔG^\ddagger were computed in intervals of 0.1 V from 0.5 to -0.9 V vs SHE and are based on interpolations using the grand canonical potential free energies to show the potential dependency of the free energy of the system. The process of quadratic fitting and interpolation is described in greater detail in Appendix C.5. The potential interval that is plotted in Figure 3.6 is the narrowest potential window within which all the values used to calculate ΔG and ΔG^\ddagger are interpolated

values, as opposed to extrapolated. The reductant potentials that correspond to the reductants used in Chapter 2 are notated on the plot to aid comparison with the experimental data. To determine the potential of *ce*MoS₂ for the no-reductant case, we made drop cast *ce*MoS₂ electrodes and measured the open circuit voltage in acetonitrile with 0.10 M tetrabutylammonium perchlorate and 0.10 M methyl iodide (see Appendix A.4), which was determined to be -0.07 V vs $E(\text{Fc}^{+/0})$, or ~ 0.3 V vs SHE, and also corresponds to the potential of the ferrocene condition. XPS of drop cast *ce*MoS₂ showed the same peaks in the Mo3*d* and S2*p* regions as the *ce*MoS₂ spectra in Chapter 2.

From Figure 3.6, we can see that at the ΔG for methylation of S10, a high-S sulfur, is consistently ~ 0.5 eV higher than the ΔG for methylation of S7, a low-S sulfur. The barrier height of S10 methylation, ΔG^\ddagger , is ~ 0.2 eV higher than the ΔG^\ddagger of S7 methylation. These results show that low-S functionalization is preferred over high-S functionalization both thermodynamically and kinetically. Figure 3.7 shows the correlation between ΔG and ΔG^\ddagger of S7 and S10 methylation. If we use the Boltzmann distribution to evaluate the significance of the difference of 0.5 eV between the ΔG values, we see that the probability of S10

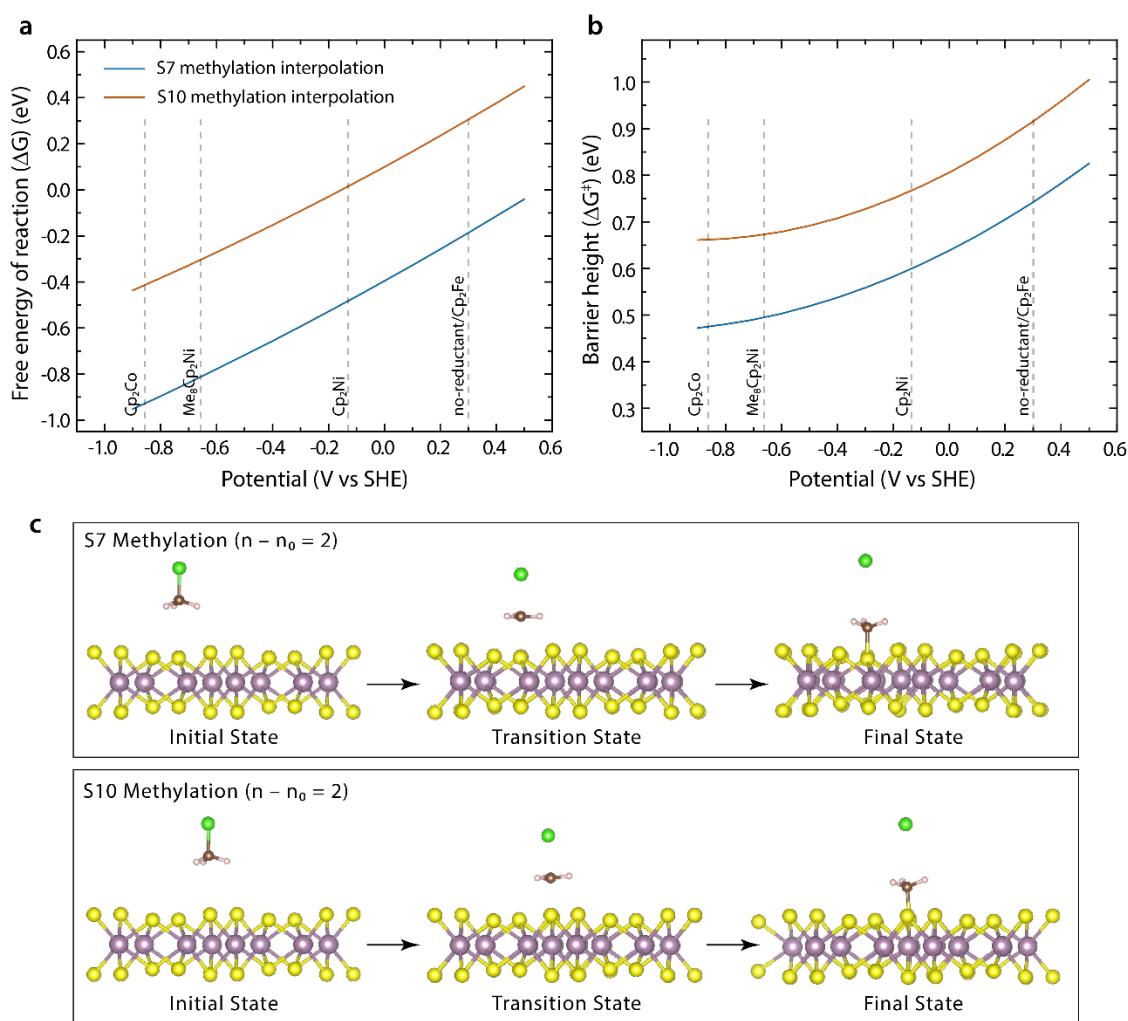


Figure 3.6. (a) Thermodynamic favorability, ΔG , and (b) kinetic barrier, ΔG^\ddagger , of methylation on S7 and S10 of 1T'-MoS₂ as a function of potential based on interpolations of the initial, transition, and final state free energies (see Appendix C.5). (c) Side-view of the initial state, transition state, and final states for S7 and S10 methylation with negative charge of 2.

methylation is 9 orders of magnitude lower than that of S7 methylation. Using the Eyring equation to evaluate the difference in rate constants, the details in Appendix C.6, we see that the rate constant k for S7 methylation is 2 s^{-1} , but only 0.002 s^{-1} for S10 methylation at 0.3 V vs SHE, a difference of 3 orders of magnitude in the rate constant. The Boltzmann distribution and Eyring equation are given by eq. 1 and 2:

$$p_i/p_j = \exp(-(E_i - E_j)/k_B T) \quad (1)$$

$$k = (k_B T/h) \exp(-\Delta G^\ddagger/RT) \quad (2)$$

where p_i is the probability of the system being in state i , E_i is the energy of state i , k_B is the Boltzmann constant, T is the temperature, k is the reaction rate constant, h is Planck's constant, and R is the gas constant.

Thus, there is a significant thermodynamic and kinetic preference for the functionalization of low-S sulfurs. The reason for this is likely due to the differences in Mo–S bond lengths between low-S and high-S. As the Mo–S bond length increases, the covalent bond is weaker, there is greater electron density localized on the sulfur atom and less stabilization with the Mo atom, making the sulfur more nucleophilic. Conversely, as the Mo–S bond shortens, more electron density from the sulfur participates in the Mo–S bond and becomes unavailable to participate in nucleophilic addition. For high-S sulfurs, the Mo–S bond distances are 2.34, 2.39, and 2.46 Å, whereas the Mo–S bond distances for low-S sulfurs are 2.35, 2.51, and 2.54 Å. Given that two of the Mo–S bonds for low-S are longer by 0.08–0.11 Å each, it is reasonable to expect that low-S sulfurs preferentially engage in nucleophilic attack compared to the high-S sulfurs. Similar conclusions have been made in computational studies of hydrogen adsorption on low-S and high-S sulfurs, with the conclusion that the ~ 0.7 eV difference in the free energy of H adsorption (0.06 eV on low-S, 0.73 eV on high-S) is due

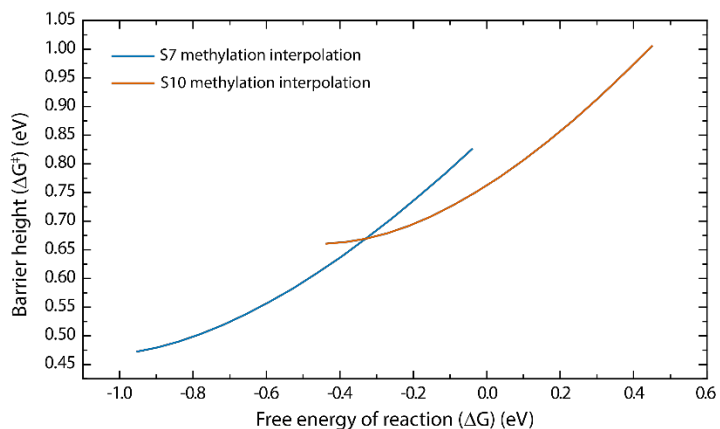


Figure 3.7. The correlation between the barrier height and the free energy of reaction for S7 and S10 methylation, plotted using the same points as shown in Figure 3.6. The reaction potential varies along each curve and can be determined using Figure 3.6.

to the more negatively charged low-S with a charge -0.54 , compared to high-S with a charge of -0.47 .¹⁶ These values were obtained using Bader's charge population analysis.⁹⁹ The same study also found that H atoms adsorbed onto high-S moved to the nearest low-S with a barrier height of 0.15 eV that can be easily

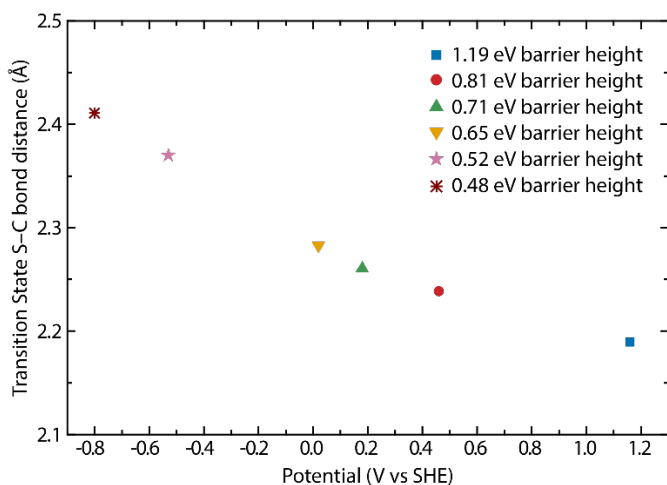


Figure 3.8. Transition state S–C bond distance as a function of potential in V vs SHE. Each point is based on a single nudged elastic band calculation. As the potential becomes more negative, the S–C bond length increases, indicating that the transition state resembles the initial state more than the final state, consistent with the data in Figure 3.6 indicating a more exothermic reaction as the potential decreases.

overcome at room temperature.¹⁶ A similar reaction was not performed in this work, which we believe would be interesting to note in future work.

Consistent with the decrease in barrier height and increased thermodynamic favorability of S7 methylation as the potential becomes more negative, we found that the S–C bond distance in the transition state increases as the potential

decreases, as illustrated in Figure 3.8. An increase in the S–C bond distance implies that the transition state occurs earlier along the reaction coordinate, closer to the reactants. According to Hammond’s postulate, the closer the energy between the transition state and another state, the more their geometries resemble each other and vice versa. In exothermic reactions, the transition state is closer in energy to the reactants than to the products, which is what we observed in Figure 3.6 as the potential becomes more negative. To summarize, as the potential becomes more negative, the reaction becomes more exothermic, and the transition state moves closer to the initial state along the reaction coordinate.

In addition to methylation of the 1T’ phase, we also performed a minimization of a methyl-functionalized 1T phase. Notably, the methylated 1T-MoS₂ distorted to a 1T’-like structure, although its minimized free energy was higher than the structures shown above. Since we were able to minimize the 1T phase by itself without observing distortion, this suggests that there is a local minimum for the 1T phase with a barrier for distortion that is overcome upon the addition of a methyl group. Thus, functionalization necessitates that the 1T phase

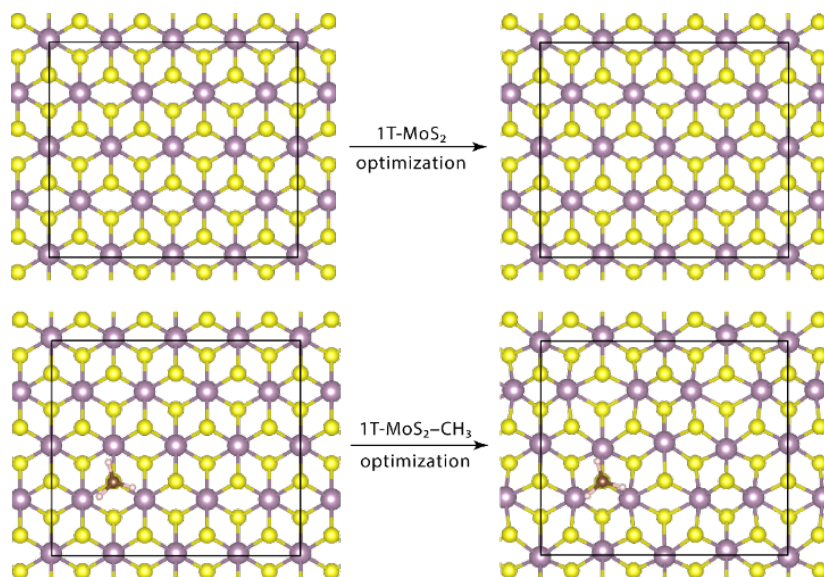


Figure 3.9. Top row: 1T-MoS₂ before and after geometry optimization. Bottom row: methylated 1T-MoS₂ before and after geometry optimization. Methylated 1T-MoS₂ resulted in a distorted structure.

becomes distorted. The structures before and after the geometry optimization of the 1T phase without and with methylation are shown in Figure 3.9.

3.3.3 Thermodynamics of progressive methyl functionalization of 1T'-MoS₂ as a function of applied potential

In this section, we will discuss the thermodynamics of progressive surface methylation and use the results to inform our understanding of coverage limitations. First, we will describe the methodology used to determine which positions to functionalize at each methyl addition. We will use this notation to represent the reaction and resulting layout surface methyls: $XN(A)[-h]B$, where X is the number of neighbors of the methyl being added, N stands for neighbors, A , B , etc. are the numbered sulfur positions that are functionalized (see Figure 3.4) and can have more or fewer positions as appropriate, “h” appears next to positions that are high-S, and the round bracket “()” appears around the position being functionalized.

We observed in the previous section that functionalization preferably occurs on low-S rather than high-S. Thus, we chose the 1st methyl addition to be on S7. To determine which sulfur should be functionalized next, we compared the free energies of every 2-methyl functionalization pattern where one of the methyls is on S7 at fixed negative charge to mimic the negatively charged experimental conditions, shown in Figure 3.10. From Figure 3.10

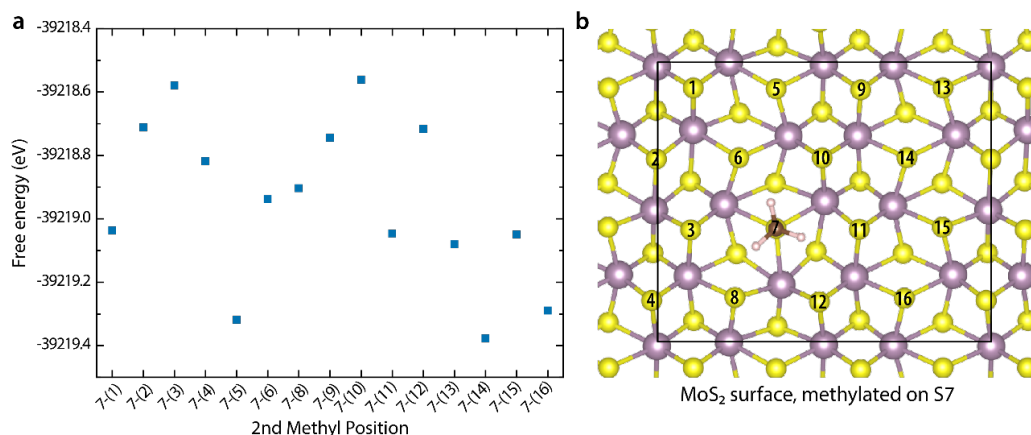


Figure 3.10. (a) Free energies of 2-methyl functionalization patterns that include one methyl on S7, minimized with a negative charge of 2. **(b)** MoS₂ surface prior to the addition of the 2nd methyl.

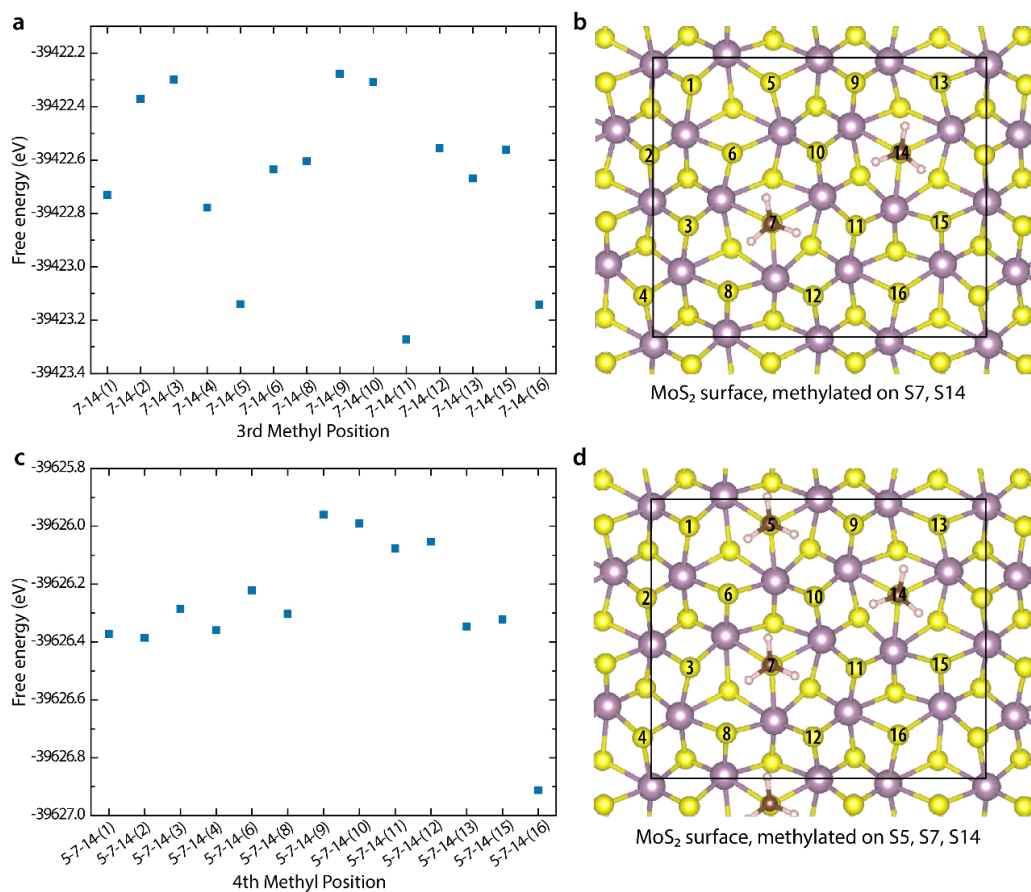


Figure 3.11. (a) Free energies of 3-methyl functionalization patterns that include methyls on S7 and S14, minimized with a negative charge of 2, **(b)** the MoS₂ surface prior to the addition of the 3rd methyl. **(c)** Free energies of 4-methyl functionalization patterns that include methyls on S5, S7, and S14, minimized with a negative charge of 2, **(d)** MoS₂ surface prior to the addition of the 4th methyl.

we see that the methylation pattern 7-5 (i.e. positions S7 and S5 are methylated) and 7-14 are the patterns with the lowest free energy. Thus, we chose to functionalize S14 for the 2nd methyl and the reaction can be represented as 0N-7-(14) using our notation.

For the 3rd methyl, we repeated the same procedure and observed that methylation at positions 5 (low-S), 11 (high-S), and 16 (low-S) resulted in the structures with the lowest free energy (Figure 3.11a, b). Since we know that low-S are preferable for functionalization compared to high-S and noting that the potential of the final structure with S11 methylated is ~ 0.15 V positive relative to all other structures, we chose S5 for the third methylation

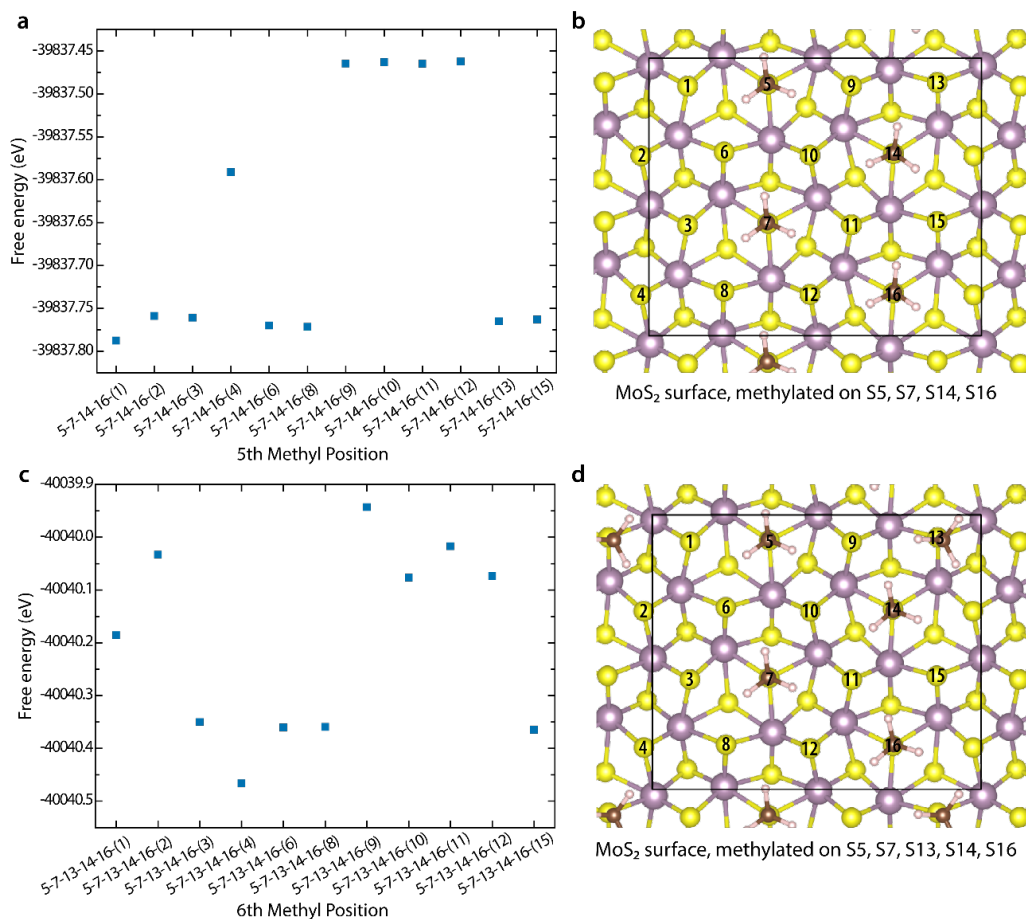
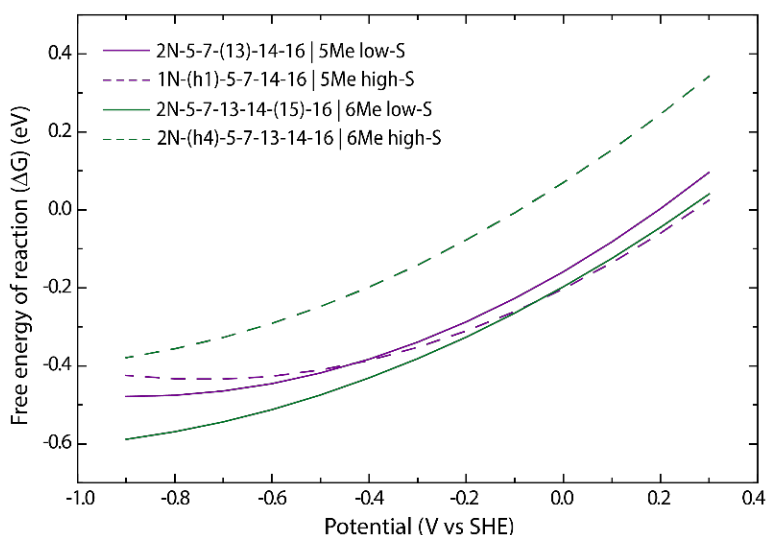


Figure 3.12. (a) Free energies of 5-methyl functionalization patterns that include methyls on S5, S7, S14, and S16, minimized with a negative charge of 4.2, (b) the MoS₂ surface prior to the addition of the 5th methyl. (c) Free energies of 6-methyl functionalization patterns that include methyls on S5, S7, S13, S14, and S16, minimized with a negative charge of 4.2, (d) MoS₂ surface prior to the addition of the 6th methyl.

reaction, 0N-(5)-7-14. For the 4th methylation, the same procedure was repeated, and resulted in a clear favored methylation position at S16, the 0N-5-7-14-(16) reaction (Figure 3.11c, d).

For the 5th methylation, we observed the free energies to be similar for positions 1, 2, 3, 6, 8, 13, and 15 (Figure 3.12a, b). Positions 1, 2, and 3 are high-S, whereas 6, 8, 13, and 15 are low-S. We encountered a similar situation during the 6th methylation, where S3 and S4 (high-S) and S6, S8, and S15 (low-S) were the lowest in energy (Figure 3.12c, d).

Figure 3.13 shows the ΔG of methylation obtained using grand canonical potential kinetics for the 5th and 6th methylation reactions on either a low-S or a high-S. The ΔG is ~ 0.3 eV lower for the low-S option relative to the high-S option when the number of neighbors is held constant, as is the case for the two 6-methyl examples (2N-5-7-13-14-(15)-16 and 2N-(h4)-5-7-13-14-16). On the other hand, the ΔG between methylation of a low-S with 2 neighbors vs a high-S with 1 neighbor is similar, which can be seen for the 5-methyl examples 2N-5-7-(13)-14-16 and 1N-(h1)-5-7-14-16. The reason for this discrepancy between comparing the free energies of the final structure and the ΔG of reaction may be due to differences in



potential at fixed charge depending on where the methyl is located. Thus, it is not immediately obvious from free energies of minimized structures at fixed charge what their relationship will be at fixed potential.

Figure 3.13. The ΔG of the methylation reaction vs potential for the 5th and 6th methylations, indicated in the notation with numbers corresponding to methylated sulfurs, brackets around the most recent methyl position, a prefix indicating the number of neighbors for the bracketed position, and “h” to indicate high-S positions.

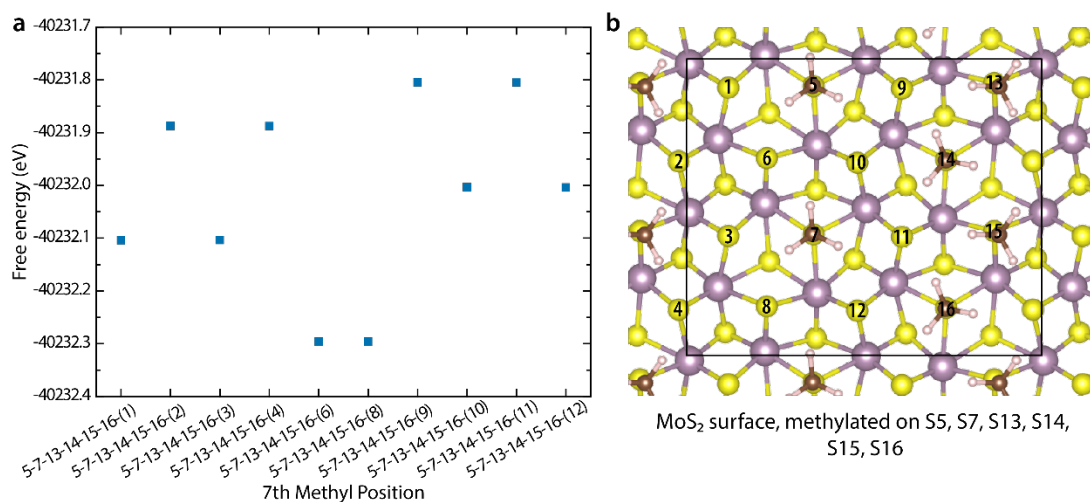


Figure 3.15. (a) Free energies of 7-methyl functionalization patterns that include methyls on S5, S7, S13, S14, S15, and S16, minimized with a negative charge of 1, (b) MoS₂ surface prior to the addition of the 7th methyl.

We also calculated the free energies of 7-methyl patterns and found that the remaining low-S positions, S6 and S8, were equally favored (Figure 3.15).

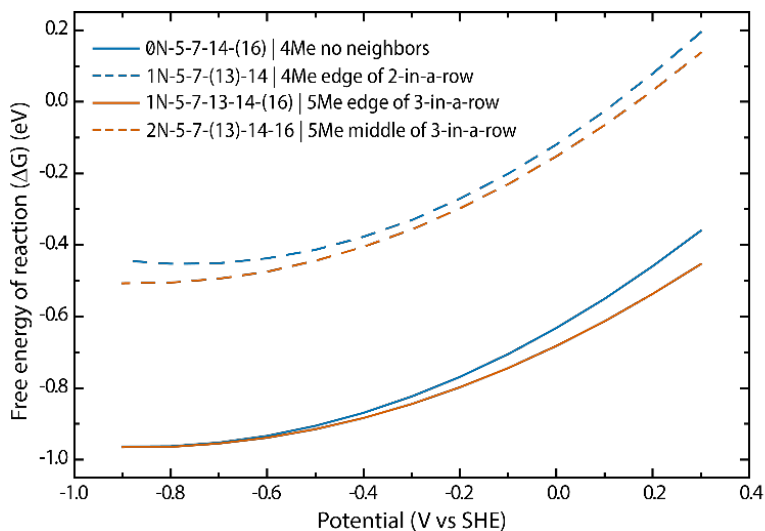


Figure 3.14. The free energy of the methylation reaction, ΔG , vs potential for the 4th and 5th methylations, comparing the effect of neighboring groups on the ΔG value. For the 4th methylation reaction (blue solid and dashed lines), 0N-5-7-14-(16) and 1N-5-7-(13)-14 functionalizes a sulfur adjacent to 0 and 1 methyl group respectively. For the 5th methylation reaction (orange solid and dashed lines), 1N-5-7-13-14-(16) and 2N-5-7-(13)-14-16 functionalizes sulfurs adjacent to 1 and 2 methyl groups, respectively. The 5-methyl reactions result in the same pattern of methyls on the surface.

In addition to calculating the thermodynamics of functionalizing the “most favorable” position at each step to determine the methylation pattern, we also calculated the thermodynamics for reactions that would yield useful comparisons in terms of steric effects. For the 4th methylation, although we found that 0N-5-7-14-(16) is the most favorable reaction,

we also calculated the thermodynamics for the 1N-5-7-(13)-14 reaction to understand the effects of functionalizing a low-S (S13) adjacent to an existing methyl group (S14) (Figure 3.14). Similarly, although the only low-S sites available were between two methyl groups for the 5th methylation, 2N-5-7-(13)-14-16, we also calculated the thermodynamics for the 1N-5-7-13-14-(16) reaction which has the same methylation pattern in the product, but the reaction was adjacent to only one methyl group rather than two (Figure 3.14). Note that positions S13 and S16 are adjacent since the unit cell repeats in all directions.

Notably, in the example shown in Figure 3.14, the ΔG of the two-neighbor (2N) reaction is substantially higher than the 1N reaction that results in the same pattern of 5 methyls (5-7-13-14-16) in the product. In the 4-methyl cases, the ΔG of the 1N reaction is higher than the 0N reaction, but they result in different methylation patterns. Also, the 1N 4-methyl reaction appears to be as thermodynamically unfavorable as the 2N 5-methyl reaction. This may be because the 5-6-13-14 pattern, with its adjacent methyls on S13 and S14, is more strained than the 5-7-14-16 pattern, where no methyls are adjacent to each other. Since their initial states are equally unstrained, this results in a more positive ΔG for the reaction that produces

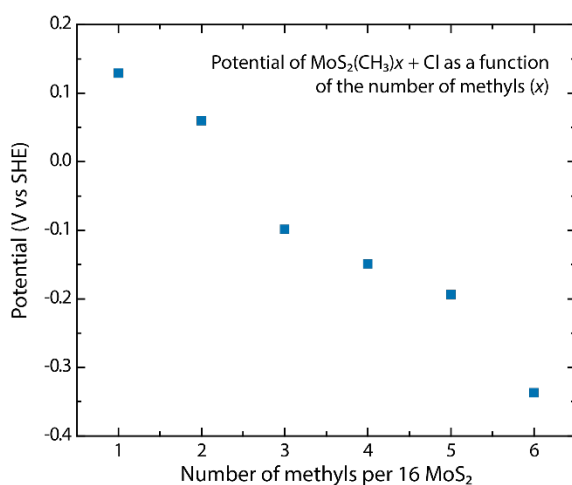


Figure 3.16. Potential in V vs SHE of the final state products $(\text{MoS}_2)_{16}(\text{CH}_3)_x + \text{Cl}$, with a fixed negative charge of 2 in the unit cell, depending on the number of methyls added to the surface ($x = 1, 2, 3, 4, 5$ or 6). The potential of the final products becomes more negative as the number of methyls increases due to additional electrons in the system.

more steric hinderance in the product. From this perspective, the similarity in free energy change in the overall system, ΔG , for the 1N-5-7-(13)-14 and 2N-4-7-(13)-14-16 reactions suggests that the addition of the S13 methyl adds a similar amount of strain to both systems.

In the process of calculating the thermodynamics of the reactions described above, we also found, perhaps unsurprisingly, that the potential of the reaction products becomes more negative as more

methyls are added to the surface. Figure 3.16 plots the potential of the MoS₂ slab after each methylation (a chlorine atom is present above the most recently added methyl) at a fixed negative charge of 2. As additional methyls are added to the system, additional electrons are added to the functionalized MoS₂, in the form of the S–C bond and the methyl groups, resulting in a more negative potential.

For all the methylation reactions described above, we calculated the ΔG as a function of potential and plotted the results altogether in Figure 3.17, interpolated using the same methods as in 3.3.2 (see Appendix C.5). Methyl additions involving 0, 1, or 2 neighboring methyls during the reaction are grouped using solid, dashed, and dotted lines. The potentials corresponding to the reductants used in Chapter 2 are indicated with vertical lines.

From the data in Figure 3.17, we can make several observations. First, methylations that occur surrounded by empty sites (i.e. those labeled 0N) have similar thermodynamic favorability. The ΔG of methylation actually *decreases* after the first methylation. This is reminiscent of the effects observed for 2H-MoS₂ vacancy-induced radical functionalization,

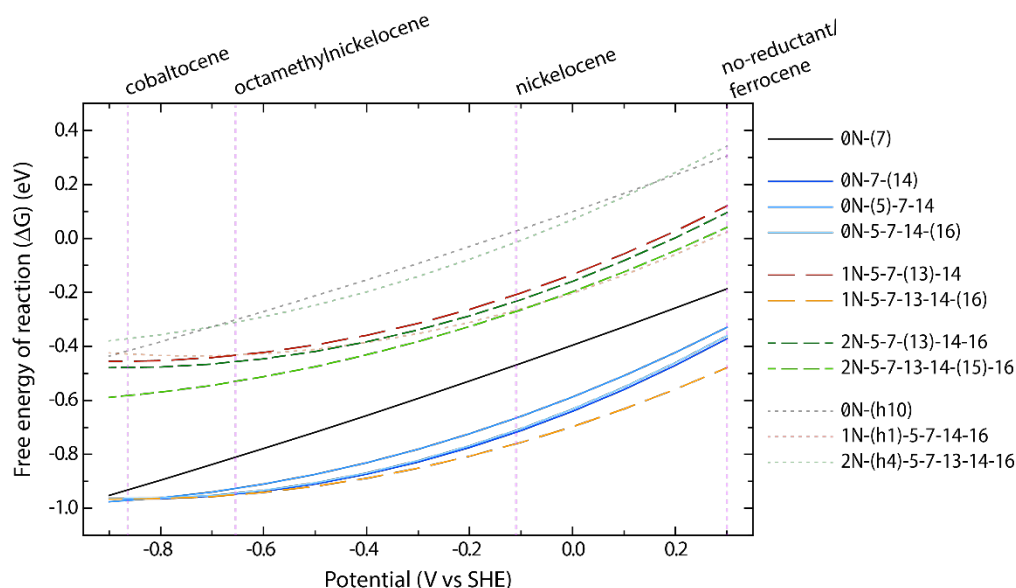


Figure 3.17. The free energy of the methylation reaction, ΔG , vs potential for all methylation reactions, where XN stands for X neighbors for the methyl being added, the numbers representing the sulfur positions that are methylated, and brackets surround the position undergoing the methylation reaction. Potentials corresponding to experimental conditions in Chapter 2 are marked with vertical lines.

whereby the initial functionalization reaction can only occur next to a vacancy, but functionalization induces higher reactivity in nearby sulfurs, resulting in a nucleation-propagation pattern of functionalization across the surface.⁷² A similar mechanism may be present in this system that promotes functionalization of non-sterically hindered nearby sites.

Second, high-S functionalizations in the 0N and 2N cases (0N-(h10) and 2N-(h4)-5-7-13-14-16) have the highest ΔG values out of all the reactions in this potential range and are thus less likely to be functionalized than low-S, except in the case of 1N-(h1)-5-7-14-16 which is comparable to 2N low-S functionalization.

Third, the ΔG of 2N methylations are substantially higher than the 0N and a subset of 1N methylations. The ΔG values of 1N methylations are split between being those of 0N or 2N, depending on the methylation pattern on the surface. If we compare the ΔG reactions that result in methyl functionalization at the same positions, as in 1N-5-7-13-14-(16) and 2N-5-7-(13)-14-16, and assume that the thermodynamics of a reaction are correlated with the kinetics of the reaction which is true in the case of the first methylation reaction (Figure 3.7), the ~ 0.5 eV increase in ΔG of the latter suggests that from both the thermodynamics and kinetics perspectives, methylation of sites with two neighboring methyl groups is substantially disfavored relative to methylation of sites with either zero or one neighbors. This difference for 2N reactions may be a key factor in limiting the achievable coverage in the experimental system. Based on Figure 3.17, for a 2N reaction to have a ΔG close to that of a 0N reaction in the no-reductant case (0.3 V vs SHE), at least -0.7 V of additional potential needs to be applied (~ -0.4 V vs SHE).

We will use these insights later in Section 3.3.5 to simulate and obtain the expected coverage distributions of random surface functionalization according to different functionalization models and suggest the models that are most likely to represent this system.

3.3.4 Effects of neighboring methyl groups on the rotational barrier

Aside from the thermodynamics and kinetics of the methylation reaction, we wanted to study the rotational barrier experienced by methyl groups on the surface and the impact of the

number of neighbors on their rotational barriers. Methyl groups with higher rotational barriers suggests that rotation occurs with lower probability, and thus certain conformations are restricted. If we assume that the kinetics of a reaction depends on the likelihood for the reactants' conformation to meet the conformation limits in the final product, then the rotational barrier of the functional group in the final product can reflect the kinetics or likelihood for the reaction to take place.

We computed the rotational barrier for seven cases using the nudged elastic band method at fixed charge for each methyl added to the surface in roughly the same order as discussed in section 3.3.3, with no methyls on high-S since these positions were shown to be substantially less favored. In three cases, the rotating methyl had 0 neighbors; in two cases, the rotating methyl had 1 neighbor, and in the remaining two cases, the rotating methyl had 2 neighbors.

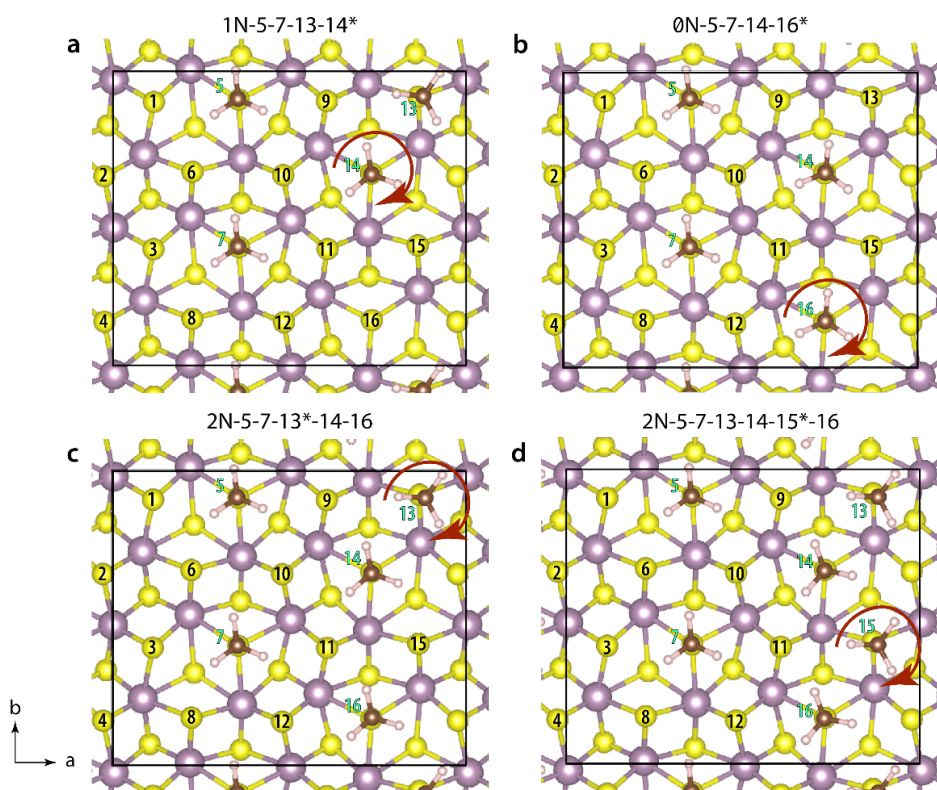


Figure 3.18. Examples of methyl patterns and the corresponding notation to indicate the pattern and the rotating methyl. (a) Example where the rotating methyl has one neighbor, (b) an example where the rotation methyl has 0 neighbors, (c) and (d) are examples where the rotating methyl has 2 neighbors. Note that positions 13 and 16 are adjacent due to the periodic repeat of the unit cell.

We will use the following notation to convey the surface conformation and the rotating methyl: $XN-A^*[-B[-C]]$, where X is the number of neighbors of the rotating methyl, N stands for neighbors, A , B , C are the sulfur positions that are functionalized and can have more or fewer positions as appropriate, and the asterisk (*) appears next to the position of the rotating methyl. Four examples of this notation are shown in Figure 3.18, with the sulfur numbering the same as in Figure 3.4.

Figure 3.19 graphs the rotational barrier depending on the number of neighbors adjacent to the rotating methyl, the maximum of being 2 if functionalization is restricted to only low-S. There is a clear demarcation in the rotational barrier for methyl groups with 0 or 1 neighbors to methyls with 2 neighbors, with the latter doubling in the barrier height from ~ 0.05 eV to ~ 0.1 eV (Figure 3.19a). Figure 3.19b plots the rotational barrier vs the number of methyls on the surface to illustrate the same data from a different perspective.

One apparent outlier to discuss is for the 1-neighbor (1N) cases. For 1N-5-7-13-14*-16 where the rotating methyl is at the end of a group of 3 methyls in a row, the barrier height is close to those of the 0N cases at ~ 0.05 eV, whereas the 1N-5-7-13*-14 case where the rotating methyl is one of 2 methyls in a row resulted in a much lower barrier of 0.02 eV. This may be

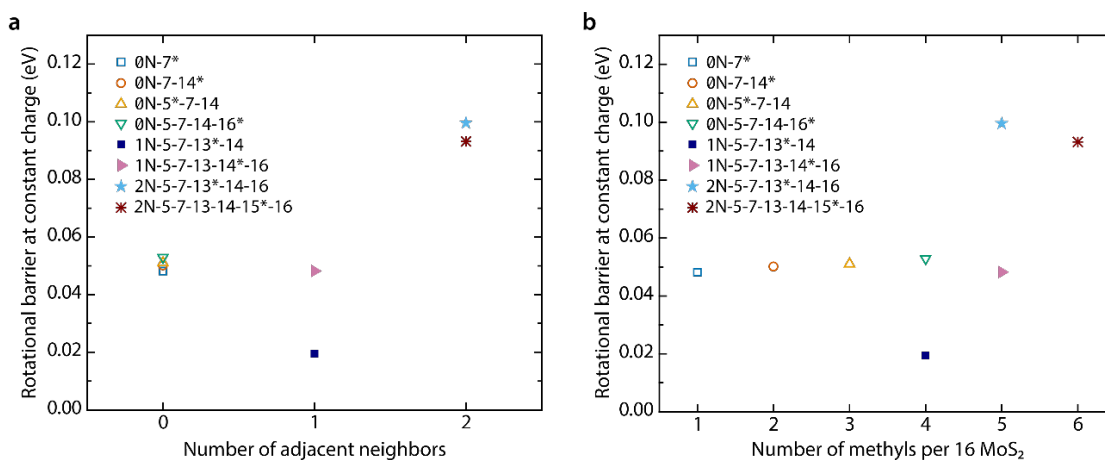


Figure 3.19. The rotational barrier for clockwise methyl rotation by 120° of various methyl patterns as a function of (a) the number of neighbors adjacent to the rotating methyl, and (b) the number of methyl groups on the MoS₂ surface per unit cell. The unique pattern and methyl rotation is specified in the legend notation as $XN-A^*[-B]$ where X is the number of neighbors next to the rotating methyl, A , B , etc. are the positions with methyls, and the asterisk (*) indicates the rotating methyl.

due to the combination of 2 factors: (1) a relatively higher free energy in the most favorable conformation for 2 adjacent methyls relative to 0N cases, and (2) a relatively lower free energy in the least favorable conformation for when there are 3 adjacent methyls relative to 2 adjacent methyls. Specifically, the free energy of the most favorable conformation of 1N-5-7-13*-14 may be higher than the 0N cases due to additional strain from the adjacent S13 and S14 positions. Additionally, for 1N-5-7-13-14*-16 with 3 adjacent methyls, the S13 methyl cannot accommodate the one on S14 due to steric hinderance from the S16 methyl on the other side, whereas for the S14 adjacent methyl can accommodate the S13 methyl for 1N-5-7-13*-14 during the peak of the rotational barrier. The relative destabilization of the rotational trough relative to 0N cases and stabilization of the rotational peak relative to 1N-5-7-13-14*-16 results in a relatively low rotational barrier for 1N-5-7-13*-14. Note that 5-7-13-14 is not the thermodynamically favored pattern for 4 methyl groups on the surface; the thermodynamically most favorable pattern is one where all methyl groups are evenly spaced, such as 5-7-14-16, which is also plotted (0N-5-7-14-16*) and has a 0.05 eV rotational barrier.

Another comparison is between the middle vs outermost methyl groups in a row of 3 methyl groups in the two cases with the same 5-methyl pattern (5-7-13-14-16): the rotational barrier for the middle of 3 adjacent methyls is 0.10 eV, as in 2N-5-7-13*-14-16, whereas the rotational barrier is 0.05 eV for the outermost of 3 adjacent methyls, as in 1N-5-7-13-14*-16. This shows that although the outermost methyls in a row of 3 restrict the rotation of the middle methyl, the outermost methyls are not themselves restricted because of the additional space they can use to accommodate the rotation. In the extreme case where there are no “outermost methyls” to speak of, such as in 2N-5-7-13-14-15*-16 where all low-S sulfurs within the same column are functionalized, the rotational barrier is 0.09 eV, similar to the barrier for the middle of 3 adjacent methyls (2N-5-7-13*-14-16) discussed above.

Given that there is a clear indication that methyl conformation is severely restricted when surrounded by 2 neighbors compared with either 0 or 1, this provides us with an additional clue in conjunction with Section 3.3.3 that the coverage limitation for methyl functionalization may reflect restrictions on the number of neighbors that methyl groups can tolerate on the surface. We can construct two types of “rules” based on this idea, the first

focused locally on the methyl being added, and the second globally by taking into account all the methyls on the surface: at every step, either (1) the number of neighbors adjacent only to the methyl being added determines the success of the reaction, or (2) the number of neighbors that *any* methyl experiences as a result of a functionalization reaction (not just the methyl being added) determines the success of the reaction. The former we will refer to as the “local” perspective, and the second as the “global” perspective. Both may contribute to our experimental observations, but we make this distinction for the purposes of thinking about whether the environment of methyls that are already on the surface need to be taken into consideration during each methylation reaction. We will explore how the coverage is limited based on these two perspectives using simulations in the next section.

3.3.5 Models of expected coverage under various constraints

We can model the simulation based on our understanding of the system from the local vs global perspectives, by focusing only on the environment of the methyl being added, or the environments of all methyls on the surface after each functionalization step. We developed models and simulated random functionalization based on both perspectives, the results of which we will discuss in this section. The common thread across the models tested is that they all rely on the idea that the number of nearest neighbors is a key factor: in the local perspective, we consider only the number of neighbors experienced by the methyl being added, and in the global perspective we consider the number of neighbors experienced by any methyl on the surface, not just the one being added. The perspective that is most applicable depends on the influence of functional groups on the thermodynamics and transition state of the reaction as a function of their distance from the reaction site.

Below, we will discuss several simulation cases that reflect certain “rules” regarding how methylation of MoS₂ proceeds based on assumptions inspired by the results discussed in sections 3.3.2–3.3.4. Under the constraints of each set of rules, which we refer to as a model, we simulated the random addition of functional groups to a 100×100 grid, $N = 2000$ times, to obtain a distribution of coverages and an average coverage per MoS₂ (i.e. every two sulfurs) for each model. For all simulations, high-S were excluded from functionalization

given the results in sections 3.3.2–3.3.3. We will discuss the models from the most restrictive constraints to the least restrictive constraints and establish non-trivial lower and upper bounds for coverage (i.e. greater than 0% and less than 100%). The code for all simulations discussed in this section can be found in Appendix D.

In the simplest and most restrictive case, no nearest neighbors are allowed for any methyl group (“0-neighbor max”). From the global perspective, every reaction step needs to result in a surface where no functional groups are adjacent to any other group. From the local perspective, each reaction occurs if the reaction site is not adjacent to existing functional groups. The implementation of these two perspectives happens to correspond to the same set of products, because an algorithm that limits functionalization next to existing functional groups (local) also produces a result where no two groups are adjacent (global). Thus, we modeled this using an algorithm that prohibits functionalization at any spot adjacent to a functional group, until all possible spots have been exhausted (Appendix D.1.1). Using this model, we obtained an average coverage and standard deviation of $43.5 \pm 0.2\%$ after 2000 simulations (Figure 3.20a).

Beyond the “0-neighbor max” case, the two perspectives diverge and require different algorithms. The reason for this is that the global perspective looks at the final state of all functional groups, for example by requiring *all* functional groups to have a maximum of X neighbors in the final state, whereas the local perspective looks only at the number of neighbors for the current reaction site and does not consider the number of neighbors for sites that are already functionalized. An algorithm that limits reactions to sites where there is at most 1 neighbor next to the reaction site (local constraint) can still produce in final state where there are multiple functional groups in a row if each group is added to the outermost position of the chain at every step. Therefore, we will discuss two models stemming from a “1-neighbor max” perspective: a “global 1-neighbor max” and a “local 1-neighbor max.”

To simulate the “global 1-neighbor max” constraint, we used an algorithm that allows functionalization at a reaction site only if there are no more than 2 adjacent low-S anywhere on the surface after the current step. If this is not the case, the site is not functionalized. This

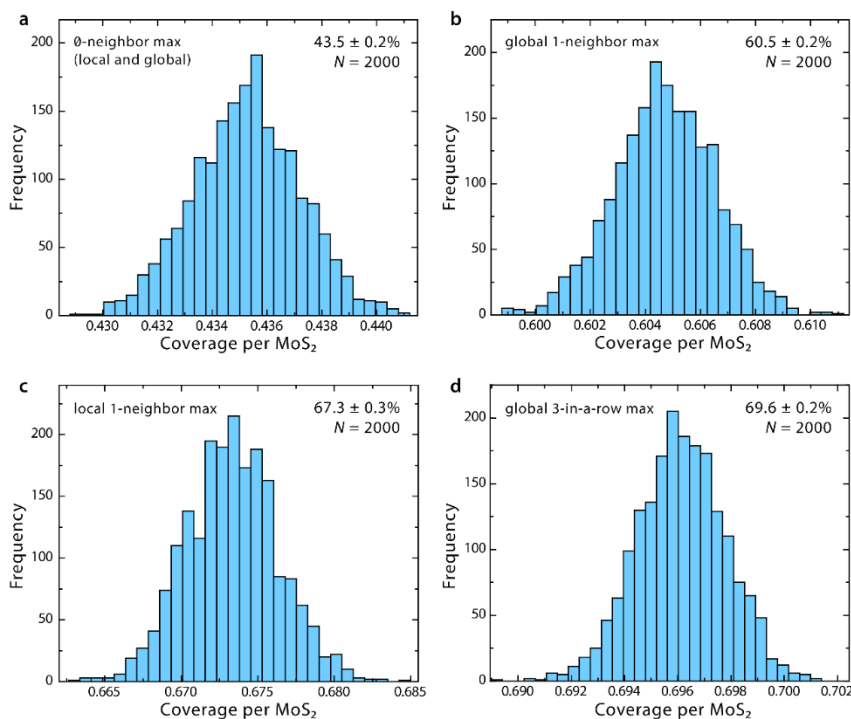


Figure 3.20. Histograms of the coverage distributions from simulations of the random functionalization of a 100×100 grid ($N = 2000$, 30 bins) of four models and the resulting average and standard deviations. Half of the sites represent low-S and half represent high-S; high-S are not functionalized in any of these models: (a) the “0-neighbor max” model that only allows functionalization on sites surrounded by empty sites, (b) the “global 1-neighbor max” model that allows functionalization if the result is no more than 1 neighbor adjacent to any group on the surface, (c) the “local 1-neighbor max” model that allows functionalization if the site being functionalized has at most 1 neighbor at the time of addition, and (d) the “global 3-in-a-row max” model that allows functionalization if the resulting layout has no more than 3 functional groups in a row.

proceeds until there are no more valid positions to functionalize (Appendix D.1.2). The resulting average coverage from this model is $60.5 \pm 0.2\%$ ($N = 2000$) (Figure 3.20b).

To simulate the “local 1-neighbor max” constraint, we used an algorithm that allows each functionalization step to proceed after first checking that there is no more than 1 adjacent functionalized site to the position being functionalized. This proceeds until there are no more valid positions to functionalize (Appendix D.1.3). The average coverage from this model is $67.3 \pm 0.3\%$ ($N = 2000$) (Figure 3.20c).

If we follow the above pattern in a similar vein to a “2-neighbor maximum” case, we would obtain 100% coverage per MoS_2 in both the global and local cases, because 2 is exactly the

maximum number of available low-S positions adjacent to any low-S position. Thus, to obtain a non-trivial coverage result, we simulated a process that allows up to 3 functional groups in a row (“global 3-in-a-row max”). The reasoning for including this model is that for a group of 3-in-a-row methyls, although the middle group experiences 2 neighbors, the outermost groups can accommodate the middle group and ease the steric hinderance, as reflected in the methyl rotational barriers discussed in Section 3.3.4. To simulate this, we employed the same algorithm as for the “global 1-neighbor max,” except this time checking for no more than 3 adjacent functionalized sites after each functionalization (Appendix D.1.4). The resulting coverage from this model is $69.6 \pm 0.2\%$ ($N = 2000$) (Figure 3.20d).

In the following paragraphs, we will discuss how the coverages from the models above may be in alignment with the experimentally observed coverages discussed in Chapter 2. The simulation and experimental results are listed side-by-side for comparison in Table 3.1.

Table 3.1. Coverage per MoS₂ obtained experimentally using reductant-activated functionalization and theoretically using simulations, expressed as an average and standard deviation. The theoretical results were obtained using simulations based on different assumptions on the allowed number of neighbors on a local vs global scale. Experimental results are based on data shown in Figure 2.8.

Experimental Coverage Data		Modeled Coverage	
Reductant	Coverage per MoS ₂ ($N = 3$)	Algorithm	Coverage per MoS ₂ (100×100 , $N = 2000$)
None	$41 \pm 4\%$	0-neighbor max	$43.5 \pm 0.2\%$
Ferrocene	$43 \pm 3\%$	Global 1-neighbor max	$60.5 \pm 0.2\%$
Nickelocene	$52 \pm 1\%$	Local 1-neighbor max	$67.3 \pm 0.3\%$
Octamethylnickelocene	$59 \pm 4\%$	Global 3-in-a-row max	$69.6 \pm 0.2\%$
Cobaltocene	$64 \pm 2\%$		
Decamethylcobaltocene	$56 \pm 0.3\%$		

For the experimental and simulation conditions with the lowest coverage, the average experimental coverage in the no-reductant case is $41 \pm 4\%$ ($N = 3$) and is close to the simulated average coverage of $43.5 \pm 0.2\%$ ($N = 2000$) in the 0-neighbor max simulation. We found through DFT calculations discussed Section 3.3.3 that the thermodynamic favorability of adding methyls with no neighbors is consistent regardless of the number of methyls prior to the reaction (except for the first methylation which is less favorable). Therefore, it is possible that the experimental coverage in the no-reductant and ferrocene

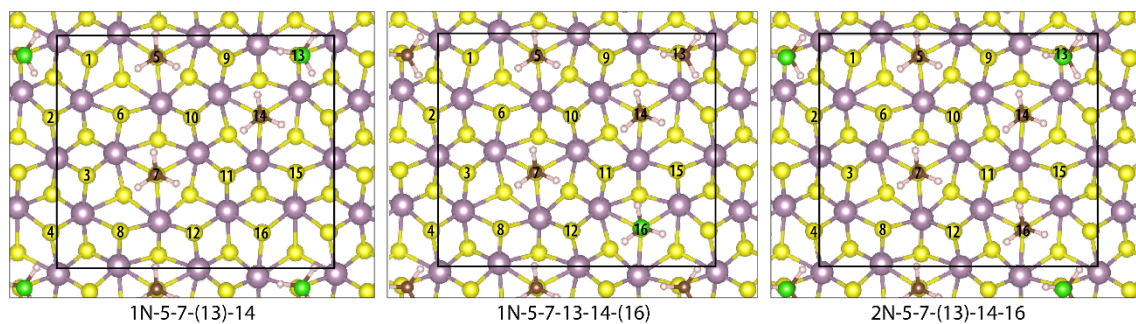


Figure 3.21. Top-down views of the final product for 3 reactions: 1N-5-7-(13)-14 (left), 1N-5-7-13-14-(16) (middle), and 2N-5-7-(13)-14-16 (right). The latter two reactions result in the same pattern of methylation on S5, S7, S13, S14, and S16. For 1N-5-7-13-14-(16) (middle), the most recent methyl added is on S16, whereas for 2N-5-7-(13)-14-16 (right), the most recent methyl added is on S13.

conditions reflect the random addition of methyl groups when there are no nearest neighbors, and that functionalization occurs on only half of all the sulfurs on the surface (low-S). Since this also implies that there are no neighbors for *any* methyls on the surface after all the functionalization steps, it is not necessary to distinguish between the local vs global perspective in this case.

However, this is not the case if we turn our attention to explain the highest observed coverage, $64 \pm 2\%$ ($N = 3$), that was obtained using cobaltocene reductant-activated addition. The simulated coverage distribution using the “global 1-neighbor max”, “local 1-neighbor max”, and “global 3-in-a-row max” models were $60.5 \pm 0.2\%$, $67.3 \pm 0.2\%$, and $69.6 \pm 0.2\%$, respectively ($N = 2000$). To decide which of these models is the most likely descriptor for the experimental data, we can use the results from Section 3.3.3 that compared the thermodynamics of two reactions which produced the same pattern of methyls on the surface (3-in-a-row) but achieved via the addition of either the middle methyl or an edge methyl, such that the reaction involved either 2 or 1 nearest neighbor(s), respectively. This comparison was made for the reactions 1N-5-7-13-14-(16) and 2N-5-7-(13)-14-16 in section 3.3.3, plotted in Figure 3.14, revealing that the ΔG for 2N-5-7-(13)-14-16 is 0.5 eV higher than for 1N-5-7-13-14-(16). The methylation pattern is shown above in Figure 3.21.

If we assume that the thermodynamics is reflective of the kinetics, which it appears to be for the first methylation reaction (Figure 3.7), then this suggests that the kinetics of the 2N-5-7-(13)-14-16 reaction is also slower than the 1N-5-7-13-14-(16) reaction. Thus, despite these

reactions both resulting in 3 methyls in a row, the reaction with only 1 neighbor next to the reaction site proceeds much more favorably than the reaction with 2 neighbors.

An interesting counterexample to using 1-neighbor as a constraint can be seen if we compare the 1-neighbor reactions 1N-5-7-(13)-14 and 1N-5-7-13-14-(16), where the ΔG of the former reaction is consistently ~ 0.5 eV more positive than the latter, which is as large as the disparity between 2N and 0N reactions. Note that the latter reaction can be viewed as an extension of the former reaction, i.e., adding the 5th methyl at S16 after the addition the 4th methyl was added at S13. By looking at the final structures resulting from 1N-5-7-(13)-14 and 1N-5-7-13-14-(16) above in Figure 3.21, we see that the S13 methyl group is more strained than any other methyl group, with the CH₃ group tilting sideways from the sulfur. After the 5th methyl is added at S16, it adopts a similar conformation to the S14 methyl that was already on the surface. It appears that although the methylation of S13 is unfavorable due to strain, once it is functionalized and provides space for the S14 methyl, space also becomes available for the S16 methyl to add with little additional strain.

From this example, it appears that the strain, and thus the ΔG of reaction, varies between reactions categorized as 1N reactions. For this reason, the 1-neighbor maximum models should be interpreted as an upper bound that captures a range of 1N reactions, some of which are much more favored than others. We did not simulate a model that includes 2N reactions with ΔG values similar to the unfavorable 1N reaction since the resultant coverage would be $> 100\%$ which was not observed experimentally.

Given this disparity in the reaction thermodynamics for two reactions that result in the exact same product and their differences isolated to the local environment of the methylation reaction site, we believe the most appropriate perspective to understand the coverage obtained using cobaltocene, which ranged from 63–67%, is that it reflects the expected outcome of the “local 1-neighbor max” model. From the simulated coverage distribution, this suggests an average upper bound of $67.3 \pm 0.3\%$ ($N = 2000$) coverage, with a range around 66.3 to 68.5% if all available sites within this constraint are functionalized each time. Methyl coverage, then, is ultimately limited by the unfavorable steric hinderance experienced

by the addition of a methyl group between two other methyl groups. It is possible that the “local 1-neighbor max” and the “global 3-in-a-row max” models are both contributing, e.g., if each methylation can occur next to at most one methyl, but not if there are already 3 methyls in a row due to the steric hinderance for the existing methyls. But, since the coverage distribution for “global 3-in-a-row” is higher than for “local 1-neighbor max,” it would not affect the upper limit of the expected coverage under our current hypothesis. More MoS₂ units would be required in the unit cell of the DFT calculations to have enough space for 4 adjacent methyls and an empty site, which we leave as future work.

In a similar fashion, we argue that the “0-neighbor max” model reflects the lower bound of coverage distributions at $43.5 \pm 0.2\%$ (range of 42.9–44.1%), since we saw that methylation is more thermodynamically favorable than the first methylation reaction regardless of the number of methyl groups on the surface, as long as each reaction is surrounded by empty sites (Figure 3.17). If we assume that methylation in the no-reductant and ferrocene conditions proceeds only for the sites that are easiest to functionalize, then the “0-neighbor max” model represents an upper bound coverage distribution for these conditions.

3.4 Conclusion

In this chapter, we used density functional theory to explain the coverage limitations observed in Chapter 2 for the methylation of chemically exfoliated MoS₂ in the 1T' phase. We discovered that it is substantially more favorable both thermodynamically and kinetically to methylate low-S rather than high-S at any potential between 0.5 to –0.9 V vs SHE, which accounts for half of the sulfurs on the surface. In addition, subsequent methylation reactions proceed depending on the steric hinderance associated with the methyl addition, which can be simplified in terms of the number of nearest neighbors during the reaction. The reaction is substantially less favored thermodynamically when there are two neighbors compared to when there are none. We can model this neighbor effect on the upper limit of coverage using a “local 1-neighbor max” algorithm to simulate random functionalization of low-S on a 100×100 grid of sulfurs, resulting in an expected coverage distribution centered at $67.3 \pm 0.3\%$ per MoS₂ based on 2000 simulations. This model encompasses the highest coverage

observed in the experimental data, which was $64 \pm 2\%$ using cobaltocene, and suggests to us that the coverage obtained using cobaltocene is indeed the highest coverage achievable on 1T'-MoS₂. However, further examples of 1-neighbor reactions should be studied to elucidate the conditions where 1-neighbor reactions are favored vs restricted, since we observed both examples here. In the next chapter, we will discuss our investigation of reductant-activated WS₂ methylation, compare the results to MoS₂ methylation, and explain the differences in coverage using a combination of experimental and theoretical techniques.

Chapter 4: Comparison of Reductant-Activated Functionalization on WS₂ vs MoS₂

4.1 Introduction

Tungsten disulfide (WS₂) is a layered material that belongs to the same group of transition metal dichalcogenides (TMDs) as MoS₂ with the formula MX₂, where M = Mo, W, and X = S, Se.² Tellurides are not typically included in discussions of TMDs because although WS₂, MoSe₂, and WSe₂ are similar to MoS₂ in their structure and phases, molybdenum and tungsten tellurides have semi-metallic characteristics in their natural 1T' phase.^{2, 21} Having developed a reductant-activated functionalization method for MoS₂ that shows a consistent increase in surface coverage as the reductant potential increases using both methyl and propyl functional groups in Chapter 2, we now seek to explore and understand the versatility and limits of this one-electron metallocene reductant-activated functionalization method in terms of how it can (or cannot) be readily applied to other materials. By investigating the adaptability of this method in various types of reactions, we can build a foundation of understanding for the important parameters that influence functionalization, which future researchers can use in untested scenarios.

To extend the utility of reductant-activated functionalization beyond MoS₂ and TMDs to other chalcogenides, pnictides, and even the carbon and boron groups, a natural starting point is to look at and compare the efficacy of reductant-activated functionalization on WS₂, MoSe₂, and WSe₂, as these TMDs belong to the same group as MoS₂, and their surface chemistry is the most similar. In fact, the intercalation and exfoliation functionalization in the absence of reductant on which this work is based is known to be applicable to MoS₂, WS₂, and MoSe₂.¹⁹ Unfortunately, the Se3*d* peaks in the XPS spectra are highly overlapping and thus not amenable for quantification of the functionalized Se–C peak, making it difficult to measure changes in coverage to a meaningful level of precision for selenides. For this reason, we focus solely on comparing WS₂ to MoS₂. We will study the methylation reaction using methyl iodide as a system with minimal impact from steric limitations. By comparing

the effects of reductant-activated functionalization on two similar materials first, we hope to set a foundation for understanding how this method may be applied to other chalcogenides and beyond.

4.2 Experimental Design

To compare the effects of reductant-activated functionalization on chemically exfoliated WS₂ (*ce*WS₂) vs MoS₂ (*ce*MoS₂), *ce*WS₂ was reacted with methyl iodide in the presence of one-electron metallocene reductants. To maintain consistency with metallocene reductants previously used to increase the methyl coverage on *ce*MoS₂, the same five reductants were used: ferrocene (Cp₂Fe), nickelocene (Cp₂Ni), octamethylnickelocene (Me₈Cp₂Ni), cobaltocene (Cp₂Co), and decamethylcobaltocene (Me₁₀Cp₂Co). The same procedure was used to intercalate and exfoliate WS₂ as for MoS₂ (Figure 2.1). We chose to compare only the case of functionalization with methyl iodide to observe the reductant effects without steric limitations. The procedure varied from 2–3 days in terms of the duration of the functionalization step. Experiments showed that these 1-day variations did not impact the coverage to an observable degree (see Results and Discussion), indicating that the coverages obtained were in the thermodynamic limit. See Appendix A for experimental details.

4.3 Results and Discussion

4.3.1 Methyl coverage of WS₂ vs MoS₂ using reductant-activated functionalization and influence of reaction time and temperature on coverage

The coverage was quantified based on the XPS S2*p* peaks using the percentage of the S2*p* peak area belonging to functionalized sulfur (S–C bonds). Figure 4.1 shows the characteristic XPS W4*f* and S2*p* regions for *ce*WS₂ before and after methyl functionalization and the additional S2*p* peak at ~163.3 eV indicative of functionalized sulfur. A new set of XPS fitting parameters was developed for WS₂ samples in addition to the one used for MoS₂ samples in Chapter 2, based on spectra of two *ce*WS₂ and two *ce*MoS₂ samples that were handled entirely under inert atmosphere with air-free transfer to the XPS instrument for XPS and UPS

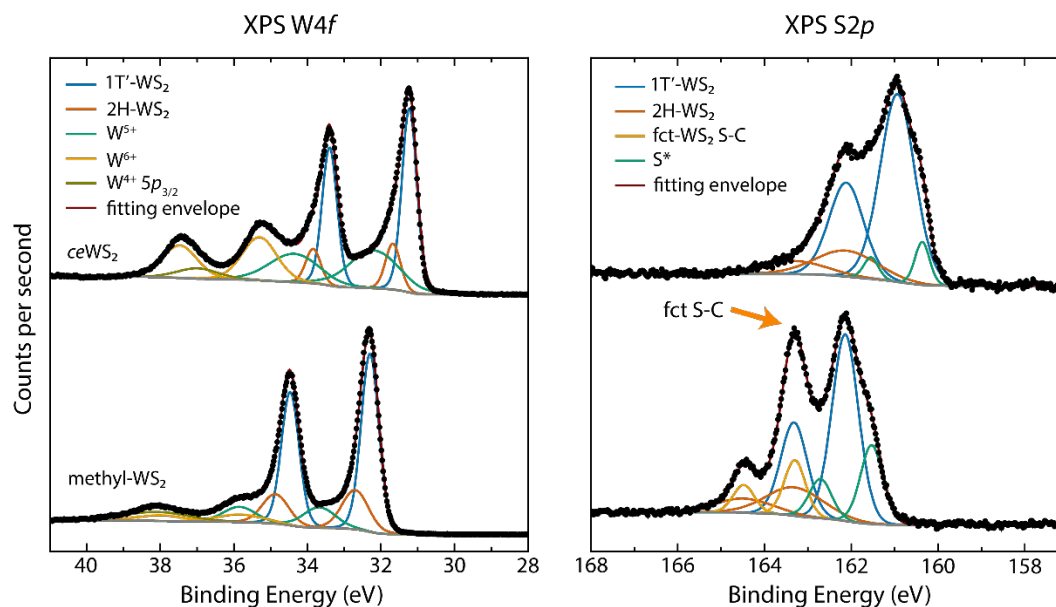


Figure 4.1. X-ray photoelectron spectra (XPS) of $W4f$ and $S2p$ regions for $ceWS_2$ and methyl- WS_2 synthesized with iodomethane and no reductant. Black dots are the raw data points and lines fit the peaks according to different species. For pure W-containing compounds, $W5p_{3/2}$ separates well from $W4f$. However, for samples in which W has several chemical states, the $W5p_{3/2}$ signal from lower chemical states overlaps with $W4f_{5/2}$ peak from higher chemical states,¹⁰⁰ which we also observe here.

measurements. These parameters are provided in Appendix B. Previous work indicates that functionalized $ceMoS_2$ and $ceWS_2$ remain in the $1T'$ phase.^{19, 85}

Figure 4.2 graphs the UPS measurements of air-free $ceMoS_2$ and $ceWS_2$ in the high-energy cutoff and valence band regions. These measurements resulted in average work functions of 4.11 eV and 3.94 eV for air-free $ceMoS_2$ and $ceWS_2$ samples (2 each), respectively. That the work function of $ceWS_2$ is lower than of $ceMoS_2$ is not surprising given that in the $2H$ phase, the conduction band minimum and valence band maximum of WX_2 s has been found experimentally and theoretically to be higher than those of the corresponding MoX_2 .¹⁰¹⁻¹⁰³ Note that these samples were not heated to remove adventitious carbon *in situ* prior to the UPS measurement, and thus unavoidably contain the influence of adventitious carbon. To determine the absolute work function with greater accuracy and precision, future work should attempt to remove adventitious carbon in the XPS instrument *in situ* with mild heating and measure more samples to verify this trend. The current data suggests that the work function of $ceWS_2$ is lower compared to $ceMoS_2$, and thus for reactions held at a particular

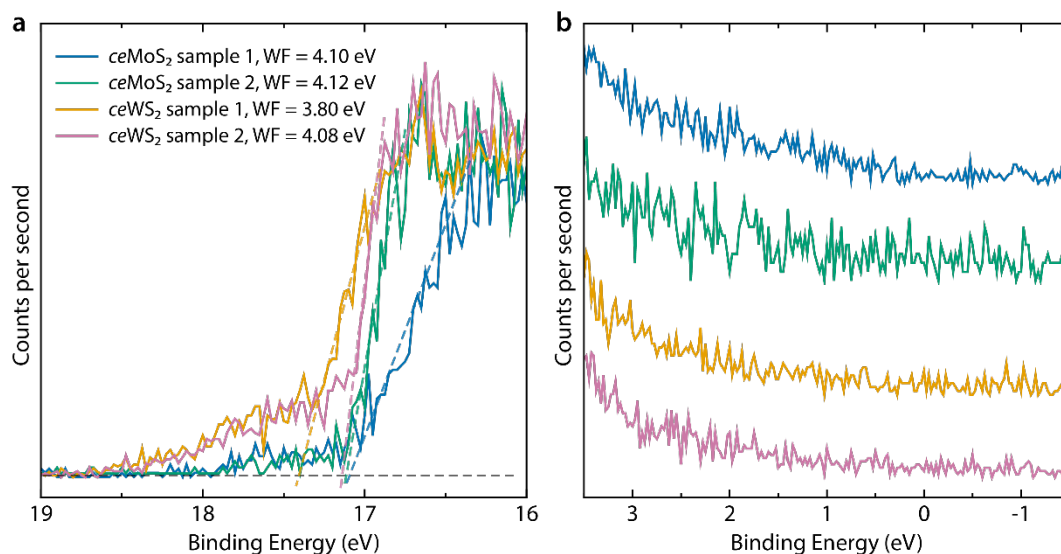


Figure 4.2. Ultraviolet photoelectron spectra (UPS) of chemically exfoliated MoS₂ and WS₂ samples prepared and transferred under inert atmosphere. (a) The high binding energy cutoff and linear fits used to obtain the work function of drop cast nanosheets. (b) Valence-band regime for the same samples, showing a band gap near zero, consistent with reported calculations.^{14, 16}

potential, there is less driving force for the reductant to donate electrons to *ceWS*₂ compared to *ceMoS*₂.

Figure 4.3a shows the coverages of functionalized *ceWS*₂ and *ceMoS*₂ samples as quantified by XPS S2*p* peaks following reductant-activated functionalization with methyl iodide, as a function of the effective solution potential assuming a reductant-to-oxidant ratio of 50:1. The methyl coverage increases as the reductant strength increases for both materials, with the highest coverages resulting from the addition of cobaltocene to the reaction. However, the average methyl coverage on WS₂ is lower than on MoS₂ for every condition. The average coverage on *ceWS*₂ is $52 \pm 7\%$ in the cobaltocene condition and $25 \pm 3\%$ in the no-reductant condition, whereas the average coverage on *ceMoS*₂ is $64 \pm 2\%$ and $41 \pm 3\%$ in the cobaltocene and no-reductant conditions respectively, resulting in a maximum relative coverage increase of 110% for *ceWS*₂ and 60% for *ceMoS*₂. Increasing the reduction potential from cobaltocene to decamethylcobaltocene resulted in lower coverages on both *ceMoS*₂ and *ceWS*₂. No significant difference was observed between ferrocene and no reductant (Figure 4.3b).

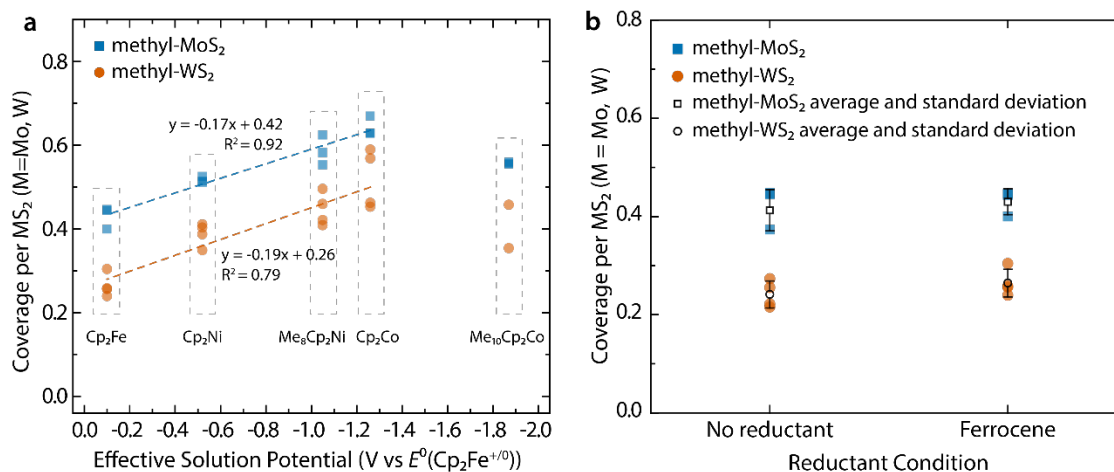


Figure 4.3. (a) Methyl coverage on $ceMoS_2$ and $ceWS_2$ after reacting with methyl iodide in the presence of various one-electron metallocene reductants as a function of the effective solution potential. The effective solution potentials were determined by correcting the formal potential with a 50:1 reductant-to-oxidant ratio for ferrocene, nickelocene, octamethylnickelocene, cobaltocene, and decamethylcobaltocene in order of reductant strength. Coverage increases as reductant strength increases for both materials, and decreases beyond cobaltocene, while $ceWS_2$ consistently achieves lower coverage compared to $ceMoS_2$. Lines are linear fits using least squares linear regression of points excluding those for decamethylcobaltocene. (b) Methyl coverage per MS_2 (M = Mo, W) after reacting with iodomethane either with no reductant added or in the presence of ferrocene, as determined by fitting XPS spectra. Individual points represent a single experiment and hollow symbols indicate the average with standard deviation as error bars. No substantial differences can be observed between these two conditions for either $ceMoS_2$ or $ceWS_2$.

We also tested the effect of reaction time on WS_2 methyl coverage in the range of 1–5 days, since the reaction times for functionalization experiments varied between 2–5 days between $ceWS_2$ and $ceMoS_2$. Figure 4.4a shows the WS_2 methyl coverage as a function of reaction time between methyl iodide and $ceWS_2$, either with no reductant or in the presence of octamethylnickelocene. Methyl coverage did not vary substantially on the time scale of 1–5 days for both conditions, indicating that the reaction reaches the thermodynamic limit at 1–2 days and that varying the reaction time between 2–5 days does not noticeably affect the coverage. ^{13}C MAS NMR spectra were not obtained for the WS_2 trend and remains to be investigated in future work.

Figure 4.4b shows the results from temperature-dependence experiments which reveal that increasing the reaction temperature above room temperature did not substantially improve the methyl coverage. For these experiments, $ceWS_2$ and methyl iodide were reacted for 2 days at four temperatures (room temperature ~ 22 °C, 50 °C, 70 °C, or 90 °C) and under 4

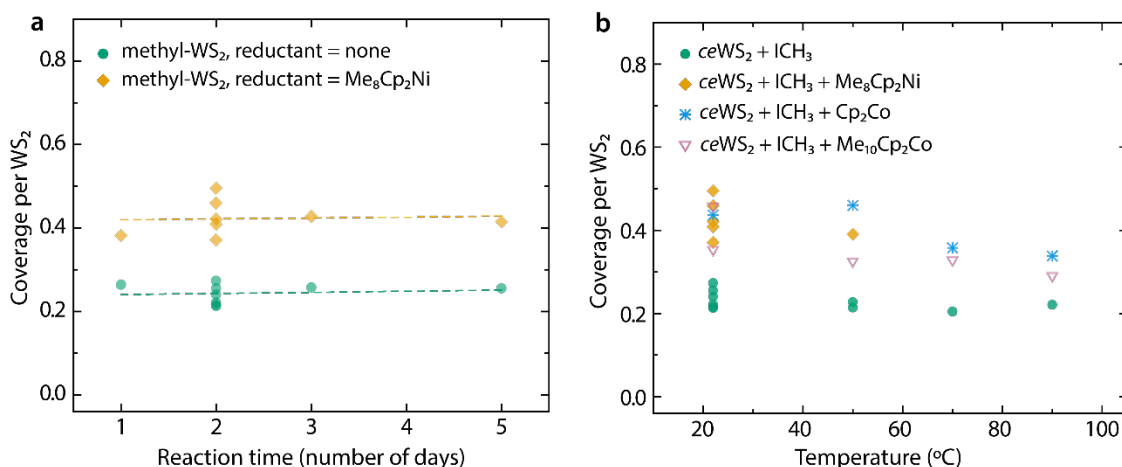


Figure 4.4. (a) Methyl coverage on *ceWS*₂ after reacting with methyl iodide in the presence of no reductant or with octamethylnickelocene as a function of reaction time. In both graphs, results from each reaction are shown as individual points to convey the distribution of values. Opacity is set of 60% to allow visualization of overlapping points. (b) Methyl coverage on *ceWS*₂ after reacting with methyl iodide in the presence of various reductants (none, octamethylnickelocene, cobaltocene, and decamethylcobaltocene) as a function of reaction temperature. No substantial differences were observed between room temperature and 50 °C, while coverage stayed the same or decreased for reaction temperatures above 50 °C.

redox conditions (no reductant, octamethylnickelocene, cobaltocene, or decamethylcobaltocene). Not only did temperatures above room temperature not result in a substantial increase in coverage for any of these conditions, but temperatures above 50 °C appear to decrease the coverage. Temperatures above 90 °C were not used in order to minimize phase conversion from 1T' to 2H.

Given that *MoS*₂ and *WS*₂ undergo the same reaction mechanism with methyl iodide, a question that remains is why the coverage on *WS*₂ is consistently lower than that of *MoS*₂. This may be due to: (1) differences in the distribution or quantity of stored negative charge, both of which would affect the number of sulfurs with sufficient nucleophilicity to participate in the *S*_N2 reaction, or (2) differences in nanosheet thickness which affects the fraction of sulfurs hidden from the surface. To address the question of charge distribution, we performed charge density calculations for 1×2 supercells of 1T'-*MS*₂ (M = Mo, W) using density functional theory (experimental details in Appendix A.6). Our results indicate that excess negative charge in 1T'-*MoS*₂ and 1T'-*WS*₂ is distributed similarly and concentrates on the sulfur atoms in both compounds. Figure 4.5 shows the charge density isosurfaces after

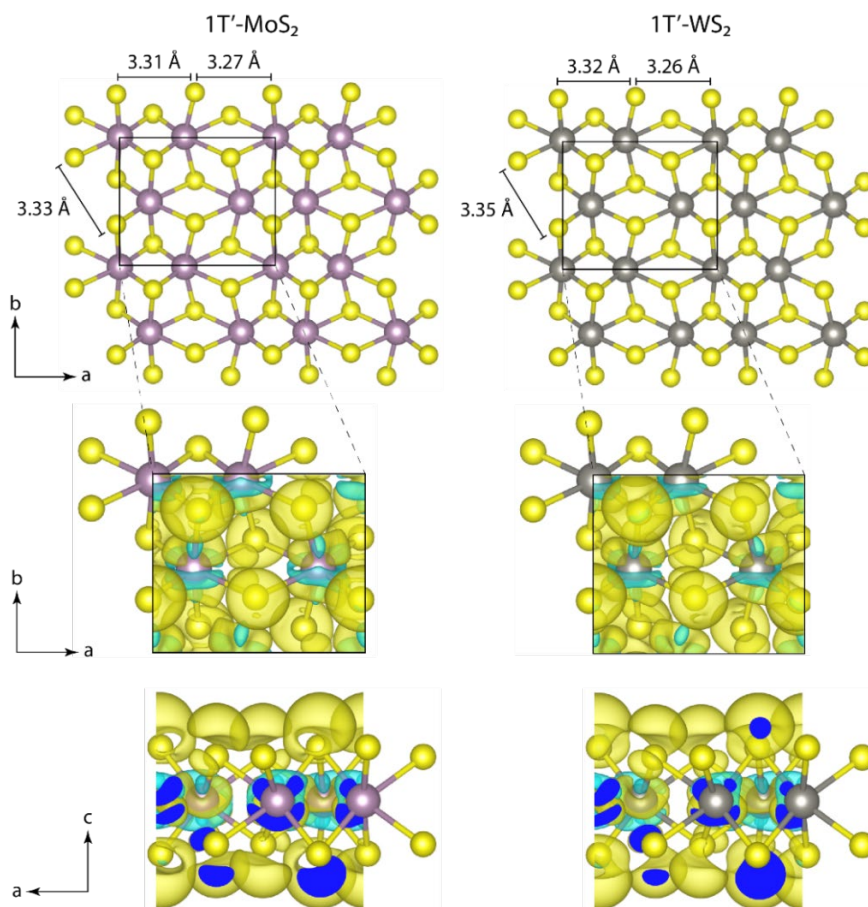


Figure 4.5. Charge density plot of 1T'-MoS₂ and 1T'-WS₂ using density functional theory (DFT) calculations after optimizing the structures. Charge density was calculated for neutral 1T'-MoS₂ and 1T'-WS₂, and with a -1 charge for both cases, to simulate a net charge of 0.25 per MS₂ (M = Mo, W). The neutral charge density plot was subtracted from the -1 charge density plot for both cases to obtain the charge density difference whose isosurface is shown above. Both structures show similar distribution of the excess negative charge.

subtracting the charge density of the neutral 1T'-MS₂ from the 1T'-MS₂ with an excess of 0.25 electrons per MS₂. The bandgaps for neutral 1T'-MoS₂ and 1T'-WS₂ were 0.09 eV and 0.07 eV, whereas for negatively charged (0.25 per MS₂) 1T'-MoS₂ and 1T'-WS₂ were 0.02 eV and 0.01 eV, respectively. The bandgap for neutral 1T'-MoS₂ matches the spectroscopic studies and calculated bandgaps from previous studies.^{16, 20}

4.3.2 Zeta potentials and particle sizes of *ce*WS₂, *ce*MoS₂, *fct*-WS₂, and *fct*-MoS₂

To determine whether the surface potential of *ce*WS₂ is as negative as *ce*MoS₂ after intercalation and exfoliation, we performed zeta potential measurements for *ce*MoS₂, *ce*WS₂,

and reaction mixtures of $ceMoS_2/ceWS_2$ with methyl iodide. The zeta potential of a particle is the electric potential at the boundary of the double layer on the particle surface, between the mobile fluid and the fluid attached to the particle, and can be used to characterize the dispersion stability of particles in solution.¹⁰⁴⁻¹⁰⁵ Zeta potential values typically range from -100 mV to $+100$ mV, with highly dispersed particles possessing values greater than $+30$ mV or less than -30 mV. Since the zeta potential is sensitive to variations in pH and ionic strength and dilution is necessary in most cases to achieve a concentration low enough to measure particle mobility by light scattering techniques, the measured zeta potential does not reflect the true value of the zeta potential.¹⁰⁴ Even so, we can gain a qualitative and comparative understanding of the zeta potentials between $ceMoS_2$ and $ceWS_2$ without knowing their true zeta potentials under reaction conditions.

The particle sizes and zeta potentials for solutions of $ceMoS_2$, $ceWS_2$, $ceMoS_2$ with ICH_3 , and $ceWS_2$ with ICH_3 , were determined using dynamic light scattering. Each set of measurements consisted of 10 individual measurements, and particle size measurements

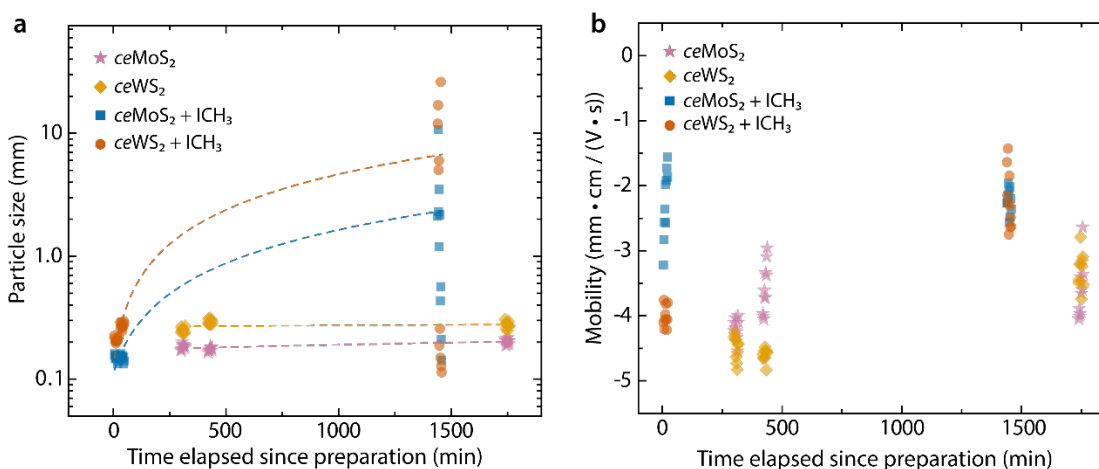


Figure 4.6. (a) Particle sizes of $ceMoS_2$, $ceWS_2$, $ceMoS_2 + ICH_3$, and $ceWS_2 + ICH_3$, as a function of time after sample preparation plotted on a log₁₀ y-axis. Linear fits are made using least squares linear regression. The accuracy of particle size measurements decreases for values above $1 \mu\text{m}$. The increase in particle size after methyl functionalization indicate increased aggregation. (b) Mobility measurements using dynamic light scattering of suspensions of $ceMoS_2$, $ceWS_2$, $ceMoS_2 + ICH_3$, and $ceWS_2 + ICH_3$, as a function of time since sample preparation. For both plots, each point is an individual measurement, with each cluster containing 10 data points, and each point is set to 60% opacity to visualize the distribution of overlapping points. Values plotted here were used to obtain the zeta potentials plotted in Figure 4.7 using the Smoluchowski model.

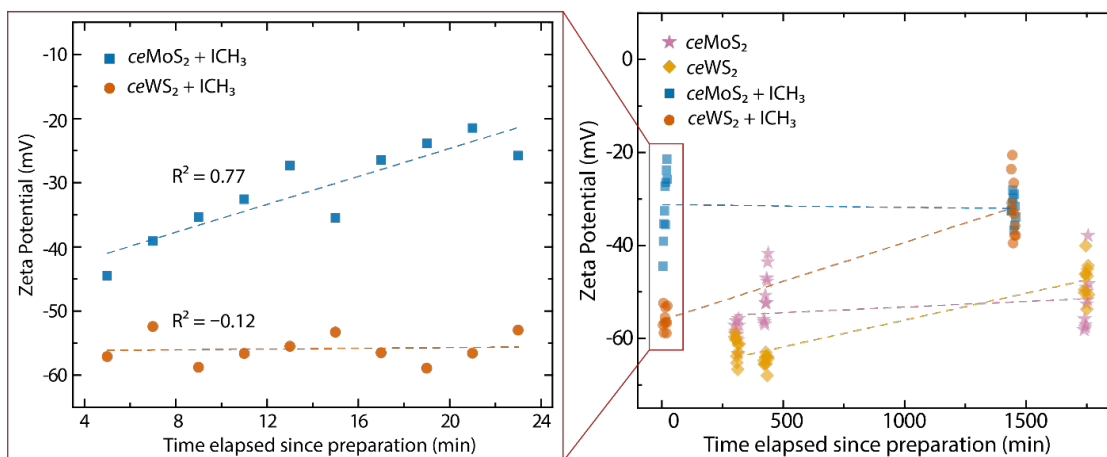


Figure 4.7. Zeta potential measurements for solutions of *ceMoS*₂, *ceWS*₂, *ceMoS*₂ + ICH₃, and *ceWS*₂ + ICH₃. Each point represents an individual measurement, with 60% opacity to show overlapping points. Left graph zooms in on the time frame from 5–25 minutes after sample preparation to show changes in zeta potential immediately after methyl iodide is added to *ceMoS*₂ and *ceWS*₂. Linear fits were made using least squares linear regression.

lasted ~ 10 seconds while zeta potential measurements lasted ~ 2 minutes. The particle size and mobility values were used to compute the zeta potential and are shown in Figure 4.6.

Figure 4.7 graphs the zeta potential measurements for *ceMoS*₂, *ceWS*₂, and the reactions *ceMoS*₂ + ICH₃, and *ceWS*₂ + ICH₃, as a function of the time elapsed since their preparation. The time of preparation for *ceMoS*₂ and *ceWS*₂ corresponds to the first addition of water to intercalated MoS₂ and WS₂, and for *ceMoS*₂ + ICH₃ and *ceWS*₂ + ICH₃ corresponds to the addition of methyl iodide. Since the exfoliated MS₂ (M = Mo, W) needed to be purified, there was a 5-hour period between the addition of water and the zeta potential measurement for *ceMS*₂, whereas the methyl iodide was added just before the particle size and zeta potential measurements for *ceMS*₂ + ICH₃. A second round of measurements for all four conditions was obtained after 24 hours. Table 4.1 lists the average and standard deviation of 10 points taken at each time cluster. Both *ceMoS*₂ and *ceWS*₂ had a zeta potential of ~ -60 mV 5 hours after exfoliation and ~ -50 mV 29 hours after exfoliation, suggesting that the surface potential is similar for both compounds. The *ceMoS*₂ zeta potential is similar to the reported value of -41 mV in a previous study.¹⁹

Table 4.1. Zeta potentials for solutions of $ceMoS_2$, $ceWS_2$, with and without methyl iodide, as a function of time after preparation. Averages and standard deviations are based on 10 measurements, each of which is plotted in Figure 4.7.

Time elapsed since preparation (minutes)	Zeta Potential (mV) (average \pm standard deviation)			
	$ceMoS_2$	$ceWS_2$	$ceMoS_2 + ICH_3$	$ceWS_2 + ICH_3$
5	–	–	-31 ± 7	-56 ± 2
300 (5 hours)	-57 ± 2	-62 ± 3	–	–
420 (7 hours)	-51 ± 5	-65 ± 1	–	–
1440 (24 hours)	–	–	-32 ± 3	-32 ± 6
1740 (29 hours)	-52 ± 4	-47 ± 4	–	–

The zoom-in graph from 5–25 minutes highlights a notable difference in kinetics between the $ceMoS_2 + ICH_3$ and $ceWS_2 + ICH_3$ reactions. Within the first 30 minutes of reacting $ceMoS_2$ with methyl iodide, the zeta potential shifted from ~ -45 mV to ~ -30 mV. In contrast, the zeta potential values for $ceWS_2 + ICH_3$ stayed relatively consistent in the first 30 minutes of reaction at ~ -55 mV. We hypothesize that at $t = 0$ in the $ceMoS_2 + ICH_3$ reaction, the zeta potential was similar to that of $ceMoS_2$ at ~ -60 mV and began to move in the positive direction as the reaction proceeded during the 5 minutes that elapsed for the particle size measurement. 24 hours later, the zeta potentials for both reactions averaged -32 mV. Using the zeta potential as an indirect measurement of the reaction progress, it appears that $ceMoS_2$ reacts orders of magnitude faster than $ceWS_2$ with methyl iodide. Given that the zeta potentials before and after functionalization are similar for both $ceMoS_2$ and $ceWS_2$, this data suggests that the lower methyl coverage on WS_2 compared to MoS_2 cannot be attributed to differences in surface potential.

4.3.3 Comparison of the thermodynamics and kinetics of WS_2 and MoS_2 methyl functionalization using density functional theory modeling

To supplement the experimental results discussed above, we performed density functional theory calculations for the methylation of 1T'- MoS_2 and WS_2 with $ClCH_3$ to assess whether theoretical calculations of the thermodynamics and kinetics for the first methyl addition can help explain the differences in coverages observed experimentally. To make the relevant

comparison, we used a previously developed grand canonical potential kinetics (GCP-K) formulation to convert the free energies obtained by fixed charge calculations to grand canonical potential (GCP) free energies at fixed potential.¹⁰⁶ The same process that was used in Chapter 3 (detailed in Appendix C.5) was used to interpolate the GCP free energy from potential for the initial, transition, and final states for the $\text{MoS}_2 + \text{ClCH}_3$ and $\text{WS}_2 + \text{ClCH}_3$ reactions. Six calculations for MoS_2 spanning 0.8 to -0.8 V vs SHE and seven calculations for WS_2 spanning 0.3 to -0.9 V vs SHE were used to interpolate the free energy vs potential curves of initial, transition, and final states. The interpolation process uses a quadratic fit of the free energy vs number of electrons, shown in Figure C.1 and discussed in Appendix C.

Figure 4.8 shows the dependence of the free energy (ΔG) of the reaction and the barrier height (ΔG^\ddagger) on the potential (V vs SHE) for the reactions $\text{MoS}_2 + \text{ClCH}_3$ and $\text{WS}_2 + \text{ClCH}_3$, with the methyl being added to S7 in both cases. At any given potential, ΔG is calculated as the final state GCP free energy subtracted by that of the initial state, and ΔG^\ddagger is calculated as the transition state GCP free energy subtracted by that of the initial state. These calculations indicate that ΔG of 1T'- MoS_2 methylation is ~ 0.2 – 0.4 eV more negative than the ΔG of 1T'- WS_2 methylation at every potential within the interpolation range, and the ΔG^\ddagger of MoS_2 and

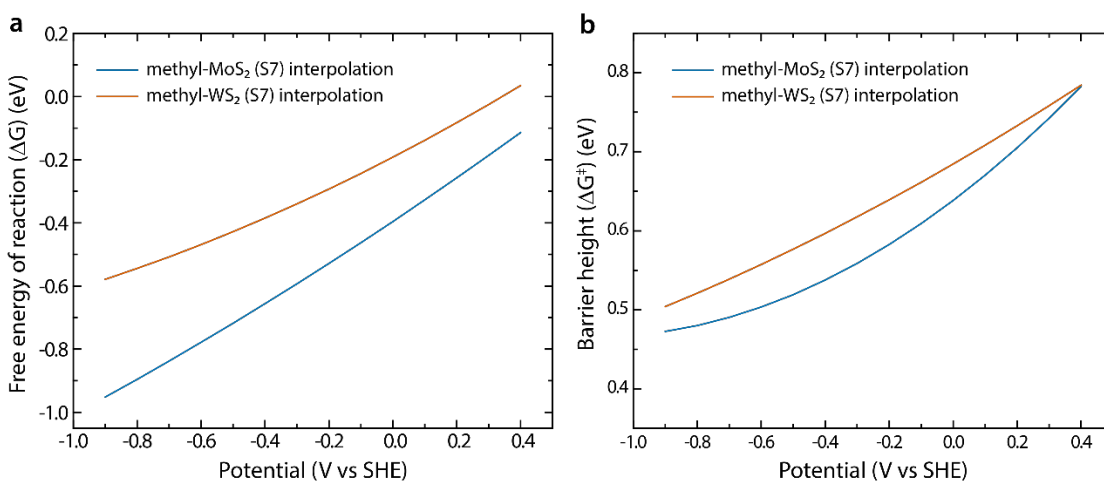


Figure 4.8. Interpolation in 0.1 V intervals of (a) the free energy and (b) the barrier height, of adding ClCH_3 to S7 (Figure 3.1) on 1T'- MoS_2 and WS_2 . The free energies and barrier heights are calculated by subtracting the initial state grand canonical potential from the final state grand canonical potential (for the free energy) or the transition state grand canonical potential (for the barrier height) at fixed potential for each reaction.

WS₂ methylation are similar at ~ -0.3 V vs SHE but diverge as the potential becomes more negative, with ΔG^\ddagger for MoS₂ methylation being ~ 0.05 eV lower than WS₂ methylation within the interpolation range. At 0.3 V vs SHE (the no-reductant condition) with a difference of 0.02 eV in barrier height, the rate constant k for MoS₂ methylation and WS₂ methylation differs by a factor of 2 at 1.7 s^{-1} and 0.9 s^{-1} , respectively. However, due to the exponential dependence of rate on the barrier height, at -0.1 V vs SHE (the nickelocene condition) with a 0.05 eV difference in barrier height, the rate differs by an order of magnitude with $k = 310 \text{ s}^{-1}$ for MoS₂ and $k = 41 \text{ s}^{-1}$ for WS₂. This difference in the rate constant is consistent with our observations that the zeta potential of the MoS₂ methylation reaction reaches the value of the functionalized product within 30 minutes, whereas for WS₂ it takes up to 24 hours.

Since our experiments show that the coverage does not change substantially after 1 day of reaction for WS₂ methylation (Figure 4.4), and we used a minimum of 2 days reaction time for the MoS₂ and WS₂ coverage data shown Figure 2.8 and Figure 4.3, the experimental coverages for WS₂ appear to be limited by thermodynamics rather than kinetics. We can deduce that the MoS₂ reactions also reached their thermodynamic limit since we observed in the zeta potential measurements (Section 4.3.2) that MoS₂ methylation occurs faster than WS₂. Figure 4.8a predicts that at any potential, MoS₂ methylation is more thermodynamically favorable than WS₂ methylation and suggests that for WS₂ methylation to have the same thermodynamic driving force as MoS₂ methylation, the potential for the WS₂ reaction should be performed between -0.3 V to -0.7 V relative to the MoS₂ reaction depending on the potential. From the linear fit of the experimental coverage data in Figure 4.3, we can calculate the potential at which WS₂ obtains the same methyl coverage that MoS₂ obtains in the absence of reductant. The ferrocene condition at -0.1 V vs $E^0(\text{Fc}^{+/0})$ showed no substantial effect on the coverage relative to the no-reductant case for both materials. At this potential, the MoS₂ methyl coverage is 0.44 per MoS₂. When the WS₂ methyl coverage is 0.44, the corresponding potential calculated using the linear fit is -0.9 V vs $E^0(\text{Fc}^{+/0})$, a difference of -0.8 V. Comparing this -0.8 V difference to the prediction based on the DFT thermodynamic calculations that WS₂ requires an additional -0.3 to -0.7 V of applied potential in order to achieve the same coverage as MoS₂, we can attribute a portion of our

experimental observations to differences in the thermodynamic favorability of the reaction, keeping in mind that these calculations are reflective of only the first methyl addition. This difference in thermodynamics between WS₂ and MoS₂ may be the result of tungsten having a higher electronegativity and larger size compared to molybdenum, allowing it to stabilize the negative charges on the sulfur which reduces the nucleophilicity of the sulfur atoms and makes WS₂ less prone to engage in a nucleophilic addition reaction.

4.4 Conclusion

Methyl coverage of chemically exfoliated WS₂ (*ceWS*₂) increases as the strength of the reductant in the reaction solution increases from nickelocene to cobaltocene, with the latter achieving a two-fold increase in coverage compared to the no-reductant case. Although this 110% increase in coverage on *ceWS*₂ is greater than the 60% increase observed on *ceMoS*₂, the methyl coverage on *ceMoS*₂ was consistently higher than on *ceWS*₂. Zeta potential measurements also confirmed that the surface potential of *ceWS*₂ is similar to that of *ceMoS*₂ before and after methylation with methyl iodide. These differences in coverage at constant potential can be explained by the thermodynamics of these reactions with support from DFT calculations showing that the ΔG of WS₂ methylation is consistently $\sim 0.2\text{--}0.4$ eV lower than the ΔG of MoS₂ methylation at constant potential, and that the driving force for WS₂ methylation can be made similar to that of MoS₂ if WS₂ methylation occurs -0.3 to -0.7 V relative to MoS₂. This explains a portion of the -0.8 V difference in the experimental data.

One hypothesis that was not tested in this work is the possibility that the average number of layers per nanosheet for *ceWS*₂ is higher than for *ceMoS*₂, resulting in fewer available basal plane sulfurs to participate in the reaction for *ceWS*₂. To address this hypothesis, atomic force microscopy (AFM) and Raman spectroscopy can be used in future work to determine the average number of layers in *ceMoS*₂ and *ceWS*₂ nanosheets. In addition, gently heating *ceMoS*₂ and *ceWS*₂ samples *in situ* in the XPS instrument prior to work function measurements in conjunction with a greater number of samples can help produce more accurate and precise absolute work function values in the future.

The results from this study suggest that reductant-activated functionalization using one-electron metallocenes has promising potential to be broadly applicable for chalcogenide functionalization, and possibly also for other nucleophilic compounds. The absolute coverage even amongst the most similar of materials will depend on the subtle differences in atomic properties, and DFT along with the grand canonical potential kinetics formulation can be useful tools to evaluate the expected differences in reactivity and coverage prior to experimental testing as a method of screening promising candidates. To evaluate the possibility of extending reductant-activated functionalization beyond chalcogenides, reductant-activated functionalization should be tested on non-chalcogenide compounds, and theoretical studies to predict the coverage as a function of reduction potential can help to direct research efforts.

Chapter 5: Conclusion and Outlook

We have developed and demonstrated a redox-based functionalization method that is versatile and tunable, enabling the control of surface functionalization coverage as a function of the solution potential. This method works by changing the solution potential using redox couples, or by applying a potential to control the potential of a *ce*MoS₂ electrode directly. Our results also indicate that a strong reductant such as cobaltocene can enable the functionalization of *ce*MoS₂ with weak electrophiles (e.g. 1-chloropropane), and of 2H-MoS₂ with good electrophiles (e.g. 1-bromo-4-fluorobutane and 2-iodo-1,1,1-trifluoroethane). We found that the highest coverage that we could obtain using reductant-activated coverage with the smallest carbon-based functional group, a methyl group, averaged ~64%.

Using density functional theory (DFT) calculations and simulations of random surface functionalization, we obtained two values which we believe represent the lower and upper bounds of expected coverage on *ce*MoS₂. From the DFT calculations, we found that methylation of low-S sulfurs is substantially more favorable than of high-S sulfurs both thermodynamically and kinetically. We also found a substantial difference in the thermodynamic favorability of methylation on sites with 2 adjacent methyl groups compared to those with none. Methylation of sites adjacent to 1 methyl group varied between these two extremes. By simulating the expected coverage based on random functionalization of the surface according to the constraint that allows either 0 or 1 adjacent functional group for each reaction, we obtained expected coverages of $43.5 \pm 0.2\%$ and $67.3 \pm 0.3\%$, which we believe can model the upper bounds of coverages in the experimental no-reductant and cobaltocene conditions, for which we observed ~40% and ~64% coverage, respectively.

Extending the experimental and theoretical methods used to functionalize *ce*MoS₂ to *ce*WS₂, we found the coverage on *ce*WS₂ also increases with increasing reduction potential. However, the coverage on *ce*WS₂ was consistently lower than on *ce*MoS₂ at every potential tested. Using zeta potential measurements, we found that the surface potentials for as-prepared *ce*MoS₂ and *ce*WS₂ are both ~ -60 mV. DFT calculations helped to explain this

coverage difference by revealing that 1T'-WS₂ methylation is consistently less favorable thermodynamically and kinetically compared to 1T'-MoS₂ methylation. The latter is consistent with zeta potential measurements, and the former helps to explain the differences in coverage observed experimentally in the thermodynamic limit. This investigation demonstrated the similarities in the coverage trend and differences in the absolute coverage that results from applying the same procedure to materials within the same group of compounds. Out of the three materials tested in this thesis, the highest coverages were achieved on *ce*MoS₂, followed by *ce*WS₂, and (unsurprisingly, due to its relatively inert properties) finally 2H-MoS₂. Understanding how to control coverage and achieve high densities is important for applying functionalized surfaces to control corrosion or recombination at edge sites, to create surface dipoles that tune relative band positions, to introduce chemically reactive handles for subsequent functionalization, and for use of such surfaces as absorption sensors. Any application that relies on the effects or signals produced by the functionalized surface requires quantitative control of the surface coverage.

In summary, we have found that the qualitative trend of increasing coverage with stronger reductants holds regardless of the phase of the material and the identity of the metal for compounds within the same group, whether it is 1T'-*ce*MoS₂ or 2H-MoS₂, or *ce*WS₂. The main difference is the absolute coverage that can be obtained with a given electrophile and a given potential. We expect that this will be the case when extending this method to other chalcogenides (such as GaS and GaSe, which has been previously functionalized with aryl halides),¹⁰⁷ the pnictides, and materials based on the carbon and boron groups. Since this method has yet to be systematically investigated on group 11, 12, 13, and other group 14 compounds, except for oxidant-activated functionalization on bulk and nanoparticle silicon, this is a fruitful area for further investigation.

As such, we propose that future work be performed in several areas: first, to extend the preliminary results herein on reductant-activated functionalization of 2H-MoS₂ with greater characterization of the product and use DFT to explain and predict the reactivity of 2H-MoS₂ to electrophiles and how reactivity does (or does not) depend on the presence of sulfur vacancies; second, to use the control afforded by reductant-activated functionalization to

synthesize multifunctional surfaces with mixed functional groups; third, to explore oxidant-activated functionalization on TMDs and merge the insights with the work herein into a holistic understanding of redox-activated functionalization on TMDs; fourth, to expand testing of redox-activated functionalization on compounds from groups 11, 12 and 13 (boron-based, carbon-based, and pnictides) and use DFT to explain the observed behavior; and finally in the course of the above, to explore oxidants, reductants, and electrochemical techniques not tested herein. Characterization of the stability and air-sensitivity of the functionalized products will also enable future researchers to identify and explore appropriate combinations for application-specific needs. Thus, there is a tremendous breadth of research to explore by employing the concept of redox-activated functionalization to the area of 2D materials functionalization.

Appendix A: Experimental and DFT Computational Methods

A.1 Materials

All organic solvents and reagents were purchased commercially and used as received without further purification. Molybdenum disulfide powder (99%), tungsten disulfide powder (99.8%), bis(cyclopentadienyl)nickel(II) (nickelocene), and bis(tetramethylcyclopentadienyl)nickel(II) (octamethylnickelocene) were purchased from Alfa Aesar. Anhydrous hexanes, anhydrous *N,N*-dimethylformamide (DMF), *n*-butyllithium (1.6 M in hexanes), bis(cyclopentadienyl)iron(II) (ferrocene), bis(pentamethylcyclopentadienyl)cobalt(II) (decamethylcobaltocene), and bis(cyclopentadienyl)cobalt(II) (cobaltocene), were purchased from Sigma-Aldrich. All the above chemicals were stored in an Ar- or N₂-filled glovebox (<5 ppm O₂), except for ferrocene. Nanopure water with a resistivity ≥ 18.2 M Ω ·cm was obtained from a Barnstead E-Pure system. The centrifuge used for purification was a Beckman Coulter Avanti J-20 XP centrifuge with a JA-17 fixed rotor, where $\text{rcf}(\times g) = 137.75 \times (\text{rpm}/1000)^2$.

A.2 Synthesis of Chemically Exfoliated MoS₂ (*ce*MoS₂) and WS₂ (*ce*WS₂)

MoS₂ or WS₂ powder (1 eq.) was intercalated with Li by heating to 98 °C with *n*-butyllithium (1.6 M in hexanes, 2.5 eq.) in a sealed glass pressure tube for 24 hours. The powder was filtered and washed with anhydrous hexanes (10 \times 2 mL), then exfoliated in H₂O at a maximum concentration of 0.14 M. The dispersion was sonicated for 1 h, then centrifuged at 2000 rpm (551 rcf) for 5 min to remove unexfoliated material. The supernatant was retained and centrifuged at 6000 rpm (4959 rcf) to obtain the precipitate, which was then washed with H₂O, and then with either H₂O if no other reactions will be performed, or anhydrous *N,N*-dimethylformamide (DMF) if the following reaction is functionalization in DMF. Samples of *ce*MoS₂ or *ce*WS₂ were drop cast from 1:1 water/methanol suspensions

onto p^+ -Si for XPS measurements and were dried *in vacuo* for 2 days for ATR-FTIR and NMR measurements.

A.3 Reductant-Activated Functionalization of $ceMoS_2$ and $ceWS_2$

Chemically exfoliated MoS_2 or WS_2 were suspended in 10 mL of DMF at a concentration of 0.1 M in a 20 mL scintillation vial. The concentration was determined by evaporating 0.1 mL of solution on tared weighing paper and measuring the mass difference using a microbalance. All functionalized MoS_2 and WS_2 samples were synthesized using DMF as the solvent unless otherwise indicated. The alkyl halide (10 eq.) and metallocene reductant (5 eq.) were added and the solution was stirred for 42 h (WS_2) or 66 h (MoS_2) while being covered in aluminum foil. No significant differences were observed in coverage between 42 h vs 66 h for MoS_2 and WS_2 functionalization. Metallocenes were added in either ambient conditions (ferrocene) or in an Ar-purged glovebox (nickelocene, octamethylnickelocene, cobaltocene, decamethylcobaltocene) after purging the TMD/DMF solution with Ar(g). The reductant was not added under no-reductant conditions. Centrifugation to wash the functionalized TMD was performed at 6500 rpm (5820 rcf) for 30 min rounds, and the precipitate was resuspended by sonication in between rounds. The product was washed with DMF until the metallocene color was not visible (typically 3-4 rounds \times 12 mL), then with isopropanol (2×12 mL) and methanol (2×12 mL). The final product was resuspended in 1:1 water/methanol for drop casting for XPS, and the solvent was removed *in vacuo* to obtain a dry powder for ATR-FTIR and NMR measurements.

A.4 Preparation of $ceMoS_2$ Electrodes and Open-Circuit Voltage Measurement

Pyrolytic graphite plates (GraphiteStore) were polished to a mirror finish with SiC polishing paper. Solutions containing $ceMoS_2$ suspended in nanopure water at a concentration of 3.4 mg/mL were diluted to 0.20 mg/mL in methanol and drop cast in 20 μ L aliquots to a total loading of 16 μ g onto graphite plates heated to 120 $^\circ$ C in air. Samples were stored under a dry nitrogen atmosphere ($O_2 < 1$ ppm) prior to testing. Silver pseudo reference electrodes

were prepared from a silver wire, polished with SiC paper to a bright finish, and sealed in a glass tube containing 0.10 M tetrabutyl ammonium perchlorate and 0.01 M silver nitrate. A Vycor frit was sealed to the end of the tube using heat-shrink tubing. Electrochemical cells were cleaned in 3:1 (v/v) $\text{HCl}_{(\text{aq})}/\text{HNO}_{3(\text{aq})}$ for 6 h, rinsed in deionized water, and dried in an oven at 120 °C. Tetrabutyl ammonium perchlorate (0.10 M) was dissolved in acetonitrile to serve as the working electrolyte, with methyl iodide (0.10 M) added immediately prior to electrochemical testing. A Pt wire served as a counter electrode and an Ag/Ag^+ wire was separated from the working electrolyte with a Vycor frit and served as the reference electrode. The potential of the Ag pseudo reference was calibrated to Fc/Fc^+ in a separate cell before and after testing. The cell was purged with N_2 prior to testing to remove dissolved O_2 and the headspace was continuously flushed with a small stream of N_2 throughout the experiment. The voltametric responses for three samples of ceMoS_2 film on polished pyrolytic graphite were obtained in a cell containing 0.10 M methyl iodide. The average open circuit voltage immediate after placement within the cell was -0.074 ± 0.006 V vs Fc/Fc^+ .

A.5 Sample Characterization

X-ray photoelectron spectroscopy (XPS) and ultraviolet photoelectron spectroscopy (UPS) data were collected using a Kratos AXIS Ultra spectrometer equipped with a hybrid magnetic and electrostatic electron lens system and a delay-line detector (DLD). The photoelectron-ejection vector was 90° with respect to the sample surface plane. XPS data were collected using a monochromatic Al $K\alpha$ X-ray source (1486.7 eV) at pressures $< 9 \times 10^{-9}$ Torr. The electron-collection lens aperture was set to sample a 700×300 μm spot, and the analyzer pass energy was 80 eV for survey spectra and 10 eV for high-resolution spectra. UPS data were collected using a He I ultraviolet source (21.2 eV) at a pressure of 1×10^{-8} Torr in the analysis chamber. The electron-collection lens aperture was set to a 55 μm spot size and the analyzer pass energy was 5 eV. The instrument energy scale and work function were calibrated using clean Au, Ag, and Cu standards. The instrument was operated by Vision Manager software v. 2.2.10 revision 5 and data was analyzed using CasaXPS software (CASA Software Ltd).

Attenuated total reflectance Fourier transform infrared spectroscopy (ATR-FTIR) data were collected using a Thermo Scientific Nicolet 6700 optical spectrometer with a IR6118 Diamond ATR Smart iTR accessory. The spectrometer was equipped with a deuterated L-alanine-doped triglycine sulfate (DLaTGS) detector, an electronically temperature-controlled (ETC) EverGlo mid-IR source, a N₂(g) purge, and a KBr beam splitter. The spectra reported herein are averages of 1000 scans at 2 cm⁻¹ resolution, background corrected using the spectrum of *ce*MoS₂. Spectra were collected and processed using OMNIC software v. 9.2.41.

Raman spectra were collected with a Renishaw inVia Raman microprobe equipped with a Leica DM 2500 M microscope, Leica N Plan 50x objective (numerical aperture = 0.75), 1800 lines mm⁻¹ grating, and CCD detector configured in a 180° backscatter geometry. A 532 nm diode-pumped solid-state (DPSS) laser (Renishaw RL532C50) was used as the excitation source. A $\lambda/4$ plate was used to circularly polarize the incident excitation. No polarizing collection optic was used.

The solid-state carbon-13 (125.4 MHz) nuclear magnetic resonance (NMR) spectra were acquired on a Bruker DSX-500 MHz NMR spectrometer using a Bruker 4.0 mm magic-angle spinning probe at ambient conditions. Samples were prepared by carefully packing dried functionalized MoS₂ powder in a zirconium rotor. For ¹³C cross-polarization magic angle spinning (¹³C CPMAS) NMR experiments, 8.0 kHz spin rate, 4 s recycle delay, 2 ms contact time, $\pi/2$ pulse width of 4 μ s, and typically 4000 scans using a TPPI ¹H decoupling method were used. The spectra were referenced to tetramethylsilane (TMS).

The particle sizes and zeta potentials were measured using Brookhaven Instruments Corporation Zeta-PALS instrument. Using nanopure H₂O, samples of *ce*MoS₂ and methyl-MoS₂ were diluted to 0.043 mg/mL (0.27 mM), *ce*WS₂ and methyl-WS₂ were diluted to 0.095 mg/mL (0.38 mM), and 150-200 μ L of each sample was loaded into a disposable cuvette (Eppendorf UVette). Particle size was measured using the Zeta-PALS particle sizing software (version 4.0, Brookhaven Instruments Corporation) with an angle of 90° and refractive index of 1.33. Zeta potential measurements were performed with conductance

values of 20-30 μS for *ce*MoS₂, 25-36 μS for methyl-MoS₂, 27-31 μS for *ce*WS₂, and 24-33 μS for methyl-WS₂. After 1 day, the conductance for methyl-MoS₂ and methyl-WS₂ increased to 89 μS and 163 μS , respectively. Electrodes were placed in the cuvette with the samples, and each set of zeta potential measurements consisted of 10 runs at 10 seconds each, fitted to the Smoluchowski model using the Zeta-PALS software.

A Cahn C-35 microbalance with a sensitivity of 10 μg was used to determine the concentration of MoS₂ and WS₂ dispersions.

A.6 Density Functional Theory Methods

Geometry optimization calculations were carried out using the Vienna *ab-initio* simulation package (VASP) with plane wave basis set and projector augmented-wave pseudopotentials (PAW). The geometries were optimized using conjugate gradient with Perdew-Burke-Ernzerhof (PBE) exchange-correlation potentials using the PBE-D3 functional with Becke-Jonson damping starting from a previously reported calculated 1T'-MoS₂ structure transformed from the hexagonal cell to a rectangular cell and the addition of a 30 Å thick vacuum slab.¹⁴ We applied a plane wave energy cutoff of 500 eV and used a Γ -centered $6\times 6\times 1$ Monkhorst-Pack k-point grid for a 1×2 periodic slab of 1T'-MS₂ (M = Mo, W). The 1×2 unit cell was then converted into a 2×4 supercell containing 16 Mo atoms and 32 S atoms and re-optimized using a $3\times 3\times 1$ k-grid (Figure 3.3). The criteria of convergence for energy and force were set to $1\text{E-}5$ eV and 0.01 eV/Å. Water was used as the solvent and cavitation energy contribution was neglected during the structural minimization with VASP. Both the MoS₂ and WS₂ structures were optimized by first allowing the unit cell parameters, volume, and atom positions to relax, and then constraining the cell parameters in subsequent optimizations for functionalized 1T'-MoS₂ and WS₂. The free energies of our optimized structures (obtained using jDFTx as described in the following paragraph) compared to the starting structure from literature differed by 0.03 eV/MoS₂, indicating minimal deviation in the formation energy. Climbing image nudged elastic band (NEB) method with was used to calculate the reaction barrier and transition states for all reactions at fixed charge.

To determine the free energy and potential of the optimized structures with greater accuracy, we used jDFTx (v.1.6.0.)¹⁰⁸ with the CANDLE solvation model¹⁰⁹ and 0.1 M KF in water, with the corresponding charge used to obtain the minimized structure in the input. The potential vs SHE was calculated using “mu,” the potential relative to vacuum in hartrees, from the Charged.out file as Potential (V vs SHE) = $\mu \times -27.2116 \text{ eV/Ha} - 4.44 \text{ eV}$.

Appendix B: Details of X-ray Photoelectron Spectroscopy (XPS) Analysis

B.1 Analysis and Quantification of Coverage from XPS Data

High-resolution XPS data were analyzed using CasaXPS software v. 2.3.17. A Shirley background was applied to all $C1s$, $S2p$, $Mo3d$, $W4f$, and $F1s$ spectra, with endpoints averaged from 21 points. Spectra were calibrated by setting the $C1s$ peak at 284.8 eV. Peaks were fitted according to the constraints listed below, and the coverage per sulfur atom was obtained using the area of the functionalized sulfur peaks divided by the total area of all sulfur peaks. This value was doubled to obtain the coverage per MS_2 unit ($M = Mo, W$). Although a similar value can be obtained by quantifying the sulfur peaks relative to the transition metal peaks, a comparison within the same XPS binding energy region removes errors associated with any changes in the inelastic mean free path (IMFP) of photoelectrons as the kinetic energy is changed.

B.1.1 Lineshapes

The $W4f$ and $Mo3d$ peaks were fit using a modified Lorentzian asymmetric lineshape with tail damping, $LF(\alpha, \beta, w, m)$, where α and β determine the tail asymmetry, w is the tail damping parameter, and m defines the width of the Gaussian. $LF(1,1,55,260)$ was used to fit all $Mo3d$ peaks based on previous reports modelling Mo XPS peaks¹¹⁰ and $LF(1.6,1.6,75,260)$ was used to fit all $W4f$ and $W5p_{3/2}$ peaks in order to minimize the residual standard deviation (residual STD) by adjusting the tail. $Mo3d$ and $W4f$ peaks are symmetrical except in the case of pure Mo and W metal.¹⁰⁰ The $S2s$ peak in the $Mo3d$ region was fit using a Lorentzian asymmetric lineshape, $LA(\alpha, \beta, m)$, with parameters $LA(2,2,50)$ by matching the experimental data and minimizing the residual STD between the fit and the data in CasaXPS. $S2p$ peaks were fit using a Voigt $GL(30)$ function with 70% Gaussian and 30% Lorentzian character, which resulted in a minimum in the residual STD.

B.1.2 Constraints

Due to spin-orbit coupling, the Mo3*d*, W4*f*, and S2*p* peaks are doublets with specific area ratios and position constraints. The following constraints were applied:

- $\text{area}(\text{Mo}3d_{3/2}) = \text{area}(\text{Mo}3d_{5/2}) \times 0.67$
- $\text{FWHM}(\text{Mo}3d_{3/2}) = \text{FWHM}(\text{Mo}3d_{5/2}) \pm 0.2$
- $\text{position}(\text{Mo}3d_{3/2}) = \text{position}(\text{Mo}3d_{5/2}) + 3.13 \text{ eV}$
- $\text{area}(\text{W}4f_{5/2}) = \text{area}(\text{W}4f_{7/2}) \times 0.75$
- $\text{FWHM}(\text{W}4f_{5/2}) = \text{FWHM}(\text{W}4f_{7/2})$
- $\text{position}(\text{W}4f_{5/2}) = \text{position}(\text{W}4f_{7/2}) + 2.17 \text{ eV}$
- $\text{area}(\text{S}2p_{1/2}) = \text{area}(\text{S}2p_{3/2}) \times 0.5$
- $\text{FWHM}(\text{S}2p_{1/2}) = \text{FWHM}(\text{S}2p_{3/2})$
- $\text{position}(\text{S}2p_{1/2}) = \text{position}(\text{S}2p_{3/2}) + 1.18 \text{ eV}$

In addition, the ratios of the areas and positions of the 2H to 1T' S2*p* peaks were determined from the average of the unconstrained fitting of *ce*MoS₂ and *ce*WS₂ samples (2 each) that were handled completely under inert atmosphere including air-free transfer to the XPS instrument. These ratios were used to constrain the ratios of 2H to 1T' S2*p* in the analysis of functionalized samples to avoid over- or under-fitting the functionalized sulfur peak. The following constraints were applied to fct-MoS₂ and fct-WS₂ spectra:

- $\text{area}(\text{MoS}_2(2\text{H}) \text{S}2p) = \text{area}(\text{MoS}_2(\text{total}) \text{S}2p) \times 0.18$
- $\text{area}(\text{MoS}_2(2\text{H}) \text{Mo}3d) = \text{area}(\text{MoS}_2(\text{total}) \text{Mo}3d) \times 0.18$
- $\text{position}(\text{MoS}_2(2\text{H}) \text{S}2p_{3/2}) = \text{position}(\text{MoS}_2(1\text{T}') \text{S}2p_{3/2}) + 1.0 \text{ eV}$
- $\text{position}(\text{MoS}_2(\text{S}^*) \text{S}2p_{3/2}) = \text{position}(\text{MoS}_2(1\text{T}') \text{S}2p_{3/2}) - 0.61 \text{ eV}$
- $\text{area}(\text{WS}_2(2\text{H}) \text{S}2p) = \text{area}(\text{WS}_2(\text{total}) \text{S}2p) \times 0.18$
- $\text{area}(\text{WS}_2(2\text{H}) \text{W}4f) = \text{area}(\text{WS}_2(\text{total}) \text{W}4f) \times 0.18$
- $\text{position}(\text{WS}_2(2\text{H}) \text{S}2p_{3/2}) = \text{position}(\text{WS}_2(1\text{T}') \text{S}2p_{3/2}) + 1.12 \text{ eV}$
- $\text{position}(\text{WS}_2(\text{S}^*) \text{S}2p_{3/2}) = \text{position}(\text{WS}_2(1\text{T}') \text{S}2p_{3/2}) - 0.61 \text{ eV}$

Note that since the values above were determined from 2 samples, additional samples will improve the accuracy of the estimate for these constraints and would change the quantification values for individual samples accordingly. Even so, a given set of constraints produces a reliable method of fitting and comparison between samples, thus we proceeded with the above constraints with the disclaimer that should different constraints be applied, the fittings would change accordingly. For instance, increasing the distance between 2H and 1T $S2p_{3/2}$ peaks from 1.12 to 1.17 eV, keeping all other parameters constant, results in a decrease of 0.7% in the calculated coverage per WS_2 , which is negligible considering the variability between samples of 2–5% in most conditions. To provide a metric of variability, below are the average \pm standard deviation of fitting parameters found from fitting $ceMoS_2$ and $ceWS_2$ samples that were used to inform the above constraints:

- $\text{area}(MoS_2(2H) S2p) / \text{area}(MoS_2(\text{total}) S2p) = 0.18 \pm 0.02$
- $\text{position}(MoS_2(2H) S2p_{3/2}) - \text{position}(MoS_2(1T') S2p_{3/2}) = 0.979 \pm 0.003 \text{ eV}$
- $\text{position}(MoS_2(S^*) S2p_{3/2}) - \text{position}(MoS_2(1T') S2p_{3/2}) = -0.62 \pm 0.006 \text{ eV}$

- $\text{area}(WS_2(2H) S2p) / \text{area}(WS_2(\text{total}) S2p) = 0.18 \pm 0.018$
- $\text{position}(WS_2(2H) S2p_{3/2}) - \text{position}(WS_2(1T') S2p_{3/2}) = 1.12 \pm 0.13 \text{ eV}$
- $\text{position}(WS_2(S^*) S2p_{3/2}) - \text{position}(WS_2(1T') S2p_{3/2}) = -0.60 \pm 0.04 \text{ eV}$

Appendix C: Calculations and Conversions

C.1 Quantification of Coverage from ^{13}C MAS NMR Data

For quantification to corroborate the XPS analysis, solid state magic angle spinning (MAS) ^{13}C NMR spectra were obtained for ^{13}C -enriched methyl-MoS₂ and methyl-WS₂ synthesized from ^{13}C -iodomethane under three conditions: no reductant, with nickelocene, and with cobaltocene. Spectra were normalized using an external standard, 1,2,4,5-tetramethyl-1H-imidazole, and corrected for the natural abundance of ^{13}C . The mmol/g of carbon was calculated per sample according to the standard spectrum, and converted to coverage per MS₂ (M = Mo, W) using the expected molecular weight of the functionalized samples based on the XPS data (e.g. for the no-reductant WS₂ case, with ~40% coverage per MoS₂, the molecular weight of MoS₂($^{13}\text{CH}_3$)_{0.4} was used). For example, with 2.4 mmol/g of ^{13}C in the no-reductant condition and 10.1 mg of sample during the measurement:

$$\begin{aligned} \text{coverage per MoS}_2 &= (\text{mmol of } ^{13}\text{C}) / (\text{mmol of Mo}) \\ &= (2.4 \text{ mmol/g} \times 0.0101 \text{ g}) / (0.0101 \text{ g} / (166.5 \text{ g/mol}) \times 1000 \text{ mg/g}) \\ &= 0.02424 \text{ mmol } ^{13}\text{C} / 0.06066 \text{ mmol Mo} \\ &= 0.40 \end{aligned}$$

C.2 Work Functions of *ce*MoS₂ and *ce*WS₂

The high-binding energy regions of the UPS spectra for *ce*MoS₂ and *ce*WS₂ (2 each) shown in Figure 2.7 and Figure 4.2 were fitted using linear regression to determine the point at which the linear fit intersects the *x*-axis. This binding energy cutoff value was then used to calculate the work function using the formula $\text{WF} = E(\text{He I}) - \text{BE}(\text{cutoff}) = 21.22 \text{ eV} - \text{BE}(\text{cutoff})$.

C.3 Effective Reduction Potential for One-Electron Reductants

The standard potential for the one-electron redox couple corresponding to each of the reductants used in our experiments was obtained from literature using values obtained in acetonitrile shifted by +30 mV based on the difference in formal potentials for the

ferrocenium/ferrocene redox couple in acetonitrile vs DMF.^{96, 111} This conversion affects only the comparison between the MoS₂ and WS₂ work functions and the reductant on the absolute energy scale, for which we used $E_{\text{vac}} = -4.44$ V vs SHE, $E(\text{Fc}^{+/0}) = 0.4$ V vs SHE, resulting in $E(\text{Fc}^{+/0}) = 4.84$ V vs E_{vac} . The effective reduction potential for a solution where only the reductant was added was estimated from the Nernst equation assuming a 50:1 ratio of reductant to oxidant (i.e. 98% purity), resulting in a correction of -0.1 V to obtain the effective potentials in Figure 2.8 and Figure 4.3, and Table 2.1.

$$E_{\text{eff}} = E(A/A^-) - \frac{RT}{zF} \ln \frac{a_{\text{Red}}}{a_{\text{Ox}}}$$

C.4 Vibrational Frequencies of Methanethiol and Propanethiol

Table C.5.1. List of all vibrational frequencies calculated using density functional theory (B3LYP with basis set 6-311G**) for methanethiol and propanethiol, assigned to experimental peaks from methyl-MoS₂ and propyl-MoS₂ (synthesized using methyl iodide and 1-iodopropane, respectively). A description is provided for characteristic (experimental) or high-intensity (theoretical) peaks. Calculated frequencies that contained substantial contribution from the S–H bond were not used to assign peaks due the absence of this bond in experimental samples.

	DFT Vibrational Frequency (cm ⁻¹)	DFT Intensity (km/mol)	Experimental Peak Frequency from MoS ₂ -CH ₃ and MoS ₂ -(CH ₂) ₂ CH ₃ (cm ⁻¹)	Description
Methanethiol	24500	16.1	--	--
	688.57	2.56	694	C–S stretch
	800.70	1.044	--	--
	978.82	11.6	946	C–H in-plane rock
	1099.55	20.8	--	CH ₃ /S–H rock
	1369.87	10.4	1289	C–H symmetrical wag (CH ₃)
	1475.65	5.49	--	--
	1486.35	8.65	--	--
	2659.60	8.76	--	S–H stretch
	3047.06	28.6	2905	C–H symmetrical stretch (CH ₃)
	3130.39	10.8	--	--
3135.79	8.24	--	--	
Propanethiol	108.54	4.44	--	--
	174.96	17.7	--	--
	231.84	2.22	--	--
	249.30	0.0700	--	--
	355.97	0.528	--	--
	721.89	3.44	727	C–S stretch
	768.36	4.94	793	C–H in-plane rock (CH ₃ /CH ₂)

847.50	3.66	--	S-H bend
882.49	0.334	--	--
944.17	1.581	898	C-H out-of-plane wag (CH ₃ /CH ₂)
1043.98	0.0873	--	--
1074.90	5.08	1054	C-H twist (CH ₂ /CH ₃)
1135.96	5.40	1082	C-C-C symmetric stretch
1250.33	0.960	--	--
1283.66	37.2	1257	C-H wag (CH ₂)
1334.70	3.45	--	--
1383.15	4.97	--	--
1418.79	2.79	--	--
1491.30	2.52	--	--
1499.35	1.56	--	--
1502.66	8.80	--	--
1511.67	5.58	--	--
2662.37	9.01	--	S-H stretch
3020.12	22.4	2862	C-H symmetric stretch (CH ₃)
3023.59	11.0	--	--
3043.41	40.4	2924	C-H symmetric stretch (CH ₂)
3050.68	1.07	--	--
3081.84	17.6	--	--
3091.20	36.7	2955	C-H asymmetric stretch (CH ₃)
3098.89	50.4		C-H asymmetric stretch (CH ₂ /CH ₃)

C.5 DFT Modeling of Grand Canonical Potential Free Energy

We used a published method to relate traditional Quantum Mechanics (QM), where the number of electrons is fixed throughout a reaction, to Grand Canonical QM, where the potential is fixed by allowing the charge to change. This method, called Grand Canonical Potential Kinetics (GCP-K), allows us to model reactions at fixed potential to make comparisons with experimental data. The relationship between the voltage-dependent grand canonical potential (GCP) for surface states can be derived from traditional fixed-electron free energies using a Legendre transformation.¹⁰⁶ The result is that GCP depends quadratically on the applied potential (U) and on the number of electrons, allowing a continuous description of the evolution of the initial state, final state, and transition state of a reaction with respect to potential, shown in Eq. $G(n; U) = F(n) - ne(U_{\text{SHE}} - U)$, (3:

$$G(n; U) = F(n) - ne(U_{\text{SHE}} - U), \quad (3)$$

where G is the grand canonical free energy, which depends on the applied voltage U vs SHE and the number of electrons n , e is the unit electronvolt in energy, F is the total free energy as a function of n , and U_{SHE} is the electronic energy at the standard hydrogen electrode (SHE) condition which is -4.44 V. U is defined such that the sign relates directly to the experimental potential, i.e. $U = 0.4$ V corresponds to 0.4 V vs SHE. For $G(n; U)$ to be used as a *thermodynamic* potential, the number of electrons in the system must be equilibrated to the applied voltage and in order to obtain the value of G at equilibrium, $F(n)$ must be minimized with respect to n , and thus the form of $F(n)$ must be at least quadratic. Although $F(n)$ appears to be linear with respect to n , as shown in the top row of plots in Figure C.1, this apparent linearity is largely due to the linear contribution of the free energy of electrons. Linearly correcting for the free energies of electrons by plotting $F(n) - nU_{\text{SHE}}$ as shown in the plots in the bottom row of Figure C.1 reveals that $F(n)$ is quadratic with respect to n .

To determine how the potential varies with charge for a particular state along the reaction, whether it is the initial state, final state, or transition state of a reaction, we fitted $F(n)$ quadratically to obtain the quadratic coefficients a , b , and c that can then be used to calculate the thermodynamic GCP free energy by substituting Eq. 4 into Eq. 3:

$$F(n) = a(n - n_0)^2 + b(n - n_0) + c, \quad (4)$$

where n_0 is the number of electrons in a neutral system.

To obtain the coefficients a , b , and c specific of the structures (all initial, transition, and final states) mentioned in this thesis, we obtained the optimized geometries using VASP at charges that span the potential of interest, then used jDFTx with CANDLE solvation to obtain the free energy and potential (V vs SHE) of the optimized geometry (see Appendix A.6). Figure C.1 shows the fitting for $F(n) - nU_{\text{SHE}}$ vs $n - n_0$ for the initial states, transition states, and final states for the reactions $\text{MoS}_2 + \text{ClCH}_3$ on S7 (a low-S sulfur), and on S10 (a high-S sulfur). The initial states and final states for MoS_2 reactions involving one or more sulfurs on

the surface, as well as the initial, transition, and final states of the $\text{WS}_2 + \text{ClCH}_3$ reaction on S7, were also fitted using this method.

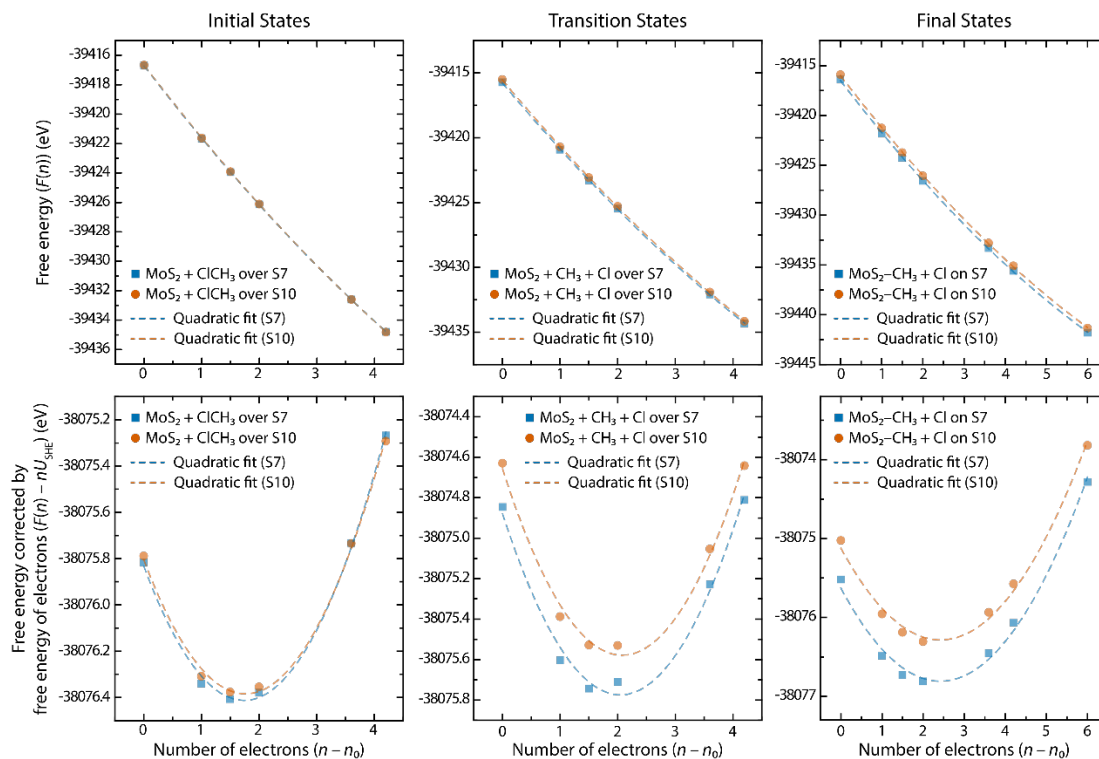


Figure C.1. Free energy as a function of the number of electrons relative to the neutral charge (n_0) for the initial state (left column), transition state (middle column), and final state (right column) of the $\text{MoS}_2 + \text{ClCH}_3$ reaction on S7 and S10. The points are energies calculated using DFT and dashed curves indicate the interpolated fit that is a quadratic fit vs the number of electrons n . The quadratic nature of the free energy dependence on the number of electrons n is more apparent once corrected for the free energy contribution of electrons (bottom row).

C.6 Calculations Using the Boltzmann Distribution and Eyring Equation

The Boltzmann distribution for the relative probabilities of two states to be populated based on their free energies is given by:

$$p_i/p_j = \exp(-(E_i - E_j)/k_B T),$$

where p_i is the probability of the system being in state i , E_i is the energy of state i , k_B is the Boltzmann constant, T is the temperature. In this work, we used the energy of the state in eV, $k_B = 8.617\text{E-}5$ eV/K, and $T = 298$ K.

The Eyring equation used to obtain the rate constant of a reaction based on the barrier height is given by:

$$k = (k_B T/h) \exp(-\Delta G^\ddagger/RT),$$

where k is the reaction rate constant, k_B is the Boltzmann constant, T is the temperature, h is Planck's constant, and R is the gas constant. We used the barrier height ΔG^\ddagger values converted to J/mol, $k_B = 1.38\text{E-}23$ J/K, $T = 298$ K, $h = 6.63\text{E-}34$ J·s, and $R = 8.31$ J/(K·mol).

Appendix D: Modeling Coverage Code

D.1 Python Code for Modeling Coverage Distributions

Python v. 3.8.5 was used to simulate the random addition of surface functional groups within a given set of constraints. For each model of coverage distribution, random surface functionalization was simulated on 100×100 grids $N = 2000$ times. Half of the positions represent low-S and half represent high-S sulfurs, corresponding to 5000 MoS₂ units. Section D.1.1 is the “0-neighbor max” model, where no functional groups are allowed to have nearest neighbors; Section D.1.2 is the “global 1-neighbor max” model, where a maximum of 2 functional groups in a row is allowed in the vertical direction (low-S sulfurs) after each functionalization step; Section D.1.3 is the “local 1-neighbor max” model, where functionalization occurs only if there is no more than 1 neighbor next to the position being functionalized; and Section D.1.4 is the “global 3-in-a-row max” model, where a maximum of 3 functional groups is allowed in the vertical direction (low-S sulfurs) after each step.

The corresponding coverage per MoS₂ from the simulations below can be calculated by taking the number of functionalized positions divided by the total number of positions multiplied by 2 to express the fractional coverage per every 2 sulfurs:

$$\text{Model coverage per MoS}_2 = 2 \times \text{Number of Functionalized Positions} / \text{Total Number of Positions.}$$

D.1.1 Coverage distribution model for low-S with no neighbors (“0-neighbor max”)

The pseudocode and code to model the coverage distribution under the constraints that (1) low-S sulfurs can be functionalized with a maximum of 0 neighbors and (2) no high-S sulfurs can be functionalized, is given below. The pseudocode is:

1. Initialize a grid of 0’s (i.e. not functionalized) with length SHEET_SIZE that is divisible by 2. Even-indexed columns are high-S and odd-indexed columns are low-

- S. Create a set of positions that correspond to low-S sulfur which is the set of odd numbers between 0 and $(\text{SHEET_SIZE})^2$.
2. Randomly select a number from this set of odd positions if it's not empty and convert it to the (row, column) location in the grid.
3. Check the value in of the corresponding position in the grid. If it's 0 (i.e. not functionalized), functionalized it (i.e. change it to 1). Then, remove this position and the position above and below it from the set of positions available.
4. Repeat steps 2–3 until the set of available positions is empty.

The Python code written in Jupyter Notebook used to obtain the coverage distribution is provided below.

```
import sys
import datetime
import numpy as np
import random as random
from matplotlib import pyplot as plt

# Define constants
SHEET_SIZE = 100 # The number of available sulfurs along both the a and b dimensions. Needs to be divisible by 2.
N_SIM = 2000 # Number of simulations

# Array to store coverage results from each simulation
sim_results = np.zeros(N_SIM)

for i in range(N_SIM):
    # Initialize the surface as a grid, represented by a 2D numpy array
    surface = np.zeros((SHEET_SIZE, SHEET_SIZE))

    # Define the set of remaining positions that can be functionalized
    # ASSUMES that SHEET_SIZE is divisible by 2
    positions_left_odd = [j for j in range(0, SHEET_SIZE **2) if j % 2 == 1] # Type 1 sulfur

    # Functionalization Loop, until the set of remaining positions is empty
    while len(positions_left_odd) > 0:

        # Randomly select a position to functionalize first
        fct_pos = random.choice(positions_left_odd)

        # Convert functionalization position to row and column indices
        col = fct_pos % SHEET_SIZE
        row = fct_pos // SHEET_SIZE

        # Functionalize the position
        surface[row, col] = 1

        # Remove the functionalized position from the appropriate set
        positions_left_odd.remove(fct_pos)
```

```

# Remove nearest neighbor positions from the set if possible.
# Assumes that SHEET_SIZE is an even number.
# Top neighbor = [row - 1, col]
# Bottom neighbor = [row + 1, col]
ind_top = fct_pos - SHEET_SIZE
ind_bot = fct_pos + SHEET_SIZE

# Removing top and bottom positions from the set
if row > 0 and (ind_top in positions_left_odd):
    positions_left_odd.remove(ind_top)
if row < SHEET_SIZE - 1 and (ind_bot in positions_left_odd):
    positions_left_odd.remove(ind_bot)

# Calculate the percentage of the surface that is functionalized per MoS2
sim_results[i] = surface.sum() / (SHEET_SIZE**2) * 2

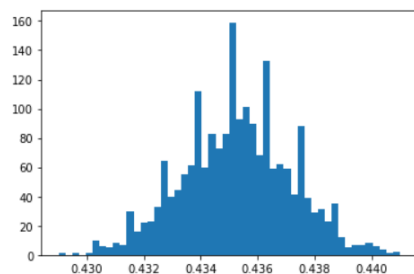
```

```
plt.hist(sim_results, bins=50)
```

```

(array([ 1.,  0.,  1.,  0.,  1., 10.,  6.,  5.,  8.,  7., 30.,
        16., 22., 23., 33., 64., 40., 44., 55., 61., 112., 60.,
         83., 73., 83., 159., 93., 101., 90., 68., 133., 59., 62.,
         59., 41., 88., 39., 29., 31., 23., 35., 12.,  5.,  7.,
          7.,  8.,  6.,  4.,  1.,  2.]),
 array([0.429 , 0.42924, 0.42948, 0.42972, 0.42996, 0.4302 , 0.43044,
        0.43068, 0.43092, 0.43116, 0.4314 , 0.43164, 0.43188, 0.43212,
        0.43236, 0.4326 , 0.43284, 0.43308, 0.43332, 0.43356, 0.4338 ,
        0.43404, 0.43428, 0.43452, 0.43476, 0.435 , 0.43524, 0.43548,
        0.43572, 0.43596, 0.4362 , 0.43644, 0.43668, 0.43692, 0.43716,
        0.4374 , 0.43764, 0.43788, 0.43812, 0.43836, 0.4386 , 0.43884,
        0.43908, 0.43932, 0.43956, 0.4398 , 0.44004, 0.44028, 0.44052,
        0.44076, 0.441 ]),
 <BarContainer object of 50 artists>

```



```

today = datetime.date.today()
savefilename = str(today) + "_sim_results_nohighS_nneighbors_" + str(SHEET_SIZE) + "x" + str(SHEET_SIZE) + \
    "_" + str(N_SIM) + "sims.csv"
np.savetxt(savefilename, sim_results)
print("Results saved to", savefilename)

```

Example output from a single simulation of a 12×12 grid:

```

Functionalization coverages from each simulation, and the average of 1 simulations:
0.4305555555555556
0.0
[[0. 1. 0. 0. 0. 0. 0. 0. 0. 1. 0. 0.]
 [0. 0. 0. 1. 0. 1. 0. 1. 0. 0. 0. 1.]
 [0. 1. 0. 0. 0. 0. 0. 0. 0. 1. 0. 0.]
 [0. 0. 0. 0. 0. 0. 0. 1. 0. 0. 0. 1.]
 [0. 1. 0. 1. 0. 1. 0. 0. 0. 0. 0. 0.]
 [0. 0. 0. 0. 0. 0. 0. 0. 1. 0. 1.]
 [0. 1. 0. 0. 0. 1. 0. 1. 0. 0. 0. 0.]
 [0. 0. 0. 1. 0. 0. 0. 0. 0. 0. 0. 1.]
 [0. 1. 0. 0. 0. 0. 0. 0. 0. 1. 0. 0.]
 [0. 0. 0. 0. 0. 1. 0. 1. 0. 0. 0. 1.]
 [0. 1. 0. 1. 0. 0. 0. 0. 0. 1. 0. 0.]
 [0. 0. 0. 0. 0. 1. 0. 1. 0. 0. 0. 1.]]

```


D.1.2 Coverage distribution model allowing a maximum of two functional groups in a row on low-S (“global 1-neighbor max”)

The pseudocode and code to model the coverage distribution under the constraints that (1) low-S sulfurs can be functionalized if the result is no more than two adjacent functional groups and (2) no high-S sulfurs can be functionalized, is given below. The pseudocode is:

1. Initialize a grid of 0's with length SHEET_SIZE that is divisible by 2. Even-indexed columns are high-S and odd-indexed columns are low-S. Create a set of positions that correspond to low-S sulfur which is the set of odd numbers between 0 and $(\text{SHEET_SIZE})^2$.
2. Randomly select a number from this set of odd positions if it's not empty and convert it to the (row, column) location in the grid. Functionalized this position. (i.e. set the value in the grid to 1).
3. If functionalization yields more than 2 functional groups in a row, remove this functional group: check every window within which this position is contained for more than 2 functional groups in a row. If there is more than 2, stop checking and remove this functional group (i.e. set the value to 0).
4. Remove this position from the set of positions available to be functionalized.
5. Repeat steps 2–4 until the set of available positions is empty.

The Python code written in Jupyter Notebook used to obtain the coverage distribution is provided below.

```
import sys
import datetime
import numpy as np
import random as random
from matplotlib import pyplot as plt
```

```
# Define constants
SHEET_SIZE = 100 # The number of available sulfurs along both the a and b dimensions. Needs to be divisible by 2.
N_SIM = 2000 # Number of simulations
```

```

# Array to store coverage results from each simulation
sim_results = np.zeros(N_SIM)

for i in range(N_SIM):
    # Initialize the surface as a grid, represented by a 2D numpy array
    surface = np.zeros((SHEET_SIZE, SHEET_SIZE))

    # Define the set of remaining positions that can be functionalized
    # ASSUMES that SHEET_SIZE is divisible by 2
    positions_left_odd = [j for j in range(0, SHEET_SIZE **2) if j % 2 == 1] # Type 1 sulfur

    # Functionalization loop, until the set of remaining positions is empty
    while len(positions_left_odd) > 0:

        # Randomly select a position to functionalize from the odd number list
        fct_pos = random.choice(positions_left_odd)

        # Convert functionalization position to row and column indices
        col = fct_pos % SHEET_SIZE
        row = fct_pos // SHEET_SIZE

        # Functionalize the position to test for 4 consecutive groups
        surface[row, col] = 1

        # Check the 3 windows if available; define start and end rows to not extend past the edge
        start_row = max(row - 2, 0)
        end_row = min(row + 2, SHEET_SIZE - 1)
        no_3_consecutive = True
        while end_row - start_row >= 2 and no_3_consecutive:
            if surface[start_row, col] == 1 and surface[start_row + 1, col] == 1 and \
                surface[start_row + 2, col] == 1:
                no_3_consecutive = False
            start_row += 1

        # Unfunctionalize the position if it results in 3 consecutive groups
        if not no_3_consecutive:
            surface[row, col] = 0

        # Remove the functionalized position from the appropriate set
        positions_left_odd.remove(fct_pos)

    # Calculate the percentage of the surface that is functionalized per MoS2
    sim_results[i] = surface.sum() / (SHEET_SIZE**2) * 2

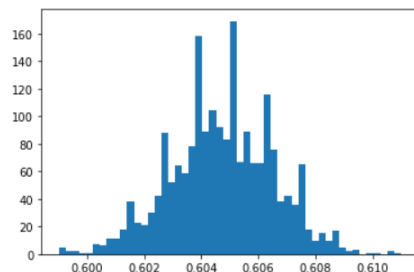
# Print results
print("Functionalization coverages from each simulation, and the average of ", N_SIM, " simulations:")
print(sim_results.mean())
print(sim_results.std())
print(surface)

Functionalization coverages from each simulation, and the average of 2000 simulations:
0.6047245
0.0017973535406257744
[[0. 0. 0. ... 1. 0. 1.]
 [0. 1. 0. ... 0. 0. 0.]
 [0. 1. 0. ... 1. 0. 1.]
 ...
 [0. 0. 0. ... 1. 0. 1.]
 [0. 1. 0. ... 0. 0. 0.]
 [0. 1. 0. ... 1. 0. 1.]]

```

```
plt.hist(sim_results, bins=50)
```

```
(array([ 5.,  2.,  2.,  1.,  1.,  7.,  6., 11., 11., 18., 38.,
        23., 21., 30., 42., 88., 52., 64., 59., 78., 158., 89.,
        104., 92., 83., 169., 67., 89., 66., 66., 116., 76., 38.,
        42., 36., 65., 18., 10., 15., 10., 17.,  5.,  2.,  3.,
         0.,  1.,  1.,  0.,  2.,  1.]),
 array([0.599 , 0.59924, 0.59948, 0.59972, 0.59996, 0.6002 , 0.60044,
        0.60068, 0.60092, 0.60116, 0.6014 , 0.60164, 0.60188, 0.60212,
        0.60236, 0.6026 , 0.60284, 0.60308, 0.60332, 0.60356, 0.6038 ,
        0.60404, 0.60428, 0.60452, 0.60476, 0.605 , 0.60524, 0.60548,
        0.60572, 0.60596, 0.6062 , 0.60644, 0.60668, 0.60692, 0.60716,
        0.6074 , 0.60764, 0.60788, 0.60812, 0.60836, 0.6086 , 0.60884,
        0.60908, 0.60932, 0.60956, 0.6098 , 0.61004, 0.61028, 0.61052,
        0.61076, 0.611  ]),
 <BarContainer object of 50 artists>)
```



```
today = datetime.date.today()
savefilename = str(today) + "_sim_results_nohighS_max2consecutive_" + str(SHEET_SIZE) + "x" + str(SHEET_SIZE) + \
"_" + str(N_SIM) + "sims.csv"
np.savetxt(savefilename, sim_results)
print("Results saved to", savefilename)
```

Example output from a single simulation of a 12×12 grid:

```
Functionalization coverages from each simulation, and the average of 1 simulations:
0.6388888888888888
0.0
[[0. 1. 0. 1. 0. 1. 0. 1. 0. 1. 0. 0.]
 [0. 0. 0. 1. 0. 1. 0. 0. 0. 1. 0. 1.]
 [0. 1. 0. 0. 0. 0. 0. 1. 0. 0. 0. 1.]
 [0. 1. 0. 1. 0. 1. 0. 1. 0. 1. 0. 0.]
 [0. 0. 0. 1. 0. 0. 0. 0. 0. 1. 0. 1.]
 [0. 1. 0. 0. 0. 1. 0. 1. 0. 0. 0. 0.]
 [0. 1. 0. 1. 0. 1. 0. 0. 0. 1. 0. 1.]
 [0. 0. 0. 1. 0. 0. 0. 1. 0. 1. 0. 1.]
 [0. 1. 0. 0. 0. 1. 0. 0. 0. 0. 0. 0.]
 [0. 1. 0. 1. 0. 1. 0. 1. 0. 1. 0. 0.]
 [0. 0. 0. 0. 0. 0. 0. 0. 0. 0. 0. 1.]
 [0. 1. 0. 1. 0. 1. 0. 1. 0. 1. 0. 1.]
```

D.1.3 Coverage distribution model with at most one adjacent functional group to functionalization site at each step (“local 1-neighbor max”)

The pseudocode and code to model the coverage distribution under the constraints that (1) a low-S sulfur site can be functionalized if there is a maximum of 1 neighbor to the

functionalization site and (2) no high-S sulfurs can be functionalized is given below. The pseudocode is:

1. Initialize a grid of 0's with length SHEET_SIZE that is divisible by 2. Even-indexed columns are high-S and odd-indexed columns are low-S. Create a set of positions that correspond to low-S sulfur which is the set of odd numbers between 0 and $(\text{SHEET_SIZE})^2$.
2. Randomly select a number from this set of odd positions if it's not empty and convert it to the (row, column) location in the grid.
3. Check the values of the position above and below to see if there is at most one of these positions that is functionalized (i.e. sum of the values in positions above and below is < 2). If this is the case, functionalize this position (change to 1). Remove this position from the set of positions available.
4. Repeat steps 2–3 until the set of available positions is empty.

The Python code written in Jupyter Notebook used to obtain the coverage distribution is provided below.

```
import sys
import datetime
import numpy as np
import random as random
from matplotlib import pyplot as plt

# Define constants
SHEET_SIZE = 100 # The number of available sulfurs along both the a and b dimensions. Needs to be divisible by 2.
N_SIM = 2000 # Number of simulations

# Array to store coverage results from each simulation
sim_results = np.zeros(N_SIM)

for i in range(N_SIM):
    # Initialize the surface as a grid, represented by a 2D numpy array
    surface = np.zeros((SHEET_SIZE, SHEET_SIZE))

    # Define the set of remaining positions that can be functionalized
    # ASSUMES that SHEET_SIZE is divisible by 2
    positions_left_odd = [j for j in range(0, SHEET_SIZE **2) if j % 2 == 1] # Type 1 sulfur

    # Functionalization loop, until the set of remaining positions is empty
    while len(positions_left_odd) > 0:

        # Randomly select a position to functionalize from the odd number list
        fct_pos = random.choice(positions_left_odd)

        # Convert functionalization position to row and column indices
        col = fct_pos % SHEET_SIZE
        row = fct_pos // SHEET_SIZE
```

```

# Check the number of neighbors this position has, if applicable
num_neighbors = 0
if row > 0:
    num_neighbors += surface[row - 1, col]
if row < SHEET_SIZE - 1:
    num_neighbors += surface[row + 1, col]

# Functionalize this position if there are less than 2 neighbors
if num_neighbors < 2:
    surface[row, col] = 1

# Remove the functionalized position from the appropriate set
positions_left_odd.remove(fct_pos)

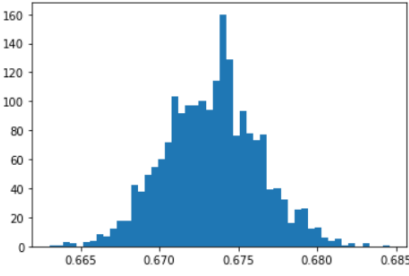
# Calculate the percentage of the surface that is functionalized per MoS2
sim_results[i] = surface.sum() / (SHEET_SIZE**2) * 2

# Print results
print("Functionalization coverages from each simulation, and the average of ", N_SIM, " simulations:")
print(sim_results.mean())
print(sim_results.std())
print(surface)

Functionalization coverages from each simulation, and the average of 2000 simulations:
0.6733208999999999
0.0030028724898003936
[[0. 1. 0. ... 1. 0. 1.]
 [0. 0. 0. ... 0. 0. 1.]
 [0. 1. 0. ... 1. 0. 1.]
 ...
 [0. 1. 0. ... 1. 0. 1.]
 [0. 0. 0. ... 0. 0. 0.]
 [0. 1. 0. ... 1. 0. 1.]]

plt.hist(sim_results, bins=50)

(array([ 1.,  1.,  3.,  2.,  0.,  3.,  4.,  8.,  7., 12., 18.,
        18., 42., 38., 49., 55., 60., 72., 103., 92., 97., 97.,
        100., 94., 114., 160., 129., 76., 93., 78., 73., 77., 39.,
        40., 32., 16., 25., 26., 12., 13., 6., 4., 5., 1.,
        2., 0., 2., 0., 0., 1.]),
 array([0.663, 0.663432, 0.663864, 0.664296, 0.664728, 0.66516,
        0.665592, 0.666024, 0.666456, 0.666888, 0.66732, 0.667752,
        0.668184, 0.668616, 0.669048, 0.66948, 0.669912, 0.670344,
        0.670776, 0.671208, 0.67164, 0.672072, 0.672504, 0.672936,
        0.673368, 0.6738, 0.674232, 0.674664, 0.675096, 0.675528,
        0.67596, 0.676392, 0.676824, 0.677256, 0.677688, 0.67812,
        0.678552, 0.678984, 0.679416, 0.679848, 0.68028, 0.680712,
        0.681144, 0.681576, 0.682008, 0.68244, 0.682872, 0.683304,
        0.683736, 0.684168, 0.6846 ]),
 <BarContainer object of 50 artists>)



today = datetime.date.today()
savefilename = str(today) + "_sim_results_nohighS_maxneighboreachtime_" + str(SHEET_SIZE) + "x" + str(SHEET_SIZE) + \
"_" + str(N_SIM) + "sims.csv"

np.savetxt(savefilename, sim_results)
print("Results saved to", savefilename)

```

Example output from a single simulation of a 12×12 grid:

```

Functionalization coverages from each simulation, and the average of 1 simulations:
0.7222222222222222
0.0
[[0. 1. 0. 1. 0. 1. 0. 1. 0. 1. 0. 1.]
 [0. 0. 0. 1. 0. 1. 0. 1. 0. 1. 0. 0.]
 [0. 1. 0. 0. 0. 0. 0. 1. 0. 1. 0. 1.]
 [0. 1. 0. 1. 0. 1. 0. 0. 0. 1. 0. 0.]
 [0. 0. 0. 1. 0. 0. 0. 1. 0. 1. 0. 1.]
 [0. 1. 0. 1. 0. 1. 0. 1. 0. 0. 0. 1.]
 [0. 0. 0. 0. 0. 0. 0. 1. 0. 1. 0. 0.]
 [0. 1. 0. 1. 0. 1. 0. 0. 0. 1. 0. 1.]
 [0. 1. 0. 1. 0. 0. 0. 1. 0. 0. 0. 1.]
 [0. 0. 0. 0. 0. 1. 0. 0. 0. 1. 0. 0.]
 [0. 1. 0. 1. 0. 1. 0. 1. 0. 1. 0. 1.]
 [0. 1. 0. 1. 0. 1. 0. 1. 0. 1. 0. 1.]]

```

D.1.4 Coverage distribution model allowing a maximum of three functional groups in a row on low-S (“global 3-in-a-row max”)

The pseudocode and code to model the coverage distribution under the constraints that (1) low-S sulfurs can be functionalized if the result is no more than three adjacent functional groups and (2) no high-S sulfurs can be functionalized, is given below. The pseudocode is:

1. Initialize a grid of 0’s with length SHEET_SIZE that is divisible by 2. Even-indexed columns are high-S and odd-indexed columns are low-S. Create a set of positions that correspond to low-S sulfur which is the set of odd numbers between 0 and (SHEET_SIZE)².
2. Randomly select a number from this set of odd positions if it’s not empty and convert it to the (row, column) location in the grid. Functionalized this position (i.e. set the value in the grid to 1).
3. If functionalization yields more than 3 functional groups in a row, remove the functional group: check every window within which this position is contained for more than 3 functional groups in a row. If there is more than 3, stop checking and remove the functional group (i.e. set the value in the functionalization position to 0).
4. Remove this position from the set of positions available to be functionalized.
5. Repeat steps 2–4 until the set of available positions is empty.

The Python code written in Jupyter Notebook used to obtain the coverage distribution is provided below.

```

import sys
import datetime
import numpy as np
import random as random
from matplotlib import pyplot as plt

# Define constants
SHEET_SIZE = 100 # The number of available sulfurs along both the a and b dimensions. Needs to be divisible by 2.
N_SIM = 2000 # Number of simulations

# Array to store coverage results from each simulation
sim_results = np.zeros(N_SIM)

for i in range(N_SIM):
    # Initialize the surface as a grid, represented by a 2D numpy array
    surface = np.zeros((SHEET_SIZE, SHEET_SIZE))

    # Define the set of remaining positions that can be functionalized
    # ASSUMES that SHEET_SIZE is divisible by 2
    positions_left_odd = [j for j in range(0, SHEET_SIZE **2) if j % 2 == 1] # Type 1 sulfur

    # Functionalization loop, until the set of remaining positions is empty
    while len(positions_left_odd) > 0:

        # Randomly select a position to functionalize from the odd number list
        fct_pos = random.choice(positions_left_odd)

        # Convert functionalization position to row and column indices
        col = fct_pos % SHEET_SIZE
        row = fct_pos // SHEET_SIZE

        # Functionalize the position to test for 4 consecutive groups
        surface[row, col] = 1

        # Check the 4 windows if available; define start and end rows to not extend past the edge
        start_row = max(row - 3, 0)
        end_row = min(row + 3, SHEET_SIZE - 1)
        no_4_consecutive = True
        while end_row - start_row >= 3 and no_4_consecutive:
            if surface[start_row, col] == 1 and surface[start_row + 1, col] == 1 and \
                surface[start_row + 2, col] == 1 and surface[start_row + 3, col] == 1:
                no_4_consecutive = False
            start_row += 1

        # Unfunctionalize the position if it results in 4 consecutive groups
        if not no_4_consecutive:
            surface[row, col] = 0

        # Remove the functionalized position from the appropriate set
        positions_left_odd.remove(fct_pos)

    # Calculate the percentage of the surface that is functionalized per MoS2
    sim_results[i] = surface.sum() / (SHEET_SIZE**2) * 2

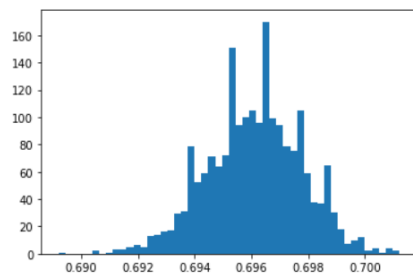
# Print results
print("Functionalization coverages from each simulation, and the average of ", N_SIM, " simulations:")
print(sim_results.mean())
print(sim_results.std())
print(surface)

Functionalization coverages from each simulation, and the average of 2000 simulations:
0.6961079
0.0016612337553758053
[[0. 1. 0. ... 1. 0. 1.]
 [0. 1. 0. ... 1. 0. 0.]
 [0. 0. 0. ... 0. 0. 1.]
 ...
 [0. 1. 0. ... 1. 0. 1.]
 [0. 1. 0. ... 1. 0. 1.]
 [0. 0. 0. ... 0. 0. 1.]]

```

```
plt.hist(sim_results, bins=50)
```

```
(array([ 1.,  0.,  0.,  0.,  0.,  2.,  0.,  1.,  3.,  3.,  5.,
        6.,  5., 13., 14., 16., 17., 29., 31., 79., 52., 59.,
        71., 64., 72., 151., 94., 100., 105., 96., 170., 99., 94.,
        79., 75., 105., 59., 38., 37., 65., 30., 18.,  7., 10.,
        12.,  2.,  4.,  1.,  4.,  2.]),
 array([0.6892, 0.68944, 0.68968, 0.68992, 0.69016, 0.6904, 0.69064,
        0.69088, 0.69112, 0.69136, 0.6916, 0.69184, 0.69208, 0.69232,
        0.69256, 0.6928, 0.69304, 0.69328, 0.69352, 0.69376, 0.694,
        0.69424, 0.69448, 0.69472, 0.69496, 0.6952, 0.69544, 0.69568,
        0.69592, 0.69616, 0.6964, 0.69664, 0.69688, 0.69712, 0.69736,
        0.6976, 0.69784, 0.69808, 0.69832, 0.69856, 0.6988, 0.69904,
        0.69928, 0.69952, 0.69976, 0.7, 0.70024, 0.70048, 0.70072,
        0.70096, 0.7012 ]),
 <BarContainer object of 50 artists>)
```



```
today = datetime.date.today()
savefilename = str(today) + "_sim_results_nohighS_max3consecutive_" + str(SHEET_SIZE) + "x" + str(SHEET_SIZE) + \
"_" + str(N_SIM) + "sims.csv"

np.savetxt(savefilename, sim_results)
print("Results saved to", savefilename)
```

Example output from a single simulation of a 12×12 grid:

```
Functionalization coverages from each simulation, and the average of 1 simulations:
0.7361111111111112
0.0
[[0. 1. 0. 0. 0. 1. 0. 1. 0. 1. 0. 1.]
 [0. 1. 0. 1. 0. 1. 0. 1. 0. 1. 0. 1.]
 [0. 1. 0. 1. 0. 1. 0. 1. 0. 0. 0. 1.]
 [0. 0. 0. 1. 0. 0. 0. 0. 0. 1. 0. 0.]
 [0. 1. 0. 0. 0. 1. 0. 1. 0. 1. 0. 1.]
 [0. 1. 0. 1. 0. 1. 0. 1. 0. 1. 0. 1.]
 [0. 0. 0. 1. 0. 0. 0. 1. 0. 0. 0. 1.]
 [0. 1. 0. 0. 0. 1. 0. 0. 0. 1. 0. 0.]
 [0. 1. 0. 1. 0. 1. 0. 1. 0. 1. 0. 1.]
 [0. 0. 0. 1. 0. 0. 0. 1. 0. 1. 0. 1.]
 [0. 1. 0. 1. 0. 1. 0. 1. 0. 0. 0. 1.]
 [0. 1. 0. 0. 0. 1. 0. 0. 0. 1. 0. 0.]
```


Appendix E: Geometries and Images of DFT Optimized Structures

Geometries are provided in VASP POSCAR format with implicit solvation (H₂O). For functionalized MoS₂ and WS₂, the numbers indicate sulfur positions that are functionalized, and brackets surround the position that was most recently functionalized. Sulfur positions 1–4 and 9–12 are high-S; positions 5–8 and 13–16 are low-S.

E.1 1T'-MoS₂ and Functionalized Structures

E.1.1 1T'-MoS₂

```
[1T'-(MoS2)16, charge = 2]
1.0000000000000000
13.1071123318841796 0.0000000000000000 0.0000000000000000
0.0000000000000000 10.9501063248573605 0.0000000000000000
0.0000000000000000 0.0000000000000000 30.0000000000000000
Mo S
16 32
Direct
0.9992564560122318 0.4869644033571848 0.4973573526197572
0.9992564560122318 0.9869644033571848 0.4973573526197572
0.4992564560122318 0.4869644033571848 0.4973573526197572
0.4992564560122318 0.9869644033571848 0.4973573526197572
0.0978526590544889 0.2368762280331037 0.4973463090323394
0.0978526590544889 0.7368762280331037 0.4973463090323394
0.5978526590544889 0.2368762280331037 0.4973463090323394
0.5978526590544889 0.7368762280331037 0.4973463090323394
0.3902563444682616 0.2369321500737897 0.4973600857028460
0.3902563444682616 0.7369321500737896 0.4973600857028460
0.8902563444682616 0.2369321500737897 0.4973600857028460
0.8902563444682616 0.7369321500737896 0.4973600857028460
0.2068526209006109 0.4869226148300467 0.4973516697567233
0.2068526209006109 0.9869226148300467 0.4973516697567233
0.7068526209006109 0.4869226148300467 0.4973516697567233
0.7068526209006109 0.9869226148300467 0.4973516697567233
0.4904648541069574 0.1501628728328316 0.5536116563576483
0.4904648541069574 0.6501628728328316 0.5536116563576483
0.9904648541069573 0.1501628728328316 0.5536116563576483
```

```

0.9904648541069573 0.6501628728328316 0.5536116563576483
0.1066546486953023 0.0736781594279838 0.4410887705444373
0.1066546486953023 0.5736781594279837 0.4410887705444373
0.6066546486953024 0.0736781594279838 0.4410887705444373
0.6066546486953024 0.5736781594279837 0.4410887705444373
0.2425247008738617 0.1560107912150419 0.5434785606052362
0.2425247008738617 0.6560107912150418 0.5434785606052362
0.7425247008738616 0.1560107912150419 0.5434785606052362
0.7425247008738616 0.6560107912150418 0.5434785606052362
0.3545790917181873 0.0678435660828590 0.4512288540193930
0.3545790917181873 0.5678435660828449 0.4512288540193930
0.8545790917181871 0.0678435660828590 0.4512288540193930
0.8545790917181871 0.5678435660828449 0.4512288540193930
0.3545759480034879 0.4060219504290737 0.5434818340969864
0.3545759480034879 0.9060219504290737 0.5434818340969864
0.8545759480034878 0.4060219504290737 0.5434818340969864
0.8545759480034878 0.9060219504290737 0.5434818340969864
0.4904299919796027 0.3236886812695851 0.4411023573466789
0.4904299919796027 0.8236886812695851 0.4411023573466789
0.9904299919796028 0.3236886812695851 0.4411023573466789
0.9904299919796028 0.8236886812695851 0.4411023573466789
0.1066704076477910 0.4001514311734428 0.5535979294909528
0.1066704076477910 0.9001514311734429 0.5535979294909528
0.6066704076477910 0.4001514311734428 0.5535979294909528
0.6066704076477910 0.9001514311734429 0.5535979294909528
0.2425377142142246 0.3178321512750594 0.4512249904269947
0.2425377142142246 0.8178321512750593 0.4512249904269947
0.7425377142142247 0.3178321512750594 0.4512249904269947
0.7425377142142247 0.8178321512750593 0.4512249904269947

```

E.1.2 (MoS₂)₁₆CH₃

[1T'-(MoS₂)₁₆(CH₃), methyl on S(7), charge = 2]

1.0000000000000000

13.1071123318841796 0.0000000000000000 0.0000000000000000

0.0000000000000000 10.9501063248573605 0.0000000000000000

0.0000000000000000 0.0000000000000000 30.0000000000000000

Mo S C H

16 32 1 3

Direct

```

0.9910641984481288 0.4696663576018736 0.4943745698752053
0.9994630217062976 0.9838952159698593 0.4946455884592282
0.5016841241764567 0.5025216331855802 0.4972445844713747
0.4988882089495732 0.9889468187762489 0.4955787583072677

```

0.0918686163883251	0.2351979638338051	0.4968247160304742
0.1079842604998191	0.7567964167903085	0.4952983620392004
0.5900952045757464	0.2321694073852996	0.4970567363269680
0.5998543024680956	0.7367724041192929	0.4950669159911030
0.3716853825412443	0.2044929519589758	0.4963953633216178
0.3930682875335947	0.7353867564847221	0.4948127742659167
0.8852750460508787	0.2395710226275227	0.4968724632096766
0.8945754174539289	0.7404798257711107	0.4946772898292267
0.2007064316753286	0.4909782614390537	0.4955389090277791
0.2150880200203815	0.9981603620491555	0.4963596840968023
0.7057175358532035	0.4858789863659538	0.4953217950516233
0.7070353671982659	0.9862313554827367	0.4945437136847488
0.4852027407181652	0.1428533143923332	0.5532379624858095
0.4938575076505316	0.6568055283378911	0.5534966588218708
0.9836858692113211	0.1474225079395808	0.5520983361688963
0.9976865285968302	0.6527434836489903	0.5478804765419341
0.1092650760631813	0.0752730973980107	0.4399723590470757
0.0986710642794293	0.5740606291717327	0.4410930644433648
0.6050310171321982	0.0770305236740256	0.4392706891779099
0.6071795765831922	0.5737953642848694	0.4387029754605294
0.2325807670524398	0.1586024820905365	0.5474001970770317
0.2443813672258059	0.6574892864885129	0.5412093387192840
0.7393380645467573	0.1558677763714229	0.5417026719304801
0.7470611076718185	0.6575573477364713	0.5399029159389030
0.3594480730580116	0.0552751303879404	0.4437216161937059
0.3536095908272330	0.5672980311642064	0.4494655291942422
0.8541252905932737	0.0696972856133797	0.4491172531611625
0.8520377671071557	0.5668876651632999	0.4497770657029818
0.3554282809326992	0.4048022069866235	0.5354708040435980
0.3558442249376199	0.9037094993440178	0.5413914022499853
0.8529589666952049	0.4092811544277808	0.5436878352218812
0.8547802831970444	0.9069525510343723	0.5403920015697778
0.4755486968585743	0.3236921108597457	0.4465521002624584
0.4934692357527481	0.8219733597166510	0.4391296115496246
0.9877159068339267	0.3174789800444913	0.4382806968557560
0.9969223519025903	0.8264712812565449	0.4378126268020637
0.1007085143021555	0.3997513829609858	0.5519791450436102
0.1081829501716243	0.9069004486539853	0.5517350520739512
0.6046834233817364	0.4019987588005662	0.5519474827912347
0.6091768413783214	0.9001210775261654	0.5510559781610311
0.2375473881144288	0.3146765781559111	0.4525062108396867
0.2464446611191065	0.8174120677750381	0.4487346701680579
0.7357439333249260	0.3157338523339561	0.4502009096233976
0.7435951391620890	0.8186035199490789	0.4483135869549386

0.3555789260307805 0.4037958309200818 0.5955703302775959
 0.3400254341122348 0.4968434854065791 0.6071619257708107
 0.4306322058383572 0.3732005213423903 0.6070712427125784
 0.2959227497792156 0.3410523257477536 0.6069578649154934

E.1.3 (MoS₂)₁₆(CH₃)₂

[1T'-(MoS₂)₁₆(CH₃)₂, methyl on S7-(14) charge = 2]

1.0000000000000000

13.1071123318841796 0.0000000000000000 0.0000000000000000

0.0000000000000000 10.9501063248573605 0.0000000000000000

0.0000000000000000 0.0000000000000000 30.0000000000000000

Mo S C H

16 32 2 6

Direct

0.0000465151793066 0.4823001460245124 0.5012078507906156

0.0049090704274593 0.9735121416973563 0.4971451028224882

0.5081164141156185 0.5021792821926820 0.5045415880286469

0.4996672348228020 0.9912050228147421 0.5010807447846845

0.0871986065663639 0.2333485838535444 0.4999689925843698

0.0984946602674406 0.7232485993235269 0.4986906314077138

0.5875159482379961 0.2397619010230775 0.5024458566661938

0.5945754727968026 0.7523702036691371 0.5031062549540128

0.3677795218353386 0.2086202465128693 0.5018769634338870

0.3890156140963626 0.7338075193327852 0.5008579597135853

0.8679125377654962 0.2595773051965470 0.5001125114832801

0.8927930681290780 0.7408146318033331 0.5008101226707475

0.2059160693141618 0.4916196741669898 0.5014124219422367

0.2220920608507738 0.0122808692578295 0.4987814267593161

0.7232148343488244 0.4568612648853057 0.5027895924716776

0.7079983580765797 0.9840700559076292 0.5007152189101014

0.4813146790007896 0.1463526645663446 0.5582365025772659

0.4921842772080542 0.6594798938323401 0.5597341908017949

0.9753045777237793 0.1464493859299394 0.5511848281503682

0.9918412372490942 0.6500819751774173 0.5567390680556434

0.1067402697199591 0.0765796341960060 0.4426183875629822

0.1055040276950091 0.5665239376645959 0.4430320284465105

0.6070471984797590 0.0767634923681575 0.4458815178979778

0.6203713840543571 0.5754676265689097 0.4511586132292507

0.2271102151070384 0.1622156640499197 0.5528286804868462

0.2394445943307179 0.6568661192799994 0.5483393202232884

0.7361733925779921 0.1569171546479924 0.5466521305605619

0.7416975686898257 0.6568500602308336 0.5408824043411530

0.3615759081883592 0.0596521604679850 0.4474342186331940

0.3601845370402548	0.5651767584064438	0.4556818064720137
0.8578658541914691	0.0669278513529980	0.4575209526335622
0.8552044403580978	0.5645907578459117	0.4569913883985544
0.3578331337787340	0.4067018113617230	0.5411528975033691
0.3538655477811959	0.9081709377914309	0.5455897097086866
0.8625138660084859	0.4109938003472058	0.5541854589583681
0.8608942259520038	0.9086315729905484	0.5463566397440919
0.4745042883673158	0.3272488480776720	0.4519348698641780
0.4890901083056949	0.8247630735566640	0.4452339322350710
0.9810979109658651	0.3255502401533004	0.4440908450593313
0.9949504145328585	0.8157807557078535	0.4420865472824125
0.1069098998931618	0.3962155387111707	0.5564425598412954
0.1169919853600935	0.9001752281464015	0.5512839724623604
0.6081117843773945	0.3969228413466846	0.5592879627016755
0.6061961920235289	0.9078178118814469	0.5588593677503252
0.2361630485897905	0.3158379888548253	0.4565874890678489
0.2409567213284335	0.8165820161133059	0.4573546016893144
0.7277203634427681	0.3068906832469180	0.4490178475948398
0.7404880464553277	0.8181826354881954	0.4542326189524084
0.3559029989302815	0.4038192443847600	0.6012240552904800
0.7419870056594383	0.6586110374172165	0.6009394600830581
0.3408489409683731	0.4966996126766290	0.6131241608813083
0.4305249464175082	0.3720230370877531	0.6128865866822522
0.2956216755475886	0.3413106629489407	0.6120895338994204
0.7553839429844138	0.7527353280828301	0.6118836759751322
0.8030710186135144	0.5983955565139355	0.6126270727064284
0.6676135359713179	0.6261971528648573	0.6126419544038441

E.1.4 (MoS₂)₁₆(CH₃)₃

[1T'-(MoS₂)₁₆(CH₃)₃, methyl on S(5)-7-14, charge = 2]

1.0000000000000000

13.1071123318841796 0.0000000000000000 0.0000000000000000

0.0000000000000000 10.9501063248573605 0.0000000000000000

0.0000000000000000 0.0000000000000000 30.0000000000000000

Mo S C H

16 32 3 9

Direct

0.0046965174596654 0.4804988765180682 0.5006128930818942

0.0023773566048455 0.9721296842566918 0.4983979314504802

0.5104836225277017 0.4981464771990225 0.5042910313131139

0.5026729581027364 0.9985956892870224 0.5025314886448972

0.0870125619211058 0.2245433334592575 0.4987981960122332

0.0947846351871672 0.7240419945497071 0.5005123686951921

0.5900619214183621	0.2400454652328793	0.5025239704862403
0.5884065032548199	0.7513171403232253	0.5044538502583671
0.3684810273581884	0.2076351955389074	0.5028548005630126
0.3714907405019279	0.7065812611651062	0.5035747526907467
0.8705811618131285	0.2600021997208211	0.4999518695801964
0.8897560686665160	0.7406727404646117	0.5016848444691427
0.2229971440773897	0.5103462491192621	0.5001286674931122
0.2189205461944216	0.0120659206783707	0.4990696454370359
0.7250921669728255	0.4573418940233692	0.5026956230512284
0.7083708135674317	0.9823323544016490	0.5009733353300466
0.4847366687167401	0.1502143702106693	0.5595151667709819
0.4883221982877230	0.6513277175508889	0.5607072583584093
0.9760184018675238	0.1475296509734113	0.5522755168073130
0.9874741953943468	0.6463383744223313	0.5571979630715758
0.1039468267615933	0.0712779760735792	0.4421345214942299
0.1098088154754332	0.5713334595711536	0.4434408308515533
0.6085415016461005	0.0759206527224215	0.4457794485376424
0.6211657317420323	0.5762012198797865	0.4514763230176695
0.2258927098759782	0.1628879093913084	0.5530851409255002
0.2312179187926288	0.6607084522775231	0.5546895249163500
0.7392663746324568	0.1566273206645334	0.5463719369980059
0.7387373043353075	0.6565420741803011	0.5412922554532255
0.3613910459679408	0.0587711547315953	0.4485101696148002
0.3668503802554831	0.5556066096266838	0.4502632558093055
0.8563083578571044	0.0659786816578205	0.4578267116241689
0.8566857976788198	0.5643561798507962	0.4571983644926618
0.3615393819144898	0.4056454563999967	0.5409140578532450
0.3567395437299316	0.9066061497252498	0.5404295778937550
0.8656415413797560	0.4115216330525979	0.5537138715486104
0.8599456436555104	0.9076446867506140	0.5479805757165177
0.4749850713440507	0.3240248668357911	0.4522209139173161
0.4749800747896878	0.8218191767707107	0.4511380868031288
0.9843702785292419	0.3242346296866184	0.4435343906319905
0.9918432939459381	0.8152686417277868	0.4432238370395160
0.1174738526205858	0.3978612756102600	0.5521267005059460
0.1150935619823757	0.9015769697993733	0.5525736167431454
0.6118526777216274	0.3961160750046410	0.5594205940616769
0.6058062005206608	0.9079126166218362	0.5595877336445285
0.2331259073266639	0.3149121331704929	0.4595458371211541
0.2367374883901904	0.8142464977190811	0.4596114207148065
0.7297664991396062	0.3078648001706915	0.4487574405147299
0.7357412714179834	0.8149688362940402	0.4551988518328201
0.3583343047829489	0.4072553386585789	0.6009226683919289
0.7394455150792857	0.6553293834309372	0.6013607776559970

0.3554787868610100	0.9116077980190048	0.6004167047717236
0.3505726829748279	0.5021315594110218	0.6119887556657400
0.4297328795466173	0.3676449282944224	0.6132167169011093
0.2928272397391714	0.3529242859410283	0.6118820658216070
0.7546711899489620	0.7485127437203372	0.6128937712147300
0.7992627292623650	0.5928061866401024	0.6126753515541461
0.6643936597351360	0.6244989561121094	0.6128371308510739
0.3477798065179890	0.0069931881095044	0.6108629961141816
0.4274259443814457	0.8730418426147463	0.6125332671954316
0.2904647485465768	0.8575410639855895	0.6120857282511322

E.1.5 (MoS₂)₁₆(CH₃)₄

[1T'-(MoS₂)₁₆(CH₃)₄, methyl on S5-7-14-(16), charge = 2]

1.0000000000000000

13.1071123318841796 0.0000000000000000 0.0000000000000000

0.0000000000000000 10.9501063248573605 0.0000000000000000

0.0000000000000000 0.0000000000000000 30.0000000000000000

Mo S C H

16 32 4 12

Direct

0.0047992376617919	0.4724597089877940	0.4996535597259520
0.0047988059711997	0.9724290790669459	0.4996433230481912
0.5079390524196357	0.4980881479299640	0.5043574128227031
0.508020522238832	0.9980787092876785	0.5043406875129258
0.0900009349769538	0.2224351104460670	0.4996479833004577
0.0900149117947520	0.7224670656931116	0.4996456092493324
0.5868542366359891	0.2480543581004772	0.5043583625497794
0.5868385619112240	0.7480624485518351	0.5043395939492291
0.3693968850851534	0.2065526950263550	0.5037067552632780
0.3693691869043993	0.7066075803182834	0.5036699315438991
0.8736447503442208	0.2606080430611685	0.4998738666213776
0.8736467795778552	0.7606129341453928	0.4998624581743417
0.2211307230975664	0.5105696551099177	0.4998937658871629
0.2211867677288445	0.0105888859579408	0.4998534983706929
0.7254160382422256	0.4565941375723959	0.5036872628709058
0.7255180399599087	0.9565411455489000	0.5037014002176263
0.4851809279466365	0.1505003337365883	0.5608037685703979
0.4850692578861561	0.6506387360243437	0.5607862997858918
0.9773248549986024	0.1488448740950537	0.5529217200334391
0.9773773107849922	0.6489071086468797	0.5529290118772300
0.1072421497250711	0.0699181010916565	0.4429413074869833
0.1072378992929513	0.5698883258339996	0.4429608650986562
0.6210204084135343	0.0726760639192222	0.4519236201702124

0.6208863357318359	0.5726577511955441	0.4518998808407506
0.2271220404834693	0.1621034873573431	0.5540138230476933
0.2271470054120401	0.6621593753122679	0.5540036792879948
0.7358571255263940	0.1559401411756912	0.5410771246148879
0.7358371486910611	0.6559564770140814	0.5410335672597613
0.3656281582808722	0.0559858915714336	0.4500662390441006
0.3655552049456337	0.5559342509217067	0.4500870224507699
0.8599398314052038	0.0637819157089046	0.4598341167811343
0.8599266496247570	0.5638048230524517	0.4598355995221763
0.3589813346947071	0.4059301682899537	0.5410867077426635
0.3590180062631992	0.9059617427108263	0.5410305663035681
0.8676462226452873	0.4121260419172401	0.5540241491784893
0.8677406750736146	0.9120537187403072	0.5540290721569058
0.4738849670914678	0.3226584145142938	0.4519225374496459
0.4738890157696668	0.8226672645826781	0.4518981742669917
0.9875785890340613	0.3198978286958533	0.4429516736030785
0.9875818550750736	0.8199128706903804	0.4429372588965406
0.1174163306027872	0.3988349751151674	0.5529449817502854
0.1174854240488328	0.8988953583538647	0.5529233293309254
0.6096583812255549	0.4006212013987047	0.5607905012911873
0.6097254470938682	0.9005255629076201	0.5607861411983417
0.2349164576844721	0.3137765410528517	0.4598635818107144
0.2348709225936421	0.8138270369119035	0.4597987125819635
0.7292046336963279	0.3059663493262449	0.4500821384293535
0.7292569421789746	0.8059896877746136	0.4500653128392392
0.3569283066516487	0.4084012328983193	0.6011230921445107
0.7378849831514465	0.6583685034044444	0.6010623146089323
0.3569330787469319	0.9083977353779044	0.6010679831136972
0.7379769261852400	0.1585576126397660	0.6011072357594922
0.3486111819811697	0.5033212235942816	0.6120649410694198
0.4290151803681665	0.3700069306408911	0.6131780457324659
0.2922202987639259	0.3533579151170371	0.6125037618489296
0.7473889573772157	0.7531405315269986	0.6119957600226762
0.8018799083578882	0.6021599995440959	0.6124475561032564
0.6652824751165551	0.6212724406009226	0.6130764905808715
0.3467441541155979	0.0030804842997025	0.6119881788921989
0.4297929552649131	0.8720592018888235	0.6130955177922744
0.2933364771183908	0.8515316366697994	0.6124516599628574
0.7444105295368788	0.2537283337775150	0.6120125495215163
0.8037973631931922	0.1054286036030130	0.6124795384719471
0.6666860263145424	0.1181454899725476	0.6131905167971254

[1T'-(MoS₂)₁₆(CH₃)₄, methyl on S5-7-(13)-14, charge = 2]

1.0000000000000000

13.1071123318841796 0.0000000000000000 0.0000000000000000
 0.0000000000000000 10.9501063248573605 0.0000000000000000
 0.0000000000000000 0.0000000000000000 30.0000000000000000

Mo S C H
 16 32 4 12

Direct

0.0041818989342124 0.4845538375554349 0.5016046991337383
 0.0023818853067106 0.9702359300901874 0.4984790758674439
 0.5102669245057913 0.4980806405781614 0.5039073232377624
 0.4996338446837152 0.9989255576359822 0.5030522705258768
 0.0852830514334245 0.2274164724983788 0.4986249020194573
 0.0963228949210941 0.7237571868510622 0.5011193349041235
 0.5875246397577548 0.2397218484771337 0.5022301627940463
 0.5886203221376585 0.7519211771212100 0.5052832485556650
 0.3661099950056266 0.2085596619217648 0.5025998857513295
 0.3715405334183149 0.7064860210913774 0.5039630076412455
 0.8689821150778905 0.2609106713750387 0.4999761544672228
 0.8918831198252301 0.7312390893354490 0.5013978780912486
 0.2235504463982805 0.5108140531192729 0.5003702863504649
 0.2179731431234865 0.0123040401576137 0.4994381479196749
 0.7251891961662232 0.4568409075571728 0.5023649696087344
 0.7033958508704122 0.9881815571666989 0.5021488309596267
 0.4817574071400344 0.1515043377261233 0.5595260789235255
 0.4884881822200421 0.6503072296116336 0.5609488789194620
 0.9754335233023673 0.1493902138986022 0.5517247929660608
 0.9901891720891488 0.6479331043768645 0.5587473930178666
 0.1034119796378387 0.0720710068723572 0.4424661146837627
 0.1100944292334074 0.5719212095030061 0.4439283685315205
 0.6047137296986863 0.0745158817711815 0.4456611088149516
 0.6213660479832449 0.5775660406658248 0.4515360979266450
 0.2243206339977673 0.1631463798435998 0.5531087116118946
 0.2319741955481218 0.6606930411923898 0.5551849691677641
 0.7367580488698674 0.1595216039557099 0.5473384269107711
 0.7376279185435956 0.6541302767123859 0.5420793101278276
 0.3594973635045682 0.0579028147186443 0.4487686292947516
 0.3668099920032529 0.5567979169400743 0.4502934915520192
 0.8554177511128264 0.0652648890599823 0.4591620049622757
 0.8564853670338388 0.5625965807314993 0.4560745214677043
 0.3615842604953243 0.4058982699964023 0.5407919229211764
 0.3551902611517700 0.9063217567391715 0.5410101255336410
 0.8650757662242479 0.4119522640531625 0.5538977191338369
 0.8569237562950905 0.9094925631210984 0.5444070505184530
 0.4735527550053572 0.3244997919107783 0.4519283547587698
 0.4755417005570211 0.8217638366255091 0.4517666472668203

```

0.9829089885792938 0.3269150517952255 0.4437985259939322
0.9937604945462344 0.8126932581959935 0.4434229720017007
0.1181710037950965 0.3978382303290385 0.5520674509909097
0.1144363474837243 0.9015717443812060 0.5529783840702920
0.6109960741372024 0.3953048305454603 0.5588372052748536
0.6021753265032580 0.9093839175161822 0.5605029162194241
0.2315215010561029 0.3160655364771850 0.4592894381779021
0.2368570728998030 0.8142974065427384 0.4600555337230600
0.7281750032880664 0.3057506342633274 0.4488285257985809
0.7391398361250259 0.8169765649078471 0.4585611489471257
0.3584979087092162 0.4071728624417569 0.6007960580790001
0.7351854843821042 0.6433456249201337 0.6021409494423002
0.3538171974281806 0.9120101386886508 0.6010040670915062
0.8677968755974416 0.9119406216337667 0.6044937034112534
0.3501005930418646 0.5019300347790482 0.6119446965317533
0.4301416539756927 0.3681448128993465 0.6130681409744755
0.2933517717778188 0.3521434377031769 0.6117407867986799
0.7160151529606099 0.7330283227132210 0.6158697669468470
0.8101116935636967 0.6128450434278527 0.6138114540036669
0.6764438284706459 0.5770419750928480 0.6115386434687726
0.3467707551762124 0.0075984779729370 0.6113349317774275
0.4254941791402519 0.8729233967345674 0.6132347017986300
0.2884445924362740 0.8586781211203196 0.6127513641522410
0.9041705429723913 -0.0014771134426889 0.6136211300228355
0.9142097969942553 0.8343998382512441 0.6153400692257209
0.7907239724463223 0.9077075675515995 0.6184296364699764

```

E.1.6 (MoS₂)₁₆(CH₃)₅

[1T'-(MoS₂)₁₆(CH₃)₅, methyl on S5-7-(13)-14-16 or S5-7-13-14-(16), charge = 4.2]

1.0000000000000000

13.1071123318841796 0.0000000000000000 0.0000000000000000

0.0000000000000000 10.9501063248573605 0.0000000000000000

0.0000000000000000 0.0000000000000000 30.0000000000000000

Mo S C H

16 32 5 15

Direct

```

0.0041003621205770 0.4762412635884324 0.4997078279852382
0.0067871341145721 0.9771451245962095 0.4997009949242658
0.5060587973092501 0.4956255643535660 0.5041489718827699
0.5065631831909310 0.9950262247915259 0.5051558570942903
0.0878588024822758 0.2272255207297025 0.4993984264222067
0.0872062857591673 0.7254385581129159 0.5001010167523028
0.5837320845707340 0.2455474045699944 0.5042260984337167

```

0.5841306063943205	0.7452031236991910	0.5051688238942026
0.3675420241914611	0.2079367069604277	0.5032756746448936
0.3674113045791701	0.7075649948763548	0.5039236529319796
0.8714899050157775	0.2615664951776124	0.4999956887695985
0.8718290361328355	0.7569989370530916	0.5007305443847158
0.2197114241775403	0.5112765087194092	0.4999625756441681
0.2200783451660162	0.0108581095137154	0.5002105198661332
0.7233562811191677	0.4578693598046116	0.5031718960824374
0.7221423512530664	0.9590439401023377	0.5049196446410493
0.4816049039978571	0.1494984881844611	0.5609375504481811
0.4817295616889398	0.6472548639085198	0.5612014095581553
0.9763191160356121	0.1525608535041559	0.5531307117818337
0.9757659841138248	0.6480722242334946	0.5536514707291734
0.1078831842055634	0.0737035900806694	0.4429117250230813
0.1059736680601163	0.5735925600163064	0.4432512530833512
0.6188539688770361	0.0715279125677566	0.4525448160310571
0.6183378751326684	0.5728127481769962	0.4518359629135740
0.2254441971770710	0.1630790713081052	0.5538776518201386
0.2249468997864628	0.6615730739109762	0.5543593756933819
0.7329947416191147	0.1587224502772723	0.5409316627749627
0.7328208779666795	0.6548357205923473	0.5411735733731534
0.3644094498345686	0.0551841184975694	0.4503663166775478
0.3638644288732130	0.5568567114884766	0.4502368482464151
0.8587161416319798	0.0634793623196710	0.4612671496740532
0.8585578401633389	0.5646786167665707	0.4596004548711073
0.3572188728439312	0.4058889367290295	0.5402880387904727
0.3573071147596216	0.9056778575616998	0.5410090477361906
0.8656739519634760	0.4127840655073226	0.5538679905354831
0.8682809353842936	0.9158272600625013	0.5509356759389525
0.4722654715775838	0.3222248361783909	0.4515453411243847
0.4725458457230272	0.8221442299445176	0.4525291299711213
0.9849659627384816	0.3237177547561083	0.4430492140026823
0.9852040830600030	0.8235064604060677	0.4438177703385835
0.1162138668669148	0.3996655167050329	0.5527732243714325
0.1170750741107996	0.8995059081065695	0.5532424392634059
0.6080055114871996	0.3987757098882693	0.5602646839305574
0.6071666003866829	0.8979869744565168	0.5619260923303709
0.2327940859979803	0.3149163434105725	0.4596270132735078
0.2324092025188698	0.8141688158012063	0.4604978854744284
0.7269346443449575	0.3056251423762091	0.4500352449292837
0.7261278778591387	0.8063484594058906	0.4517035270905747
0.3546829519065479	0.4068401842555859	0.6002771425754472
0.7334806333684469	0.6503898154043726	0.6011821581630121
0.3542986931745741	0.9076620355094109	0.6009940013389514

0.7351675655810935 0.1633765185969236 0.6009013273179602
 0.8849905743183549 0.9056008652297380 0.6108519800170717
 0.3444319765967154 0.5013709375188015 0.6113902300953873
 0.4275386076391889 0.3700917307024218 0.6121926583733772
 0.2908683871927936 0.3495398076210439 0.6111731964116967
 0.7184255281567392 0.7424623678337049 0.6138323165321049
 0.8081713683935964 0.6171549688614266 0.6121963701444155
 0.6727839171774781 0.5879913568403037 0.6117929378752548
 0.3457206365527868 0.0025992441031175 0.6119274346569307
 0.4263383471622926 0.8691639541583787 0.6131153630771037
 0.2893353505288902 0.8522639316238787 0.6119094587298657
 0.7190238979638351 0.2573124975519057 0.6113653940144190
 0.8113104553277303 0.1360981264701856 0.6121248322665455
 0.6764961076845121 0.1009541639942998 0.6134982312498434
 0.9328511215363473 0.9828582061073885 0.6210839283411482
 0.9233450635629349 0.8186682572935565 0.6178734903040355
 0.8101206985113123 0.9096865565451528 0.6269621805928436

[1T'-(MoS₂)₁₆(CH₃)₅, methyl on S(1)-5-7-14-16, charge = 4.2]

1.0000000000000000

13.1071123318841796 0.0000000000000000 0.0000000000000000

0.0000000000000000 10.9501063248573605 0.0000000000000000

0.0000000000000000 0.0000000000000000 30.0000000000000000

Mo S C H

16 32 5 15

Direct

0.0056974069103479 0.4761818579343221 0.5007009886657446
 0.0020733305179469 0.9791272790979365 0.4999311163076921
 0.5082553785564699 0.4949856863056015 0.5052472020783533
 0.5082900156549490 0.9953689983783947 0.5047061537387566
 0.0883052033346055 0.2257610064426005 0.5007455470365959
 0.0877316521311081 0.7216849796439594 0.5003942130990771
 0.5857464700204945 0.2456468333734103 0.5048751836782593
 0.5857634654120860 0.7455436519534895 0.5048192925679501
 0.3688894308826881 0.2079380161318241 0.5044950388335541
 0.3688418944924875 0.7071058382554576 0.5047648320969572
 0.8728217145898910 0.2604254065524420 0.5006577176375837
 0.8724127933762342 0.7602041219820295 0.5004835152341591
 0.2210890264843987 0.5097320936993989 0.5013443597584382
 0.2222900433690817 0.0125156144419457 0.5012658852180348
 0.7249390536587442 0.4571224240824125 0.5041116610260810
 0.7247584377512707 0.9575357811619705 0.5033947505334583
 0.4845326622838760 0.1479437354060517 0.5613351913145829
 0.4847854863953500 0.6483241162123433 0.5615710769881083

0.9761004352634908 0.1496342950380606 0.5539990915646392
0.9753202393181369 0.6483638216182441 0.5539145571704369
0.1080548700792481 0.0740970361114227 0.4441625657855519
0.1078444378267958 0.5716112551117037 0.4438966414973968
0.6195320765810355 0.0723171464124058 0.4520040578506876
0.6197546095384393 0.5714531548802242 0.4525168820078583
0.2271356172230334 0.1633471999348070 0.5554418267456873
0.2278215539723614 0.6603679360154175 0.5558761109731573
0.7348211760606678 0.1553249331769852 0.5406535840771099
0.7345980552703909 0.6555317777717361 0.5409540409212599
0.3649484417199023 0.0561519046986291 0.4510449456782535
0.3648020883753186 0.5556881668671313 0.4513845006628787
0.8591974979102874 0.0646008473329694 0.4591736049368766
0.8601184672920432 0.5633927000332769 0.4607337375710261
0.3594842184642550 0.4055359530582284 0.5416304269122836
0.3606030077759094 0.9054540697757314 0.5415852273946764
0.8669562253291864 0.4114250555296106 0.5546942368859433
0.8663279924419536 0.9125476484199340 0.5542199757869888
0.4733354674430757 0.3222853668310402 0.4525316366330195
0.4728781539668702 0.8214707006211326 0.4525046769085958
0.9868535539668063 0.3227353113548136 0.4441269854307744
0.9864012720615252 0.8212588459134705 0.4439144938216266
0.1169039014106597 0.3993796899624289 0.5543873250096972
0.1167898749871526 0.8978183496586007 0.5500360782094748
0.6103194229599169 0.3979404250568380 0.5614810001112513
0.6107391514756991 0.8986144527510409 0.5609134329189998
0.2335040849790905 0.3143525961093053 0.4612466478766006
0.2327573689539136 0.8146666464659635 0.4622668978472342
0.7285604879193260 0.3058740506765662 0.4507870642056863
0.7283905755022571 0.8048375309891611 0.4505166936340496
0.3579297138747720 0.4060744110888301 0.6016101485696893
0.7372114778028226 0.6571385780210892 0.6009430733997909
0.3616929517155412 0.9067337259007486 0.6016477727278616
0.7372383550266280 0.1556607900193472 0.6006399701049406
0.1033209294520228 0.9053877159898859 0.6101325345046775
0.3534302841480224 0.5012098231238448 0.6127995848203428
0.4286234537868762 0.3632291182425998 0.6132754446122490
0.2910555544604497 0.3542565061280896 0.6126557743436265
0.7463859613285779 0.7519293315404748 0.6119640574470465
0.8016394951834960 0.6009777312808021 0.6119448454392153
0.6647424058100860 0.6194051594756745 0.6129053358103548
0.3371442909549222 0.9971320883031494 0.6131062578949877
0.4399540259127489 0.8877603763955272 0.6125325660690641
0.3098703224212351 0.8352216704686510 0.6134612614676999

0.7465155446051915 0.2502161199746210 0.6118926573865894
 0.8015385451049583 0.0991400269090729 0.6115190353266224
 0.6646539542616724 0.1178517234066460 0.6124203200889461
 0.1396708875055868 0.9897441771532162 0.6216477115131451
 0.1398573782434280 0.8245998748335782 0.6246485685856145
 0.0211984272101850 0.9061547425116524 0.6172035052764621

E.1.7 (MoS₂)₁₆(CH₃)₆

[1T'-(MoS₂)₁₆(CH₃)₆, methyl on S5-7-13-14-(15)-16, charge = 4.2]

1.0000000000000000

13.1071123318841796 0.0000000000000000 0.0000000000000000
 0.0000000000000000 10.9501063248573605 0.0000000000000000
 0.0000000000000000 0.0000000000000000 30.0000000000000000

Mo S C H

16 32 6 18

Direct

0.0064181863168910 0.4799892537234002 0.4998795134982707
 0.0063655017939882 0.9799259211172837 0.4998819316486425
 0.5055042429498376 0.4948701820918474 0.5047994034197040
 0.5054548071339010 0.9948520839895836 0.5048364492279065
 0.0877106752828707 0.2282895015446002 0.5001071408430167
 0.0877656563123584 0.7282670750128463 0.5000917331624835
 0.5830578028578669 0.2450341711948109 0.5047872418821493
 0.5831072471469407 0.7450933977115339 0.5047897337150332
 0.3669592951635034 0.2085307877614407 0.5036479357327420
 0.3669839810048174 0.7085396108693922 0.5036527499730341
 0.8713881181994355 0.2579348572435035 0.5008337489852264
 0.8714452265198919 0.7579755900506109 0.5008417825249384
 0.2196210572693603 0.5120276124092303 0.5003091118883747
 0.2195732469165845 0.0120222490289656 0.5003036336119073
 0.7214516635922513 0.4594160281614633 0.5043308461250632
 0.7214286428226837 0.9593973503620630 0.5043924209807770
 0.4805306809000400 0.1484549928328149 0.5612013336215813
 0.4805922414591906 0.6483953651789288 0.5611890847769032
 0.9761537011693248 0.1524816318163779 0.5542291731386386
 0.9762427170009954 0.6524302314606641 0.5542089143178294
 0.1074634381277464 0.0757828024412047 0.4431654761585501
 0.1075125910965120 0.5757480665713915 0.4431527698970613
 0.6178670645148732 0.0721689995903885 0.4523363863407242
 0.6178826578217217 0.5722175009592557 0.4522858690779804
 0.2252464823629475 0.1632672861935557 0.5544150513522437
 0.2252972190921771 0.6632861460551421 0.5544160150096102
 0.7315464269033873 0.1577780133991507 0.5415096548609877

0.7316481581759536	0.6577659561096990	0.5414500313309211
0.3635542360620826	0.0564154061891761	0.4503691772524012
0.3635681238700841	0.5564690654293852	0.4503696756584936
0.8580825836999021	0.0643619388309074	0.4606098174979850
0.8581412953278666	0.5644069049422146	0.4605726313321885
0.3566507098906672	0.4061466349878456	0.5408057446862374
0.3565935445442361	0.9061436339165247	0.5408213863887409
0.8669780848434789	0.4173845655298568	0.5507543040073350
0.8670246370341224	0.9173125220677529	0.5508091560872413
0.4718879982393782	0.3223586471138019	0.4519911343654289
0.4718934502337105	0.8224009806637085	0.4519942953795486
0.9846186692190776	0.3256530275071093	0.4440173960477520
0.9846883568079160	0.8256691930982339	0.4440167229447756
0.1166266564924856	0.4011701391697242	0.5533159064314990
0.1166697095282131	0.9011583130789270	0.5533135528541102
0.6065429126942534	0.3980875681802457	0.5612641578870566
0.6064768509857941	0.8980551874308677	0.5613106273044227
0.2321734392767047	0.3156318895927385	0.4601547701527563
0.2322440585813632	0.8156478870052677	0.4601581953705514
0.7258187734912378	0.3059364919030897	0.4513271765931953
0.7258519004684948	0.8060449481236199	0.4513483670619025
0.3544699893453168	0.4076593871119199	0.6007931398946247
0.7303048200625647	0.6555690050626075	0.6015160340722463
0.3543807872864438	0.9076403877417342	0.6008029939664615
0.7298640798804239	0.1555614615926404	0.6015737228915756
0.8815952804981007	0.9046877406760159	0.6107687996244179
0.8809485362836879	0.4045495080100749	0.6107251407814424
0.3476958600163927	0.5027189736936984	0.6118140858803031
0.4260670833027216	0.3673351127777457	0.6126296817192947
0.2887736528565740	0.3536698137193783	0.6117993287075384
0.7030343085078339	0.7444503944106564	0.6133245178094886
0.8078996595875437	0.6380378720645673	0.6134255870702378
0.6779886496821892	0.5832088616282097	0.6122490355269417
0.3473639403658830	0.0026757106017494	0.6118171490935442
0.4260879718795009	0.8675787624531089	0.6126213089466616
0.2888208234234128	0.8534146697472590	0.6118148611068697
0.7021148117782290	0.2442698896795359	0.6133512145644371
0.8074362609635994	0.1384449413505991	0.6136039944805124
0.6777008004891050	0.0829235082426449	0.6122194585491388
0.9291020364973864	0.9814057318686571	0.6217858955432697
0.9199349532633883	0.8174101508454215	0.6174162227608930
0.8062139014428003	0.9078271966239840	0.6264596276997223
0.9274845203709051	0.4818800351828512	0.6219867880597659
0.9200878176634382	0.3177915819100048	0.6173651693288086

0.8053264840534596 0.4064016933627595 0.6262200077478887

[1T'-(MoS₂)₁₆(CH₃)₆, methyl on S(4)-5-7-13-14-16, charge = 4.2]

1.0000000000000000

13.1071123318841796 0.0000000000000000 0.0000000000000000

0.0000000000000000 10.9501063248573605 0.0000000000000000

0.0000000000000000 0.0000000000000000 30.0000000000000000

Mo S C H

16 32 6 18

Direct

0.0029211772833670 0.4685084553910487 0.5004586889197979

0.0071580113846895 0.9612756816730122 0.4946821493638870

0.5055855860533238 0.4902651373690408 0.5034974086153842

0.5057719920612089 0.9898164072962834 0.5044020266305461

0.0851789839693299 0.2192597710793913 0.5042915550009582

0.0869048934445147 0.7152354362865375 0.4985554566294986

0.5830936256327821 0.2401914059252445 0.5043632336674251

0.5829055860874077 0.7405268591309632 0.5040902403351321

0.3663648982831067 0.2011116311455051 0.5033024243425914

0.3663415339955995 0.7012331742955088 0.5025569325516431

0.8718313122368163 0.2540132643394393 0.5047074785502798

0.8711380966012582 0.7513649646550836 0.4990879250544740

0.2190248033713871 0.5043945751431695 0.4992846659351584

0.2191084352576116 0.0050663545072172 0.4994523870057112

0.7217612119706523 0.4534980357984570 0.5027922168690020

0.7217386850395815 0.9527556616489690 0.5040703713957658

0.4811029590277927 0.1434552755726502 0.5606268286456969

0.4806436233888988 0.6423102863189589 0.5600347689218520

0.9753814811752672 0.1593714394728909 0.5663552242564260

0.9742176546965713 0.6436196021064947 0.5526173774574848

0.1059194797844892 0.0726164943122641 0.4433839685478165

0.1036975885070570 0.5608924042572506 0.4425449475933505

0.6184024989620724 0.0665386366115593 0.4521641815363354

0.6173893102794723 0.5672389245918447 0.4509584231694558

0.2262602954818470 0.1528029868587667 0.5549223393133791

0.2239605246589338 0.6563339558364495 0.5530350939501369

0.7303065107521787 0.1509925051679454 0.5421941673401279

0.7319360815725575 0.6520997461801404 0.5401382145652930

0.3634784789897186 0.0497522119064360 0.4499661057214340

0.3630574291660791 0.5492495334345034 0.4491936577545886

0.8590127798892322 0.0599477312885744 0.4624887340421868

0.8585055564123071 0.5564000907692711 0.4587342527791859

0.3566331900537372 0.3997443507338135 0.5397897042671730

0.3563542095522618 0.8990325222008310 0.5399282820127070

0.8607339917106747	0.4143153222977536	0.5544069968622998
0.8730252721911995	0.9150612616511641	0.5481510149397173
0.4713105162369367	0.3157292184636358	0.4514410174592843
0.4712635786394369	0.8172520504900462	0.4514782371000641
0.9834708293696158	0.3111550614238278	0.4468589143210502
0.9853974923258445	0.8106402261099356	0.4408719413654368
0.1179520342652532	0.3971504385124099	0.5534988225536160
0.1132980781649877	0.8917771574069520	0.5506257030840961
0.6069399800973584	0.3944707796567332	0.5600606073799520
0.6067692417821358	0.8921637470201438	0.5609262111868329
0.2278622714314317	0.3045167674793777	0.4611367950155165
0.2313269374988335	0.8074774154607688	0.4592477133987150
0.7307512456100588	0.2970159135280112	0.4518682480829227
0.7253349001448689	0.8012297462042888	0.4504070614564605
0.3545369777401759	0.4016749014601487	0.5997961404734811
0.7314056501768552	0.6476173776099282	0.6001674680823481
0.3535676642349517	0.8992973807655862	0.5999201829249101
0.7273017518093364	0.1529379142831345	0.6021416233762226
0.8853174355984413	0.8973879569269542	0.6080777899538969
-0.0052427089317723	0.2486099347088078	0.6185275916465351
0.3457685259664547	0.4965312622946330	0.6107773378224867
0.4269588038438399	0.3635681948701632	0.6116488365199193
0.2899304777381040	0.3459025400636159	0.6108670366134270
0.7161538350896157	0.7396524481487742	0.6127715522810456
0.8058380587150847	0.6142904011131105	0.6114461001120581
0.6705216586780766	0.5851711500596490	0.6105317015599073
0.3470001567888162	-0.0058848155368743	0.6112210502413922
0.4247505118856695	0.8582185156373057	0.6118836382795791
0.2875076256370557	0.8454920820613017	0.6106531448192920
0.7207090342877991	0.2483524968005484	0.6128240221363120
0.7986229543685675	0.1134903453739897	0.6144220344401539
0.6611753532149088	0.1000050473992323	0.6133778180704356
0.9334726538369649	0.9729032489494166	0.6197420031183498
0.9216739994090987	0.8088973318307471	0.6144158732922205
0.8094348885457240	0.9013794259743063	0.6232655113418694
-0.0240034702628023	0.3456297737696439	0.6158318826241630
0.0751753633610898	0.2375585844771237	0.6279468816126177
0.9454996944762174	0.2050758819481648	0.6435851599415313

E.1.8 (MoS₂)₁₆(CH₃)₇

[1T'-(MoS₂)₁₆(CH₃)₆, methyl on S5-(6)-7-13-14-15-16, charge = 1]

1.0000000000000000

13.1071123318841796 0.0000000000000000 0.0000000000000000

0.0000000000000000 10.9501063248573605 0.0000000000000000
 0.0000000000000000 0.0000000000000000 30.0000000000000000

Mo S C H
 16 32 7 21

Direct

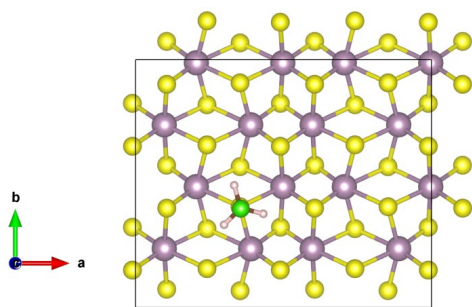
0.0048214502018683 0.4728116053703166 0.4995134293019557
 0.0054419443377889 0.9745276121127782 0.4989131094288935
 0.5065547924099599 0.4972444820402347 0.5048951066766476
 0.5071262628833220 0.9969463022246846 0.5040547823262278
 0.0873871302890867 0.2251244086716641 0.4988521180191434
 0.0866769475369624 0.7237158086429781 0.4994378698136389
 0.5835410630993459 0.2479532789290261 0.5040025620139527
 0.5835318499166990 0.7474119114611277 0.5050411125135735
 0.3671909640170475 0.2073158715976219 0.5026142293741724
 0.3691803139549458 0.7087462763932314 0.5046143084535682
 0.8720414662035390 0.2586470699057978 0.4999574567742180
 0.8724263496923120 0.7584242774355188 0.5001011195796629
 0.2187097577673225 0.5077616769155090 0.5001411237046693
 0.2200786513149394 0.0117733176981398 0.4991936892636329
 0.7215477183571168 0.4590534025625986 0.5043506302805256
 0.7218190025645250 0.9590796011202907 0.5039432752190978
 0.4820984057878295 0.1498882672444551 0.5599282202594055
 0.4839415840772977 0.6491195242559997 0.5616573123763983
 0.9769713453967606 0.1498586706812985 0.5524254801084476
 0.9756613445461916 0.6490037503621926 0.5529166420029358
 0.1064929967984805 0.0727614632838922 0.4420788923804368
 0.1055115766843249 0.5714015244861959 0.4429184144906259
 0.6190476170200367 0.0733589357985823 0.4516205036220085
 0.6183594081257225 0.5736360396672515 0.4523641437018084
 0.2252448883620794 0.1622942373708512 0.5532046118558465
 0.2231812312937167 0.6642264414884470 0.5510735981304945
 0.7320634837225265 0.1583544511158005 0.5410406191910958
 0.7324852098431097 0.6583538766623703 0.5415413629402230
 0.3645567388332029 0.0561269269611895 0.4493453130288337
 0.3649516748994791 0.5575481170070125 0.4512377508023889
 0.8581074506886237 0.0637320021033294 0.4602078797829514
 0.8580506583318889 0.5633539349155765 0.4606699862106687
 0.3577640528001083 0.4050034232819439 0.5408621824818027
 0.3577540676997066 0.9091956416094856 0.5408365938581277
 0.8676234207906174 0.4146768211478553 0.5508961069833314
 0.8682980739687228 0.9160470374906056 0.5504507542367347
 0.4719702610700927 0.3243302280540566 0.4515197102599567
 0.4717655155075093 0.8228356042656481 0.4522032824886805
 0.9849520727073584 0.3217284029818663 0.4426211578374061

0.9855902242918217	0.8214511463470562	0.4426988193488099
0.1166918984927411	0.3961291882729874	0.5528028158342903
0.1170769589898251	0.9012244346359656	0.5522362112972172
0.6061180106295418	0.3985147075022724	0.5610239681460591
0.6064498451139050	0.9008361860387393	0.5609537443274096
0.2325222035413493	0.3149979910041299	0.4590798811175691
0.2330401043722400	0.8129346870781851	0.4609599847760196
0.7258728954194240	0.3079007331264789	0.4508435034756704
0.7257848162949513	0.8065242368114347	0.4510622209641849
0.3570687290453953	0.4014829034588389	0.6008898103715896
0.7318360985908836	0.6581144275350841	0.6016437571162644
0.3559451471340993	0.9154159577094702	0.6008354891009161
0.7314365645242061	0.1574587759980428	0.6011387817740379
0.8884569457890882	0.9075555399365738	0.6101044151418900
0.8875821410343291	0.4062915195044916	0.6105747303627547
0.2028735899862408	0.6564977882120620	0.6107446370469173
0.3705717388447969	0.4938951349666946	0.6134571103696617
0.4187982575365846	0.3409405361686325	0.6117356209889709
0.2831919463857166	0.3664165210379141	0.6121333390133372
0.7045959671071425	0.7470906672875216	0.6133045623838196
0.8093801744255458	0.6410716297730337	0.6136441179016919
0.6797688533417534	0.5863001187630237	0.6129570464774198
0.3687894520855906	0.0102291990850601	0.6110358615428129
0.4167658127211784	0.8564719612747222	0.6136394294008981
0.2810638860342551	0.8849159344101433	0.6124904219317576
0.7042673787280684	0.2463599428017477	0.6129018382466915
0.8090046304285839	0.1403212730063675	0.6130834440452224
0.6793501906251300	0.0856466266166398	0.6124292206942638
0.9324093137431696	0.9881388493808227	0.6200922304458941
0.9315766726441613	0.8238642464350303	0.6169384727219653
0.8140782731699018	0.9058386211258734	0.6266310165582624
0.9310065765935291	0.4872415181358462	0.6206053238507561
0.9312040293626631	0.3229993897261803	0.6174284621345045
0.8131624283583881	0.4040198068675381	0.6270595104312415
0.1554395215365196	0.7346333282602991	0.6203082452240809
0.2771224757938285	0.6601450675143782	0.6273744435218285
0.1635190741053441	0.5703714352728433	0.6178872481920540

E.2 1T'-MoS₂ Initial, Transition and Final States of Reactions

E.2.1 (MoS₂)₁₆ + ClCH₃ reactions on S7 and S10

Methylation of S7 (low-S). Methyls on the surface before reaction: None



[1T'-(MoS₂)₁₆ + ClCH₃, S(7) INITIAL STATE, charge = 2]

1.0000000000000000

13.1071123318841796 0.0000000000000000 0.0000000000000000

0.0000000000000000 10.9501063248573605 0.0000000000000000

0.0000000000000000 0.0000000000000000 30.0000000000000000

Mo S C H Cl

16 32 1 3 1

Direct

0.9975861212489048 0.4874274574428786 0.4994053850453433

0.9976735396756059 0.9872923981162771 0.4995062796662182

0.4977440609836358 0.4877056389078596 0.4993261389730131

0.4976237339575163 0.9872176940530315 0.4995330258887995

0.0969893927261534 0.2373737765217110 0.4993823023422635

0.0969490176426455 0.7371373917318004 0.4994406875978200

0.5969825857240119 0.2375964334049023 0.4994805510792653

0.5969407961862585 0.7374777109140346 0.4995910286200768

0.3891766556067693 0.2369225272946630 0.4991395884244864

0.3890688385909749 0.7372639255739487 0.4995117362865298

0.8891401897915253 0.2374758290201592 0.4994938790653740

0.8890683337330986 0.7374317913514098 0.4995609557460150

0.2053747167193548 0.4875748363618633 0.4991935817843915

0.2055329363533296 0.9875566616699147 0.4995370388939827

0.7055373743884388 0.4873403746540969 0.4994733546590922

0.7054631315593517 0.9873051488050444 0.4995912987377195

0.4890642285084891 0.1511435194882865 0.5556277874692266

0.4892187961200673 0.6505900873411613 0.5557497763136117

0.9894869071872531 0.1508945630582897 0.5556711466638949

0.9894454636950487 0.6506505380010115 0.5556999049636259

0.1052409445573380 0.0737542135666023 0.4432558752529921

0.1048425113224557 0.5740871568902280 0.4430694078224763

0.6053527047518501 0.0738268039289782 0.4433556361082586

0.6055116026764327 0.5742641092687268 0.4432472493787928

0.2415114132073674 0.1568567637588766 0.5455255925135286

0.2413781860796201 0.6562615309306417 0.5455408424021843

0.7413937738499465 0.1567187678598525 0.5455987864296690

0.7414151243412826	0.6565065380206569	0.5456406905371627
0.3532711919414514	0.0677289682857844	0.4532255163252875
0.3532799593229425	0.5684910788773964	0.4531807401729218
0.8531225522554113	0.0681085045761979	0.4534796597871588
0.8530905867178999	0.5682594233886119	0.4534178223246403
0.3529013937598850	0.4067002295333181	0.5446412673172208
0.3531135736952183	0.9065464085921252	0.5456243135618689
0.8532507803044600	0.4065877416871093	0.5455946131316262
0.8532604673573554	0.9066011069070677	0.5456771215636107
0.4896780262321780	0.3240161743428631	0.4431061171795180
0.4893977804144087	0.8239321175068310	0.4433298606399330
0.9892455317421124	0.3238655955635523	0.4432076542796622
0.9892265142074882	0.8238958900874181	0.4432973048005273
0.1055450625861970	0.4008903274178180	0.5555432302611423
0.1053299238382126	0.9006956898692380	0.5556920610131236
0.6050141788724424	0.4010123979699899	0.5556737479161749
0.6051058974168051	0.9008559328441342	0.5558257773969871
0.2413466159901880	0.3180440072625996	0.4531342396295661
0.2414077685463764	0.8182148250305977	0.4534532256248747
0.7414284696897753	0.3181637594659303	0.4533703671716457
0.7413882795883565	0.8182092900814105	0.4534815484036688
0.3549142158650113	0.4012556869642001	0.6540427414756765
0.3334811196132213	0.4931419074212631	0.6433512113440175
0.4315702801398737	0.3781388918344309	0.6424580501296081
0.2993011776842363	0.3339675526334678	0.6424928796592793
0.3556635385817176	0.3985957477062875	0.7141919392681899

[1T'-(MoS₂)₁₆ + ClCH₃, S(7) TRANSITION STATE, charge = 2]

1.0000000000000000

13.1071123318841991 0.0000000000000000 0.0000000000000000

0.0000000000000000 10.9501063248573995 0.0000000000000000

0.0000000000000000 0.0000000000000000 30.0000000000000000

Mo S C H Cl

16 32 1 3 1

Direct

0.9918346085597275	0.4706957109144003	0.4985419186601842
0.9992043718253236	0.9858964269962739	0.4981078037494657
0.4981630717787110	0.4866648464100197	0.4998440390755040
0.4991203631681139	0.9880572246664014	0.4990487297663562
0.0955262529453276	0.2376109277518805	0.4998120039393305
0.1025504928309134	0.7530701967604387	0.4993688058805035
0.5954609327092528	0.2393724072324747	0.4998002658702430
0.5974283897798437	0.7400983544626346	0.4991563476402407
0.3881112608323434	0.2317273389388282	0.4990797341587738

0.3908154269489654 0.7354817093026905 0.4986666802927539
0.8873334677772560 0.2382230144589072 0.4996570851365683
0.8924239701171811 0.7367890707276653 0.4984930858478523
0.2009624748041162 0.4903559645687155 0.5000945612332317
0.2078503648768008 0.9878712993453062 0.4986986754447291
0.7045379347523634 0.4858222488955273 0.4996373534198604
0.7065763308384406 0.9857351925894834 0.4978820458324830
0.4888448624363733 0.1493003989825632 0.5558586016663265
0.4909077196617615 0.6521534968133720 0.5554808634742840
0.9871293574686222 0.1487455864271436 0.5551225182027104
0.9938171670368877 0.6512909135446489 0.5528559061576589
0.1075294010830266 0.0750310503160685 0.4428157575595699
0.1000104502356559 0.5731011144684908 0.4450350128322018
0.6058037545598426 0.0763690480186827 0.4428000699268135
0.6053499115448306 0.5738469998119804 0.4435227210210227
0.2405129274106194 0.1550471926829788 0.5464118936628838
0.2424112210296489 0.6593883052418882 0.5451403236303909
0.7414337099989972 0.1548818384676684 0.5447223623335201
0.7431837443440171 0.6569721706452472 0.5444025695258339
0.3547687522023926 0.0672402172808785 0.4518538272272845
0.3523033523420583 0.5670305414919948 0.4536268058853707
0.8537801181341690 0.0693203249737543 0.4521238357057196
0.8516375661018023 0.5655300629920662 0.4536008586735168
0.3516745846320267 0.4073007222777406 0.5433585786289341
0.3549113242252007 0.9054285765037540 0.5446354575200142
0.8523683836363872 0.4070336170186746 0.5469821330865847
0.8540912662875051 0.9053935214814469 0.5438023382137239
0.4881860929640093 0.3245786467773798 0.4435062618867884
0.4901738210463061 0.8249389816769453 0.4426585458353700
0.9903143238017895 0.3185536842674576 0.4417449609102633
0.9925422461465315 0.8258507947408971 0.4417920681210356
0.1013740795469117 0.3983401532705554 0.5562622666810598
0.1047618141740126 0.9054741419530988 0.5560720989350761
0.6047379622985518 0.4001055698488561 0.5564260618515678
0.6071986109646030 0.9014218287074688 0.5551012256970758
0.2412691048477205 0.3195507067400186 0.4551902266815950
0.2430260355075474 0.8169557902561382 0.4517044782475537
0.7390896806181012 0.3186394015756972 0.4531324465040184
0.7415555830838598 0.8170561827142685 0.4521057465317644
0.3538708020289433 0.4033984148076050 0.6194321524655881
0.3317556420796235 0.4987110495470469 0.6204302487789880
0.4338509097918313 0.3785067443892803 0.6195500528132841
0.2958036367043343 0.3329314234310493 0.6196210749699466
0.3551683330276073 0.4006822956188625 0.6970604106106291

[1T'-(MoS₂)₁₆ + ClCH₃, S(7) FINAL STATE, charge = 2]

1.0000000000000000

13.1071123318841796 0.0000000000000000 0.0000000000000000

0.0000000000000000 10.9501063248573605 0.0000000000000000

0.0000000000000000 0.0000000000000000 30.0000000000000000

Mo S C H Cl

16 32 1 3 1

Direct

0.9924257410815982 0.4707727347425814 0.4941800947904575

-0.0000301356036127 0.9834393675680480 0.4945054001555181

0.5027511574680542 0.5005880873829377 0.4975461053376077

0.5005659661839790 0.9887223334773599 0.4956981663404538

0.0915142392760285 0.2351560816405606 0.4964659941625572

0.1063747106193111 0.7546775698557957 0.4952740637930841

0.5892481462840675 0.2401834706354361 0.4975535159153827

0.5987091251405906 0.7414270652455348 0.4957753388992110

0.3722954012235393 0.2058547492430542 0.4959309209554211

0.3924266943731010 0.7335336860853866 0.4947928249431541

0.8851745386512472 0.2394466554471194 0.4966439489105133

0.8934073250844254 0.7408846933351205 0.4949040564921010

0.2006681824307670 0.4909757460205683 0.4956500529308698

0.2153434311661098 0.9980665925042496 0.4962592299578833

0.7068575471456023 0.4823250623180846 0.4950302064683761

0.7077076734937499 0.9830407694612543 0.4943191890688481

0.4848499109080205 0.1445174476531203 0.5529556361366421

0.4934537857861915 0.6565367206303248 0.5534901645980804

0.9838621157559673 0.1470117359864897 0.5517870520386909

0.9956332104394021 0.6520707616008159 0.5481151962835112

0.1092654185232941 0.0749571490684264 0.4397529691178629

0.0997641643680724 0.5734355255493292 0.4406319017187385

0.6066664599424880 0.0791032556187736 0.4400839394340719

0.6081047702796496 0.5754014523479419 0.4395197824191788

0.2330004631618393 0.1588092630854578 0.5468414174247774

0.2433828916892393 0.6569851939898959 0.5412938179254234

0.7394282954681846 0.1550363834194508 0.5409561340403959

0.7462219260070739 0.6567265646504951 0.5394698173742046

0.3597637989658574 0.0557846351822161 0.4438809233851524

0.3549027549092266 0.5664802681077613 0.4494846560113104

0.8541905064767769 0.0685170422363647 0.4491534480888925

0.8524345215828888 0.5665711037313765 0.4499163478450393

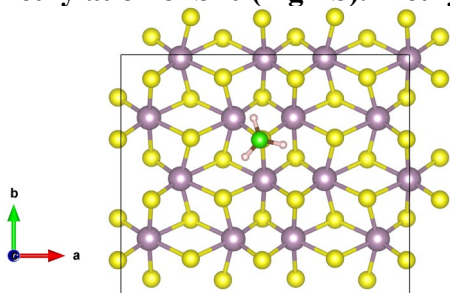
0.3550230934276728 0.4052889610294002 0.5357349985458715

0.3560913199419746 0.9035250238744180 0.5409907157578920

0.8538463366379808 0.4077187231344750 0.5437179101200625

0.8556650110135970	0.9066739997286795	0.5409086144700644
0.4761561961648603	0.3250434692613622	0.4457529298565568
0.4923550295840697	0.8236584442062660	0.4392420903910635
0.9870855779346437	0.3176371784453319	0.4380739689601741
0.9958312102661644	0.8257988438286873	0.4378220104621003
0.1012117285342238	0.3990892648071078	0.5518546357072727
0.1086987757498150	0.9060105794391516	0.5515453751021452
0.6053487482810459	0.4030887670041218	0.5528916173018987
0.6088660635809090	0.9011055357302760	0.5518174868482876
0.2373907892155875	0.3153378200432784	0.4521865521239838
0.2454730146264889	0.8167500146938068	0.4489698713529739
0.7349364517486646	0.3150080589733997	0.4494005467893246
0.7416180288281508	0.8179445688338468	0.4477418869193005
0.3555188018641587	0.4035138063646510	0.5958689276928298
0.3395727896421239	0.4962389552650880	0.6076236181456866
0.4307356855028114	0.3734429353688064	0.6072957924635330
0.2963355568543650	0.3403420690939776	0.6073109499665165
0.3469230198659199	0.4193172568390159	0.7226297271027831

Methylation of S10 (high-S). Methyls on the surface before reaction: None



[1T'-(MoS₂)₁₆ + ClCH₃, S(10) INITIAL STATE, charge = 2]

1.0000000000000000		
13.1071123318841796	0.0000000000000000	0.0000000000000000
0.0000000000000000	10.9501063248573605	0.0000000000000000
0.0000000000000000	0.0000000000000000	30.0000000000000000
Mo	S	C H Cl
16	32	1 3 1

Direct

0.9981268007524423	0.4845597836005430	0.4992390445849335
0.9981666508355171	0.9845618765668858	0.4992337568941715
0.4979334508950951	0.4832884750572587	0.4988914850349467
0.4980828103671117	0.9838788397319631	0.4990395807705924
0.0973324137196303	0.2394940003379842	0.4996623803471895
0.0973703905859064	0.7396135008237906	0.4995801329157828
0.5973844548421898	0.2400014708313107	0.4996563245397295

0.5975549198043982 0.7406367924836983 0.4994194818318950
0.3895319284983091 0.2371706271489327 0.4994752458145953
0.3895733367590151 0.7372182163741625 0.4991212095655602
0.8895440981631820 0.2370274967477538 0.4995324867616082
0.8895826290567868 0.7370048980970136 0.4994037640964573
0.2059034257531344 0.4869815549119982 0.4993371083981030
0.2059692332250029 0.9868669122219842 0.4993179351606227
0.7057758388125990 0.4870723343361096 0.4993194048941680
0.7059726119909605 0.9869793470328276 0.4993353336306782
0.4896176176163227 0.1500891201131370 0.5552667196281432
0.4896300180603528 0.6502264658847403 0.5547090939339808
0.9896805431072649 0.1501809683007871 0.5554352817860255
0.9896678960058632 0.6502968937508480 0.5553552452508185
0.1058135242679198 0.0738984503324965 0.4434738532365528
0.1057420451860241 0.5737675008196367 0.4434455097110869
0.6059805036985981 0.0738469702677506 0.4434724557660222
0.6058951093893175 0.5736770532549800 0.4433871657295818
0.2420708853965227 0.1561438938922032 0.5454256287223999
0.2421777180481313 0.6563331621177396 0.5453105942300654
0.7418536428116640 0.1561549503498699 0.5455205064420483
0.7417703261063953 0.6563425753845580 0.5453675336675947
0.3534919247069875 0.0679341209360342 0.4533166774229054
0.3534055845037536 0.5676512986422769 0.4531798659885882
0.8535476221965449 0.0678924878827919 0.4534091576376756
0.8535085967433510 0.5677466509592777 0.4533619173757681
0.3539135185569328 0.4064765213460872 0.5455794767686909
0.3539225376403669 0.9060020108523691 0.5454519448516834
0.8537142644792424 0.4063081807835100 0.5455864715758341
0.8538235368038937 0.9061155683217661 0.5455572406382947
0.4900477405053749 0.3228944175391977 0.4427285942997621
0.4901983376242850 0.8237226205370005 0.4425818500732163
0.9898853788643446 0.3234157139544803 0.4429820238983832
0.9899357140438302 0.8235699987000623 0.4429052785167518
0.1056269486212157 0.4006422241447651 0.5559197530283662
0.1056362001563732 0.9005363366854359 0.5558907044936008
0.6051527352110443 0.4007398853554894 0.5558995047058964
0.6053018207971772 0.9005468970909429 0.5558930971337072
0.2415544050014008 0.3177928847970067 0.4532442969948955
0.2414121492139122 0.8179471266447418 0.4530492314954727
0.7417693599274660 0.3177427498193393 0.4533033610238554
0.7418941729278222 0.8179141203433696 0.4531086422138393
0.4838102989424408 0.6476867350092972 0.6660328617160370
0.4602720575287315 0.7380834333646177 0.6544896876947137
0.5618477160152104 0.6273960626669906 0.6555425287981631

0.4310003061433023 0.5774362708448161 0.6542999027541829
 0.4807731787050200 0.6479948766091356 0.7261227332977874

[1T'-(MoS₂)₁₆ + ClCH₃, S(10) TRANSITION STATE, charge = 2]

1.0000000000000000

13.1071123318841991 0.0000000000000000 0.0000000000000000
 0.0000000000000000 10.9501063248573995 0.0000000000000000
 0.0000000000000000 0.0000000000000000 30.0000000000000000

Mo S C H Cl
 16 32 1 3 1

Direct

0.9979426262489037 0.4852658650097316 0.5009608942971120
 0.9999270535440354 0.9856367738938908 0.5000845324807136
 0.4912889565427097 0.4687483553530047 0.5010162127073667
 0.4994395278788674 0.9870880958571785 0.5003399476053784
 0.0953724125128102 0.2368308797093130 0.5010773223220332
 0.0973514651388363 0.7373066513496013 0.5000611919240593
 0.5956075923522565 0.2370853785611130 0.5017737928205285
 0.6052008302420966 0.7561032720520000 0.5014084986194358
 0.3870608013645445 0.2374303557469614 0.5016661414308198
 0.3917811497183059 0.7368288152256417 0.5001151190098845
 0.8883729469952096 0.2376945838582755 0.5017955235764165
 0.8912251664069853 0.7372626916601454 0.4999997857743362
 0.2040580538904622 0.4872336833449369 0.5014678082458385
 0.2068516638743049 0.9871586952247426 0.4999493470477355
 0.7024046321345804 0.4877128542713585 0.5013908023770003
 0.7081300851279413 0.9861964526353085 0.5001928202917855
 0.4873544173475381 0.1491168532546215 0.5573622023224476
 0.4967360760079315 0.6498716925522577 0.5527747732107990
 0.9889961313568920 0.1474841066762877 0.5571284264357388
 0.9904503676332269 0.6505135709334061 0.5565099985989274
 0.1064708634974657 0.0753652080120780 0.4441002957676727
 0.1049603177619256 0.5724336069619838 0.4445444141460982
 0.6075962850874583 0.0750131313708378 0.4447448171612994
 0.5992837806591514 0.5731716836901969 0.4477044312716781
 0.2405438267536399 0.1548098961905877 0.5470402009498708
 0.2425670139502301 0.6571129125878459 0.5463347663628878
 0.7414287119064785 0.1544579196785482 0.5478479207413733
 0.7441933409392079 0.6586442124280073 0.5463410137542654
 0.3543821004743382 0.0692242969119413 0.4539398629916485
 0.3514455049930429 0.5649111723003696 0.4555221504176214
 0.8540413508673164 0.0690814007946221 0.4547653647757349
 0.8521357052718892 0.5668624691527626 0.4552295678913990
 0.3515277054149183 0.4068091459860237 0.5491718398236134

0.3541972134079007	0.9049177776929699	0.5456207385435157
0.8534843900954072	0.4068157981992197	0.5476097493204209
0.8562098655313493	0.9050856130193369	0.5464166003211265
0.4902427030053286	0.3179302865591218	0.4438038562628872
0.4933246110573572	0.8263217544326943	0.4440362656828880
0.9878309029075142	0.3233471374619851	0.4448786658936792
0.9908146541944474	0.8242936162182821	0.4434977446682456
0.1043670234013507	0.3987969549699337	0.5576360967904946
0.1071770658563355	0.8994377040911932	0.5563238523717188
0.6034212984783066	0.3966556945328514	0.5581469450632810
0.6051148590371718	0.9068923110083532	0.5583942210316953
0.2397447832508568	0.3185560912828831	0.4552733506451669
0.2424698788491839	0.8174405280584826	0.4539048077360665
0.7407753168858925	0.3188438883656508	0.4562714992823617
0.7432320372321519	0.8168581892659742	0.4526207940008239
0.4864069531616030	0.6487038316206512	0.6270174368268572
0.4633746932088338	0.7438380536885609	0.6275988139650436
0.5662239337567704	0.6249776221464283	0.6307379327780815
0.4290068054146276	0.5774315204979538	0.6270603236326324
0.4756034769877449	0.6518922682556425	0.7063784470052986

[1T'-(MoS₂)₁₆ + ClCH₃, S(10) FINAL STATE, charge = 2]

1.0000000000000000

13.1071123318841796 0.0000000000000000 0.0000000000000000

0.0000000000000000 10.9501063248573605 0.0000000000000000

0.0000000000000000 0.0000000000000000 30.0000000000000000

Mo S C H Cl

16 32 1 3 1

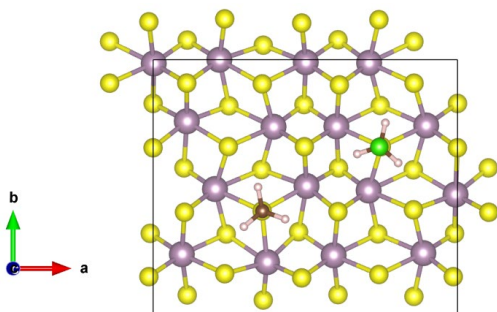
Direct

0.9979341816222393	0.4849742409802880	0.5003393365142201
0.0001997999641550	0.9852951594027723	0.4995240094831934
0.4907631040397952	0.4679339694141377	0.5008470260311156
0.4995455013600903	0.9879041717100758	0.4997257204028884
0.0951266891770234	0.2365969642202489	0.5006112725395319
0.0971713971806901	0.7371387520142819	0.4993216397636566
0.5954704865638435	0.2366462041293413	0.5011207198532980
0.6067600278119903	0.7578156133343159	0.5010050378181766
0.3867252551569366	0.2377768024011388	0.5011234450029527
0.3903271698659014	0.7379543499042542	0.4989230821211748
0.8882556383789088	0.2382535968315987	0.5014442484927751
0.8912568603982396	0.7379083371966519	0.4994878901192012
0.2037533045067379	0.4874906209200444	0.5008251276405603
0.2069463846388844	0.9879878690924853	0.4995843479491994
0.7026709139351686	0.4872024699537804	0.5005928278071383

0.7083906772476459	0.9861168047238732	0.4995598627566421
0.4870976398300702	0.1493096637807292	0.5568084962176472
0.4973085954861322	0.6492336708559436	0.5505175306136699
0.9887876468558128	0.1470818620469689	0.5566431311899567
0.9905098155412507	0.6504716776517264	0.5558456824192367
0.1065603057518767	0.0754618716977918	0.4436091726209533
0.1045443829814293	0.5723493530820992	0.4438209207476996
0.6079944998068412	0.0751078753728162	0.4440720906673990
0.5985857893384684	0.5736318646306738	0.4476169760635633
0.2401897564973183	0.1550212242323511	0.5467105021412949
0.2422816047140718	0.6575092700338867	0.5455548941183606
0.7414759368956274	0.1543001382763545	0.5472562194668877
0.7445749894859924	0.6584811690049248	0.5458049496626817
0.3543982620357028	0.0693433126416166	0.4534010825169322
0.3506741585147746	0.5643673083804268	0.4549087231310026
0.8543345741982292	0.0692233873060706	0.4543243089045097
0.8521803038072656	0.5670697210010971	0.4547143057033765
0.3509603153804969	0.4066464722588393	0.5487748933129643
0.3546452176790881	0.9047698990613753	0.5450639269294694
0.8538196432514606	0.4069945020554571	0.5472539437646201
0.8565684190645761	0.9052365174903620	0.5459643722573728
0.4901044434212198	0.3175127522070172	0.4432325775603343
0.4941901051618476	0.8266673209379868	0.4434622068004950
0.9877225032376722	0.3231353852697538	0.4443622173852100
0.9907618959235778	0.8244779576024952	0.4428446340661025
0.1043020052022095	0.3988210316047173	0.5570976722345630
0.1073001503113008	0.8990585429367406	0.5557592136378460
0.6042244869583983	0.3953374910404855	0.5575243039338412
0.6051143316013535	0.9081875026339117	0.5579348657745243
0.2393782563535773	0.3183649767801381	0.4547739829649333
0.2424066358243460	0.8181417833028416	0.4531313871423430
0.7407538112253599	0.3187184702646469	0.4556113273262046
0.7434067720144436	0.8169801077685055	0.4518314761241949
0.4865777870012643	0.6452912527713516	0.6103532530658784
0.4661510641494458	0.7374508472652668	0.6213708443376380
0.5604722798914042	0.6173835846249029	0.6239098739067644
0.4268269869988120	0.5793423372515514	0.6187412435936710
0.4806681653747056	0.6640252932506571	0.7265282711436061

E.2.2 (MoS₂)₁₆(CH₃) + ClCH₃ reaction on S14

Methylation of S14 (low-S). Methyls on the surface before reaction: S7



[1T'-(MoS₂)₁₆(CH₃) + ClCH₃, S7-(14) INITIAL STATE, charge = 2]

1.0000000000000000

13.1071123318841796 0.0000000000000000 0.0000000000000000

0.0000000000000000 10.9501063248573605 0.0000000000000000

0.0000000000000000 0.0000000000000000 30.0000000000000000

Mo S C H Cl

16 32 2 6 1

Direct

0.9934964096503418 0.4712021150965980 0.4953091054610599

0.0020001123589596 0.9854903843085365 0.4956094241152728

0.5039422237147395 0.5047202108128135 0.4979587798540326

0.5014885153965151 0.9902683240137464 0.4964927207596616

0.0943712961187134 0.2367812264627896 0.4979913190896919

0.1105360044728237 0.7585455175673592 0.4961955035139467

0.5928775963311761 0.2326146539673429 0.4979129562990361

0.6021060418978427 0.7389943298476658 0.4956016085226513

0.3742452711966077 0.2059103181782541 0.4975529942768206

0.3955084392074051 0.7370993160379116 0.4956198769748151

0.8877708493204169 0.2411679957426755 0.4979418505357370

0.8972266816853229 0.7420042576650495 0.4951188912163624

0.2031629325162228 0.4926625068227213 0.4966000396843925

0.2176760883797847 -0.0001240900393611 0.4974888802536608

0.7079928543101457 0.4868354981514339 0.4957395366027598

0.7096881159971123 0.9877159475674286 0.4953777681664056

0.4881223433832732 0.1440546589231987 0.5542708577615351

0.4967990282931724 0.6587637566718451 0.5542394198667911

0.9860334424126607 0.1488285771109762 0.5531826883938457

-0.0002501164105415 0.6544529219056351 0.5486278394952057

0.1120209032550151 0.0770741858897989 0.4410884185540377

0.1012677246754710 0.5755468506006826 0.4420922453225845

0.6074044791765049 0.0783023727871749 0.4400651486055110

0.6092870565331102 0.5755012852594712 0.4392676968562971

0.2351296104944745 0.1602276948859279 0.5486163766343389

0.2469003284328526 0.6592736192840677 0.5421653526725299

0.7417805041621466 0.1572381665289004 0.5427277513521211

0.7497757060176174 0.6591529114758934 0.5394846378809812
 0.3618130807784642 0.0570427787558479 0.4448061570213014
 0.3558468777615053 0.5689077641108568 0.4503051096349509
 0.8567912266844017 0.0713978264493684 0.4501036074882805
 0.8547583056941939 0.5680011080961848 0.4503074500035426
 0.3581375824728499 0.4066446046474764 0.5364439860690233
 0.3585203401944366 0.9051728495043059 0.5423951590777906
 0.8550802272778378 0.4111530350532766 0.5445340825540741
 0.8571804764491918 0.9079485012881884 0.5411399862130772
 0.4779433523461649 0.3249368223127526 0.4476257835702250
 0.4955355555351818 0.8239719621974632 0.4398151522339990
 0.9903909981329876 0.3186984335704206 0.4393519113040492
 0.0000467138387728 0.8285097423301166 0.4385366347913486
 0.1029705646658900 0.4015764863158464 0.5530637116942938
 0.1105732105049513 0.9083241502560160 0.5527424282588181
 0.6071925154639340 0.4038723406267632 0.5525399222183480
 0.6118991074416393 0.9013187869573741 0.5518770036739206
 0.2401143054024339 0.3162246519327579 0.4537190985248610
 0.2489702016712158 0.8192896017586108 0.4497182448584580
 0.7382568993744102 0.3165342256617634 0.4509357601545826
 0.7460904409169334 0.8205496435318748 0.4488214193006120
 0.3587525303710466 0.4063936856182280 0.5965559849546048
 0.7456899730450689 0.6590573787855644 0.6478118510474434
 0.3445553683113109 0.4999014145592259 0.6079849929312288
 0.4334866791355677 0.3745443975429611 0.6080040942063518
 0.2983464969388133 0.3450084704337739 0.6081617451345084
 0.7629295061913228 0.7519555897335098 0.6368641020130330
 0.8048612896626220 0.5955010479869333 0.6368618885254039
 0.6707421791047441 0.6302877609840630 0.6358016408478995
 0.7430055267947629 0.6580585100982284 0.7080210050242832

[1T'-(MoS₂)₁₆(CH₃) + ClCH₃, S7-(14) FINAL STATE, charge = 2]

1.0000000000000000

13.1071123318841796 0.0000000000000000 0.0000000000000000

0.0000000000000000 10.9501063248573605 0.0000000000000000

0.0000000000000000 0.0000000000000000 30.0000000000000000

Mo S C H Cl

16 32 2 6 1

Direct

0.0026734581846541 0.4838534789337848 0.4965161303905235

0.0070280078049859 0.9772078523619002 0.4927328236711952

0.5113589117650013 0.5030016152510762 0.5001561752719428

0.5022911474750061 0.9926141141874709 0.4964868860233118

0.0909721687452593 0.2350725814696326 0.4951324273006679

0.1007003615507910	0.7260683084396692	0.4942733352280170
0.5912157073452642	0.2410349729556377	0.4981329502042398
0.5964065062255013	0.7537058942710606	0.4984837151119798
0.3724393589734678	0.2104971190849164	0.4970523703940761
0.3908815312393364	0.7348570796875845	0.4962768730785218
0.8732062987768967	0.2593567720464839	0.4959179598346119
0.8947914794879930	0.7433958221426028	0.4962412012004002
0.2086262847917831	0.4938446339670326	0.4971218127189500
0.2233130439397781	0.0122853889370122	0.4943755294326935
0.7247037689832164	0.4596115621506555	0.4979277432052530
0.7103080540711395	0.9852300435855995	0.4959316471305310
0.4847720304824942	0.1477643484560541	0.5536979165768090
0.4939303704631849	0.6607739959205040	0.5551160530271450
0.9801134024716202	0.1484497299182486	0.5472371512928456
0.9933183811709483	0.6515885868372967	0.5520094496207271
0.1094115234222339	0.0778056839580419	0.4378890702578548
0.1083638593444607	0.5688380694843582	0.4386620813993398
0.6093839483901083	0.0790772668175764	0.4411795404910934
0.6222116864815233	0.5775197521640915	0.4463710334666845
0.2314812335132992	0.1634612938714794	0.5478860280910705
0.2411395656636152	0.6589339829598467	0.5440069226908667
0.7399306290630291	0.1578071216162571	0.5420677260599935
0.7439452719234183	0.6590266093820308	0.5366785018619393
0.3638127373657645	0.0622387919213353	0.4428253514754307
0.3630643080402512	0.5667673958804526	0.4510893867715854
0.8590910489520102	0.0688976914136926	0.4525071226480235
0.8575753684998094	0.5667432051552892	0.4524872564555391
0.3604506506600121	0.4082822162234476	0.5370600747348042
0.3560099269677535	0.9097406087282079	0.5409036193852823
0.8643793184418155	0.4123589760655334	0.5491847720257357
0.8632796006255438	0.9104025119845768	0.5419164248326740
0.4782930977583574	0.3295445112426587	0.4473403479159221
0.4905152103605827	0.8267365906047472	0.4406527363220268
0.9845074465909261	0.3268745671972920	0.4394472283487025
0.9967746958278826	0.8186602722064532	0.4376725381450343
0.1093596753593779	0.3977567828553836	0.5519277927139441
0.1182074305331467	0.9025570720256454	0.5470900766168737
0.6113303372037165	0.3986808866210068	0.5549050877880063
0.6086790007512139	0.9091420539625932	0.5542155063394588
0.2398304844636391	0.3179971966917755	0.4521042662622709
0.2434522268098190	0.8184614587068237	0.4524342525720788
0.7316405657193989	0.3098922065574515	0.4446399486156495
0.7420322565971627	0.8195952479011818	0.4494975944019868
0.3592515615849681	0.4050666944866861	0.5971680007273213

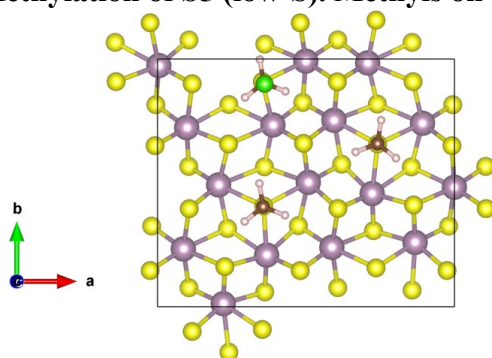
```

0.7439628981276137 0.6597390643681899 0.5967805366490694
0.3448163927444363 0.4979678627856654 0.6091540927187146
0.4338132428729359 0.3727072138475139 0.6086628538330693
0.2987810609536210 0.3430068209445697 0.6081559873976236
0.7560355735717599 0.7537989237197891 0.6080448150337577
0.8057172223568395 0.6005457111988476 0.6084605584835603
0.6700755070732185 0.6256390626633704 0.6083902267465884
0.7451764502332782 0.6586033218350920 0.7346521806389326

```

E.2.3 (MoS₂)₁₆(CH₃)₂ + ClCH₃ reaction on S5

Methylation of S5 (low-S). Methyls on the surface before reaction: S7, S14



[1T'-(MoS₂)₁₆(CH₃)₂ + ClCH₃, S(5)-7-14 INITIAL STATE, charge = 2]

```

1.0000000000000000
13.1071123318841796 0.0000000000000000 0.0000000000000000
0.0000000000000000 10.9501063248573605 0.0000000000000000
0.0000000000000000 0.0000000000000000 30.0000000000000000
Mo S C H Cl
16 32 3 9 1

```

Direct

```

0.9997462897609107 0.4822943265914555 0.5019188333835085
0.0043893199868143 0.9734198016600782 0.4976445052209248
0.5077634921176367 0.5020638560223036 0.5052946201999957
0.4993315609465236 0.9913006363957657 0.5015144115169918
0.0867599679654757 0.2332227878731690 0.5005088319995744
0.0981480822723360 0.7231513604631744 0.4992702846070496
0.5871193320661353 0.2398332838327386 0.5031763511084992
0.5941348877897477 0.7525076795071575 0.5037917141863488
0.3673413679359175 0.2085775798161758 0.5024210828701341
0.3886005285187485 0.7336074819580899 0.5012837745807568
0.8674840869095454 0.2595856497069285 0.5008707718435995
0.8924273679851891 0.7406548669657471 0.5015252806131270
0.2056501965561256 0.4917295100588079 0.5020666409465928

```


0.2214911793792175 0.0124482351025800 0.4990501307897497
0.7227698375140796 0.4568188296382681 0.5036402114157748
0.7075712824978651 0.9841208526879081 0.5013952596458445
0.4806589143228729 0.1459863618877099 0.5588125239282068
0.4914573380977882 0.6597655125607744 0.5603661497484557
0.9751452892215700 0.1462628866533955 0.5518050505755724
0.9916740720883184 0.6500749705296043 0.5574254929166437
0.1058244157605761 0.0767173610818952 0.4430035803410029
0.1051023378929443 0.5663715204009877 0.4436767191680878
0.6069108949453137 0.0770498234452846 0.4464855853527219
0.6201092184694114 0.5753844694674111 0.4519793938569601
0.2266637989218832 0.1618320121349958 0.5532910662298536
0.2390917249606328 0.6570874773962144 0.5489665709518212
0.7357710686516574 0.1568212880089792 0.5473881628740063
0.7411832736308764 0.6569169320539650 0.5416514233796930
0.3612720801041310 0.0599252607925973 0.4477995669701301
0.3599758059299190 0.5648684317941950 0.4562476294995120
0.8572954720420000 0.0670411927176933 0.4582094249846739
0.8546783654083920 0.5644185601243017 0.4578056799171826
0.3574095858806621 0.4065839281921221 0.5417604851488670
0.3530484292297822 0.9085066941949999 0.5452362402922891
0.8622509874781285 0.4109516273744251 0.5549672575262665
0.8605621588318807 0.9086518373764360 0.5469924417713644
0.4742981987752566 0.3273846782229102 0.4526213243707374
0.4889711555841106 0.8246565530512620 0.4457471738911054
0.9804330398632101 0.3256665113678761 0.4447798341060177
0.9943460983291721 0.8154762959781380 0.4426859089368261
0.1067403372812614 0.3959721615872213 0.5570370537518983
0.1167376337951414 0.9003209832810423 0.5517272344120340
0.6075072313325269 0.3967204797555260 0.5601099192263691
0.6054336138055567 0.9080467918648563 0.5595000790470349
0.2357521076457788 0.3159105670615663 0.4572015534273712
0.2404029595000203 0.8163402032644320 0.4577013906580840
0.7273082317229187 0.3070054924895221 0.4498324806286248
0.7401895672110791 0.8181223522897546 0.4549939123481206
0.3554063610154046 0.4039610371678830 0.6018340999138114
0.7410301370498431 0.6586114858419788 0.6017203236371074
0.3572493167581384 0.9033241678441388 0.6533877229289907
0.3429733258111092 0.4974774852842748 0.6136546365861568
0.4290754394589582 0.3692429112999496 0.6135384622291760
0.2933616202105507 0.3440021351533244 0.6127180312117140
0.7529694564884167 0.7529292291455107 0.6127572088502241
0.8028728547864670 0.5995729315549790 0.6134648644430679
0.6670517529379973 0.6246118137985273 0.6133022042392231

0.3446659467235010 0.9977367877270396 0.6429817887574690
 0.4304708210931509 0.8696857580515447 0.6410591650469932
 0.2948150326291409 0.8446911220595907 0.6422359471512142
 0.3605200756787296 0.8995548670517405 0.7135658528581733

[1T'-(MoS₂)₁₆(CH₃)₂ + ClCH₃, S(5)-7-14 FINAL STATE, charge = 2]

1.0000000000000000

13.1071123318841796 0.0000000000000000 0.0000000000000000

0.0000000000000000 10.9501063248573605 0.0000000000000000

0.0000000000000000 0.0000000000000000 30.0000000000000000

Mo S C H Cl

16 32 3 9 1

Direct

0.0068798361492700 0.4844977279129045 0.4992439835657845
 0.9976383826728211 0.9749759231261190 0.4984211812203659
 0.5120279261915518 0.4988235869222369 0.5035435131411440
 0.4995585806329855 0.9978130148769020 0.5018907654871985
 0.0863548033406299 0.2238468875524363 0.4971014128796130
 0.0971189375445380 0.7360754272519251 0.5013397661315996
 0.5888370544182555 0.2391323365802583 0.5015329987576163
 0.5881160667132230 0.7507846269256885 0.5037668834018908
 0.3741654153329460 0.2110582107714453 0.4997305706044426
 0.3720501666502429 0.7074831319728215 0.5025950942131879
 0.8702292527721917 0.2614527850166542 0.4986808733721971
 0.8904575961733437 0.7427566975726559 0.5007334122174539
 0.2241563270638356 0.5112450758073577 0.4993588048089845
 0.2055064444240672 0.9954291149497823 0.5015209874334958
 0.7265397923787428 0.4587627864999447 0.5015214687787964
 0.7056648018554663 0.9839107560511057 0.5005015348226409
 0.4832790554401548 0.1508086702485892 0.5581944817944992
 0.4877406867788532 0.6511455397066535 0.5599072717632870
 0.9756217880538547 0.1504754166644402 0.5514740721107432
 0.9888244967692549 0.6472275609884877 0.5557497197911195
 0.1021619426120612 0.0675847457665428 0.4422104193348887
 0.1125327286392114 0.5777595400981400 0.4435362975975912
 0.6062206252554898 0.0763936226902729 0.4449303705284527
 0.6223839024710641 0.5776357512990509 0.4507092844583067
 0.2290180324131341 0.1624312860442631 0.5486825980493721
 0.2324291766793250 0.6604191271031422 0.5540011854785404
 0.7382908749961361 0.1580697987369686 0.5453007335630548
 0.7393484745467467 0.6573183564712701 0.5406346493602288
 0.3602592861667309 0.0592367200778155 0.4489395500042368
 0.3677409654455858 0.5563477804119480 0.4494356751937046
 0.8541300474880824 0.0668136279720652 0.4570912009840361

0.8584467836760139 0.5673200863190287 0.4561394150156330
 0.3623856751126872 0.4068786434595943 0.5403974820274756
 0.3529274624989425 0.9051899616188700 0.5411902346745571
 0.8669378093632274 0.4123759811712868 0.5523859066224740
 0.8561665333582952 0.9075729497542829 0.5476136130602731
 0.4783023387544862 0.3285316601274814 0.4500975152648772
 0.4772696991328709 0.8214167535453759 0.4499129861589847
 0.9847556890560731 0.3268985967325286 0.4424127789755391
 0.9916846812731404 0.8189640748486574 0.4427488152853236
 0.1182523243745795 0.3980724138438740 0.5504944066591371
 0.1040868244224755 0.9030804955381374 0.5564904383777824
 0.6137465977012355 0.3958854093737413 0.5582328636080296
 0.6033386224071591 0.9077372037165765 0.5589376223763073
 0.2336344553236799 0.3150937382062338 0.4581641059629014
 0.2417004488913283 0.8170174974583531 0.4568559023133617
 0.7298493768320086 0.3096002979039725 0.4475499032420547
 0.7357861695701532 0.8165843380439162 0.4550154185009464
 0.3593848628731945 0.4045470135361330 0.6004372944403626
 0.7402813638025116 0.6551841342204341 0.6007484858106540
 0.3531544910561871 0.9076786037058039 0.6012426272311481
 0.3491884379192738 0.4983753526993422 0.6122795233439837
 0.4316786056528881 0.3668262149203955 0.6124740726477131
 0.2952575996352579 0.3473342833753174 0.6110160769513217
 0.7544603621779772 0.7483865704131969 0.6125014387224634
 0.8007834847756214 0.5934864975622939 0.6119658492379181
 0.6657037507494028 0.6229584640566715 0.6122836392343937
 0.3429584743889172 0.0023029674744586 0.6122123546345560
 0.4263572737797965 0.8717000554963464 0.6129285954252144
 0.2901459552549368 0.8505729826160667 0.6130499882183651
 0.3532137056743039 0.9075908128547244 0.7393412081471015

E.2.4 (MoS₂)₁₆(CH₃)₃ + ClCH₃ reactions

Methylation of S16 (low-S). Methyls on the surface before reaction: S5, S7, S14

[1T'-(MoS₂)₁₆(CH₃)₃ + ClCH₃, S5-7-14-(16) INITIAL STATE, charge = 2]

1.0000000000000000

13.1071123318841796 0.0000000000000000 0.0000000000000000

0.0000000000000000 10.9501063248573605 0.0000000000000000

0.0000000000000000 0.0000000000000000 30.0000000000000000

Mo S C H Cl

16 32 4 12 1

Direct

0.0062440188551238 0.4802927734528745 0.5014834499203353

0.0038339131031149	0.9719491959341537	0.4992010606935308
0.5118985706713098	0.4978580681137516	0.5052792576372112
0.5042574068213226	0.9982777092113911	0.5033632164311984
0.0885799903530334	0.2243229202940083	0.4996397772880340
0.0962313923437309	0.7237804446645211	0.5014190121217220
0.5914812590593693	0.2398511886971103	0.5032123484390439
0.5899017295432313	0.7507855197500676	0.5053622012047501
0.3699893122478036	0.2073487098093218	0.5038343042474452
0.3730238310439754	0.7063302661882624	0.5045876491656217
0.8722670253454879	0.2598704739022897	0.5005036389385494
0.8911733718583132	0.7405423208523733	0.5026194833594732
0.2245867294397563	0.5101093923809858	0.5011525637053503
0.2205099321820848	0.0118862845647069	0.4999671650225127
0.7266008607190588	0.4569778861954790	0.5035516800886533
0.7099156794708523	0.9815614564039041	0.5014880692183896
0.4866048892984869	0.1498621221544416	0.5603798684107308
0.4899003450197212	0.6510503961481472	0.5617075445145343
0.9772823705014579	0.1473788285926824	0.5530300518328877
0.9889110870339208	0.6460401376220509	0.5580827576724027
0.1056120405217922	0.0710054034920074	0.4429798381368439
0.1116248506160210	0.5711161741169573	0.4443856597242462
0.6097188724508404	0.0755829221596495	0.4464573420312578
0.6225315944616212	0.5758207279925146	0.4524042260654119
0.2272829657964217	0.1625929786196109	0.5540162996184936
0.2326317343471144	0.6605473222374324	0.5556701167747861
0.7410597536063961	0.1564637904939120	0.5461413742061118
0.7402893372537301	0.6560979303230715	0.5422874610254838
0.3629267132378385	0.0585966259764397	0.4494443157289938
0.3683842345087093	0.5553148562155305	0.4513006090229799
0.8579086147127869	0.0655359319852727	0.4583663286178819
0.8582326474522524	0.5641102936359651	0.4581222402123893
0.3630698355282996	0.4052688395212533	0.5420750997270735
0.3583357059301681	0.9064696171577893	0.5414210916015003
0.8671521038588721	0.4108892129908457	0.5544913002296959
0.8613229367748163	0.9077277846815169	0.5487778630451807
0.4761600213655932	0.3239672070480976	0.4531068195166188
0.4763571646108137	0.8213571120263102	0.4520892576657251
0.9864427876022781	0.3242669938550594	0.4442479889894336
0.9933462710818964	0.8149002035497831	0.4441164441845956
0.1188957688276453	0.3975510834747034	0.5530521119428434
0.1165302539076812	0.9014079729023791	0.5534195398469579
0.6134884910968544	0.3954312767263437	0.5602859542018075
0.6077480990598243	0.9077472165585388	0.5603460986731493
0.2348024546106660	0.3147588855938885	0.4605659246616859

0.2383053541303798 0.8140231268079413 0.4606176619311617
 0.7311702488768458 0.3079094641557454 0.4494184284728053
 0.7371327263317624 0.8140440331985997 0.4558996167915954
 0.3601989111533806 0.4066119668061399 0.6021092044487771
 0.7410884455407910 0.6547742885053480 0.6023647670654164
 0.3573050298480719 0.9113659761816668 0.6014253288940893
 0.7350698333896377 0.1561225680260198 0.6539004082308053
 0.3520493657359987 0.5013822519997148 0.6132717916261543
 0.4318866825105860 0.3674933449603325 0.6143043396461466
 0.2950912190529749 0.3517412169569898 0.6131777614013150
 0.7544862836975634 0.7483225515091279 0.6139430793777455
 0.8021191262476541 0.5939287118005940 0.6136689209162683
 0.6667033669738170 0.6218086435589193 0.6138935234569270
 0.3490901727172834 0.0066266325920332 0.6119684629522345
 0.4295267950021018 0.8733655688165100 0.6134639753135896
 0.2926977165753715 0.8566867203987083 0.6131456601529961
 0.7425904488937028 0.2508963247530588 0.6429798844026363
 0.8006524931165007 0.1020576882588096 0.6431461447285020
 0.6639278374397064 0.1163545470445811 0.6416665972855735
 0.7315176049696678 0.1546547010837401 0.7141223227013113

[1T'-(MoS₂)₁₆(CH₃)₃ + ClCH₃, S5-7-14-(16) FINAL STATE, charge = 2]

1.0000000000000000

13.1071123318841796 0.0000000000000000 0.0000000000000000

0.0000000000000000 10.9501063248573605 0.0000000000000000

0.0000000000000000 0.0000000000000000 30.0000000000000000

Mo S C H Cl

16 32 4 12 1

Direct

0.0089933565380269 0.4758002089363169 0.4981501942331234
 0.0021103050449639 0.9755296719954313 0.5003062405027834
 0.5106201885487286 0.4991575084683969 0.5035286667841159
 0.5065198928223654 0.9966811240546251 0.5032360285405463
 0.0906320913450858 0.2215294828051326 0.4983073041246250
 0.0944423271661144 0.7360662822421487 0.5010822450455985
 0.5875072093689165 0.2477187402927638 0.5033933568160025
 0.5879671307864645 0.7475077998502750 0.5034133776251291
 0.3762590776997265 0.2091714421258973 0.5006314592312325
 0.3710344845748501 0.7069493731621769 0.5027243499838472
 0.8750566665266687 0.2615380635554098 0.4990846399163290
 0.8747864237102482 0.7618451878097843 0.4993736414293208
 0.2237252345411331 0.5117141064105917 0.4992941563300384
 0.2091438748237924 0.9937125898781975 0.5023835868255500
 0.7278959400456932 0.4577884504013975 0.5025629196977003

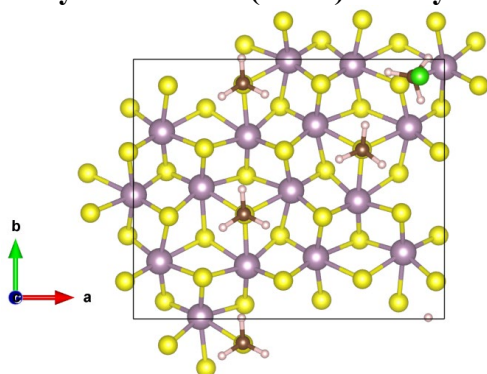
0.7248600238443444	0.9564269695795032	0.5030311149851925
0.4860042807594389	0.1503432733993485	0.5592269741697586
0.4862306379047244	0.6508183974955581	0.5599217656518261
0.9789265984530225	0.1519383981486645	0.5528408553944661
0.9793772644045728	0.6492942061619814	0.5512081584827871
0.1060072428262559	0.0659261592489525	0.4432951174234911
0.1109335671394910	0.5769463832907936	0.4432198357394037
0.6215173721395144	0.0732982231603983	0.4513050956660403
0.6234011080721720	0.5735310267222944	0.4509184137451758
0.2318701421811264	0.1614725835664530	0.5498418862047404
0.2303523467926984	0.6608588704569979	0.5538378012443125
0.7365052139730335	0.1562760162870828	0.5403354413392092
0.7372399274416246	0.6562839957775020	0.5405095589232143
0.3661497793858782	0.0565489441703373	0.4502964080842194
0.3674298019230460	0.5560229607354480	0.4492716834683337
0.8594499621240498	0.0645279980104066	0.4593132598674590
0.8631928962090777	0.5659594397825212	0.4589767071304108
0.3612982547998707	0.4067637759957494	0.5404677470521034
0.3568813550307575	0.9041932660147770	0.5417003165093511
0.8700409046435926	0.4131719249458863	0.5527646679133472
0.8653609396501455	0.9117850122890369	0.5540446955370044
0.4779630896711167	0.3269479593907849	0.4500733773693321
0.4773477819285306	0.8215901523810156	0.4503546366988760
0.9891723039417544	0.3215149056476592	0.4420251177054506
0.9887495460190779	0.8235829704726122	0.4431695819781383
0.1196909923617426	0.3987095059848727	0.5514785722125604
0.1086907095320554	0.9004914938296377	0.5574318644033152
0.6123633038130840	0.4004770985539949	0.5596360651048430
0.6088292031984506	0.9000197276345336	0.5598175835311677
0.2363387771617887	0.3136192463738285	0.4588265257469019
0.2419453745132716	0.8167921813154406	0.4566765880187652
0.7312805050472505	0.3075979592575607	0.4489711900894440
0.7306819424800087	0.8061625261130326	0.4494070614364668
0.3595427713190160	0.4060287386176897	0.6005314387463929
0.7395151265250062	0.6578606072516123	0.6005661539307382
0.3567485294756677	0.9049433742264712	0.6017608762948521
0.7387006661244299	0.1591830780326887	0.6003732731025860
0.3503584703507450	0.5002841850990400	0.6121013418203434
0.4319843172806290	0.3680729364824090	0.6123239737720372
0.2953612841359339	0.3497597542803390	0.6116846413945919
0.7472864380162697	0.7526357978120298	0.6117271934895586
0.8046272183990669	0.6032761425988105	0.6118081996166983
0.6678714428717614	0.6184314288244684	0.6126685643239916
0.3455137689526792	0.9992388867838670	0.6129533833861017

```

0.4303923471975936 0.8698973973950288 0.6133265203095762
0.2943961083705288 0.8466008172414394 0.6134212905346778
0.7464790855874448 0.2540642176338052 0.6113763343108691
0.8038104172180874 0.1048454544968804 0.6117090136732622
0.6671123850694514 0.1200088044588287 0.6125925897757060
0.7322639005322644 0.1571465802633503 0.7373316607645507

```

Methylation of S13 (low-S). Methyls on the surface before reaction: S5, S7, S14



[1T'-(MoS₂)₁₆(CH₃)₃ + ClCH₃, S5-7-(13)-14 INITIAL STATE, charge = 1.5]

```

1.0000000000000000
13.1071123318841796 0.0000000000000000 0.0000000000000000
0.0000000000000000 10.9501063248573605 0.0000000000000000
0.0000000000000000 0.0000000000000000 30.0000000000000000
Mo S C H Cl
16 32 4 12 1

```

Direct

```

0.0010296925015231 0.4774404907908601 0.5014497799342099
0.9987890249455190 0.9696562618806038 0.4992462175182544
0.5069795327800948 0.4950484165842811 0.5051696851622094
0.4990560391086726 0.9953633562081718 0.5031867284959544
0.0839556451011991 0.2215253829862051 0.4996527986819589
0.0916474231977181 0.7213721505448301 0.5014485198645492
0.5870813949242156 0.2368570642437760 0.5032605869503646
0.5848762276578542 0.7481169713083231 0.5050769691457542
0.3654745565285915 0.2044968562703041 0.5037355134357429
0.3681418199594285 0.7035584047530697 0.5043561357753956
0.8678054206491143 0.2562287842684658 0.5008521291255579
0.8863722730272896 0.7376343692310842 0.5023372421601452
0.2191239969582060 0.5069199608020484 0.5011221469452850
0.2151243962685049 0.0085749468360714 0.5000721031127334
0.7213043492627630 0.4543345260724426 0.5033534091832602
0.7048768417207880 0.9790006950125236 0.5014321138666118
0.4818915397593952 0.1469717486861485 0.5602347214837202

```

0.4849641695257902	0.6485166175863253	0.5614504915811662
0.9730983504927603	0.1445624175843907	0.5532608728789336
0.9838325786049102	0.6434441325587344	0.5579719555023404
0.1007987253857647	0.0681796237722366	0.4430025276450140
0.1063865176718778	0.5682914489521810	0.4443901036505585
0.6048506179791105	0.0731429024159424	0.4463720334917550
0.6173370890853183	0.5729952861139777	0.4521599174278935
0.2229667473412227	0.1597158932542555	0.5539827202028796
0.2279204824716777	0.6575672644627522	0.5555628467190875
0.7360776181889374	0.1530318216358802	0.5470720836958597
0.7353292125099847	0.6535030445441198	0.5420943562693343
0.3577462470703092	0.0559662220700860	0.4493702518861146
0.3629617663103859	0.5524004292308694	0.4511833675398193
0.8526193872975717	0.0631225885312535	0.4583009034747224
0.8532192471091545	0.5612922810648840	0.4578921453732336
0.3580338318456678	0.4024976284103135	0.5421018825871072
0.3531227202958314	0.9034312859252919	0.5415404872977548
0.8616624204221006	0.4082370861978382	0.5544274126226028
0.8560859787885802	0.9047300477451351	0.5482501584879098
0.4714559355741844	0.3211450015585067	0.4530477692421486
0.4713465795270552	0.8185901853231626	0.4517659753092508
0.9812986848497373	0.3209421681191911	0.4443765722666929
0.9886869795656293	0.8124924984445288	0.4440481741115390
0.1136893532412155	0.3947424172894401	0.5531384740530864
0.1111659059054606	0.8988375539159743	0.5535798788648093
0.6084712767385877	0.3930056709297925	0.5601848560114725
0.6026038237049240	0.9047075639723595	0.5601393770257023
0.2301202824477907	0.3118373873665022	0.4603696000116749
0.2336891516005653	0.8114672906161291	0.4603256382258447
0.7267992381555987	0.3051823539712027	0.4494789511300199
0.7320400161923318	0.8116279283868946	0.4556964595234239
0.3550967022378596	0.4039587681869185	0.6021440086859492
0.7356829934397421	0.6520279994793996	0.6021580439428297
0.3520642021529580	0.9080914651559820	0.6015571348853306
0.9010571988539881	0.9331876681633803	0.6573704573143451
0.3499922811952971	0.4990100995228616	0.6133032091295103
0.4253560987841414	0.3615013292153494	0.6144158995021896
0.2881798647780152	0.3522113470870831	0.6131401041977905
0.7452097504322293	0.7461881605383988	0.6137757627646353
0.7989249519559288	0.5946916268134205	0.6135872924018044
0.6625942453202324	0.6150221266301937	0.6136084023443518
0.3480514981244761	0.0036836229407329	0.6121475323291415
0.4223793139574468	0.8654351153763474	0.6136756331900692
0.2850341222051713	0.8576080757637321	0.6131844286832708

0.9481075360331657 0.0049700601478971 0.6425805204579425
 0.9238061745417686 0.8434293232032826 0.6449159138770044
 0.8201818762981595 0.9502820631837026 0.6510772889040429
 0.9208469323963054 0.9349183321540605 0.7168444571455953

[1T'-(MoS₂)₁₆(CH₃)₃ + ClCH₃, S5-7-(13)-14 FINAL STATE, charge = 1.5]

1.0000000000000000

13.1071123318841796 0.0000000000000000 0.0000000000000000

0.0000000000000000 10.9501063248573605 0.0000000000000000

0.0000000000000000 0.0000000000000000 30.0000000000000000

Mo S C H Cl

16 32 4 12 1

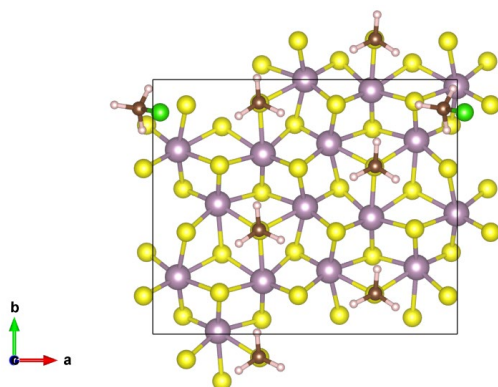
Direct

-0.0014741979639001 0.4713541967212340 0.5000958298520417
 0.0032306223121967 0.9746512722798863 0.4990058627707642
 0.5062641410267774 0.4951376841421762 0.5041099934692299
 0.5083137599306765 0.9956094193227716 0.5025189993484416
 0.0908569974564335 0.2341227060698567 0.5004841836159164
 0.0873052064960360 0.7199240040828440 0.4990764055577647
 0.6116211340615462 0.2443734330991937 0.5012172303250036
 0.5839282743438656 0.7469468253520222 0.5040874148800296
 0.3671665551360351 0.1997349412480243 0.5046207955178803
 0.3729949037541671 0.7069731809436631 0.5015023369860051
 0.8548398021116892 0.2608440070441299 0.4985808102057524
 0.8725934826312916 0.7573791185524994 0.5003391502898749
 0.2087198367221241 0.4943458123350712 0.5028754902226081
 0.2197492673060236 0.0100574720589300 0.4990739201117280
 0.7227532555026109 0.4603684985383696 0.5021621140028093
 0.7223621037764932 0.9627583520086661 0.5029705322075131
 0.4921199002685576 0.1513123703831311 0.5575785027152347
 0.4838061839506617 0.6478607476330881 0.5601246764249734
 0.9764598781779524 0.1530169348020395 0.5502593191115108
 0.9764336670874164 0.6468761976919059 0.5533738343655051
 0.1058615971479400 0.0746799594061731 0.4433802298318724
 0.1037272270430979 0.5633108094920227 0.4439745671683745
 0.6198176498087858 0.0674161217534873 0.4484708404220263
 0.6161358076292510 0.5750197743702011 0.4507212988884562
 0.2258737456600084 0.1582126457587698 0.5544510099944623
 0.2288237684826465 0.6601538553755609 0.5510578428234245
 0.7378931429063684 0.1521936328512090 0.5486138465061251
 0.7325254557353365 0.6557488280965964 0.5413611899187738
 0.3643642292641513 0.0543625090877063 0.4492149401591957
 0.3631039411614384 0.5516066654727039 0.4516723961775261
 0.8568594569667586 0.0653935108748668 0.4587321873140289

0.8582128964006609	0.5659108501812898	0.4585913635672075
0.3565091943788136	0.4004537328479900	0.5423737905975912
0.3586191094607884	0.9062523245989209	0.5402660508009155
0.8595658760391776	0.4099676234909342	0.5537628923536871
0.8664571847146246	0.9149361488393032	0.5507084003165061
0.4772388068089146	0.3147761149753607	0.4548630130459456
0.4742076060499403	0.8223027965142096	0.4500284065503660
0.9807547775737246	0.3177556194374830	0.4442775610379420
0.9858327717024210	0.8200350715487332	0.4430213597286312
0.1063352933534880	0.3986283655232856	0.5569691391899254
0.1160643739044406	0.8978800883920195	0.5518429086165966
0.6105607689360608	0.3968848837791891	0.5590641778094863
0.6080051332788786	0.9010225362755332	0.5598357636031596
0.2393709528510186	0.3127915906526959	0.4579933696057036
0.2328761395252809	0.8113820200062671	0.4596472484364151
0.7279423060723971	0.3171050906701475	0.4441215617238101
0.7279045221942791	0.8073555680139167	0.4508048109953289
0.3550095781733043	0.4021459784861121	0.6025044917157850
0.7327511797954444	0.6521243080514778	0.6014195690226537
0.3576132376169968	0.9089627417922189	0.6003193790740726
0.8792223700251333	0.9221543139006976	0.6106581141415082
0.3465611839925797	0.4971101063615956	0.6133822449586891
0.4271532323307908	0.3639926445831638	0.6145288457783388
0.2904676600180963	0.3471823412633682	0.6140725244599751
0.7202161734706005	0.7447087805002462	0.6139903570038395
0.8063287562478462	0.6162512552073117	0.6126712555337801
0.6706200942577490	0.5923624366186990	0.6123342492262657
0.3532584925152001	0.0042809843899895	0.6112954861092195
0.4280574942127315	0.8664741087179895	0.6123165964102030
0.2907742454596578	0.8579748973352033	0.6118659368689616
0.9258526405707916	0.0021404872399569	0.6187260182726080
0.9165076635640678	0.8380271563776205	0.6217698736086469
0.8029196136629450	0.9315774828026415	0.6250242607679399
0.8816747279045194	0.9138676757677523	0.7312523625906798

E.2.5 (MoS₂)₁₆(CH₃)₄ + ClCH₃ reactions

Methylation of S13 (low-S). Methyls on the surface before reaction: S5, S7, S14, S16



[1T'-(MoS₂)₁₆(CH₃)₄ + ClCH₃, S5-7-(13)-14-16 INITIAL STATE, charge = 2]

1.0000000000000000

13.1071123318841796 0.0000000000000000 0.0000000000000000

0.0000000000000000 10.9501063248573605 0.0000000000000000

0.0000000000000000 0.0000000000000000 30.0000000000000000

Mo S C H Cl

16 32 5 15 1

Direct

0.9968992287217425 0.4739382391810462 0.5004224880457110

0.9968403400712255 0.9739521082615477 0.5003008957362949

0.5001031776546035 0.4996603568528846 0.5051057294831373

0.5000519419350717 0.9997479406043883 0.5049960812937450

0.0821380661185806 0.2239368270179021 0.5003917256168521

0.0820954456787897 0.7239970168836869 0.5003479284798557

0.5789484609833867 0.2497122944266997 0.5050482149200746

0.5789096480519199 0.7496153966841641 0.5050395468585825

0.3614804627395963 0.2081393837094658 0.5044352182985676

0.3614401346837637 0.7081685845453403 0.5044507408148092

0.8657642015655442 0.2621062800478357 0.5006280749963363

0.8657827099263672 0.7620327178576153 0.5005010998441878

0.2132775350452908 0.5121684776823978 0.5006417240515075

0.2133325038329234 0.0122810538862550 0.5004467663003687

0.7175878889602315 0.4581276941325663 0.5044585757708648

0.7172740567307696 0.9582838679648050 0.5041410590727351

0.4773645409946280 0.1521316606268168 0.5614982042133154

0.4772877715296248 0.6522198714555252 0.5615340190897742

0.9695592572345597 0.1502350756019550 0.5536711312995934

0.9694385039589044 0.6505573225357707 0.5536411332926637

0.0991926488236418 0.0715139094104829 0.4435983033020100

0.0993640402653798 0.5713406051319445 0.4437006764121922

0.6127529080573525 0.0745398228629090 0.4524720713788424

0.6130677830236517 0.5741824327845160 0.4526488400425904

0.2192388650839201 0.1634700646228710 0.5547259691446146

0.2191736243168760	0.6637383145539376	0.5547806836011526
0.7279422677460015	0.1574580154084806	0.5417059847131315
0.7279874450754888	0.6575847822634618	0.5417683446358216
0.3577552064311529	0.0577433578946055	0.4507155004237958
0.3576684737626063	0.5575592556279224	0.4508418278405862
0.8520111075815492	0.0654404324302491	0.4604277952867248
0.8520196569167316	0.5651448033150485	0.4605484062311622
0.3511108786927950	0.4074838295491596	0.5418034164890209
0.3510635405056091	0.9076252858388386	0.5417240714779457
0.8597885023419489	0.4135831295224723	0.5547943717747675
0.8591630555477243	0.9140807525474267	0.5543273478060706
0.4659109815851524	0.3243627502552042	0.4526524160659284
0.4658816289917863	0.8242091284983040	0.4526236778123373
0.9797105794960527	0.3214628077975543	0.4437041969060860
0.9797878681685436	0.8213434826607146	0.4435996330040567
0.1095515404569771	0.4003863993873014	0.5536905156859844
0.1099056917561953	0.9004898904005175	0.5534625124796393
0.6017818258104700	0.4021282628918632	0.5615412411744964
0.6018553819505449	0.9022544954587354	0.5613858831766850
0.2269978615792866	0.3153615253435379	0.4606048420869044
0.2270026861916004	0.8152817954693570	0.4605101170847132
0.7213628962228077	0.3076159835973294	0.4508213437365796
0.7212966369684584	0.8073888089307263	0.4506637453022070
0.3488075774321392	0.4098829898848047	0.6018239419976111
0.7304398201725394	0.6600524954432351	0.6017931123976217
0.3485098486913361	0.9102391253547153	0.6017534491130316
0.7305548894048512	0.1597092088280208	0.6017294316463100
0.9544787048147395	0.8859771231771822	0.6567858513363726
0.3421404788011031	0.5049744508141124	0.6127906312000591
0.4201174653179954	0.3695785178530145	0.6139321723032395
0.2830373951653469	0.3564946291042797	0.6130945852879416
0.7354873349580711	0.7552944990813587	0.6127421926395047
0.7971272037103502	0.6083002115697818	0.6130475459426379
0.6598800684823646	0.6180305332500174	0.6139551740497605
0.3422606877052288	0.0054267792808907	0.6126603231219869
0.4195610451041460	0.8694701061361209	0.6139513132382526
0.2824044692516233	0.8574023593683883	0.6130071323621530
0.7367251409957569	0.2548515692548915	0.6126918668654351
0.7967783628104262	0.1069772913137146	0.6128981802462209
0.6596139388985330	0.1187394371411351	0.6139528664074407
0.9858435914474084	0.9636878573864669	0.6384967214987950
0.9650693978445709	0.8017500874123884	0.6377780745382226
0.8740520875891892	0.9004503622664332	0.6648254726459989
0.0239713566528295	0.8713749368945464	0.7084309468554356

[1T'-(MoS₂)₁₆(CH₃)₄ + ClCH₃, S5-7-(13)-14-16 FINAL STATE, charge = 2]

1.0000000000000000

13.1071123318841796 0.0000000000000000 0.0000000000000000

0.0000000000000000 10.9501063248573605 0.0000000000000000

0.0000000000000000 0.0000000000000000 30.0000000000000000

Mo S C H Cl

16 32 5 15 1

Direct

0.0031105164011905 0.4724852174849808 0.4989875036089435

0.0048992053266808 0.9711055060694451 0.4995074710591801

0.5047300925412082 0.4979274239675421 0.5033685302593930

0.5060677367230512 0.9974062895586209 0.5044234332378423

0.0891567422095634 0.2247676628965776 0.4990699999361757

0.0888863993041637 0.7214411447839661 0.4996630790528560

0.5839335728557510 0.2483727897715638 0.5035656537460095

0.5842572036574195 0.7479241589647917 0.5045569724319239

0.3673137623993997 0.2064370311225835 0.5029030306104983

0.3678143234162512 0.7064482790104050 0.5033384358491803

0.8713958445211455 0.2615747291216138 0.4990438352062543

0.8721475856561000 0.7576462819087837 0.5001369661721508

0.2185092302374695 0.5098994425801506 0.4995204013638522

0.2191629677923478 0.0098381579613716 0.4996356757046121

0.7231195144303083 0.4562184189309053 0.5029016982450607

0.7217747287498752 0.9581613625612524 0.5046859244956156

0.4826911066942405 0.1513643010470636 0.5602681243039908

0.4826002250417645 0.6488890030792658 0.5604797357723378

0.9763774085344161 0.1515974992904238 0.5519720169314846

0.9760949602175841 0.6465621094784321 0.5528042879212089

0.1056467200852851 0.0703229652176111 0.4426404858850962

0.1051768441203782 0.5698754133966673 0.4424729315208544

0.6194662948168522 0.0720624184244428 0.4519742571741378

0.6186285544344542 0.5734353799852840 0.4514333593599072

0.2256813439700737 0.1620453203794734 0.5534752610033098

0.2260174500032256 0.6612689745303565 0.5537263504095078

0.7330875653409242 0.1592254672535966 0.5409857927861896

0.7327843041117034 0.6545407680018395 0.5412528144093927

0.3637209773375812 0.0550329113098103 0.4497357190280787

0.3629157325710896 0.5570307810976474 0.4494098952816827

0.8582181078086417 0.0622803410676690 0.4609548947596446

0.8578374891703161 0.5643041040760498 0.4590796920443598

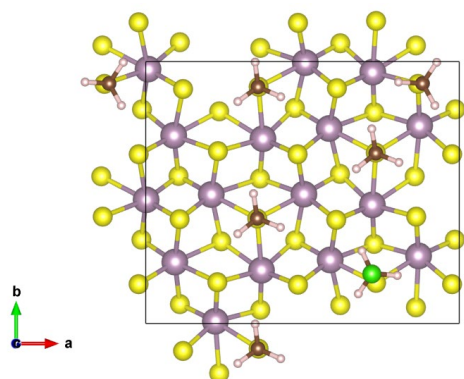
0.3561590926865503 0.4053191296923302 0.5407076841549376

0.3569558066087678 0.9056685718091927 0.5410903102793011

0.8653623644582047 0.4122693527379018 0.5532979192046206

0.8681806917901519	0.9146560690949124	0.5512831478366056
0.4717220634376149	0.3225292143562735	0.4508316112415537
0.4721945147971426	0.8228534664597962	0.4517701672867662
0.9854756392118259	0.3201971636606755	0.4421307157242801
0.9861231628702564	0.8189633068059817	0.4431036328319978
0.1150193465374592	0.3993312970644976	0.5527197688886955
0.1171398072894788	0.8980485702273777	0.5529632546625493
0.6064124679406414	0.4009754526322281	0.5596592441409042
0.6058038868265746	0.8998592667859158	0.5613296747999587
0.2338793922271670	0.3142690210348214	0.4586629154455270
0.2331588395593416	0.8134294256742447	0.4595739382415732
0.7268869039098076	0.3055749298033237	0.4492203245306600
0.7263114842952395	0.8069379316152085	0.4511324693708414
0.3543380244345714	0.4076269587348030	0.6007558941179206
0.7334375049218986	0.6512725379271251	0.6013131804285028
0.3544191183995682	0.9084735987248109	0.6011331840765904
0.7349682050537629	0.1661570658313865	0.6009982782406391
0.8878265335851728	0.9068647074919783	0.6109693545972251
0.3452926063568078	0.5023768037335260	0.6117527077767588
0.4266831937267103	0.3699521955762882	0.6128110758775883
0.2900898916749313	0.3518863001802612	0.6121572323981359
0.7187794626682634	0.7434568672825423	0.6138213077365656
0.8077554425389422	0.6177699622808749	0.6126106317637544
0.6726195707661503	0.5896963965365325	0.6123173141890006
0.3471883389356066	0.0035527538718740	0.6120305296967156
0.4258243824877759	0.8687845990921715	0.6133927679855035
0.2888876592294214	0.8547463192490770	0.6124407127464713
0.7197464043226957	0.2604857572035567	0.6111421118473502
0.8106756389634964	0.1386923199183930	0.6126258227107009
0.6758693105452253	0.1051384090795071	0.6140227235711823
0.9352865639268986	0.9847673871497390	0.6206291308962445
0.9270042252667936	0.8208088919883220	0.6182830101862337
0.8137891978083165	0.9108110720949643	0.6276677855576663
0.8822910744786842	0.9027561374971025	0.7293593136368122

Methylation of S16 (low-S). Methyls on the surface before reaction: S5, S7, S13, S14



[1T'-(MoS₂)₁₆(CH₃)₄ + ClCH₃, S5-7-13-14-(16) INITIAL STATE, charge = 1.5]

1.0000000000000000

13.1071123318841796 0.0000000000000000 0.0000000000000000

0.0000000000000000 10.9501063248573605 0.0000000000000000

0.0000000000000000 0.0000000000000000 30.0000000000000000

Mo S C H Cl

16 32 5 15 1

Direct

0.0011589352092365 0.4723428489967874 0.5012096020580746

0.0072421936235156 0.9713583577876226 0.4997086590452712

0.5044311250799561 0.4936764989308187 0.5041976891527165

0.5089878299910751 0.9958942588292105 0.5047840732980918

0.0927176054403311 0.2345549816076019 0.5021434313088506

0.0891560054006614 0.7179859377658833 0.5001368179673168

0.5883961556703018 0.2426532489928110 0.5043573355366610

0.5851611149702751 0.7444871005533708 0.5049158327434955

0.3691227959794372 0.2033137102732376 0.5038215124741521

0.3738454265641681 0.7055623235567449 0.5023404327652399

0.8703824920496716 0.2580796735788558 0.5001491589421676

0.8738320381146176 0.7554074282137540 0.5010806438481865

0.2090043928152782 0.4924525937170912 0.5032726303663498

0.2218557156748117 0.0082890086109332 0.5005393624412021

0.7228616559241294 0.4530514776656570 0.5037186176026633

0.7242159177406956 0.9598850193537407 0.5042588151819350

0.4856520191754022 0.1479050182393034 0.5610169512364956

0.4843318073855111 0.6463301280753787 0.5607615985960415

0.9771869766630827 0.1501216449926559 0.5520709286166292

0.9774879002779667 0.6462633024194206 0.5545851922446676

0.1088636842666179 0.0739461491748778 0.4447079834477306

0.1046013890155339 0.5633553756284323 0.4444699089946070

0.6207088268991157 0.0700054766149696 0.4512348246687299

0.6196590549728708 0.5713207056676617 0.4523817634998806

0.2284448919070135 0.1576616214654306 0.5550547141603274

0.2303698435126435	0.6580486643648763	0.5518810041971662
0.7346818758137511	0.1551755228241011	0.5438762614523970
0.7336604111961512	0.6521542724184197	0.5415985423451765
0.3655320521191597	0.0523601462455148	0.4504148722932502
0.3644391693108521	0.5533350823823929	0.4514344200883591
0.8618644901547959	0.0615735945143542	0.4601009139933065
0.8580817412441911	0.5620501423059818	0.4601084760127545
0.3556606270144144	0.4006571876341185	0.5424740121564018
0.3600391174298180	0.9037589146402669	0.5414460773523222
0.8627848197747896	0.4079961791618049	0.5548190166482102
0.8683896387169334	0.9148513204050356	0.5510476346845524
0.4769886290139640	0.3176242668165642	0.4514052781440041
0.4757796776071608	0.8230238253376457	0.4515388628438457
0.9861826981068434	0.3201148656980308	0.4441438461864730
0.9879194141602604	0.8174805995234089	0.4439110363701255
0.1079698398208273	0.3982563436112045	0.5582289429993585
0.1189377266606746	0.8951697265032666	0.5530845494944898
0.6076457722405065	0.3956801031649340	0.5604514691642170
0.6096909683557354	0.8983951669545193	0.5611519284111091
0.2408584153793097	0.3135592004490932	0.4578369950473410
0.2342667047480327	0.8100217534488637	0.4604230557551612
0.7283380251256071	0.3036870111475696	0.4494529991078497
0.7289545213984967	0.8065299228902451	0.4512457093305791
0.3555503500175909	0.4014365075061612	0.6025115387618228
0.7338321114981142	0.6502595205386853	0.6016610606661400
0.3580845054345267	0.9035679259963741	0.6014745410695826
0.7230950590318733	0.1907845766640562	0.6526605917917021
0.8829002674175432	0.9165309903718162	0.6110425320408168
0.3437374948569268	0.4956334183781205	0.6137105694632081
0.4295200680201972	0.3670720668995102	0.6139978522322035
0.2935979858878350	0.3424342480616099	0.6141649496908131
0.7209283491284987	0.7431791857657225	0.6138757005934024
0.8075042455679957	0.6149785485482235	0.6130921242046451
0.6717463351304718	0.5905102302094629	0.6127068814667552
0.3490409437220988	-0.0020286168166975	0.6129129736181552
0.4304723869157955	0.8655447488632286	0.6133271146824202
0.2937492602045190	0.8474474185481008	0.6125864223173693
0.6896832858415601	0.2768809904063143	0.6414110984126671
0.8023536731287253	0.1833460663004664	0.6417585852920777
0.6780783032882892	0.1134176754177968	0.6407646843738092
0.9280603786401191	0.9971016006002561	0.6199449167786550
0.9222155164998199	0.8324914089801192	0.6209024819025143
0.8066130692882826	0.9218978037687677	0.6257482619980971
0.7212809577618339	0.1891469690397393	0.7128725949319854

[1T'-(MoS₂)₁₆(CH₃)₄ + ClCH₃, S5-7-13-14-(16) FINAL STATE, charge = 1.5]

1.0000000000000000

13.1071123318841796 0.0000000000000000 0.0000000000000000

0.0000000000000000 10.9501063248573605 0.0000000000000000

0.0000000000000000 0.0000000000000000 30.0000000000000000

Mo S C H Cl

16 32 5 15 1

Direct

0.9999467578396195 0.4752527601119307 0.5001880791669050

0.0068653217731529 0.9733572078646587 0.4989438700414649

0.5028218869170047 0.4963542027651651 0.5029995295212277

0.5075542816683974 0.9979667896017229 0.5043751636040783

0.0915213613212328 0.2369767200228024 0.5011139331961598

0.0881310649480117 0.7208271800530053 0.4989831582579941

0.5836227892652976 0.2473505316633086 0.5033510097770894

0.5838528653280591 0.7473670813480906 0.5043248911998373

0.3670896312983250 0.2064426491506939 0.5026983790185592

0.3725417069303637 0.7084835945315739 0.5011539623453660

0.8712358511176245 0.2622435401165678 0.4992866505312300

0.8724278777136041 0.7580750471685304 0.5001029156701678

0.2069978458706023 0.4948622984173058 0.5022932619965127

0.2206142737888311 0.0109796725526631 0.4995669845436256

0.7216484248370499 0.4559556337541353 0.5029169940560039

0.7230375269650194 0.9590160031304790 0.5043681550402542

0.4822349599093264 0.1511625350426873 0.5601304658313684

0.4822192227194140 0.6484063487430298 0.5596406744044260

0.9770190789440719 0.1525403031437088 0.5512348719459627

0.9767471637926037 0.6489770260986374 0.5533976680554359

0.1074938978198467 0.0765369773879495 0.4436703160385748

0.1031629175314970 0.5664553068465736 0.4433374926123522

0.6205550826876161 0.0724686557838874 0.4517528675800094

0.6184951574057899 0.5737974481694877 0.4515564387154932

0.2269669832270669 0.1606022342205234 0.5539724732727164

0.2291338264120135 0.6607507784690669 0.5505694026697834

0.7330430727896196 0.1593588832123071 0.5408620859705138

0.7323992332807349 0.6546488817646359 0.5411042930311569

0.3644735462340273 0.0548709342543648 0.4495899315618133

0.3628760374248634 0.5573055487545369 0.4501387117390037

0.8599898126795816 0.0638099295748849 0.4607693464572974

0.8566727424900236 0.5645940200735837 0.4592230901683612

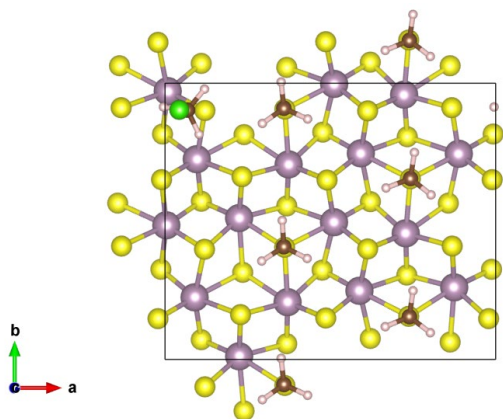
0.3536006838470616 0.4037097237891438 0.5415877890751690

0.3581191708618163 0.9062014864636589 0.5408511731051071

0.8625098864396803 0.4118795439340300 0.5539341387122744

0.8694500687168016	0.9152477624019547	0.5509896239689489
0.4736208250011578	0.3213499128028801	0.4501553215221399
0.4749797178532005	0.8265370288644009	0.4508077232802487
0.9853754981431292	0.3232978416133545	0.4430277754421197
0.9864238063770843	0.8204539585982846	0.4428534097770944
0.1068069714469233	0.4008960589155808	0.5572763027018715
0.1184604406828449	0.8974794677572823	0.5521324542366546
0.6047396591828560	0.3999513692621832	0.5594437194322296
0.6072213198212346	0.8994728622317496	0.5609886166817630
0.2388809060725442	0.3169523465550683	0.4566247955942743
0.2331877619360554	0.8131224810798688	0.4592325492876352
0.7269086794459844	0.3055134308816139	0.4492834296861348
0.7272369018335826	0.8080659534393289	0.4508496440143702
0.3534254977143103	0.4047887943872723	0.6016481690499491
0.7327168662077063	0.6515393285145471	0.6011800298793308
0.3557095030865202	0.9058924510253676	0.6009059726889279
0.7346574866473919	0.1660471208733379	0.6009067103813311
0.8894283444237714	0.9079354593796496	0.6106303062790996
0.3439822261488645	0.4994098931482849	0.6127785567783779
0.4263508036315461	0.3677675208082437	0.6132736346265701
0.2899346937226485	0.3482542727735004	0.6133206218241399
0.7186070194702180	0.7438210814488274	0.6137192884761472
0.8067448331967219	0.6172354974729624	0.6125277221346986
0.6714692445031458	0.5904820357401501	0.6121217102521967
0.3486141917160009	0.0004860847643277	0.6123812780399975
0.4270374828793069	0.8655385449779812	0.6129226257490441
0.2900491564819084	0.8518885468256443	0.6119051588349920
0.7203053610820753	0.2604423503141015	0.6111372725150924
0.8098765358984841	0.1377461397414218	0.6127590589165580
0.6750981903817951	0.1059771953240620	0.6140117872360087
0.9365685758001335	0.9862852688724805	0.6202058932051198
0.9291460342806847	0.8221315259851432	0.6178872032887573
0.8150607892877758	0.9114310793198289	0.6271362098980195
0.7346913398455417	0.1660128431223206	0.7211071159716423

Methylation of S1 (high-S). Methyls on the surface before reaction: S5, S7, S13, S16



[1T'-(MoS₂)₁₆(CH₃)₄ + ClCH₃, S(h1)-5-7-14-16 INITIAL STATE, charge = 1.5]

1.0000000000000000

13.1071123318841796 0.0000000000000000 0.0000000000000000

0.0000000000000000 10.9501063248573605 0.0000000000000000

0.0000000000000000 0.0000000000000000 30.0000000000000000

Mo S C H Cl

16 32 5 15 1

Direct

0.0039672920020118 0.4857881480272472 0.5029617150808723

0.0081349089634925 0.9713307800428597 0.5000273584546469

0.5110969725355710 0.4968363995032564 0.5052556347244499

0.5115703231583121 0.9972750370941263 0.5052767388992642

0.0894412805047467 0.2249479896846572 0.5000171533494178

0.0959937848093015 0.7249231629241992 0.5017382117938770

0.5879746382171586 0.2486427213539585 0.5053616957280702

0.5922620473274072 0.7460418922235107 0.5050604519849050

0.3706884295112898 0.2075055709509597 0.5043197863664829

0.3739078521404030 0.7060037850582394 0.5049161476687798

0.8747258258976841 0.2611335542985865 0.5011437272456722

0.8886315940857067 0.7445413909892985 0.5038362646235075

0.2240511544821149 0.5117465146961881 0.5011478695948933

0.2242431805011305 0.0114767438463212 0.5005689932936797

0.7280788527626300 0.4565627204460271 0.5044904963347004

0.7231616639562147 0.9585384916864989 0.5026335235525989

0.4861670279935203 0.1500882871055713 0.5614555485244022

0.4900569991177029 0.6495282245571655 0.5617180388473203

0.9787657017851980 0.1478273645760463 0.5534149972717621

0.9895486011461442 0.6508450360509389 0.5589202541604439

0.1095598395985106 0.0715761022498638 0.4436805295381482

0.1098703625337547 0.5727414404764271 0.4448723909320763

0.6209293401625319 0.0761386685888966 0.4519966410836774

0.6212684851106235 0.5711549904928483 0.4521666196509641

0.2284979095890800	0.1623621810995955	0.5545102851997793
0.2327993166095780	0.6615796128466411	0.5557948994951069
0.7370617347904860	0.1562788198375534	0.5420889999538794
0.7419929008955368	0.6539493151274517	0.5432164857568377
0.3681404279940811	0.0571028485903282	0.4506622060268374
0.3682490944048789	0.5557342080635790	0.4512760827033557
0.8623715124968940	0.0631661699639804	0.4607190286032304
0.8569175974963275	0.5659597744010136	0.4583700283270943
0.3617369667364348	0.4060221408681536	0.5420500538017986
0.3623946086087971	0.9059836960651572	0.5419113813333922
0.8685915833674396	0.4104065317121746	0.5557166420061994
0.8673457771484748	0.9113441704200353	0.5518839772807154
0.4752282223090501	0.3233124057955022	0.4527431506543047
0.4771012863527643	0.8227517691181540	0.4532517660449439
0.9875420668323112	0.3263175051620689	0.4451635180710990
0.9924793173574019	0.8160117482178653	0.4447955829415450
0.1194688708721669	0.3987955734722939	0.5528794563053809
0.1207205900629315	0.9009919533695787	0.5538921156938140
0.6129444542057425	0.4001177330932550	0.5617428050316225
0.6128428545196936	0.8997549478082169	0.5611368139332672
0.2350007055047930	0.3153915937509488	0.4609423609351411
0.2390016056579180	0.8138630498152500	0.4611040000767717
0.7312060300816942	0.3054305102197547	0.4511397729235246
0.7326305007700095	0.8061551103512400	0.4519929647959113
0.3593367248294292	0.4079555901094348	0.6021125444715344
0.7424290796107418	0.6548804871759535	0.6032507582054726
0.3595284320914955	0.9091597829668382	0.6019700502426540
0.7390244353388773	0.1548096802128316	0.6021182007066205
0.0678767624499452	0.9026280110885060	0.6618603324791819
0.3544765977810234	0.5030828526277561	0.6131885552598239
0.4297589952401044	0.3655759303516441	0.6142357679741465
0.2925577662275112	0.3562850128125240	0.6133068459433673
0.7543822531100888	0.7491721115068151	0.6143957271753004
0.8044580935343496	0.5960039503283279	0.6148471099103167
0.6685363057187974	0.6206948472918026	0.6148397961920757
0.3512203168761717	0.0041496018192886	0.6128881815377075
0.4312919342432160	0.8704624482942938	0.6143164017090568
0.2944821824772729	0.8543936852450171	0.6131689826102759
0.7500455606486930	0.2487393208597147	0.6137941138032660
0.8022923263796879	0.0968165657083070	0.6130396195646232
0.6660055485625627	0.1186178675215812	0.6139469686664863
0.1194365478435155	0.9785299641337301	0.6543563483539768
0.1031093112861581	0.8152180030756667	0.6533385937354317
-0.0047434376702321	0.9138976020916793	0.6445301553450052

0.0432048506050140 0.9033860146747227 0.7210554122502210

[1T'-(MoS₂)₁₆(CH₃)₄ + ClCH₃, S(h1)-5-7-14-16 FINAL STATE, charge = 1.5]

1.0000000000000000

13.1071123318841796 0.0000000000000000 0.0000000000000000

0.0000000000000000 10.9501063248573605 0.0000000000000000

0.0000000000000000 0.0000000000000000 30.0000000000000000

Mo S C H Cl

16 32 5 15 1

Direct

0.0003059951586039 0.4863616231240808 0.5023567223660897

0.0026431101265938 0.9727644115230427 0.4987724627176137

0.5080448665009045 0.4973020023680920 0.5040111356353014

0.5088672588945179 0.9980256856001037 0.5037811679138967

0.0861247980303212 0.2265871581019483 0.4993065982554521

0.0913873999306518 0.7239605182473418 0.5017138407974950

0.5849773878730684 0.2488432873215866 0.5038318579368249

0.5894167081001837 0.7462100270186351 0.5034286114326061

0.3672977348203963 0.2082561422793545 0.5036014771174925

0.3709072645127374 0.7060414832632893 0.5042107350401616

0.8716865743213544 0.2611976278426343 0.4998906824023063

0.8847259454856414 0.7440018845602423 0.5030102858240182

0.2214647860111167 0.5121097233305490 0.5004476612152933

0.2231962332310252 0.0135361024419776 0.5009033573419743

0.7250616537549505 0.4561852418414861 0.5031642234186199

0.7198397816180659 0.9589159255660132 0.5005511952396791

0.4840005873557934 0.1502140682992742 0.5602032286249984

0.4880914125084679 0.6497926487905208 0.5604663096430046

0.9750133167791389 0.1484593022556474 0.5523873458335875

0.9842905699035691 0.6493819276205837 0.5585770908219529

0.1084434649559124 0.0724247202380452 0.4435652665615621

0.1068958126462379 0.5724733914908455 0.4443469865268282

0.6174635643280397 0.0767367814000694 0.4500824435693801

0.6179808832186823 0.5708843384436812 0.4507010041452659

0.2259957030889821 0.1652817426285087 0.5544107246504327

0.2308172801301250 0.6602064525886993 0.5554323293264500

0.7339850112734800 0.1559859499801162 0.5405580663993015

0.7381871987288096 0.6532562609385417 0.5422105118555050

0.3641828653785116 0.0573585059239703 0.4500447339213853

0.3648731876136507 0.5563040726408339 0.4503725596574703

0.8597210678300583 0.0636828712566532 0.4584120573751164

0.8535181805831631 0.5663666046312936 0.4573180072163154

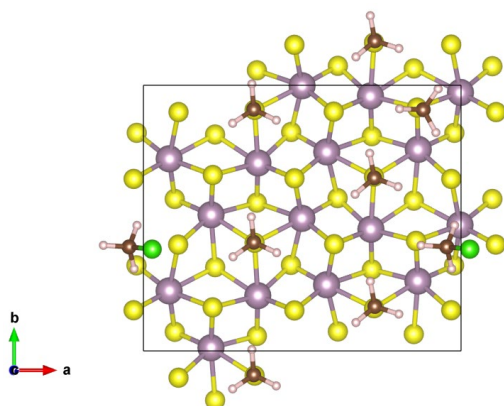
0.3591302364576670 0.4065629376980876 0.5413999092245174

0.3620069089397767 0.9058599262778327 0.5416288275459991

0.8645041679036898	0.4091848469125041	0.5547330681654070
0.8625553554011457	0.9120018312315468	0.5503263199602150
0.4716148493525693	0.3235073567025153	0.4516016098204270
0.4729687190164049	0.8229787564260641	0.4520793495692841
0.9848974256151850	0.3271904900650295	0.4442139999690794
0.9891179805944016	0.8145808774584614	0.4441648453140589
0.1160793553003654	0.3995411015062830	0.5521919561237032
0.1170931604730061	0.8996141134958475	0.5506522706083175
0.6097082435896927	0.4000011833502329	0.5603333886614817
0.6107409985172139	0.9001116819876467	0.5592347163307453
0.2319454418016487	0.3162909414451661	0.4603455219530986
0.2346353632321121	0.8151525551445362	0.4619836260039631
0.7283840243296369	0.3053649258484111	0.4496652416862703
0.7294821623238882	0.8056942911440120	0.4503428541833529
0.3574050979894447	0.4084169715171854	0.6014515944571245
0.7383859447133796	0.6541461399172809	0.6022657289838977
0.3640651807879722	0.9094009837414397	0.6017606245568002
0.7357072184600087	0.1538840550122763	0.6006082318738839
0.1012981828158607	0.8993713467376591	0.6104406399933996
0.3547735636733352	0.5035911795040904	0.6126340577819482
0.4269649568117986	0.3637234471584369	0.6134203108319826
0.2896615399995137	0.3588558963902972	0.6127916806914441
0.7485478182053965	0.7486169189459279	0.6134488787328705
0.8014158232319130	0.5968284877537438	0.6138996909983889
0.6651792745351818	0.6178501074860465	0.6138370568738176
0.3424142657511120	0.0009063116496087	0.6130453467596423
0.4415997203745159	0.8874859299255572	0.6127786688636473
0.3107202127523870	0.8405982413063178	0.6142538007091062
0.7443545368669507	0.2479651600470346	0.6124312546651700
0.8002186432449118	0.0979101934650062	0.6115797299005340
0.6635114582714430	0.1150801426746433	0.6123018150779070
0.1322698342203326	0.9852140493875059	0.6232724672569173
0.1415833647345801	0.8205170170374108	0.6242580639755118
0.0192619685246927	0.8929642720183563	0.6171137263414846
0.1014620766461522	0.9103645640622128	0.7319640775079549

E.2.6 (MoS₂)₁₆(CH₃)₅ + ClCH₃ reactions

Methylation of S15 (low-S). Methyls on the surface before reaction: S5, S7, S13, S14, S16



[1T'-(MoS₂)₁₆(CH₃)₅ + ClCH₃, S5-7-13-14-(15)-16 INITIAL STATE, charge = 2]

```
1.0000000000000000
13.1071123318841796  0.0000000000000000  0.0000000000000000
0.0000000000000000  10.9501063248573605  0.0000000000000000
0.0000000000000000  0.0000000000000000  30.0000000000000000
```

```
Mo S C H Cl
16 32 6 18 1
```

Direct

```
0.9967585149937568  0.4741440291507839  0.4999597446529597
0.9981357588695853  0.9729696764644384  0.5006977864446075
0.4989367184143604  0.4989527031909574  0.5047472676146630
0.4995548208390788  0.9981464794557255  0.5059370359224403
0.0808361870463046  0.2258643506763334  0.4999105856190910
0.0810885817274010  0.7232194247803071  0.5007554497156377
0.5766313282130618  0.2489854415063838  0.5049321991522139
0.5771755625601812  0.7490475650873542  0.5059591336365012
0.3601190015497923  0.2079016778522119  0.5041964082048801
0.3605447150596677  0.7077260627613979  0.5046922633404229
0.8641418476498539  0.2628338698376761  0.5001270147219107
0.8652998879566633  0.7586744936275408  0.5014535133935125
0.2127722964394024  0.5122723071629943  0.5003476771970332
0.2125648975406199  0.0116730217029725  0.5007680248666267
0.7161827124916434  0.4580985158186710  0.5036899124504697
0.7148268481957570  0.9596931291099430  0.5060034799662270
0.4753290276087478  0.1523240118811066  0.5616893822669546
0.4756146854997804  0.6497452729256805  0.5618590094218028
0.9690133702722544  0.1530989356367619  0.5532426201224329
0.9692039485246815  0.6473832645090049  0.5540661010021830
0.0987022027205143  0.0718420599099785  0.4437122107465996
0.0985771159416917  0.5720703749445953  0.4435016005994135
0.6121877886567594  0.0731810645217257  0.4533666991114128
0.6113666580874677  0.5751799570693223  0.4525147938146786
```

0.2178326763652451	0.1639215146889635	0.5545521478039162
0.2184281383947818	0.6622321335403351	0.5549785297198704
0.7260865795793889	0.1606733977876065	0.5419264502700665
0.7258649719441705	0.6559644924700669	0.5420929128913874
0.3572033246411771	0.0563048285665357	0.4510766573843873
0.3569498688443791	0.5581749987386809	0.4506628240488691
0.8512172063999670	0.0633288633582485	0.4622008295691063
0.8512657396763224	0.5657188078295883	0.4601701076726597
0.3500375603916167	0.4070689252820837	0.5413717439233459
0.3501378447714756	0.9069997871922539	0.5419353445952924
0.8582504672716916	0.4142832499464844	0.5538711575914045
0.8614302765274734	0.9159589568845991	0.5522992636919865
0.4644213485923095	0.3238486088630203	0.4523575006196849
0.4651282170408446	0.8241913102216188	0.4532853987001274
0.9781699687277554	0.3220099722336838	0.4431069821627632
0.9789895264586220	0.8208391438205966	0.4443161252063011
0.1094197935914514	0.4002629397547310	0.5532058557602697
0.1104860953311868	0.8991690252719323	0.5539902723877804
0.6004719494451142	0.4018306796501706	0.5608938425637069
0.5991706184837823	0.9008634550712712	0.5628366437008940
0.2259555281490978	0.3152617639954422	0.4602588592242490
0.2256604500218139	0.8146234800353500	0.4611227489161505
0.7193642267087255	0.3067061446082568	0.4503312092739184
0.7191479505394327	0.8082998548264252	0.4525628159846958
0.3475190406842327	0.4090329614362429	0.6013974525737363
0.7270587075017190	0.6516466751284682	0.6021260945904543
0.3472933351511743	0.9096224482331625	0.6019426170611859
0.7286116591698243	0.1672283720967020	0.6019203609992657
0.8809796350878649	0.9080562019446928	0.6120179355746033
0.9548801551370997	0.3915567934936159	0.6549463165434793
0.3397433221030872	0.5039268618555367	0.6124437446826826
0.4192630868630517	0.3697926652755619	0.6134987170278904
0.2823255933901641	0.3544937209545404	0.6125734865954972
0.7123878228710216	0.7436509240172047	0.6148439104832664
0.8015882961904738	0.6180902981120552	0.6131694429506108
0.6663709215288709	0.5897165414828188	0.6130233167996565
0.3414477644491300	0.0048398983201566	0.6128549157201787
0.4181491191381136	0.8684020808706142	0.6141655786046692
0.2809694038330701	0.8570899880412380	0.6131155536161519
0.7142672883685717	0.2617638497987845	0.6121044159669871
0.8042108174733932	0.1386341375018577	0.6133469083587535
0.6690399056050763	0.1068413714242543	0.6149496887342294
0.9279784633247719	0.9864458662999949	0.6217200739270669
0.9206494966430421	0.8221875269288229	0.6192222724558439

0.8065033142373079 0.9111833743725877 0.6284599976603512
 0.9798105309174496 0.4724756715917128 0.6366197081584593
 0.9705746546791714 0.3092074669504312 0.6355201707287621
 0.8740917673402274 0.3975709274546444 0.6636916415691499
 0.0275813805389475 0.3830388602025225 0.7059677799829578

[1T'-(MoS₂)₁₆(CH₃)₅ + ClCH₃, S5-7-13-14-(15)-16 FINAL STATE, charge = 2]

1.0000000000000000
 13.1071123318841796 0.0000000000000000 0.0000000000000000
 0.0000000000000000 10.9501063248573605 0.0000000000000000
 0.0000000000000000 0.0000000000000000 30.0000000000000000

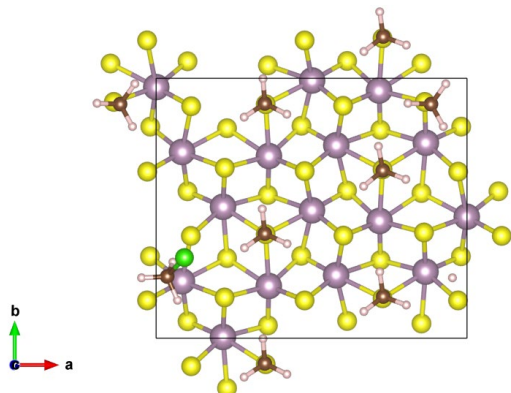
Mo S C H Cl
 16 32 6 18 1

Direct

0.0067164243197835 0.4723251328813396 0.4999341085437029
 0.0067619461352440 0.9722499968038554 0.5000355498196393
 0.5073660387995752 0.4973302861853550 0.5045489802866594
 0.5075146202692939 0.9972551119299159 0.5048641393512726
 0.0899616557993528 0.2241049863390630 0.4998754342606372
 0.0900361007245827 0.7239664649336874 0.4999024898408656
 0.5848548334118224 0.2484377001891881 0.5048231086341921
 0.5850518041261572 0.7484263520110138 0.5050741691569691
 0.3689419278578858 0.2067670231705574 0.5036463375602873
 0.3690528729955547 0.7067042813659040 0.5037651244486265
 0.8735180681127861 0.2589536903550441 0.5006938883431368
 0.8735909176912914 0.7587906423353263 0.5007947266894102
 0.2210382962469444 0.5107405564845788 0.5000345766205759
 0.2210564178702692 0.0106616214969861 0.5000910029710156
 0.7230154898870030 0.4588033857482407 0.5048456781889962
 0.7230322142232206 0.9590032232624733 0.5050742370103333
 0.4835085263631643 0.1501881379197240 0.5611033020768001
 0.4837498867460761 0.6494463589302742 0.5611404768926367
 0.9786518516730004 0.1498096378508827 0.5532732452163208
 0.9787578845069564 0.6494887566743831 0.5532642347512702
 0.1071739121988684 0.0712163357157522 0.4431408786401790
 0.1071667045515872 0.5713081577903599 0.4430829163356343
 0.6204678951563627 0.0731875192367052 0.4526189521805197
 0.6205776630236750 0.5735881289916052 0.4524929232637491
 0.2272893157994062 0.1620465034356042 0.5541689683701703
 0.2273180566520544 0.6619006718774719 0.5541963131123133
 0.7332898464193264 0.1588924964004104 0.5421477150226219
 0.7334416958731862 0.6580974427055234 0.5422814152270491
 0.3653634015033689 0.0559448178544652 0.4502339886100263
 0.3652461214669395 0.5563663502812822 0.4501574496168124

0.8596489451065916	0.0633612726785366	0.4613236599993354
0.8596943541951524	0.5635392016481624	0.4612190445967320
0.3584509481740374	0.4058593781424393	0.5411763126053442
0.3584487274369785	0.9058250778234549	0.5413224501690667
0.8693750240729792	0.4156517235023163	0.5516759363657204
0.8695361884390800	0.9157082652940342	0.5516756131190766
0.4731323872208284	0.3230870853496881	0.4519235149448868
0.4733418812985603	0.8232107765654032	0.4521916209954181
0.9869660177317767	0.3203390410719765	0.4433845411548996
0.9869522505949686	0.8203747521847157	0.4434733438896685
0.1191813064160521	0.3986586426318749	0.5532628156403152
0.1192722617847373	0.8985397060396567	0.5533362981305965
0.6067026254226345	0.4003365768107577	0.5612704205131755
0.6069095553792233	0.9002870649877829	0.5616483204235619
0.2344346237921196	0.3141335945299509	0.4599544119342997
0.2345189851353617	0.8140700481939170	0.4600479538126299
0.7275058017908261	0.3071501995549780	0.4514556304892338
0.7275104269508926	0.8072818050420475	0.4517007556955372
0.3561404586977285	0.4082012406582931	0.6012148110796575
0.7335418453921284	0.6562360455693707	0.6024440107166951
0.3558359107588119	0.9082124622419976	0.6013586207189269
0.7325605056032800	0.1593614805941901	0.6022470800475386
0.8892787976189136	0.9066951012516136	0.6113208348516949
0.8896577777990012	0.4069374596057256	0.6111739687441914
0.3487787422149998	0.5031716611773366	0.6122213005566775
0.4277410646358724	0.3687266062186914	0.6133420312698865
0.2908056097915327	0.3540714941222982	0.6124851782013949
0.7008996939273435	0.7422028113202243	0.6144598497465218
0.8123189639263422	0.6464533134402054	0.6139665878093744
0.6876527471893142	0.5790341347254452	0.6142176641049231
0.3494908233622484	0.0032871402334670	0.6123656953700313
0.4268800421820402	0.8674748995542030	0.6135581248070889
0.2898529362203545	0.8551352913779767	0.6125690380902774
0.7079434975762715	0.2490599587647776	0.6144724173138347
0.8096837489058811	0.1392932065471301	0.6141244645044389
0.6789016062328870	0.0892840362603375	0.6135906241884879
0.9320620460068679	0.9879242185930558	0.6215521353032177
0.9334920358928436	0.8238158499570556	0.6180953190914346
0.8147487311461126	0.9033866662859832	0.6276667881011099
0.9333238312828541	0.4879540749216503	0.6209552575616090
0.9339536531024705	0.3239038350874862	0.6176883338940431
0.8156195100989394	0.4044777171560229	0.6285015956317591
0.6836910060711540	0.4023428191368703	0.6902375317866855

Methylation of S4 (high-S). Methyls on the surface before reaction: S5, S7, S13, S14, S16



[1T'-(MoS₂)₁₆(CH₃)₅ + ClCH₃, S(h4)-5-7-13-14-16 INITIAL STATE, charge = 2]

```
1.0000000000000000
13.1071123318841796 0.0000000000000000 0.0000000000000000
0.0000000000000000 10.9501063248573605 0.0000000000000000
0.0000000000000000 0.0000000000000000 30.0000000000000000
```

```
Mo S C H Cl
16 32 6 18 1
```

Direct

```
0.9991611105765645 0.4674327015982737 0.4995352659428935
0.0005515716901270 0.9661026288934562 0.5000831129882652
0.5013875575666428 0.4921045639346988 0.5044397025871669
0.5019014513516364 0.9914182575835653 0.5054703370562077
0.0831943897864265 0.2190745485031209 0.4995880703234561
0.0834613412639489 0.7164665071809252 0.5002090385096869
0.5790140605807568 0.2423098880446697 0.5045684512350117
0.5795591276585464 0.7422239806581082 0.5055293093995684
0.3624686428017435 0.2011059247256092 0.5037963107187232
0.3629308530870938 0.7009394205285097 0.5042461170985070
0.8664756331244453 0.2561467521025523 0.4998155304945429
0.8676926252194622 0.7518593069014545 0.5008725852896195
0.2152331396156672 0.5055533096378626 0.4998879143151329
0.2149326998957717 0.0049633534250960 0.5002877240535866
0.7188508220009748 0.4511228896872273 0.5036524491871525
0.7171535118437656 0.9528713893916327 0.5055017417701120
0.4776700203505971 0.1454465777853289 0.5612786678730527
0.4779122973263346 0.6430353418678192 0.5614704566584153
0.9710571320759233 0.1455943477302080 0.5526588542908364
0.9715868610387247 0.6408030569530991 0.5535328193862182
0.1011422393855325 0.0653293562395662 0.4432342803938321
0.1010259972766674 0.5652383216044307 0.4430253729498095
0.6144989152841838 0.0665560863781923 0.4529142725179734
```

0.6141203105889510	0.5679959342347581	0.4523030431107781
0.2202347458068485	0.1569678007549938	0.5541726104548109
0.2207404965444458	0.6556108349786500	0.5544901551123693
0.7283599633226741	0.1537383515587680	0.5414607269383284
0.7282934342357348	0.6492940063960504	0.5416907872584766
0.3595919075521555	0.0496321474809557	0.4506388647435335
0.3594639667092803	0.5512939982392570	0.4502566252174453
0.8535153665501635	0.0567324167035296	0.4617165414365446
0.8535770851531955	0.5586383956203873	0.4598459292774812
0.3523745196329610	0.4002709884510553	0.5409738266105466
0.3524954630757001	0.9002468530477684	0.5414711720882408
0.8615262985369675	0.4069494489532924	0.5539693662218114
0.8639346089791409	0.9090396261588282	0.5516979887678489
0.4668219149225162	0.3171703493029208	0.4519900299780319
0.4675462369719521	0.8173197691816391	0.4528323657754665
0.9804370581662470	0.3152105652202411	0.4427719720205877
0.9813741621689370	0.8139666194403565	0.4437107609183606
0.1118030656924574	0.3937428668588072	0.5527206836595684
0.1127691725254439	0.8924163115272258	0.5534354045424543
0.6026844118105086	0.3948969605094466	0.5606879890461447
0.6015164121740310	0.8940837248335092	0.5623598195703570
0.2282608563367166	0.3084628638961095	0.4598861566144997
0.2280955202345055	0.8079122540805913	0.4606417284298694
0.7217749452426430	0.3002169732847769	0.4501110388435652
0.7214111803285012	0.8014573603475332	0.4520620905974575
0.3495608808276687	0.4023131156846984	0.6009963116632012
0.7290479089511592	0.6456206960549213	0.6017185512586292
0.3496565261292971	0.9029661604281084	0.6014795797484749
0.7303317771277726	0.1602019886805710	0.6014317303395028
0.8842798551942697	0.9005198868664909	0.6113467507146348
0.0356276334839962	0.2374028383148827	0.6580881229063027
0.3414636498354066	0.4972038100330283	0.6120088911665251
0.4213355822374691	0.3633650153756879	0.6131908729720492
0.2844436396530631	0.3475105620075338	0.6121054608433741
0.7150900632360330	0.7379621959642891	0.6142905113168116
0.8031551271657773	0.6111318971512022	0.6129311019617023
0.6676279714366700	0.5846481798041134	0.6125876290068373
0.3438157140032172	0.9982076880039775	0.6123685266328668
0.4204824916541604	0.8617451547771162	0.6137320475595233
0.2832962557730440	0.8504721963995536	0.6126482141972440
0.7193047234747613	0.2554286926727432	0.6115483627124967
0.8046394520603172	0.1277304692735244	0.6130579340119316
0.6684533001557879	0.1029716651707485	0.6143144910722949
0.9317113977074348	0.9785896144291497	0.6209632357447148

0.9238959198701607 0.8144700051873340 0.6183143264019740
 0.8101327474066455 0.9037910335220386 0.6280546156527923
 0.0540456263224591 0.2928577652190525 0.6288493929479269
 0.0690130848673134 0.1463442687755560 0.6550518786681387
 0.9531644343599379 0.2324964767907452 0.6632214349148460
 0.0911981747702037 0.3103226257048789 0.7062246531893924

[1T'-(MoS₂)₁₆(CH₃)₅ + ClCH₃, S(h4)-5-7-13-14-16 FINAL STATE, charge = 2]

1.0000000000000000

13.1071123318841796 0.0000000000000000 0.0000000000000000

0.0000000000000000 10.9501063248573605 0.0000000000000000

0.0000000000000000 0.0000000000000000 30.0000000000000000

Mo S C H Cl

16 32 6 18 1

Direct

0.0034447311349960 0.4739179983261173 0.4991342405912216

0.0056256480347316 0.9706338470937753 0.5017203776105180

0.5054111493870279 0.4976509149983952 0.5032598571085414

0.5056214319717952 0.9966008112653204 0.5045942592731285

0.0899477739106307 0.2252668575956548 0.4983180943670067

0.0880374591458103 0.7227493975463192 0.5001754633488247

0.5826349321656186 0.2483079095202527 0.5035639627018751

0.5836221442240807 0.7477651805642630 0.5047924262393798

0.3666072908014267 0.2069003023908832 0.5021494820358513

0.3672110360813353 0.7059255433829283 0.5033946012813970

0.8687328643400097 0.2633251871641419 0.5006981808217880

0.8714798574025219 0.7577170709683295 0.5008036689581952

0.2192715206467503 0.5113199611362280 0.4989112812352163

0.2192215566448719 0.0091619147813631 0.5001105947173718

0.7231914065833357 0.4570900305643098 0.5031068312405492

0.7207021817577257 0.9578153890319260 0.5059852376835370

0.4803887095188455 0.1514254253082545 0.5598582560784255

0.4820176679996576 0.6478928814016706 0.5604989146853516

0.9767405230043592 0.1525750245949696 0.5507600486314856

0.9760443667297281 0.6460654310365901 0.5532618358949912

0.1047358201981334 0.0676771493480866 0.4432884410050809

0.1041697165179299 0.5718928140833839 0.4425286450813771

0.6197700333622677 0.0713090887872508 0.4525069754303623

0.6186317636790492 0.5738511589011381 0.4514368095356249

0.2260896264989542 0.1637093681749585 0.5530429034110114

0.2260320583832078 0.6597310638745363 0.5539650821175801

0.7296470953670946 0.1589134141607472 0.5419420983729647

0.7314368714975261 0.6545640025763297 0.5415233929729460

0.3630798982128945 0.0538562153541816 0.4497194863634039

0.3633567902597204	0.5569020788672679	0.4491516110709490
0.8588873705705360	0.0625822228851600	0.4642162314466080
0.8576088532325208	0.5651519843390221	0.4596288420897419
0.3564485035875443	0.4057097923581492	0.5397992196934077
0.3570904053248380	0.9049592537340363	0.5411627429615694
0.8646846685953586	0.4155223925922739	0.5540292347096774
0.8664737353306566	0.9104441807268800	0.5534390867583622
0.4714056711647239	0.3229930690614685	0.4504709549177100
0.4718452253131399	0.8225029795552057	0.4519120924671188
0.9820267762877816	0.3210899096257072	0.4428647470467771
0.9855399789334395	0.8206019029557249	0.4441486673568845
0.1170310111035742	0.3993571482457665	0.5519008218177370
0.1194668373727274	0.8961722458440127	0.5541743456276842
0.6060934775525273	0.4002367615492680	0.5597324877874357
0.6036047470087624	0.8992488290044809	0.5619674970779589
0.2320608518540026	0.3147910103979433	0.4579226971954986
0.2323764207111856	0.8131572392138725	0.4601004020153674
0.7266337916345663	0.3048850686853723	0.4498693359900375
0.7259411712862067	0.8078058031615989	0.4519555727969482
0.3540634921727366	0.4070694699501810	0.5998381193525603
0.7295593602748833	0.6484504117286619	0.6015487692177177
0.3545394063020210	0.9077885747192597	0.6012061050503917
0.7253900114080645	0.1657022989180781	0.6019587649501775
0.8853976971865031	0.8882362886128480	0.6128704130373271
0.9999035387398091	0.1725051637363705	0.6097778613140348
0.3462050691893861	0.5018272885030901	0.6110118388435138
0.4258649625787240	0.3679037821001666	0.6118761663662419
0.2890192930222855	0.3523628667466120	0.6110480472008051
0.7132619866378377	0.7396779811466813	0.6145959756763382
0.8034011555468441	0.6147814494170658	0.6133659718551092
0.6686805032150481	0.5855624936291566	0.6114502061683866
0.3481887165744285	0.0029460570551740	0.6121185022528318
0.4255717037783700	0.8671430476228935	0.6134591813121153
0.2885624036391265	0.8548392158647646	0.6124969616350681
0.7425445007823185	0.2591796793665833	0.6125258768095356
0.7812598254480267	0.1021228709717241	0.6157630894305057
0.6486137482047990	0.1393756614645748	0.6127137607295093
0.9423779905239201	0.9531932796204371	0.6247864512081149
0.9135172979512868	0.7949641502122363	0.6177326692522790
0.8124142174096151	0.9018743725245617	0.6298448840865842
0.0232430704117165	0.2679243043658764	0.6140212108265837
0.0622913175735899	0.1111594509742827	0.6191422408943089
0.9313471086998433	0.1546548955840956	0.6293332506425678
0.9730172421709549	0.2422696531379535	0.7260363321434473

E.3 1T'-WS₂ Initial, Transition and Final States of Reactions

E.3.1 1T'-WS₂

[1T'-(WS₂)₁₆, charge = 2]

1.0000000000000000

13.0971896471307101 0.0000000000000000 0.0000000000000000

0.0000000000000000 11.0464090652851095 0.0000000000000000

0.0000000000000000 0.0000000000000000 30.0000000000000000

W S

16 32

Direct

0.0015508440338749 0.4869165775477646 0.4973515288784553

0.0015508440338749 0.9869165775477646 0.4973515288784553

0.5015508440338748 0.4869165775477646 0.4973515288784553

0.5015508440338748 0.9869165775477646 0.4973515288784553

0.0955579535121251 0.2369227774526517 0.4973512307610420

0.0955579535121251 0.7369227774526518 0.4973512307610420

0.5955579535121251 0.2369227774526517 0.4973512307610420

0.5955579535121251 0.7369227774526518 0.4973512307610420

0.3891389950020174 0.2369312916064001 0.4973545467256978

0.3891389950020174 0.7369312916064001 0.4973545467256978

0.8891389950020174 0.2369312916064001 0.4973545467256978

0.8891389950020174 0.7369312916064001 0.4973545467256978

0.2079707428671272 0.4869237113842883 0.4973504503350732

0.2079707428671272 0.9869237113842882 0.4973504503350732

0.7079707428671272 0.4869237113842883 0.4973504503350732

0.7079707428671272 0.9869237113842882 0.4973504503350732

0.4890263298951142 0.1479284772341163 0.5537243947722880

0.4890263298951142 0.6479284772341163 0.5537243947722880

0.9890263298951142 0.1479284772341163 0.5537243947722880

0.9890263298951142 0.6479284772341163 0.5537243947722880

0.1080802814825485 0.0759164219049084 0.4409801079292389

0.1080802814825485 0.5759164219049084 0.4409801079292389

0.6080802814825486 0.0759164219049084 0.4409801079292389

0.6080802814825486 0.5759164219049084 0.4409801079292389

0.2409165100814003 0.1557582845954345 0.5433490592815593

0.2409165100814003 0.6557582845954345 0.5433490592815593

0.7409165100814002 0.1557582845954345 0.5433490592815593

0.7409165100814002 0.6557582845954345 0.5433490592815593

0.3561936397776908 0.0680915758920437 0.4513575556235076

0.3561936397776908 0.5680915758920437 0.4513575556235076

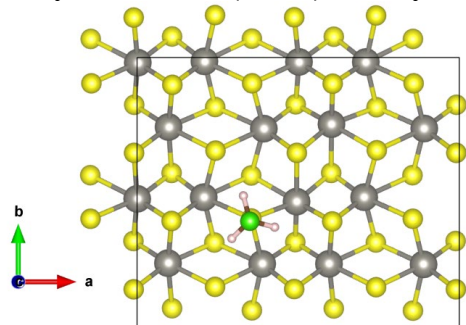
```

0.8561936397776909 0.0680915758920437 0.4513575556235076
0.8561936397776909 0.5680915758920437 0.4513575556235076
0.3561937220786320 0.4057633429521189 0.5433519890435533
0.3561937220786320 0.9057633429521188 0.5433519890435533
0.8561937220786320 0.4057633429521189 0.5433519890435533
0.8561937220786320 0.9057633429521188 0.5433519890435533
0.4890205784041136 0.3259172246588019 0.4409803988943242
0.4890205784041136 0.8259172246588019 0.4409803988943242
0.9890205784041136 0.3259172246588019 0.4409803988943242
0.9890205784041136 0.8259172246588019 0.4409803988943242
0.1080869230322468 0.3979283787640973 0.5537238804452502
0.1080869230322468 0.8979283787640973 0.5537238804452502
0.6080869230322468 0.3979283787640973 0.5537238804452502
0.6080869230322468 0.8979283787640973 0.5537238804452502
0.2409189175080888 0.3180869360073765 0.4513552273099966
0.2409189175080888 0.8180869360073765 0.4513552273099966
0.7409189175080888 0.3180869360073765 0.4513552273099966
0.7409189175080888 0.8180869360073765 0.4513552273099966

```

E.3.2 (WS₂)₁₆ + ClCH₃ reaction on S7

Methylation of S7 (low-S). Methyls on surface before reaction: None



[1T'-(WS₂)₁₆ + ClCH₃, S(7) INITIAL STATE, charge = 2]

```

1.0000000000000000
13.0971896471307101 0.0000000000000000 0.0000000000000000
0.0000000000000000 11.0464090652851095 0.0000000000000000
0.0000000000000000 0.0000000000000000 30.0000000000000000
W S C H Cl
16 32 1 3 1

```

Direct

```

0.0003415987955735 0.4799577728940430 0.4977865550740627
0.0021695169959865 0.9809544704037438 0.4971073991702385
0.4949272676973723 0.4696439619093395 0.4973677538717180
0.5024262422190489 0.9837029896865396 0.4971475556053571

```


0.0959076668211633	0.2432897129759261	0.4985201920896281
0.0976918410405677	0.7442751667458440	0.4978125330530045
0.5955399779817978	0.2406960203676231	0.4984551381361665
0.6032221769219251	0.7548208293285585	0.4980818737215512
0.3882046817538556	0.2405716150809015	0.4981414103452652
0.3933201775214500	0.7382644057788588	0.4972285654416753
0.8890720078980667	0.2386698968513093	0.4985768453094127
0.8912513656367442	0.7387427401602575	0.4971318815340394
0.2067198442418585	0.4858875895216809	0.4983826147206172
0.2089861369292765	0.9858776281825552	0.4971231122250633
0.7047386132591240	0.4860170352525399	0.4983475845637377
0.7098555102506448	0.9833782183915915	0.4973347885722971
0.4875756292262318	0.1479721262504612	0.5533803275336917
0.4958103005261387	0.6491246224724733	0.5511207887773367
0.9895045798895966	0.1469769856767869	0.5534792104373086
0.9906849438669040	0.6491059148141248	0.5528789419744378
0.1085666841397736	0.0773128523827074	0.4421623479551330
0.1071148388032402	0.5752338129993507	0.4426478837735934
0.6104201322050971	0.0765386628306363	0.4422464794237199
0.6023857146386931	0.5752255262314335	0.4444015947457575
0.2419771642846983	0.1560592595714554	0.5432435980876109
0.2433873976815136	0.6573538159100490	0.5428949557839780
0.7416925924788704	0.1546975490451737	0.5438398946928041
0.7438483060801856	0.6586426125645803	0.5427041650402733
0.3562687029062913	0.0694680659888382	0.4516891987967810
0.3541930365259888	0.5659077857596234	0.4527539685348151
0.8561655338435368	0.0684018442065991	0.4524529381017718
0.8546980890232456	0.5668726699642033	0.4527428991912703
0.3547939645376556	0.4075865363817113	0.5457125534777456
0.3570223723267630	0.9050679958829039	0.5430646511807620
0.8556016292271093	0.4065842487940738	0.5448346101756509
0.8582298250632644	0.9049614363278254	0.5440514657651317
0.4910161938316883	0.3205862077771024	0.4396250199741206
0.4923391807823799	0.8277267109923366	0.4401722863338920
0.9886499728757723	0.3247206064440011	0.4409848871065831
0.9911309405223316	0.8259221192768414	0.4399374572429697
0.1071322070268782	0.3984770380492890	0.5556542671462725
0.1093908652394187	0.8994811139911713	0.5546568723052459
0.6055578459076482	0.3967756513353346	0.5553968390851054
0.6070315597727438	0.9036912976130773	0.5558983781792860
0.2397878323461072	0.3193412381900173	0.4515279129942559
0.2424362585341404	0.8178349943736065	0.4508566661113482
0.7410189073764601	0.3192446225603311	0.4525426218331249
0.7430891726629602	0.8169249433657831	0.4493100260117023

0.3502326422168456 0.3998203491046077 0.6566295553431105
 0.3299404665256713 0.4911924387915372 0.6458459921209129
 0.4269188967244308 0.3757334568606353 0.6453391066042072
 0.2940951761501505 0.3339072506012291 0.6449267160491665
 0.3498562790684341 0.3973497914457846 0.7167954440135440

[1T'-(WS₂)₁₆ + ClCH₃, S(7) TRANSITION STATE, charge = 2]

1.0000000000000000
 13.0971896471306994 0.0000000000000000 0.0000000000000000
 0.0000000000000000 11.0464090652851006 0.0000000000000000
 0.0000000000000000 0.0000000000000000 30.0000000000000000

W S C H Cl
 16 32 1 3 1

Direct

0.9992667365827446 0.4796465718933763 0.4983342636724087
 0.0021367232596309 0.9805725394558263 0.4974355999017612
 0.4946114082747062 0.4694388942293719 0.4985450312263708
 0.5026196240161186 0.9861880889491513 0.4982067755261444
 0.0957596998276145 0.2423903507282892 0.4992799092880275
 0.0975982025943237 0.7431362626091295 0.4983059278720087
 0.5965040346549323 0.2406566838666352 0.4994507517848062
 0.6036416412670612 0.7560025053749178 0.4990430707552240
 0.3892648647841788 0.2370007118433712 0.4988135123466893
 0.3938000540919197 0.7374891616139760 0.4983612330389685
 0.8890836505506978 0.2385786142512107 0.4992595985444883
 0.8911600566623366 0.7387299006745559 0.4975368169394397
 0.2044983502335126 0.4889325896313623 0.4996769268675601
 0.2088953587791370 0.9867788792539327 0.4978672320650646
 0.7048143820778840 0.4845475426005638 0.4989929565433353
 0.7100524498466166 0.9833307998617644 0.4978215605245996
 0.4887179009531671 0.1484493231758488 0.5549030247045539
 0.4971966708786399 0.6494742656774699 0.5522057213735380
 0.9891703123892267 0.1462052331028414 0.5540851368916727
 0.9898838103904025 0.6491900081365872 0.5533881117373890
 0.1088004691128075 0.0774839488870059 0.4426215215009932
 0.1061206278431486 0.5747737288745385 0.4430465847400815
 0.6105418352200682 0.0770482971706928 0.4429355217771517
 0.6017014630112312 0.5753049955221096 0.4456574540302823
 0.2418892817687138 0.1554328400522982 0.5442833488360752
 0.2428244759880193 0.6582819478951631 0.5443430809338529
 0.7423045887856947 0.1543338955224990 0.5445293678581657
 0.7442114234573329 0.6584421353593732 0.5430736886803335
 0.3565317294918087 0.0692717737908760 0.4518994885702993
 0.3536342027075213 0.5658403514586829 0.4540958912951440

0.8562977750503067	0.0683604201747090	0.4529176410979187
0.8540323902908364	0.5663954166791713	0.4532761560726323
0.3531062467160305	0.4078796052208188	0.5449504223989384
0.3568728515140480	0.9052888626323159	0.5436466962453763
0.8554505921795795	0.4061694710375092	0.5456133256110477
0.8583488769390196	0.9047756082598296	0.5444371566982151
0.4917974381521373	0.3204552754108406	0.4406479560101966
0.4920770637736638	0.8284022777963485	0.4414642737593775
0.9889614547605670	0.3240722164596624	0.4416372918346619
0.9916085171414754	0.8255416130001224	0.4403226826006742
0.1053207972740643	0.3984146881461600	0.5564681000773252
0.1089859724616463	0.8992157499239215	0.5550282661943123
0.6059328196038716	0.3968856649335757	0.5563755139187265
0.6074432586008778	0.9045304081481889	0.5567161224640230
0.2408568174774446	0.3204146983193246	0.4536672537306830
0.2430565693288138	0.8177016078684849	0.4520062338165830
0.7409580767120251	0.3186749224094329	0.4530481737662272
0.7426453581338280	0.8168136920958272	0.4497728591465601
0.3508263534920108	0.4008678761036431	0.6215820835481225
0.3281999677309487	0.4951589228181287	0.6226549091655117
0.4309875590666324	0.3767493339251307	0.6220180232793130
0.2931273248989718	0.3306287909836287	0.6210591311342081
0.3498103500033187	0.3962242445487908	0.6994109838751145

[1T'-(WS₂)₁₆ + ClCH₃, S(7) FINAL STATE, charge = 2]

1.0000000000000000

13.0971896471307101 0.0000000000000000 0.0000000000000000

0.0000000000000000 11.0464090652851095 0.0000000000000000

0.0000000000000000 0.0000000000000000 30.0000000000000000

W S C H Cl

16 32 1 3 1

Direct

0.9984200902086094	0.4800577328764765	0.4968045857676496
0.0022110242423442	0.9804361094003198	0.4959392054859840
0.4948259861727342	0.4692893514938966	0.4970962236283293
0.5029885508221675	0.9884008021655268	0.4969027763012217
0.0957937597277696	0.2416238774703152	0.4978332672432313
0.0972791608392023	0.7416839760080898	0.4967819225483618
0.5978190956374790	0.2408291424538749	0.4979355573433958
0.6038268989101161	0.7568233288939026	0.4978304389001516
0.3903381450789196	0.2340406724032956	0.4967499636340340
0.3940607842945453	0.7369569193999180	0.4970816424595558
0.8893601897642993	0.2386860183062014	0.4978996929247252
0.8908093139518588	0.7391254374190992	0.4963591667384174

0.2024271241286024	0.4911508313019846	0.4983438924602588
0.2090236884965460	0.9873413701236470	0.4962987060829506
0.7051893430246818	0.4829905328945414	0.4973445331406429
0.7104472636927011	0.9834912794371146	0.4963993125165379
0.4896584768808505	0.1489222314603767	0.5536457643135880
0.4979652163843603	0.6494267326728231	0.5508833567269807
0.9893289895650331	0.1459433586673641	0.5527115118293743
0.9893767793526028	0.6492032917665065	0.5521248807257332
0.1086810262767727	0.0774487503322694	0.4409994901734087
0.1048429532807149	0.5749043666023627	0.4412108753704093
0.6113446098866493	0.0770610006345516	0.4413923052924981
0.6019164728542570	0.5755469582326193	0.4444898174430421
0.2422242577302315	0.1548595243397972	0.5427522872484933
0.2422322153246974	0.6586989625812703	0.5432885446217606
0.7428180846442525	0.1545383414289314	0.5431186512321948
0.7440709892960069	0.6579312947961218	0.5415260278786582
0.3571162924831850	0.0683255952331876	0.4497198732269719
0.3532650447021893	0.5654907516735018	0.4530316722923454
0.8566539338105323	0.0683009539408331	0.4515307442835916
0.8536240177345394	0.5666249618379103	0.4518603134653636
0.3518443367166991	0.4079720455439758	0.5417219197113976
0.3569459177493589	0.9054371575252846	0.5419514132018609
0.8553933594444412	0.4060796053280128	0.5442326908229131
0.8585254195526999	0.9050727724799538	0.5432132781222855
0.4932989531892588	0.3202302125631856	0.4389805236468522
0.4920948767215231	0.8286606775225480	0.4403864499142642
0.9892733671111111	0.3238466276156605	0.4402247015637233
0.9913641459517492	0.8252564972336840	0.4389829239800350
0.1041525346117199	0.3986689856991905	0.5549722717278380
0.1093159231924263	0.8989252123911393	0.5533232982094468
0.6060711972452381	0.3970950398339024	0.5548929342422758
0.6075398772966530	0.9051167017397100	0.5553767921687554
0.2417901280827679	0.3212842023285981	0.4532001817704575
0.2431776791346321	0.8172864095807846	0.4508184207218802
0.7415711576499288	0.3180174990253257	0.4512823041874927
0.7424827939294391	0.8169192753107368	0.4484456259771594
0.3501440454499904	0.4007725696979596	0.6019179732072223
0.3292124032328698	0.4907002749567452	0.6142415904206093
0.4263794203553016	0.3751009860083485	0.6133844166252078
0.2932917566800494	0.3334758375667990	0.6119660749618564
0.3501313883060194	0.4005011601588344	0.7215455368548599

Bibliography

- (1) Li, X.; Zhu, H., Two-dimensional MoS₂: Properties, preparation, and applications. *J. Materiomics* **2015**, *1*, 33-44.
- (2) Chhowalla, M.; Shin, H. S.; Eda, G.; Li, L. J.; Loh, K. P.; Zhang, H., The chemistry of two-dimensional layered transition metal dichalcogenide nanosheets. *Nat. Chem.* **2013**, *5*, 263-75.
- (3) Duan, X. D.; Wang, C.; Pan, A. L.; Yu, R. Q.; Duan, X. F., Two-dimensional transition metal dichalcogenides as atomically thin semiconductors: opportunities and challenges. *Chem. Soc. Rev.* **2015**, *44*, 8859-8876.
- (4) Voudouris, P. C.; Melfos, V.; Spry, P. G.; Bindi, L.; Kartal, T.; Arikas, K.; Moritz, R.; Ortelli, M., Rhenium-rich Molybdenite and Rheniite in the Pagoni Rachi Mo–Cu–Te–Ag–Au Prospect, Northern Greece: Implications for the Re Geochemistry of Porphyry-style Cu–Mo and Mo Mineralization. *Can. Mineral* **2009**, *47*, 1013-1036.
- (5) Nicolosi, V.; Chhowalla, M.; Kanatzidis, M. G.; Strano, M. S.; Coleman, J. N., Liquid Exfoliation of Layered Materials. *Science* **2013**, *340*, 1226419.
- (6) Castellanos-Gomez, A.; Buscema, M.; Molenaar, R.; Singh, V.; Janssen, L.; van der Zant, H. S. J.; Steele, G. A., Deterministic transfer of two-dimensional materials by all-dry viscoelastic stamping. *2D Mater.* **2014**, *1*.
- (7) Fan, X. B.; Xu, P. T.; Li, Y. C.; Zhou, D. K.; Sun, Y. F.; Nguyen, M. A. T.; Terrones, M.; Mallouk, T. E., Controlled Exfoliation of MoS₂ Crystals into Trilayer Nanosheets. *J. Am. Chem. Soc.* **2016**, *138*, 5143-5149.
- (8) Zhang, L.; Zunger, A., Evolution of electronic structure as a function of layer thickness in group-VIB transition metal dichalcogenides: emergence of localization prototypes. *Nano Lett.* **2015**, *15*, 949-57.
- (9) Heine, T., Transition metal chalcogenides: ultrathin inorganic materials with tunable electronic properties. *Acc. Chem. Res.* **2015**, *48*, 65-72.
- (10) Mak, K. F.; Lee, C.; Hone, J.; Shan, J.; Heinz, T. F., Atomically Thin MoS₂: A New Direct-Gap Semiconductor. *Phys. Rev. Lett.* **2010**, *105*, 136805.
- (11) Splendiani, A.; Sun, L.; Zhang, Y.; Li, T.; Kim, J.; Chim, C.-Y.; Galli, G.; Wang, F., Emerging Photoluminescence in Monolayer MoS₂. *Nano Lett.* **2010**, *10*, 1271-1275.
- (12) Wang, Z.; Li, R.; Su, C.; Loh, K. P., Intercalated phases of transition metal dichalcogenides. *SmartMat* **2020**, *1*, e1013.
- (13) Calandra, M., Chemically exfoliated single-layer MoS₂: Stability, lattice dynamics, and catalytic adsorption from first principles. *Phys. Rev. B* **2013**, *88*.
- (14) Chou, S. S.; Sai, N.; Lu, P.; Coker, E. N.; Liu, S.; Artyushkova, K.; Luk, T. S.; Kaehr, B.; Brinker, C. J., Understanding catalysis in a multiphase two-dimensional transition metal dichalcogenide. *Nat. Commun.* **2015**, *6*, 8311.
- (15) Toh, R. J.; Sofer, Z.; Luxa, J.; Sedmidubsky, D.; Pumera, M., 3R phase of MoS₂ and WS₂ outperforms the corresponding 2H phase for hydrogen evolution. *Chem. Commun.* **2017**, *53*, 3054-3057.

- (16) Fan, X.-L.; Yang, Y.; Xiao, P.; Lau, W.-M., Site-specific catalytic activity in exfoliated MoS₂ single-layer polytypes for hydrogen evolution: basal plane and edges. *J. Mater. Chem. A* **2014**, *2*, 20545-20551.
- (17) Heising, J.; Kanatzidis, M. G., Exfoliated and restacked MoS₂ and WS₂: Ionic or neutral species? Encapsulation and ordering of hard electropositive cations. *J. Am. Chem. Soc.* **1999**, *121*, 11720-11732.
- (18) Qin, X. R.; Yang, D.; Frindt, R. F.; Irwin, J. C., Real-space imaging of single-layer MoS₂ by scanning tunneling microscopy. *Phys. Rev. B* **1991**, *44*, 3490-3493.
- (19) Voiry, D.; Goswami, A.; Kappera, R.; Silva, C. d. C. C. e.; Kaplan, D.; Fujita, T.; Chen, M.; Asefa, T.; Chhowalla, M., Covalent functionalization of monolayered transition metal dichalcogenides by phase engineering. *Nat. Chem.* **2015**, *7*, 45-49.
- (20) Pal, B.; Singh, A.; G, S.; Mahale, P.; Kumar, A.; Thirupathaiyah, S.; Sezen, H.; Amati, M.; Gregoratti, L.; Waghmare, U. V.; Sarma, D. D., Chemical exfoliation of MoS₂ leads to semiconducting 1T' phase and not the metallic 1T phase. **2017**.
- (21) Tang, C. S.; Yin, X.; Wee, A. T. S., 1D chain structure in 1T' -phase 2D transition metal dichalcogenides and their anisotropic electronic structures. *Appl. Phys. Rev.* **2021**, *8*, 011313.
- (22) Kappera, R.; Voiry, D.; Yalcin, S. E.; Branch, B.; Gupta, G.; Mohite, A. D.; Chhowalla, M., Phase-engineered low-resistance contacts for ultrathin MoS₂ transistors. *Nat. Mater.* **2014**, *13*, 1128-1134.
- (23) Lee, H.; Bak, S.; An, S.-J.; Kim, J. H.; Yun, E.; Kim, M.; Seo, S.; Jeong, M. S.; Lee, H., Highly Efficient Thin-Film Transistor via Cross-Linking of 1T Edge Functional 2H Molybdenum Disulfides. *ACS Nano* **2017**.
- (24) Jariwala, D.; Sangwan, V. K.; Lauhon, L. J.; Marks, T. J.; Hersam, M. C., Emerging device applications for semiconducting two-dimensional transition metal dichalcogenides. *ACS Nano* **2014**, *8*, 1102-20.
- (25) Sun, Y.; Gao, S.; Lei, F.; Xiao, C.; Xie, Y., Ultrathin Two-Dimensional Inorganic Materials: New Opportunities for Solid State Nanochemistry. *Acc. Chem. Res.* **2015**, *48*, 3-12.
- (26) Akbari, E.; Jahanbin, K.; Afroozeh, A.; Yupapin, P.; Buntat, Z., Brief review of monolayer molybdenum disulfide application in gas sensor. *Physica B Condens. Matter* **2018**, *545*, 510-518.
- (27) Kim, S. J.; Mondal, S.; Min, B. K.; Choi, C.-G., Highly sensitive and flexible strain-pressure sensor with cracked paddy shaped MoS₂/graphene foam/Ecoflex hybrid nanostructures. *ACS Appl. Mater. Interfaces* **2018**.
- (28) Feng, Z.; Chen, B.; Qian, S.; Xu, L.; Feng, L.; Yu, Y.; Zhang, R.; Jiancui, C.; Li, Q.; Li, Q.; Sun, C.; Zhang, H.; Liu, J.; Pang, W.; Zhang, D., Chemical sensing by band modulation of a black phosphorus/molybdenum diselenide van der Waals hetero-structure. *2D Mater.* **2016**, *3*, 035021.
- (29) Zhang, S. L.; Choi, H. H.; Yue, H. Y.; Yang, W. C., Controlled exfoliation of molybdenum disulfide for developing thin film humidity sensor. *Curr. Appl. Phys.* **2014**, *14*, 264-268.

- (30) Sarkar, D.; Xie, X.; Kang, J.; Zhang, H.; Liu, W.; Navarrete, J.; Moskovits, M.; Banerjee, K., Functionalization of Transition Metal Dichalcogenides with Metallic Nanoparticles: Implications for Doping and Gas-Sensing. *Nano Lett.* **2015**, *15*, 2852-2862.
- (31) Cho, B.; Hahm, M. G.; Choi, M.; Yoon, J.; Kim, A. R.; Lee, Y.-J.; Park, S.-G.; Kwon, J.-D.; Kim, C. S.; Song, M.; Jeong, Y.; Nam, K.-S.; Lee, S.; Yoo, T. J.; Kang, C. G.; Lee, B. H.; Ko, H. C.; Ajayan, P. M.; Kim, D.-H., Charge-transfer-based Gas Sensing Using Atomic-layer MoS₂. *Sci. Rep.* **2015**, *5*, 8052.
- (32) Park, M.; Park, Y. J.; Chen, X.; Park, Y.-K.; Kim, M.-S.; Ahn, J.-H., MoS₂-Based Tactile Sensor for Electronic Skin Applications. *Adv. Mater.* **2016**, *28*, 2556-2562.
- (33) Tsai, M.-Y.; Tarasov, A.; Hesabi, Z. R.; Taghinejad, H.; Campbell, P. M.; Joiner, C. A.; Adibi, A.; Vogel, E. M., Flexible MoS₂ Field-Effect Transistors for Gate-Tunable Piezoresistive Strain Sensors. *ACS Appl. Mater. Interfaces* **2015**, *7*, 12850-12855.
- (34) Zhu, M.; Sakamoto, K.; Li, J.; Inomata, N.; Toda, M.; Ono, T., Piezoresistive strain sensor based on monolayer molybdenum disulfide continuous film deposited by chemical vapor deposition. *J. Micromechanics Microengineering* **2019**, *29*, 055002.
- (35) Yin, W.; Yan, L.; Yu, J.; Tian, G.; Zhou, L.; Zheng, X.; Zhang, X.; Yong, Y.; Li, J.; Gu, Z.; Zhao, Y., High-Throughput Synthesis of Single-Layer MoS₂ Nanosheets as a Near-Infrared Photothermal-Triggered Drug Delivery for Effective Cancer Therapy. *ACS Nano* **2014**, *8*, 6922-6933.
- (36) Deng, R.; Yi, H.; Fan, F.; Fu, L.; Zeng, Y.; Wang, Y.; Li, Y.; Liu, Y.; Ji, S.; Su, Y., Facile exfoliation of MoS₂ nanosheets by protein as a photothermal-triggered drug delivery system for synergistic tumor therapy. *RSC Adv.* **2016**, *6*, 77083-77092.
- (37) Yin, F.; Anderson, T.; Panwar, N.; Zhang, K.; Tjin, S. C.; Ng, B. K.; Yoon, H. S.; Qu, J.; Yong, K.-T., Functionalized MoS₂ Nanosheets as Multi-Gene Delivery Vehicles for In Vivo Pancreatic Cancer Therapy. *Nanotheranostics* **2018**, *2*, 371-386.
- (38) Wang, S.; Chen, Y.; Li, X.; Gao, W.; Zhang, L.; Liu, J.; Zheng, Y.; Chen, H.; Shi, J., Injectable 2D MoS₂ - Integrated Drug Delivering Implant for Highly Efficient NIR - Triggered Synergistic Tumor Hyperthermia. *Adv. Mater.* **2015**, *27*, 7117-7122.
- (39) Chou, S. S.; Kaehr, B.; Kim, J.; Foley, B. M.; De, M.; Hopkins, P. E.; Huang, J.; Brinker, C. J.; Dravid, V. P., Chemically Exfoliated MoS₂ as Near-Infrared Photothermal Agents. *Angew. Chem. Int. Ed.* **2013**, *52*, 4160-4164.
- (40) Yadav, V.; Roy, S.; Singh, P.; Khan, Z.; Jaiswal, A., 2D MoS₂-Based Nanomaterials for Therapeutic, Bioimaging, and Biosensing Applications. *Small* **2019**, *15*, 1803706.
- (41) Walton, A. S.; Lauritsen, J. V.; Topsøe, H.; Besenbacher, F., MoS₂ nanoparticle morphologies in hydrodesulfurization catalysis studied by scanning tunneling microscopy. *J. Catal.* **2013**, *308*, 306-318.
- (42) Mom, R. V.; Louwen, J. N.; Frenken, J. W. M.; Groot, I. M. N., In situ observations of an active MoS₂ model hydrodesulfurization catalyst. *Nat. Commun.* **2019**, *10*, 2546.
- (43) Hinnemann, B.; Moses, P. G.; Bonde, J.; Jorgensen, K. P.; Nielsen, J. H.; Horch, S.; Chorkendorff, I.; Nørskov, J. K., Biornimetic hydrogen evolution: MoS₂ nanoparticles as catalyst for hydrogen evolution. *J. Am. Chem. Soc.* **2005**, *127*, 5308-5309.
- (44) Voiry, D.; Salehi, M.; Silva, R.; Fujita, T.; Chen, M. W.; Asefa, T.; Shenoy, V. B.; Eda, G.; Chhowalla, M., Conducting MoS₂ Nanosheets as Catalysts for Hydrogen Evolution Reaction. *Nano Lett.* **2013**, *13*, 6222-6227.

- (45) Ding, Q.; Song, B.; Xu, P.; Jin, S., Efficient Electrocatalytic and Photoelectrochemical Hydrogen Generation Using MoS₂ and Related Compounds. *Chem* **2016**, *1*, 699-726.
- (46) Kwon, K. C.; Choi, S.; Hong, K.; Moon, C. W.; Shim, Y.-S.; Kim, D. H.; Kim, T.; Sohn, W.; Jeon, J.-M.; Lee, C.-H.; Nam, K. T.; Han, S.; Kim, S. Y.; Jang, H. W., Wafer-scale transferable molybdenum disulfide thin-film catalysts for photoelectrochemical hydrogen production. *Energy Environ. Sci.* **2016**, *9*, 2240-2248.
- (47) Li, H.; Tsai, C.; Koh, A. L.; Cai, L.; Contryman, A. W.; Fragapane, A. H.; Zhao, J.; Han, H. S.; Manoharan, H. C.; Abild-Pedersen, F.; Nørskov, J. K.; Zheng, X., Activating and optimizing MoS₂ basal planes for hydrogen evolution through the formation of strained sulphur vacancies. *Nat. Mater.* **2016**, *15*, 48-53.
- (48) Yin, Y.; Han, J.; Zhang, Y.; Zhang, X.; Xu, P.; Yuan, Q.; Samad, L.; Wang, X.; Wang, Y.; Zhang, Z.; Zhang, P.; Cao, X.; Song, B.; Jin, S., Contributions of Phase, Sulfur Vacancies, and Edges to the Hydrogen Evolution Reaction Catalytic Activity of Porous Molybdenum Disulfide Nanosheets. *J. Am. Chem. Soc.* **2016**, *138*, 7965-72.
- (49) Kim, T. I.; Kim, J.; Park, I.-J.; Cho, K.-O.; Choi, S.-Y., Chemically exfoliated 1T-phase transition metal dichalcogenide nanosheets for transparent antibacterial applications. *2D Mater.* **2019**, *6*, 025025.
- (50) Tang, K.; Wang, L.; Geng, H.; Qiu, J.; Cao, H.; Liu, X., Molybdenum disulfide (MoS₂) nanosheets vertically coated on titanium for disinfection in the dark. *Arab. J. Chem.* **2020**, *13*, 1612-1623.
- (51) Wu, S.; Zeng, Z.; He, Q.; Wang, Z.; Wang, S. J.; Du, Y.; Yin, Z.; Sun, X.; Chen, W.; Zhang, H., Electrochemically reduced single-layer MoS₂ nanosheets: characterization, properties, and sensing applications. *Small* **2012**, *8*, 2264-2270.
- (52) Novoselov, K. S.; Geim, A. K.; Morozov, S. V.; Jiang, D.; Zhang, Y.; Dubonos, S. V.; Grigorieva, I. V.; Firsov, A. A., Electric Field Effect in Atomically Thin Carbon Films. *Science* **2004**, *306*, 666.
- (53) Mas-Ballesté, R.; Gómez-Navarro, C.; Gómez-Herrero, J.; Zamora, F., 2D materials: to graphene and beyond. *Nanoscale* **2011**, *3*, 20-30.
- (54) Krishnan, U.; Kaur, M.; Singh, K.; Kumar, M.; Kumar, A., A synoptic review of MoS₂: Synthesis to applications. *Superlattice Microst.* **2019**, *128*, 274-297.
- (55) Backes, C.; Berner, N. C.; Chen, X.; Lafargue, P.; LaPlace, P.; Freeley, M.; Duesberg, G. S.; Coleman, J. N.; McDonald, A. R., Functionalization of Liquid-Exfoliated Two-Dimensional 2H-MoS₂. *Angew. Chem. Int. Ed.* **2015**, *54*, 2638-2642.
- (56) Chen, Y.; Tan, C. L.; Zhang, H.; Wang, L. Z., Two-dimensional graphene analogues for biomedical applications. *Chem. Soc. Rev.* **2015**, *44*, 2681-2701.
- (57) Chou, S. S.; De, M.; Kim, J.; Byun, S.; Dykstra, C.; Yu, J.; Huang, J.; Dravid, V. P., Ligand conjugation of chemically exfoliated MoS₂. *J. Am. Chem. Soc.* **2013**, *135*, 4584-7.
- (58) Crouse, C. A.; Pierce, C. J.; Spowart, J. E., Influencing Solvent Miscibility and Aqueous Stability of Aluminum Nanoparticles through Surface Functionalization with Acrylic Monomers. *ACS Appl. Mater. Interfaces* **2010**, *2*, 2560-2569.
- (59) Gan, X.; Zhao, H.; Wong, K.-Y.; Lei, D. Y.; Zhang, Y.; Quan, X., Covalent functionalization of MoS₂ nanosheets synthesized by liquid phase exfoliation to construct electrochemical sensors for Cd (II) detection. *Talanta* **2018**, *182*, 38-48.

- (60) McCaig, H. C.; Myers, E.; Lewis, N. S.; Roukes, M. L., Vapor Sensing Characteristics of Nanoelectromechanical Chemical Sensors Functionalized Using Surface-Initiated Polymerization. *Nano Lett.* **2014**, *14*, 3728-3732.
- (61) Nguyen, E. P.; Carey, B. J.; Ou, J. Z.; van Embden, J.; Gaspera, E. D.; Chrimes, A. F.; Spencer, M. J.; Zhuiykov, S.; Kalantar-Zadeh, K.; Daeneke, T., Electronic Tuning of 2D MoS₂ through Surface Functionalization. *Adv. Mater.* **2015**, *27*, 6225-9.
- (62) Presolski, S.; Wang, L.; Loo, A. H.; Ambrosi, A.; Lazar, P.; Ranc, V.; Otyepka, M.; Zboril, R.; Tomanec, O.; Ugolotti, J.; Sofer, Z.; Pumera, M., Functional Nanosheet Synthons by Covalent Modification of Transition-Metal Dichalcogenides. *Chem. Mater.* **2017**, *29*, 2066-2073.
- (63) Taleb, S.; Noyer, E.; Godeau, G.; Darmanin, T.; Guittard, F., Switchable Surface Wettability by Using Boronic Ester Chemistry. *ChemPhysChem* **2016**, *17*, 305-309.
- (64) Ang, A.; Sinelnikov, R.; Meldrum, A.; Veinot, J. G. C.; Balberg, I.; Azulay, D.; Millo, O.; Rieger, B., Photoluminescence through in-gap states in phenylacetylene functionalized silicon nanocrystals. *Nanoscale* **2016**, *8*, 7849-7853.
- (65) Brown, E. S.; Peczonczyk, S. L.; Wang, Z.; Maldonado, S., Photoelectrochemical Properties of CH₃-Terminated p-Type GaP(111)A. *J. Phys. Chem. C* **2014**, *118*, 11593-11600.
- (66) Leong, W. S.; Li, Y.; Luo, X.; Nai, C. T.; Quek, S. Y.; Thong, J. T., Tuning the threshold voltage of MoS₂ field-effect transistors via surface treatment. *Nanoscale* **2015**, *7*, 10823-31.
- (67) Plymale, N. T.; Ramachandran, A. A.; Lim, A.; Brunshwig, B. S.; Lewis, N. S., Control of the Band-Edge Positions of Crystalline Si(111) by Surface Functionalization with 3,4,5-Trifluorophenylacetylenyl Moieties. *J. Phys. Chem. C* **2016**, *120*, 14157-14169.
- (68) Chen, X.; McDonald, A. R., Functionalization of Two-Dimensional Transition-Metal Dichalcogenides. *Adv. Mater.* **2016**, *28*, 5738-5746.
- (69) Amani, M.; Lien, D. H.; Kiriya, D.; Xiao, J.; Azcatl, A.; Noh, J.; Madhvapathy, S. R.; Addou, R.; Kc, S.; Dubey, M.; Cho, K.; Wallace, R. M.; Lee, S. C.; He, J. H.; Ager, J. W., 3rd; Zhang, X.; Yablonovitch, E.; Javey, A., Near-unity photoluminescence quantum yield in MoS₂. *Science* **2015**, *350*, 1065-8.
- (70) Schmidt, H.; Giustiniano, F.; Eda, G., Electronic transport properties of transition metal dichalcogenide field-effect devices: surface and interface effects. *Chem. Soc. Rev.* **2015**, *44*, 7715-7736.
- (71) Liu, J.; Xue, Y.; Wang, Z.; Xu, Z.-Q.; Zheng, C.; Weber, B.; Song, J.; Wang, Y.; Lu, Y.; Zhang, Y.; Bao, Q., Two-Dimensional CH₃NH₃PbI₃ Perovskite: Synthesis and Optoelectronic Application. *ACS Nano* **2016**, *10*, 3536-3542.
- (72) Chu, X. S.; Yousaf, A.; Li, D. O.; Tang, A. A.; Debnath, A.; Ma, D.; Green, A. A.; Santos, E. J. G.; Wang, Q. H., Direct Covalent Chemical Functionalization of Unmodified Two-Dimensional Molybdenum Disulfide. *Chem. Mater.* **2018**, *30*, 2112-2128.
- (73) Addou, R.; Colombo, L.; Wallace, R. M., Surface Defects on Natural MoS₂. *ACS Appl. Mater. Interfaces* **2015**, *7*, 11921-9.
- (74) Hong, J. H.; Hu, Z. X.; Probert, M.; Li, K.; Lv, D. H.; Yang, X. N.; Gu, L.; Mao, N. N.; Feng, Q. L.; Xie, L. M.; Zhang, J.; Wu, D. Z.; Zhang, Z. Y.; Jin, C. H.; Ji, W.; Zhang, X.

X.; Yuan, J.; Zhang, Z., Exploring atomic defects in molybdenum disulphide monolayers. *Nat. Commun.* **2015**, *6*.

(75) Shen, J.; Wu, J.; Wang, M.; Ge, Y.; Dong, P.; Baines, R.; Brunetto, G.; Machado, L. D.; Ajayan, P. M.; Ye, M., Insight into In Situ Amphiphilic Functionalization of Few-Layered Transition Metal Dichalcogenide Nanosheets. *Adv. Mater.* **2016**, *28*, 8469-8476.

(76) Vera-Hidalgo, M.; Giovanelli, E.; Navío, C.; Pérez, E. M., Mild Covalent Functionalization of Transition Metal Dichalcogenides with Maleimides: A “Click” Reaction for 2H-MoS₂ and WS₂. *J. Am. Chem. Soc.* **2019**, *141*, 3767-3771.

(77) Quirós-Ovies, R.; Vázquez Sulleiro, M.; Vera-Hidalgo, M.; Prieto, J.; Gómez, I. J.; Sebastián, V.; Santamaría, J.; Pérez, E. M., Controlled Covalent Functionalization of 2H-MoS₂ with Molecular or Polymeric Adlayers. *Chem. Eur. J.* **2020**, *n/a*.

(78) Vázquez Sulleiro, M.; Quirós-Ovies, R.; Vera-Hidalgo, M.; Gómez, I. J.; Sebastián, V.; Santamaría, J.; Pérez, E. M., Covalent Cross-Linking of 2H-MoS₂ Nanosheets. *Chem. Eur. J.* **2021**, *27*, 2993-2996.

(79) Chen, X.; Berner, N. C.; Backes, C.; Duesberg, G. S.; McDonald, A. R., Functionalization of Two-Dimensional MoS₂: On the Reaction Between MoS₂ and Organic Thiols. *Angew. Chem. Int. Ed. Engl.* **2016**, *55*, 5803-8.

(80) Ding, Q.; Czech, K. J.; Zhao, Y.; Zhai, J.; Hamers, R. J.; Wright, J. C.; Jin, S., Basal-Plane Ligand Functionalization on Semiconducting 2H-MoS₂ Monolayers. *ACS Appl. Mater. Interfaces* **2017**, *9*, 12734-12742.

(81) Makarova, M.; Okawa, Y.; Aono, M., Selective Adsorption of Thiol Molecules at Sulfur Vacancies on MoS₂(0001), Followed by Vacancy Repair via S–C Dissociation. *J. Phys. Chem. C* **2012**, *116*, 22411-22416.

(82) Zheng, J.; Zhang, H.; Dong, S. H.; Liu, Y. P.; Nai, C. T.; Shin, H. S.; Jeong, H. Y.; Liu, B.; Loh, K. P., High yield exfoliation of two-dimensional chalcogenides using sodium naphthalenide. *Nat. Commun.* **2014**, *5*.

(83) Vishnoi, P.; Sampath, A.; Waghmare, U. V.; Rao, C. N. R., Covalent Functionalization of Nanosheets of MoS₂ and MoSe₂ by Substituted Benzenes and Other Organic Molecules. *Chem. Eur. J.* **2017**, *23*, 886-895.

(84) Knirsch, K. C.; Berner, N. C.; Nerl, H. C.; Cucinotta, C. S.; Gholamvand, Z.; McEvoy, N.; Wang, Z.; Abramovic, I.; Vecera, P.; Halik, M.; Sanvito, S.; Duesberg, G. S.; Nicolosi, V.; Hauke, F.; Hirsch, A.; Coleman, J. N.; Backes, C., Basal-Plane Functionalization of Chemically Exfoliated Molybdenum Disulfide by Diazonium Salts. *ACS Nano* **2015**, *9*, 6018-6030.

(85) Yan, E. X.; Cabán-Acevedo, M.; Papadantonakis, K. M.; Brunshwig, B. S.; Lewis, N. S., Reductant-Activated, High-Coverage, Covalent Functionalization of 1T' -MoS₂. *ACS Materials Lett.* **2020**, *2*, 133-139.

(86) Tuxen, A.; Kibsgaard, J.; Gøbel, H.; Lægsgaard, E.; Topsøe, H.; Lauritsen, J. V.; Besenbacher, F., Size Threshold in the Dibenzothiophene Adsorption on MoS₂ Nanoclusters. *ACS Nano* **2010**, *4*, 4677-4682.

(87) Canton-Vitoria, R.; Sayed-Ahmad-Baraza, Y.; Pelaez-Fernandez, M.; Arenal, R.; Bittencourt, C.; Ewels, C. P.; Tagmatarchis, N., Functionalization of MoS₂ with 1,2-dithiolanes: toward donor-acceptor nanohybrids for energy conversion. *NPJ 2D Mater. Appl.* **2017**, *1*, 13.

- (88) Divigalpitiya, W. M. R.; Frindt, R. F.; Morrison, S. R., Inclusion Systems of Organic Molecules in Restacked Single-Layer Molybdenum Disulfide. *Science* **1989**, *246*, 369.
- (89) Plymale, N. T.; Dasog, M.; Brunschwig, B. S.; Lewis, N. S., A Mechanistic Study of the Oxidative Reaction of Hydrogen-Terminated Si(111) Surfaces with Liquid Methanol. *J. Phys. Chem. C* **2017**, *121*, 4270-4282.
- (90) Dasog, M.; Thompson, J. R.; Lewis, N. S., Oxidant-Activated Reactions of Nucleophiles with Silicon Nanocrystals. *Chem. Mater.* **2017**, *29*, 7002-7013.
- (91) Fantauzzi, M.; Elsener, B.; Atzei, D.; Rigoldi, A.; Rossi, A., Exploiting XPS for the identification of sulfides and polysulfides. *RSC Adv.* **2015**, *5*, 75953-75963.
- (92) Freeman, F.; Angeletakis, C. N., ¹³C NMR chemical shifts of thiols, sulfinic acids, sulfinyl chlorides, sulfonic acids and sulfonic anhydrides. *Org. Magn. Reson.* **1983**, *21*, 86-93.
- (93) Eda, G.; Yamaguchi, H.; Voiry, D.; Fujita, T.; Chen, M.; Chhowalla, M., Photoluminescence from chemically exfoliated MoS₂. *Nano Lett.* **2011**, *11*, 5111-5116.
- (94) Hamann, T. W.; Lewis, N. S., Control of the Stability, Electron-Transfer Kinetics, and pH-Dependent Energetics of Si/H₂O Interfaces through Methyl Termination of Si(111) Surfaces. *J. Phys. Chem. B* **2006**, *110*, 22291-22294.
- (95) Cabán-Acevedo, M.; Papadantonakis, K. M.; Brunschwig, B. S.; Lewis, N. S., Surface Passivation and Positive Band-Edge Shift of *p*-Si(111) Surfaces Functionalized with Mixed Methyl/Trifluoromethylphenylacetylene Overlayers. *J. Phys. Chem. C* **2020**, *124*, 16338-16349.
- (96) Grimm, R. L.; Bierman, M. J.; O'Leary, L. E.; Strandwitz, N. C.; Brunschwig, B. S.; Lewis, N. S., Comparison of the Photoelectrochemical Behavior of H-Terminated and Methyl-Terminated Si(111) Surfaces in Contact with a Series of One-Electron, Outer-Sphere Redox Couples in CH₃CN. *J. Phys. Chem. C* **2012**, *116*, 23569-23576.
- (97) Yu, H.; Webb, L. J.; Ries, R. S.; Solares, S. D.; Goddard, W. A.; Heath, J. R.; Lewis, N. S., Low-Temperature STM Images of Methyl-Terminated Si(111) Surfaces. *J. Phys. Chem. B* **2005**, *109*, 671-674.
- (98) Tang, Q.; Jiang, D.-e., Stabilization and Band-Gap Tuning of the 1T-MoS₂ Monolayer by Covalent Functionalization. *Chem. Mater.* **2015**, *27*, 3743-3748.
- (99) Sanville, E.; Kenny, S. D.; Smith, R.; Henkelman, G., Improved grid-based algorithm for Bader charge allocation. *J. Comput. Chem.* **2007**, *28*, 899-908.
- (100) Qiu, L.; Xu, G., Peak overlaps and corresponding solutions in the X-ray photoelectron spectroscopic study of hydrodesulfurization catalysts. *Appl. Surf. Sci.* **2010**, *256*, 3413-3417.
- (101) Gong, C.; Zhang, H.; Wang, W.; Colombo, L.; Wallace, R. M.; Cho, K., Band alignment of two-dimensional transition metal dichalcogenides: Application in tunnel field effect transistors. *Appl. Phys. Lett.* **2013**, *103*, 053513.
- (102) Terrones, H.; López-Urías, F.; Terrones, M., Novel hetero-layered materials with tunable direct band gaps by sandwiching different metal disulfides and diselenides. *Sci. Rep.* **2013**, *3*, 1549.
- (103) Kaushik, V.; Ahmad, M.; Agarwal, K.; Varandani, D.; Belle, B. D.; Das, P.; Mehta, B. R., Charge Transport in 2D MoS₂, WS₂, and MoS₂-WS₂ Heterojunction-Based Field-Effect Transistors: Role of Ambipolarity. *J. Phys. Chem. C* **2020**, *124*, 23368-23379.

- (104) Barhoum, A.; García-Betancourt, M. L.; Rahier, H.; Van Assche, G., Chapter 9 - Physicochemical characterization of nanomaterials: polymorph, composition, wettability, and thermal stability. In *Emerging Applications of Nanoparticles and Architecture Nanostructures*, Barhoum, A.; Makhoulouf, A. S. H., Eds. Elsevier: 2018; pp 255-278.
- (105) Campbell, J.; Burkitt, S.; Dong, N.; Zavaleta, C., Chapter 9 - Nanoparticle characterization techniques. In *Nanoparticles for Biomedical Applications*, Chung, E. J.; Leon, L.; Rinaldi, C., Eds. Elsevier: 2020; pp 129-144.
- (106) Huang, Y.; Nielsen, R. J.; Goddard, W. A., Reaction Mechanism for the Hydrogen Evolution Reaction on the Basal Plane Sulfur Vacancy Site of MoS₂ Using Grand Canonical Potential Kinetics. *J. Am. Chem. Soc.* **2018**, *140*, 16773-16782.
- (107) Manjunatha, S.; Rajesh, S.; Vishnoi, P.; Rao, C. N. R., Reaction with organic halides as a general method for the covalent functionalization of nanosheets of 2D chalcogenides and related materials. *J. Mater. Res.* **2017**, *32*, 2984-2992.
- (108) Sundararaman, R.; Letchworth-Weaver, K.; Schwarz, K. A.; Gunceler, D.; Ozhabes, Y.; Arias, T. A., JDFTx: Software for joint density-functional theory. *SoftwareX* **2017**, *6*, 278-284.
- (109) Sundararaman, R.; Goddard, W. A., The charge-asymmetric nonlocally determined local-electric (CANDLE) solvation model. *J. Chem. Phys.* **2015**, *142*, 064107.
- (110) Baltrusaitis, J.; Mendoza-Sanchez, B.; Fernandez, V.; Veenstra, R.; Dukstiene, N.; Roberts, A.; Fairley, N., Generalized molybdenum oxide surface chemical state XPS determination via informed amorphous sample model. *Appl. Surf. Sci.* **2015**, *326*, 151-161.
- (111) Noviandri, I.; Brown, K. N.; Fleming, D. S.; Gulyas, P. T.; Lay, P. A.; Masters, A. F.; Phillips, L., The Decamethylferrocenium/Decamethylferrocene Redox Couple: A Superior Redox Standard to the Ferrocenium/Ferrocene Redox Couple for Studying Solvent Effects on the Thermodynamics of Electron Transfer. *J. Phys. Chem. B* **1999**, *103*, 6713-6722.